

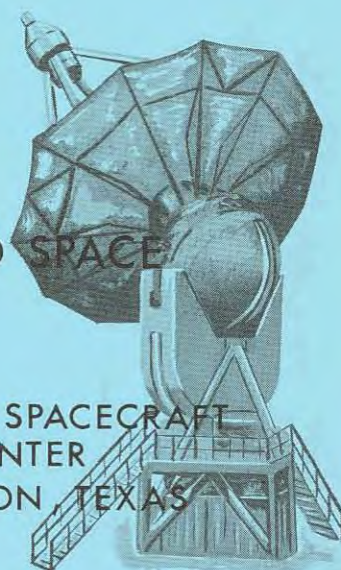
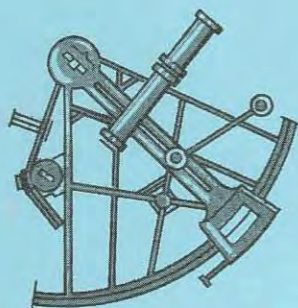


# APOLLO NAVIGATION WORKING GROUP

TECHNICAL REPORT  
NO. 65-AN-2.0

## APOLLO NAVIGATION GROUND AND ONBOARD CAPABILITIES

SEPTEMBER 1, 1965



NATIONAL AERONAUTICS AND SPACE  
ADMINISTRATION

GODDARD SPACE FLIGHT  
CENTER  
GREENBELT, MARYLAND

MANNED SPACECRAFT  
CENTER  
HOUSTON, TEXAS

# APOLLO NAVIGATION WORKING GROUP

## TECHNICAL REPORT



*F. O. Vonbun*

F. O. Vonbun

Chief, Mission Analysis  
Office

Goddard Space Flight Center  
Greenbelt, Maryland

*John P. Mayer*

John P. Mayer

Chief, Mission Planning  
and Analysis Division  
Manned Spacecraft Center  
Houston, Texas



## Contributors

### EARTH ASCENT PHASE

P. G. Brumberg, Chapter Chairman, GSFC  
B. Bryant, GSFC

### EARTH ORBIT PHASE

E. R. Schiesser, Chapter Chairman, MSC  
P. T. Pixley, MSC  
W. York, MSC

### TRANSLUNAR PHASE

P. H. Mitchell, Chapter Chairman, MSC  
A. C. Bond, MSC  
S. Z. Shaper, MSC  
D. B. Grammer, MSC

### CSM LUNAR PARKING ORBITS

W. D. Kahn, Chapter Chairman, GSFC  
J. A. Behuncik, GSFC  
V. R. Bond, MSC  
J. L. Cooley, GSFC  
A. Marlow, GSFC  
S. J. Paddack, GSFC  
D. S. Woolston, GSFC

### LEM OPERATIONS PHASE

S. O. Mayfield, Chapter Chairman, MSC  
A. C. Bond, MSC  
S. Z. Shaper, MSC  
R. H. Kidd, MSC

### TRANSEARTH PHASE

P. H. Mitchell, Chapter Chairman, MSC  
A. C. Bond, MSC  
S. Z. Shaper, MSC  
D. B. Grammer, MSC

Contributors (Continued)

REENTRY PHASE

R. E. Coady, Chapter Chairman, GSFC

J. H. Adams, MSC

A. Cohen, MSC

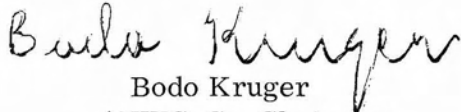
C. A. Graves, Jr., MSC

R. T. Groves, GSFC

J. W. Tolin, Jr., MSC

Acknowledgement

Special mention is merited for James C. McPherson for his untiring efforts in critically reviewing all phases of the manuscripts and proofs.




Bodo Kruger

ANWG Co-Chairman

Goddard Space Flight Center

Greenbelt, Maryland



James F. Dalby

ANWG Co-Chairman

Manned Spacecraft Center

Houston, Texas



# CONTENTS

	<u>Page</u>
1.0 INTRODUCTION . . . . .	1-1
2.0 CHANGES AND ADDITIONS. . . . .	2-1
3.0 EARTH ASCENT PHASE. . . . .	3-1
3.1 Introduction. . . . .	3-1
3.2 Description of Phase. . . . .	3-1
3.3 General Discussion. . . . .	3-3
3.4 Procedure and Results . . . . .	3-4
3.5 Conclusions. . . . .	3-8
3.6 Future Studies . . . . .	3-9
3.7 References . . . . .	3-10
4.0 EARTH ORBIT PHASE. . . . .	4-1
4.1 Introduction. . . . .	4-1
4.2 Description of Phase and Procedures. . . . .	4-1
4.3 Results. . . . .	4-5
4.4 Conclusions. . . . .	4-7
4.5 References . . . . .	4-8
5.0 TRANSLUNAR PHASE . . . . .	5-1
5.1 Introduction. . . . .	5-1
5.2 Assumptions . . . . .	5-1
5.3 Results. . . . .	5-2
5.4 Discussion of Results . . . . .	5-6
5.5 Conclusions. . . . .	5-9
5.6 Appendix A, Coordinate Systems . . . . .	5-10
5.7 Appendix B, Trajectories. . . . .	5-10
5.8 Appendix C, Components for Assumed A Priori Knowledge. .	5-11
5.9 Appendix D, Check Out Procedures . . . . .	5-12
5.10 References . . . . .	5-12
6.0 CSM LUNAR PARKING ORBITS. . . . .	6-1
6.1 Introduction. . . . .	6-1
6.2 Description of the Lunar Orbit Phase. . . . .	6-1
6.3 Ground Navigation System . . . . .	6-2
6.4 Level of Confidence . . . . .	6-6

## CONTENTS (Continued)

	<u>Page</u>
6.5 Conclusions. . . . .	6-6
6.6 References . . . . .	6-7
 7.0 LEM OPERATIONS PHASE . . . . .	 7-1
7.1 Introduction. . . . .	7-1
7.2 Procedures and Assumptions . . . . .	7-3
7.3 Results. . . . .	7-4
7.4 Conclusions. . . . .	7-9
7.5 References . . . . .	7-9
 8.0 TRANSEARTH PHASE . . . . .	 8-1
8.1 Introduction. . . . .	8-1
8.2 Assumptions . . . . .	8-1
8.3 Results. . . . .	8-2
8.4 Discussion of Results . . . . .	8-6
8.5 Summary . . . . .	8-7
8.6 Conclusions. . . . .	8-8
8.7 Appendix A, Coordinate Systems . . . . .	8-9
8.8 Appendix B, Trajectories. . . . .	8-10
8.9 Appendix C, Components of Assumed A Priori Knowledge . .	8-11
8.10 Appendix D, Check Out Procedures . . . . .	8-12
8.11 References . . . . .	8-12
 9.0 REENTRY PHASE . . . . .	 9-1
9.1 Introduction. . . . .	9-1
9.2 Assumption and Procedures . . . . .	9-1
9.3 Results and Conclusions . . . . .	9-6
9.4 Level of Confidence . . . . .	9-7
9.5 Acknowledgment. . . . .	9-7
9.6 References . . . . .	9-8



## 1.0 INTRODUCTION

The purpose of the Apollo Navigation Working Group (ANWG) is to coordinate the analysis and study of problems of the Apollo missions from the navigations point of view. Emphasis is placed on the total system rather than on the onboard and ground systems individually in order that the optimum combination of them can be achieved.

This report presents the results of studies of navigation systems capabilities. The ultimate goal of these studies is to verify the adequacy of the combined onboard and ground systems and to recommend corrective action if needed. In this, the first issue of this report, the results of ground network navigation studies are given. It was the consensus that the publication should not be delayed until the studies of the onboard and the combined systems are completed. The publication of the results from these studies is therefore left for future issues of this report.

The lunar mission has been divided into seven consecutive phases, each of which has been analyzed under conservative assumptions. The results, therefore, are conservative compared with the results of an analysis of a continuous mission. Note that the results are given in  $3\sigma$  values. The analysis was based on a ground tracking network performance as specified in 65-AN-1.0 "Apollo Missions and Navigation Systems Characteristics."

The units used are consistent with the rules of 65-AN-1.0. Scales in both English and metric units are included on diagrams and graphs with the exception of logarithmic scales, which are given only in English units. The term speed uncertainty, as used in this report, means the uncertainty of only the magnitude of the velocity vector in contrast to velocity uncertainty, which reflects both the uncertainty in orientation and magnitude.

## **2.0 CHANGES AND ADDITIONS**

This document is the first publication of the "Apollo Navigation – Ground and Onboard Capabilities" document. In future issues, this section will consist of a summary of the additions and revisions to the document.



## 3.0 EARTH ASCENT PHASE

### 3.1 INTRODUCTION

The earth ascent of the Apollo mission begins at liftoff of the launch vehicle and terminates with abort initiation or the GO/NO-GO decision. The launch is separated into two phases. The first is from liftoff to S-IVB cutoff and represents the powered flight phase. The second is from S-IVB cutoff to the GO/NO-GO decision and represents the hold phase. The hold phase is studied in this chapter.

### 3.2 DESCRIPTION OF PHASE

The Apollo space configuration will be launched from Merritt Island, Launch Complex 39, Cape Kennedy, on a launch azimuth of 72 degrees to 108 degrees. The operational launch azimuths have a daily range of 26 degrees within this range of azimuths. Referring the 26 degrees to time, they amount to a daily launch window of at least 2-1/2 hours, based on the requirement for insertion tracking using one ship. (Reference 1). A minimum of 2-1/2 to 3 minutes of tracking is obtainable following termination of the powered flight phase of the trajectory. The nominal orbit is circular at an altitude of 100 nm (185 km). An elliptical trajectory is not ruled out, in which case perigee may be at 85 nm (157 km) and apogee at 150 nm (278 km). Cutoff of the powered flight phase occurs approximately 1440 nm (2667 km) downrange from the launch area.

Figure 3.1 shows the position coverage of the insertion tracking ship relative to the ground track of six launch azimuths. The ship would be near point A for northerly launch azimuths and point C for southerly launch azimuths. During a month, the ship would have to travel approximately 350 nm (648 km) to adequately cover the 36 degree range of launch azimuths, but it would not move significantly during the day of launch. Also shown are coverage circles for Cape Kennedy, Bermuda, San Salvador and Antigua.

During the powered flight phase of the earth ascent, the Apollo Saturn configuration utilizes closed loop inertial guidance. No steering commands are sent from the ground during this phase as they were for Projects Mercury and Gemini. Consequently, the ground stations can only perform monitoring during the powered flight phase.

These are five sources of trajectory data available during this phase. The ground tracking systems (land based and ship based) consists of AZUSA, C-band and the Unified S-band Systems. Two sources of on-board position and velocity measurements are available to the ground station via the telemetry link; one from the Inertial Guidance Computer in the Saturn Vehicle and the second from the Apollo Guidance Computer in the Spacecraft. As the data is received, it is processed and used to compute data quality parameters which are used to select the best source. The selected source is then used to compute trajectory monitoring, guidance monitoring and trajectory planning parameters.

During the powered flight phase, coverage from the ground stations is sufficient and in part redundant (Figure 3.1) and land based coverage of the flight essentially terminates at cutoff of the S-IVB as it occurs 1440 nm (2667 km) down-range. Antigua can view the cutoff and insertion phase, but only for launch azimuths greater than 95 degrees. The insertion ship then becomes, for most launch azimuths, the primary site for the insertion phase. Four data sources are available to the ship at this time; shipboard C-Band and Unified S-Band, and telemetry data from the two on board inertial guidance systems. With this information, the GO/NO-GO decision will be made.

Important questions that must be answered are:

1. What data rates and tracking arcs (time) are required for shipboard tracking to make the GO/NO-GO decision?
2. What criteria are to be used in selecting the best data source for the GO/NO-GO decision?
3. What data or combination of data are to be transmitted from the ship to the Mission Control Center?

Of the studies required to answer these questions, the analysis of the C-band capability from the insertion ship was chosen first and is presented in this Chapter.

Measurement noise and bias and station errors over three different time arcs for various data sampling rates were used. The assumptions used in this study are given below and discussed in more detail in paragraph 3.4.



1. Trajectory Parameters (circular orbit) (reference 2)

Velocity 25568 ft/s (7793 m/s)

Flight path angle 0.0 degrees

Altitude 100 nm (185 km)

Launch Azimuth 108 degrees

2. Data Type and Uncertainties, C-Band Shipboard Radar,  $1\sigma$  Values (reference 3)

	NOISE	BIAS
Range	30 feet	60 feet
Azimuth	0.4 m. rad.	0.8 m. rad.
Elevation	0.4 m. rad.	0.8 m. rad.

3. Ship Location and Biases,  $1\sigma$  Values

Latitude  $21^{\circ} 15'$  North  $\pm 0.3'$  or 0.3 nm bias

Longitude  $48^{\circ} 45'$  West  $\pm 0.3'$  or 0.3 nm bias

4. The data was not degraded due to any other uncertainties than those given above. It was assumed that the data had been corrected for ships motion, speed, local vertical and refraction.

### 3.3 GENERAL DISCUSSION

The studies using the before mentioned assumptions were generated with the Short Arc Digital Program (reference 4). This program uses range, azimuth and elevation data to compute the orbit of the spacecraft in the form of inertial position and velocity vectors. The Short Arc method is based on a least squares curve fit to a truncated Taylor's series expansion of the inertial position from the center of the earth to the spacecraft. It utilizes the two-body equations of motion to obtain the expansion as a function of initial position and velocity (drag and oblateness terms are neglected). Time arcs of twenty, forty and sixty seconds were used for the present study, with the solution referenced to the mid point of the time arc.

The Short Arc Program was selected to study the insertion phase because this method was used to compute the actual GO/NO-GO decision for the Mercury Missions and a similar method is currently used in Gemini. Possibly, a Short Arc or similar method will be selected for Apollo. The results of this study should apply regardless of the method selected.

In Project Mercury, the GO/NO-GO decision was made following shutdown and separation of the spacecraft from the booster. In less than a minute, the tracking data was evaluated to decide if the mission should continue or be aborted. The GO decision was based on the insertion velocity magnitude, flight path angle and altitude, and an orbit lifetime of 1-1/2 orbits with a minimum perigee of 75 n. mi. (139 km). Any orbit outside of these constraints would have resulted in a NO-GO decision and subsequent abort.

For the Gemini Missions, the GO/NO-GO decision is similar. However, the spacecraft has on board propulsion to obtain orbital velocity, should analysis of the tracking data indicate an underspeed at insertion.

The earth insertion phase for Apollo is somewhat more complicated than for Mercury and Gemini. The nominal Saturn V launch phase to the earth parking orbit insertion consists of S-IC, S-II, and S-IVB burns with the first S-IVB cutoff occurring approximately 12 minutes after liftoff. Guidance and sequencing are under the programmed control of the launch vehicle computer and inertial reference system. The spacecraft crew and ground personnel monitor the programmed sequence of events, the performance of the vehicle systems and the achieved trajectory. The orbit insertion verification comes from the first S-IVB cutoff data.

If necessary the spacecraft crew can:

1. Override automatic event sequence timing
2. Select back-up modes
3. Cut off the S-IVB propulsion to prevent overspeed, or
4. Initiate abort sequences including selection of the appropriate guidance program.

### 3.4 PROCEDURE AND RESULTS

The studies for this Chapter have been concerned with determining the errors in speed, flight path angle, altitude, position vector and velocity vector based on shipboard C-band tracking. A total of 40 Monte Carlo runs were made with the Short Arc Program for each of the uncertainty combinations listed below. Five data sampling rates were considered: 10/sec, 5/sec, 2/sec, 1/sec and 10/min over tracking arcs of 20, 40 and 60 seconds. Table 3.1 lists the combinations of uncertainties that were studied for the three tracking intervals.

Error free radar data (range, azimuth and elevation) were generated for the insertion ship and used in the Short Arc Program to determine the accuracy of the Program. The errors caused by round-off and truncation as well as mathematical models errors, were found to be negligible. For this study the uncertainties were then added to the data as follows:

1. NOISE:

The noise was added to the data via a random number generator. Forty separate runs were made, each with a different random number starter for the three radar parameters.

2. NOISE AND + BIAS:

Positive biases in all three radar quantities (range, azimuth and elevation) were added simultaneously with the noise.

3. NOISE AND - BIAS

Same runs as 2, except with negative biases.

4. NOISE, BIAS, AND STATION ERROR:

To the noise and bias were added errors in the latitude and longitude of the ship of  $\pm 0.3'$ . The positive and negative signs indicate the error direction used for placement of the ship.

Table 3.1

MEASUREMENT UNCERTAINTIES	STATION LOCATION UNCERTAINTIES
1. Noise	0
2. Noise and + bias	0
3. Noise and - bias	0
4. Noise, - bias	{ + latitude - longitude
5. Noise, + bias	{ + latitude + longitude
6. Noise, + bias	{ + latitude - longitude
7. Noise, + bias	{ - latitude + longitude
8. Noise, + bias	{ - latitude - longitude

As indicated above, selective combinations of noise, bias and station error studies were made. The data given in the figures present the most conservative results obtained thus far in the study.

The  $3\sigma$  results as shown on the graphs are based on the expected shipboard C-band tracking accuracies. The noise and data bias uncertainties used for this study were based on the results of the performance of the two C-band tracking ships used in support of the Mercury – Atlas 9 (MA-9) mission. The average noise of the ships' observations and the noise values used for the Apollo insertion ship studies are given in Table 3.2.

Table 3.2

STANDARD DEVIATIONS (NOISE) OF SHIPS' OBSERVATIONS			
Data Type	Range Tracker (RTK)	Twin Falls Victory (TFV)	Apollo Insertion Ship
Range (feet)	48.	27.	30.0
Azimuth (m. rad.)	0.68	0.32	0.4
Elevation (m. rad.)	1.20	0.40	0.4

The data biases (not shown) on MA-9 ships' observations were roughly double the noise figures. Therefore in this study, data biases of 60 feet in range and 0.8 m. rad. in angles were used for the insertion ship.

The  $1\sigma$  total error in ship position for this study was assumed to be 0.4 n. mi. (0.74 km). This value is more optimistic than those on MA-9, but with the Insertion Ship's Inertial Navigation System, and other navigational aids, it should be attainable.

The above assumptions, based on actual shipboard C-band tracking, make the results presented in this Chapter realistic. But, if the new Apollo ships perform as well as expected, these results are conservative.

The 108 degree launch azimuth was chosen because it gave low elevation angles and maximum values of slant range for the insertion ship. Antigua was also able to view the spacecraft at insertion for the 108 degree launch azimuth. All of the studies for the ship were also made for Antigua using the same assumptions with only the geometry being different (Figure 3.1). Table 3.3 gives the values of the tracking data over the longest arc used in the studies.



Table 3.3

TRACKING COVERAGE - 108 DEGREE LAUNCH AZIMUTH						
INSERTION SHIP				ANTIGUA		
Time From SIV-B Cutoff (sec)	Range (nm)	Azimuth (deg.)	Elevation (deg.)	Range (nm)	Azimuth (deg.)	Elevation (deg.)
0	501.	259.	7.6	320.	62.	15.9
20	449.	251.	9.4	368.	73.	13.0
40	405.	242.	11.2	426.	80.	10.3
60	373.	232.	12.7	488.	86.	8.0

From Table 3.3, it can be seen that the spacecraft is approaching the ship while for Antigua, the converse is taking place. Since essentially the same results were obtained from Antigua and the ship, only the ship results are given. It should be noted, however, that because of the close agreement, a somewhat greater level of confidence is placed on the study.

It was mentioned previously that the GO/NO-GO decision was based on three critical orbital parameters. They were: speed, flight-path angle and altitude. Figures 3.2 through 3.4 give the  $3\sigma$  uncertainties in these parameters as a function of tracking sampling rates and arc length of data. The position and velocity vectors are not used for the earth orbit insertion decision but rather the scalar components given above. Figures 3.5 and 3.6 give the  $3\sigma$  errors in the position and velocity. They have been included to show the relative comparison between the scalar and vector errors.

In Figures 3.2 the  $3\sigma$  uncertainty in speed is given as a function of five different data rates. The graphs are presented for 20, 40 and 60 second tracking intervals. It is shown that bias on the measurement and station location contribute little to the uncertainty in speed, but noise on the other hand, contributes significantly to this uncertainty. Furthermore, there is a significant improvement in accuracy if the tracking interval is increased from 20 seconds to 40 or 60 seconds.

In Figures 3.3, the  $3\sigma$  uncertainty in flight-path angle is given for various data rates and tracking time arcs. High data rates do not give significant improvement to this parameter for tracking intervals of 40 seconds and longer. Station location biases do not affect the error in this parameter.

In Figures 3.4, the  $3\sigma$  uncertainty in altitude is given for various data rates and tracking intervals. Again, station location biases have little effect, and noise is not significant. Data bias errors cause the greatest uncertainty in the altitude, and increasing the tracking arc or data rate will not reduce this error. Increasing the data rate above 2/sec does not significantly reduce the uncertainties.

In Figures 3.5, the  $3\sigma$  uncertainty in position is given for the various data rates and tracking time intervals. It is noted that the station location bias causes the greatest uncertainty, and the effect of measurement bias, though significant, is smaller. Measurement noise has no effect. In addition, data rates and tracking interval have no effect.

In Figures 3.6, the  $3\sigma$  uncertainty in velocity is given for the various data rates and tracking intervals. The greatest uncertainty is caused by the measurement bias for tracking intervals of 40 to 60 seconds. The effect of measurement noise and station location bias can be significant and the uncertainty is sensitive to both data rates and tracking interval.

The results of this study have been checked with similar runs made with the ERRAN error analysis program, Mission Analysis Office, Goddard Space Flight Center. The results of the two programs agree to within  $\pm 10\%$ . Checks have also been made with the operational Gemini "Real-Time Program" at GSFC, with even closer agreement.

### 3.5 CONCLUSIONS

The results presented in this Chapter pertain to the tracking intervals and data rates of the earth insertion phase, based on the expected accuracies of a shipboard C-band radar. From the enclosed graphs, the following conclusions may be made.

1. A 40 second tracking interval is significantly more accurate than a 20 second tracking interval, both for speed and flight path angle (Altitude error is insensitive to both tracking interval and data rate.) Therefore the GO/NO-GO decision should be based on a tracking interval which is longer than 20 seconds.

2. Data rates of 5/sec give essentially the same results as 10/sec for a tracking interval of 40 seconds. For a 60 second interval, a 2/sec data rate is adequate.
3. Table 3.4 summarizes the approximate uncertainty percentage contributed by measurement noise, measurement bias, and station location bias to the three critical insertion parameters for a tracking interval of 40 seconds.

Table 3.4

Uncertainty	Speed	Flight Path Angle	Altitude
Measurement Noise	~ 95%	~40%	~10%
Measurement Bias	~5%	~60%	~85%
Station Location Bias	~0%	~0%	~5%

4. Table 3.5 summarizes the percentage of uncertainty contributed to the insertion position and velocity for a tracking interval of 40 seconds.

Table 3.5

Uncertainty	Position	Velocity
Measurement Noise	~ 5%	~20%
Measurement Bias	~45%	~60%
Station Location Bias	~50%	~20%

### 3.6 FUTURE STUDIES

1. Expansion of the present study to a tracking interval of 90 seconds.
2. Investigation of the use of data from other sources (paragraph 3.2) in making the GO/NO-GO decision.
3. Obtaining results of the Bermuda GO/NO-GO decision based on C-Band data for Gemini 3, 4 and 5.

### 3.7 REFERENCES

1. MSC, Mission Planning and Analysis Division, "Trajectory Studies for use in Determining Tracking Requirements for Project Apollo." NASA Project Apollo Working Paper No. 1114, March 9, 1964.
2. J. L. Cooley, GSFC Report No. X-513-64-359, "The Influence of Venting on the Apollo Earth Parking Orbit," Nov. 24, 1964.
3. "Radar Tracking Ship Performance During MA-9," X-554-63-161, Data Operations Branch, Goddard Space Flight Center, July 31, 1963.
4. IBM Demonstration Report, "Project Mercury Bermuda Program System," August 22, 1961.
5. MSC-GSFC, ANWG Report No. 65-AN-1.0, "Apollo Missions and Navigation Systems Characteristics," Feb. 5, 1965.

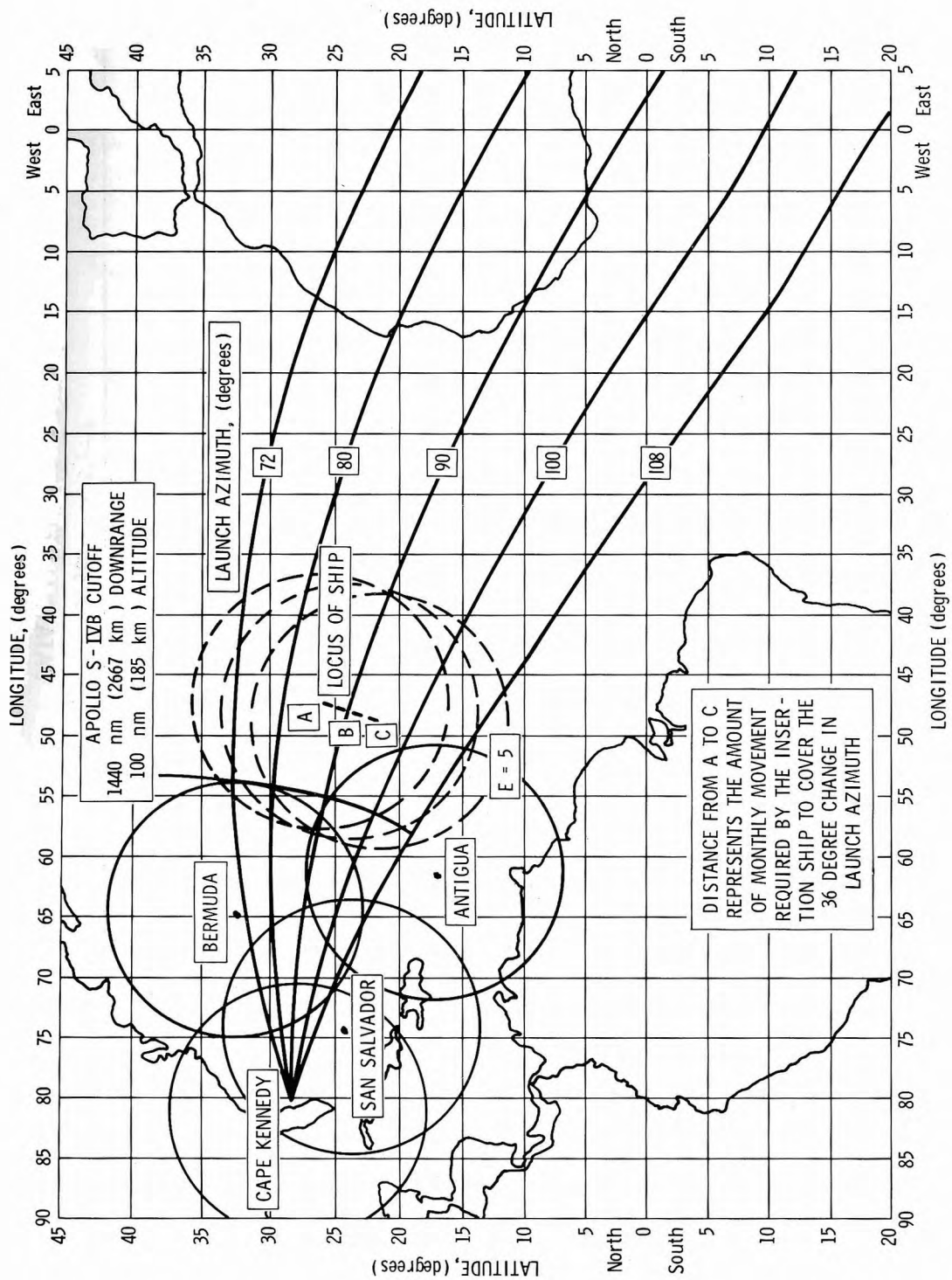


Figure 3.1

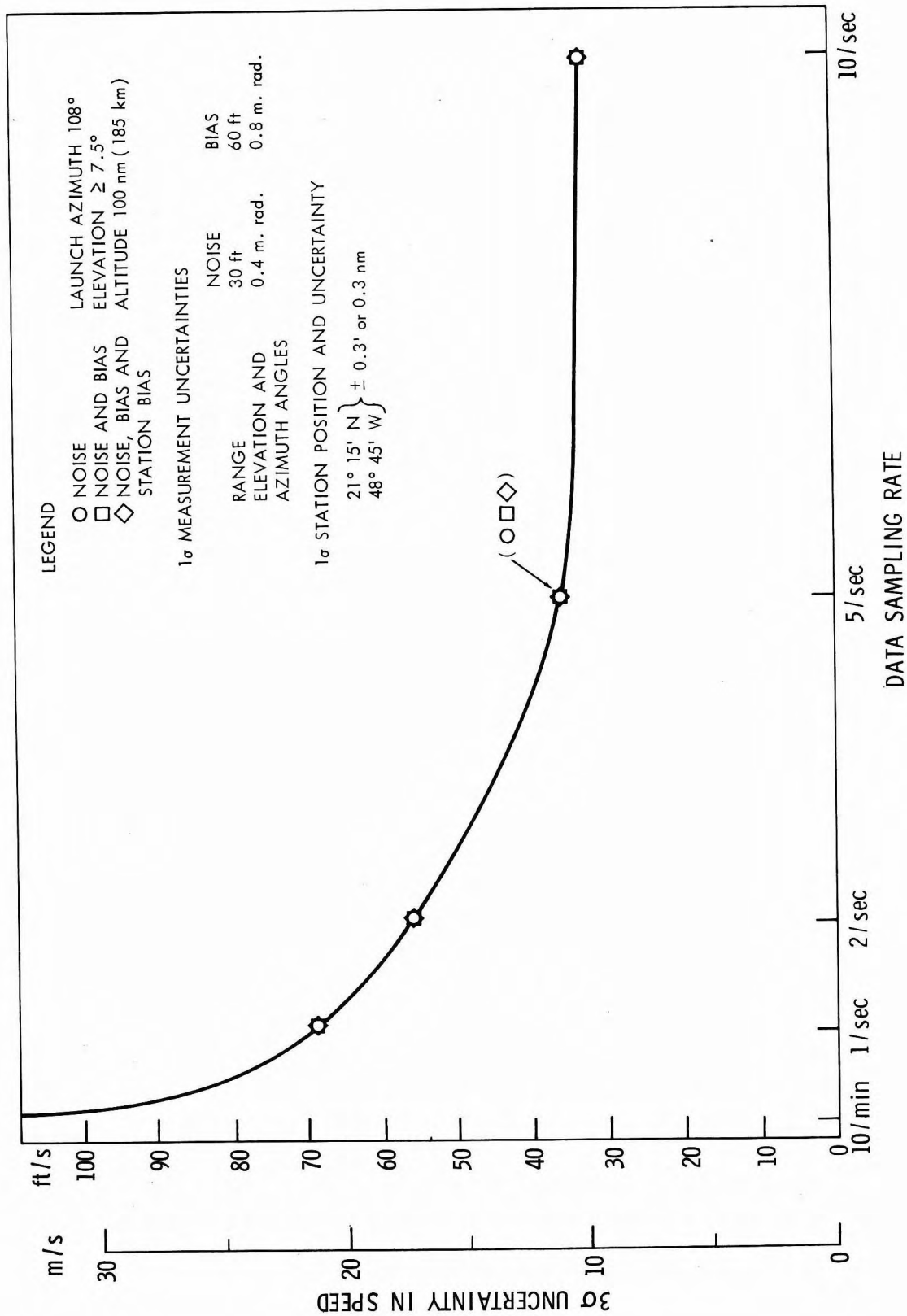


Figure 3.2a—Speed uncertainty, 20 second tracking interval.



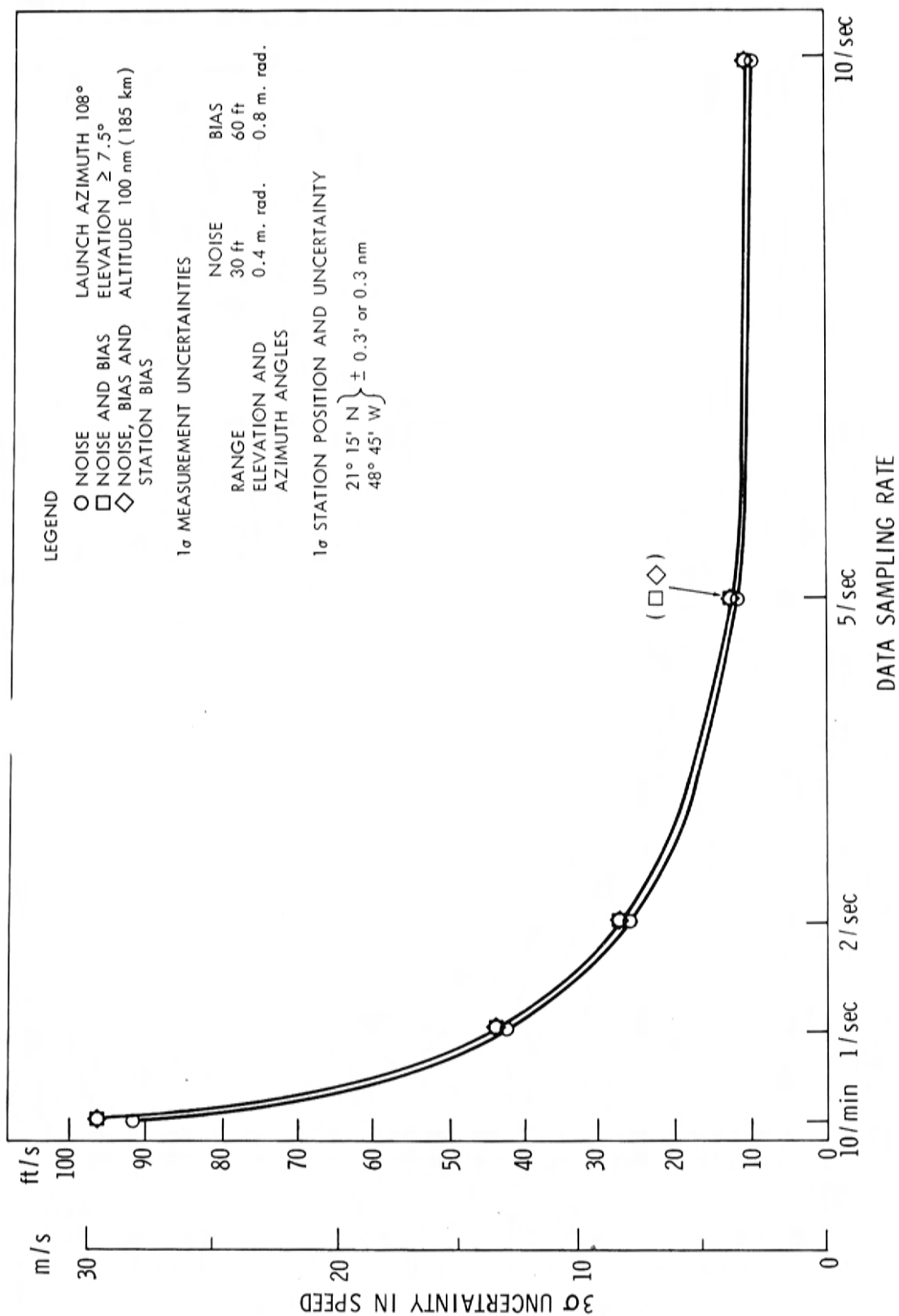


Figure 3.2b—Speed uncertainty, 40 second tracking interval.

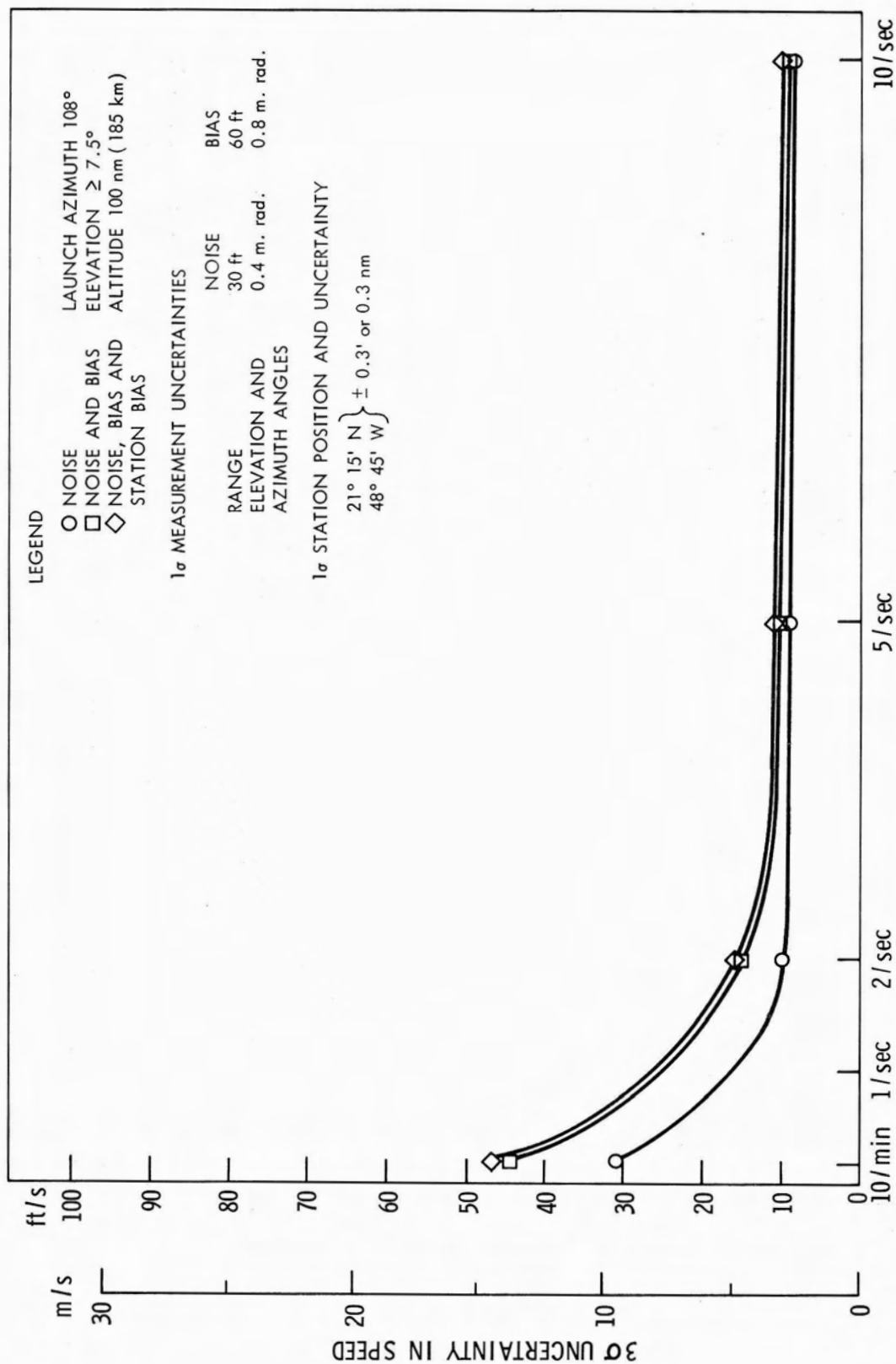


Figure 3.2c—Speed uncertainty, 60 second tracking interval.

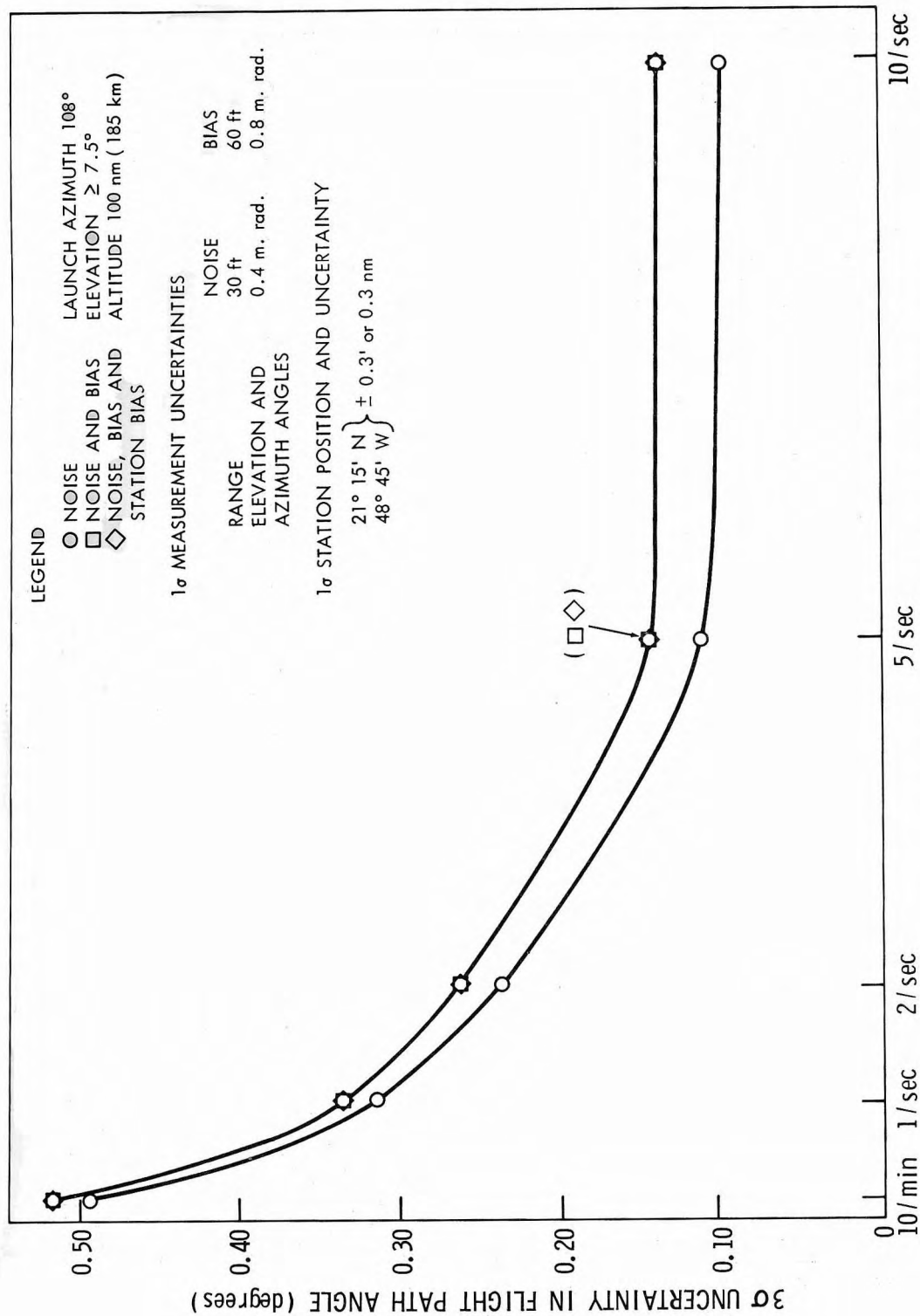


Figure 3.3a—Flight path angle uncertainty, 20 second tracking interval.

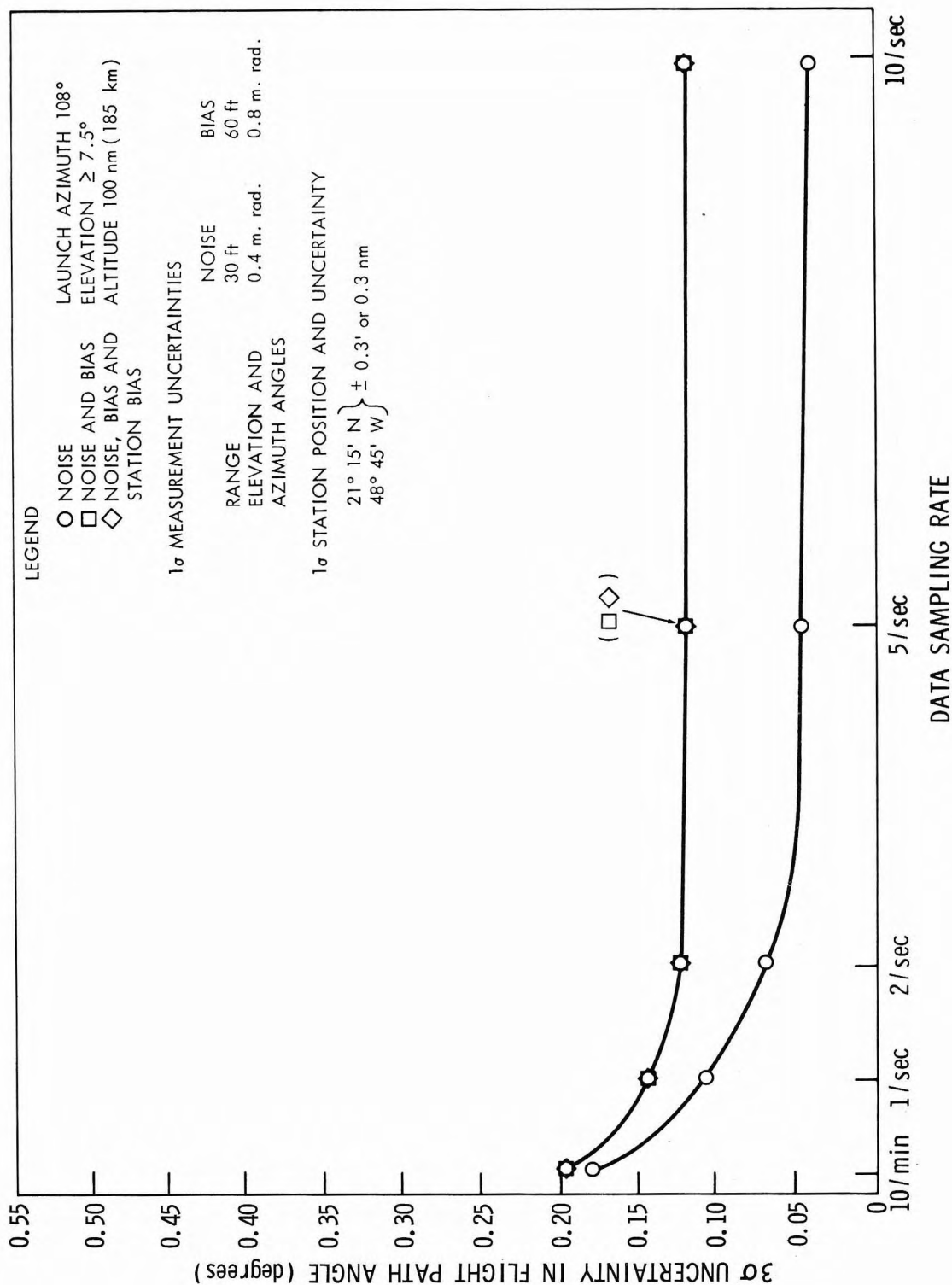


Figure 3.3b—Flight path angle uncertainty, 40 second tracking interval.

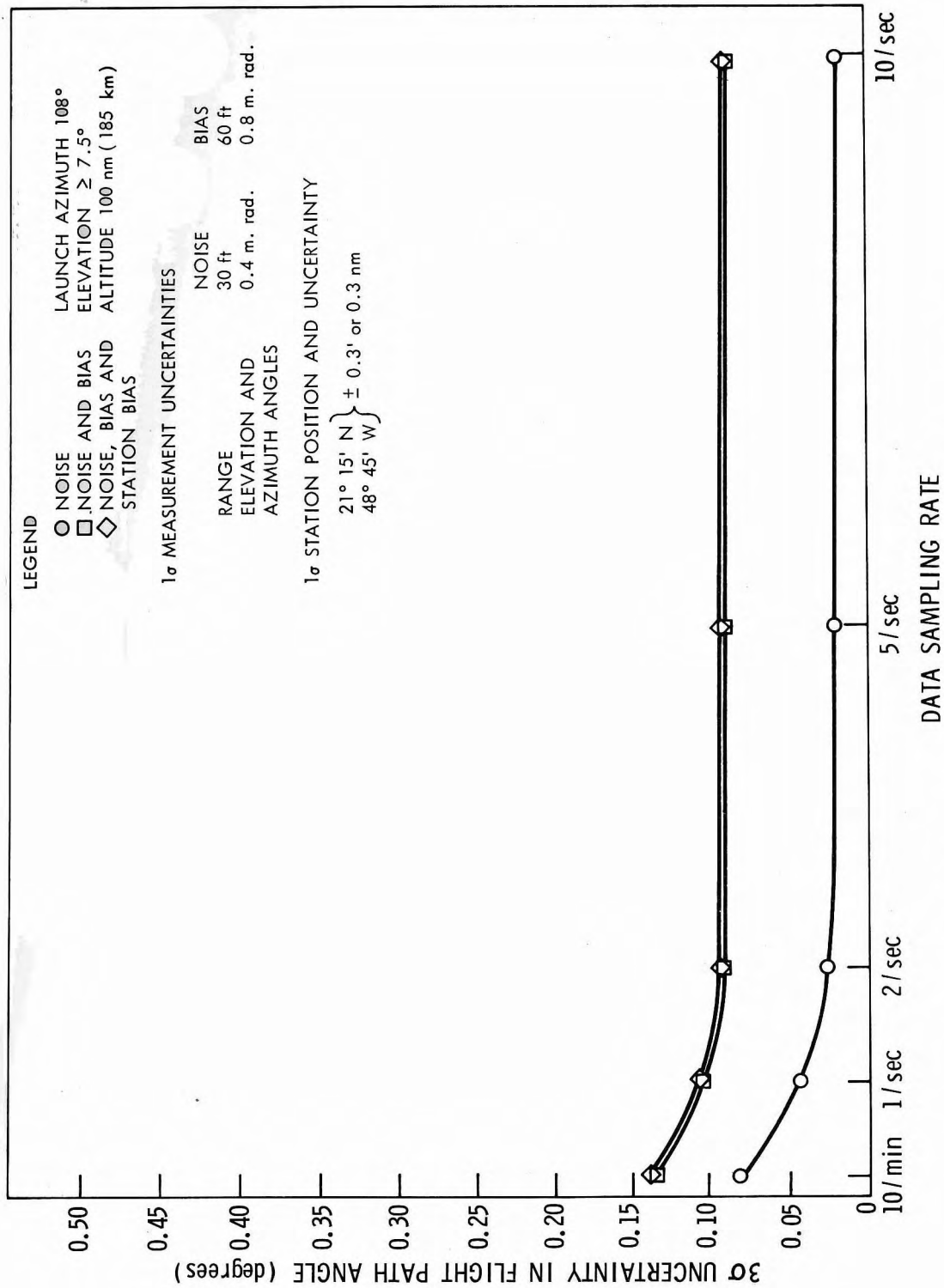


Figure 3.3c—Flight path angle uncertainty, 60 second tracking interval.

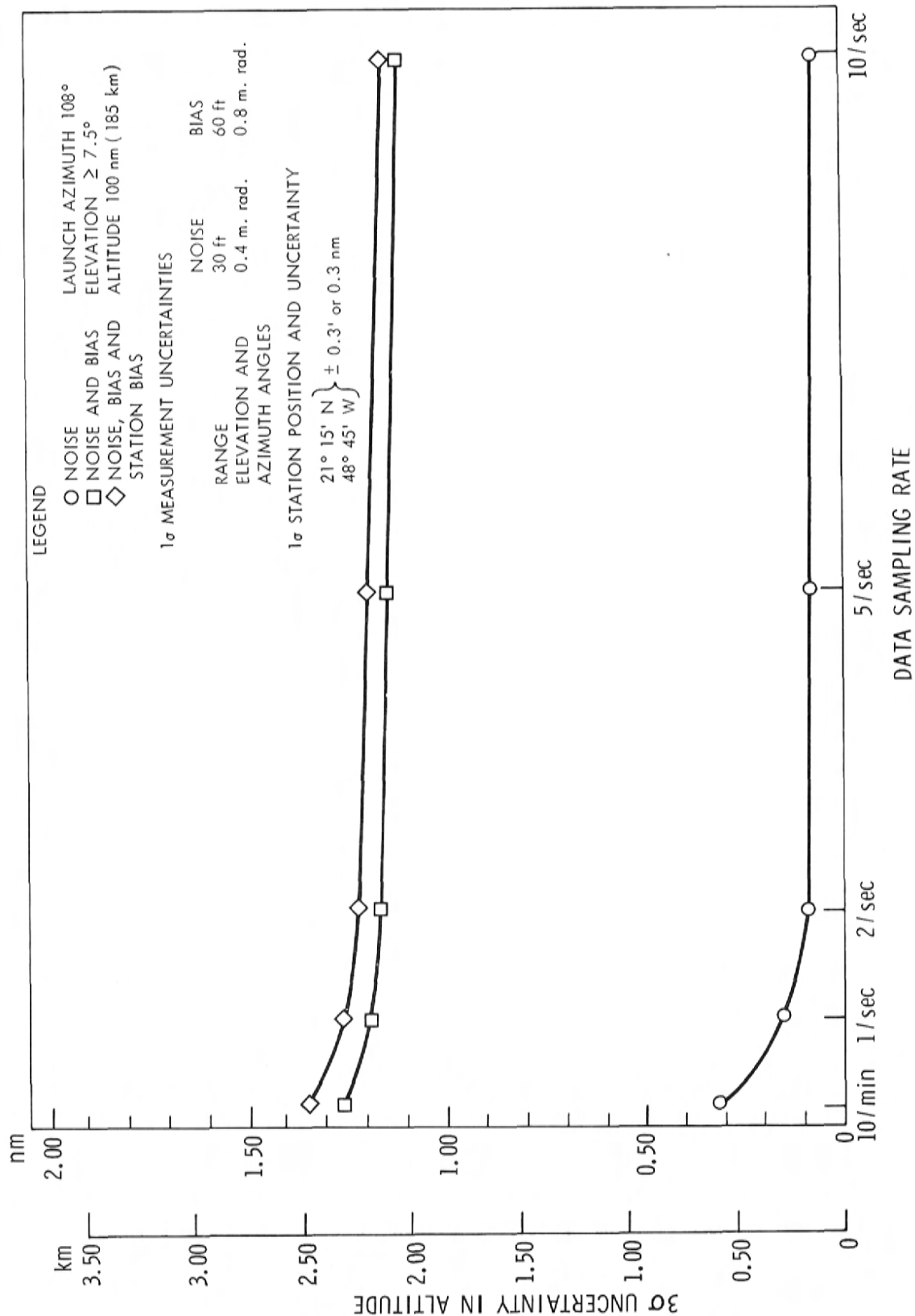


Figure 3.4a—Altitude uncertainty, 20 second tracking interval.



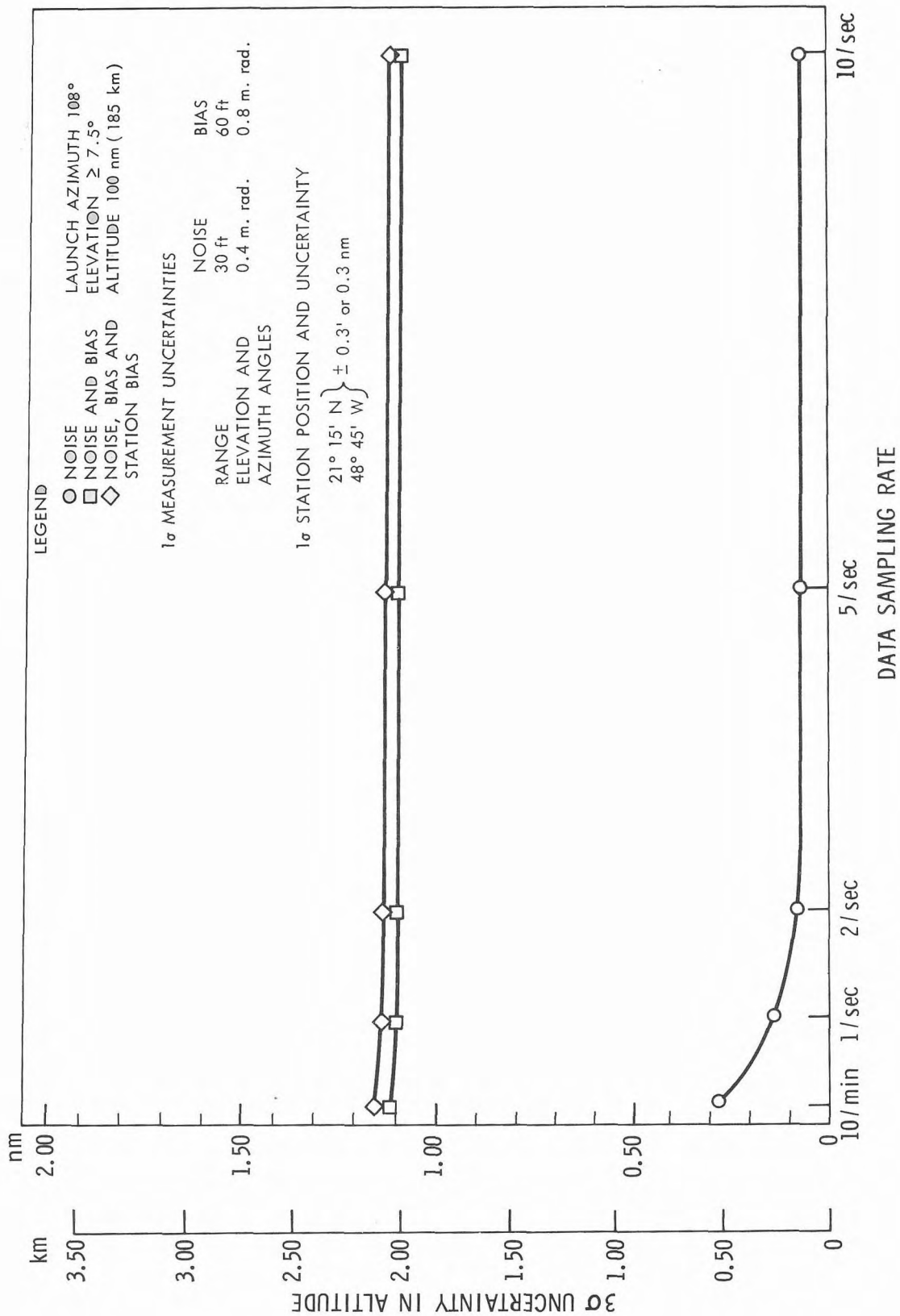


Figure 3.4b—Altitude uncertainty, 40 second tracking interval.

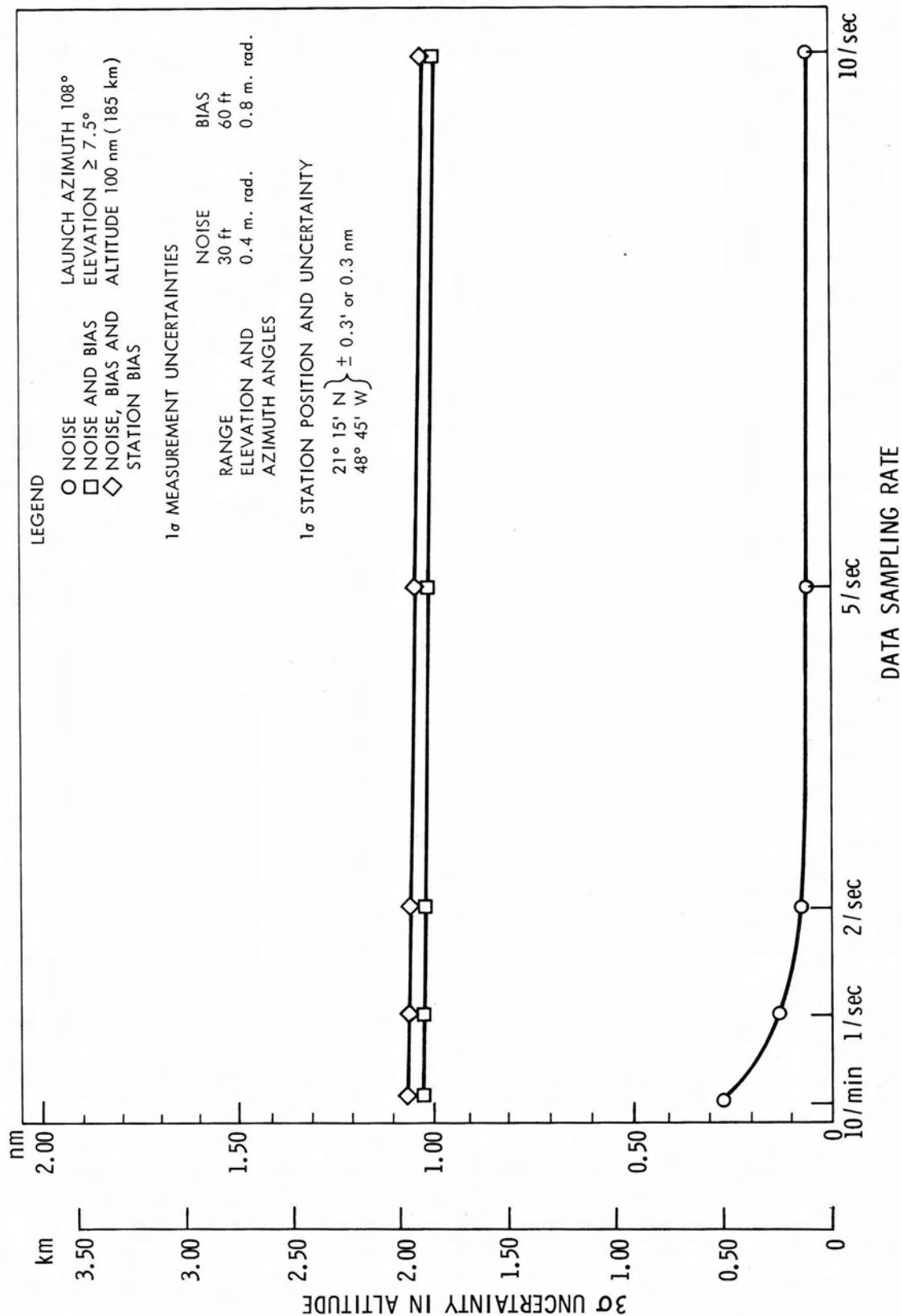


Figure 3.4c—Altitude uncertainty, 60 second tracking interval.

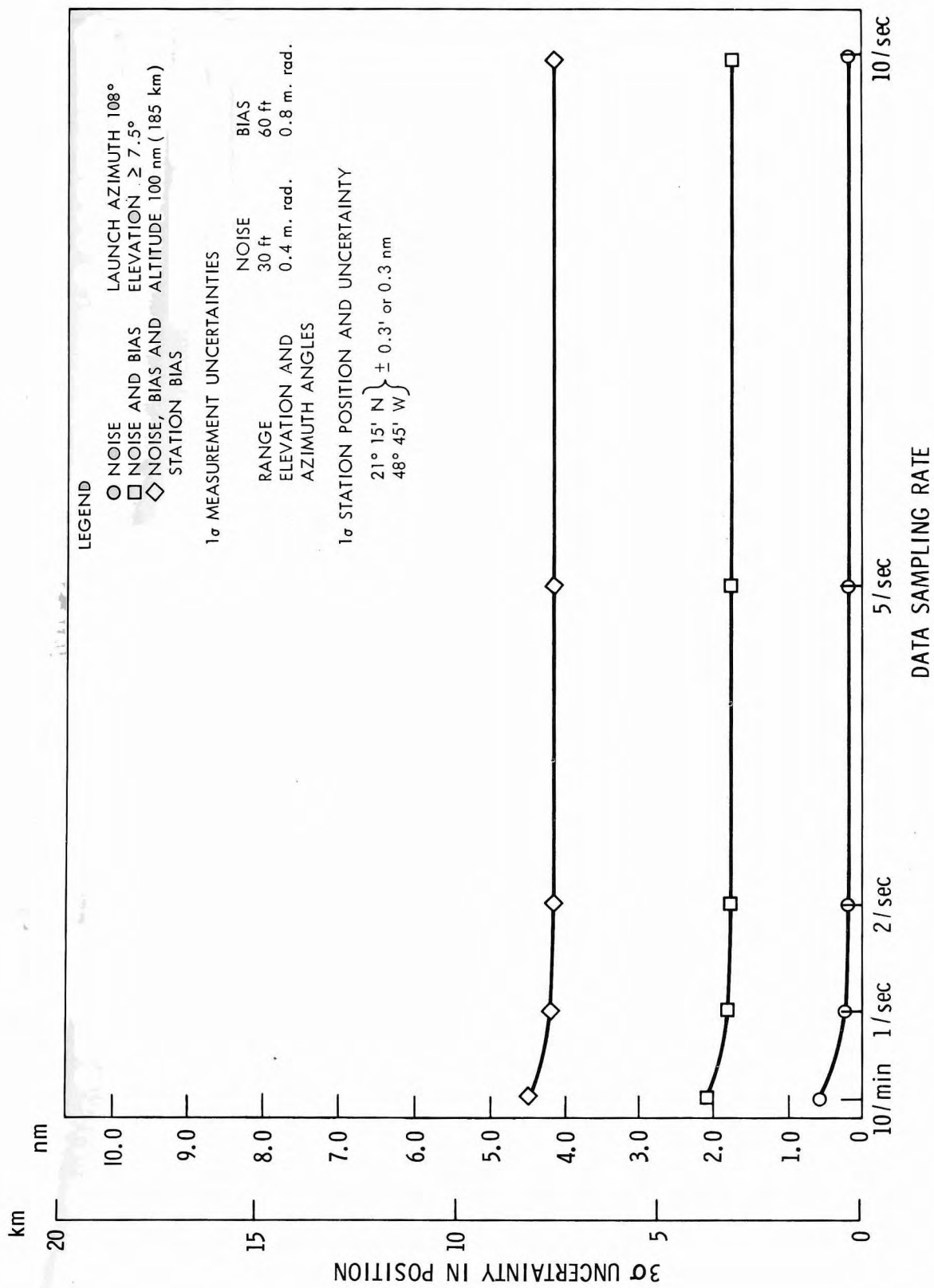


Figure 3.5a—Position uncertainty, 20 second tracking interval.

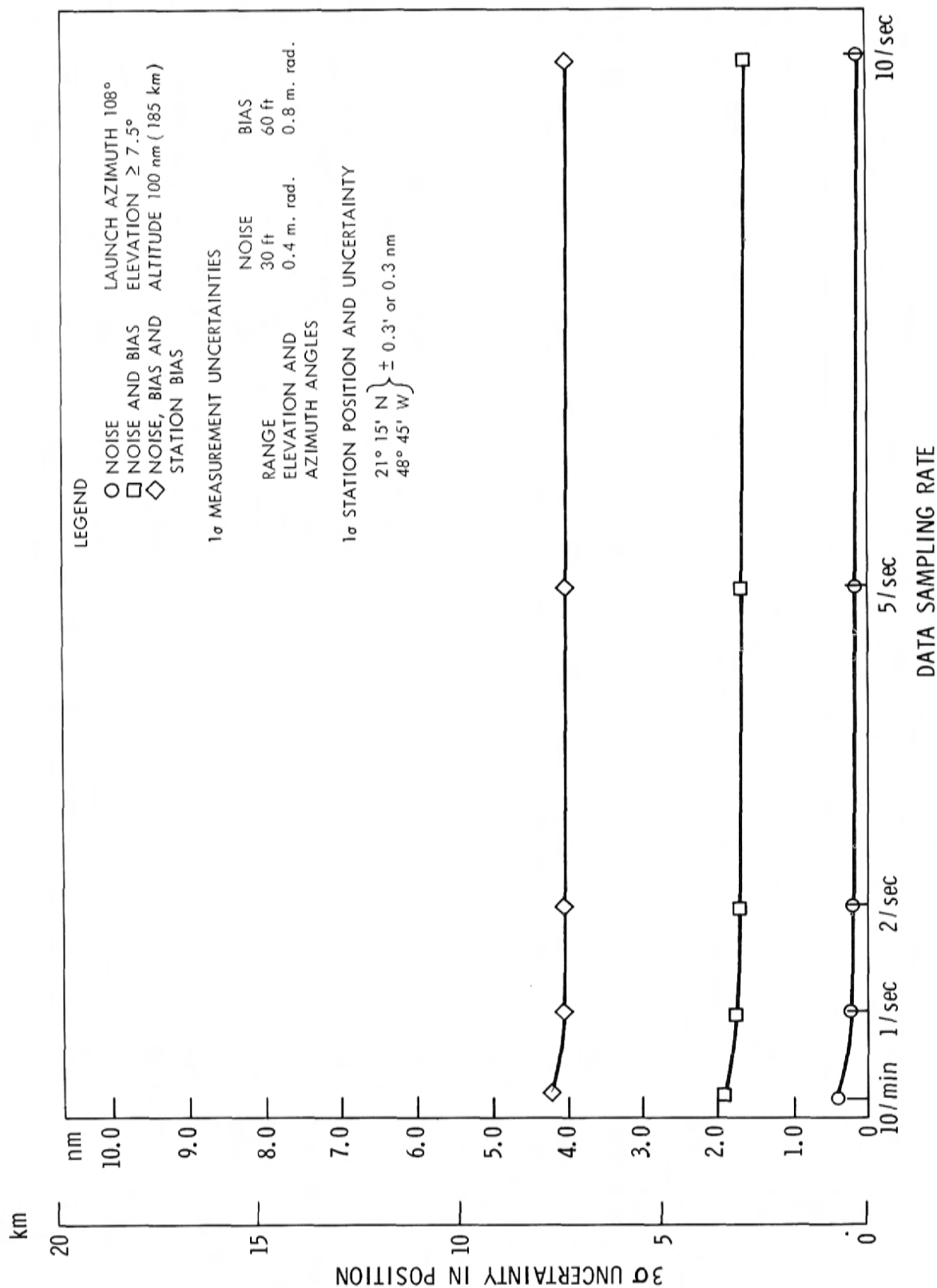


Figure 3.5b—Position uncertainty, 40 second tracking interval.

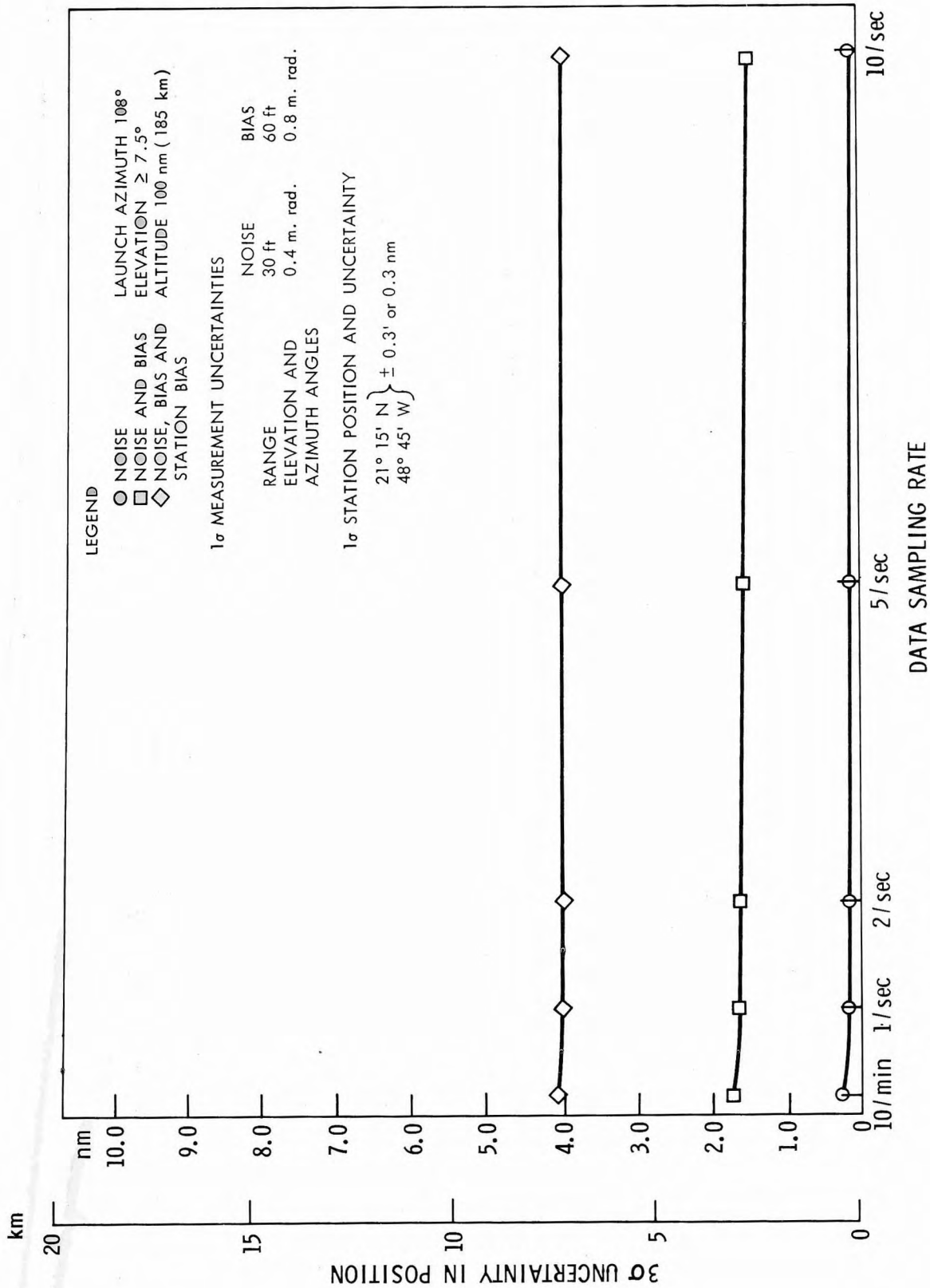


Figure 3.5c—Position uncertainty, 60 second tracking interval.

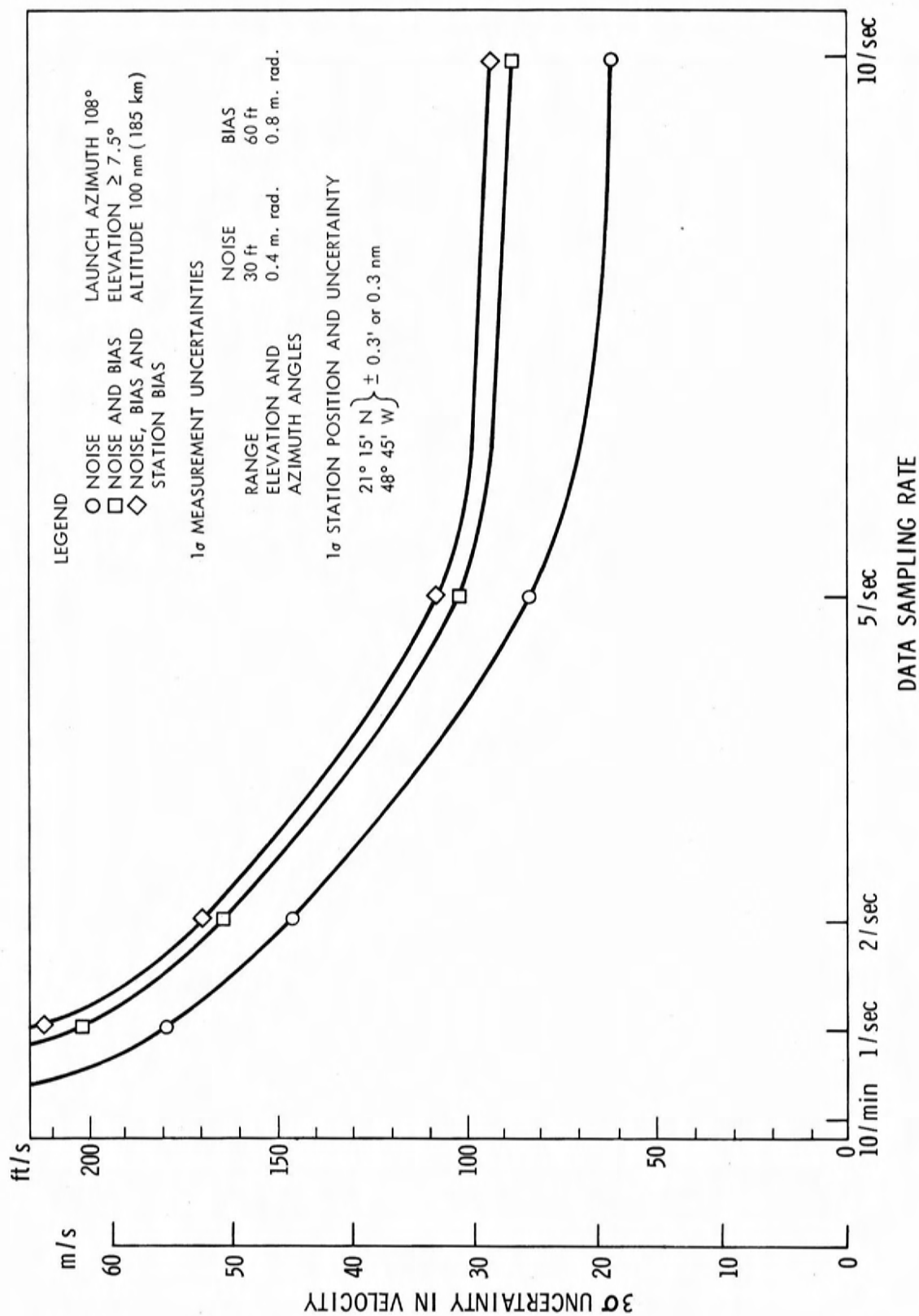


Figure 3.6a— Velocity uncertainty, 20 second tracking interval.



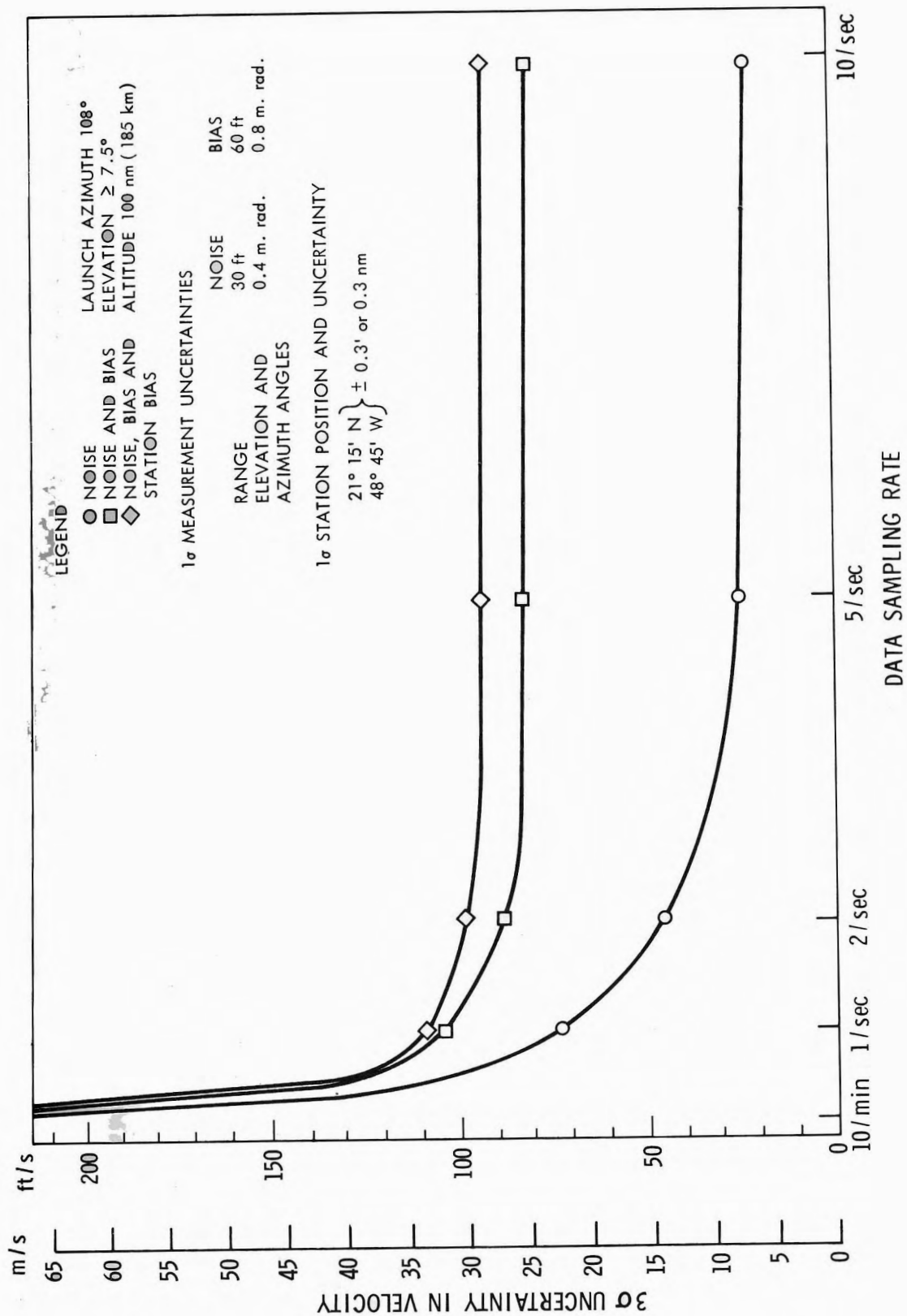


Figure 3.6b—Velocity uncertainty, 40 second tracking interval.

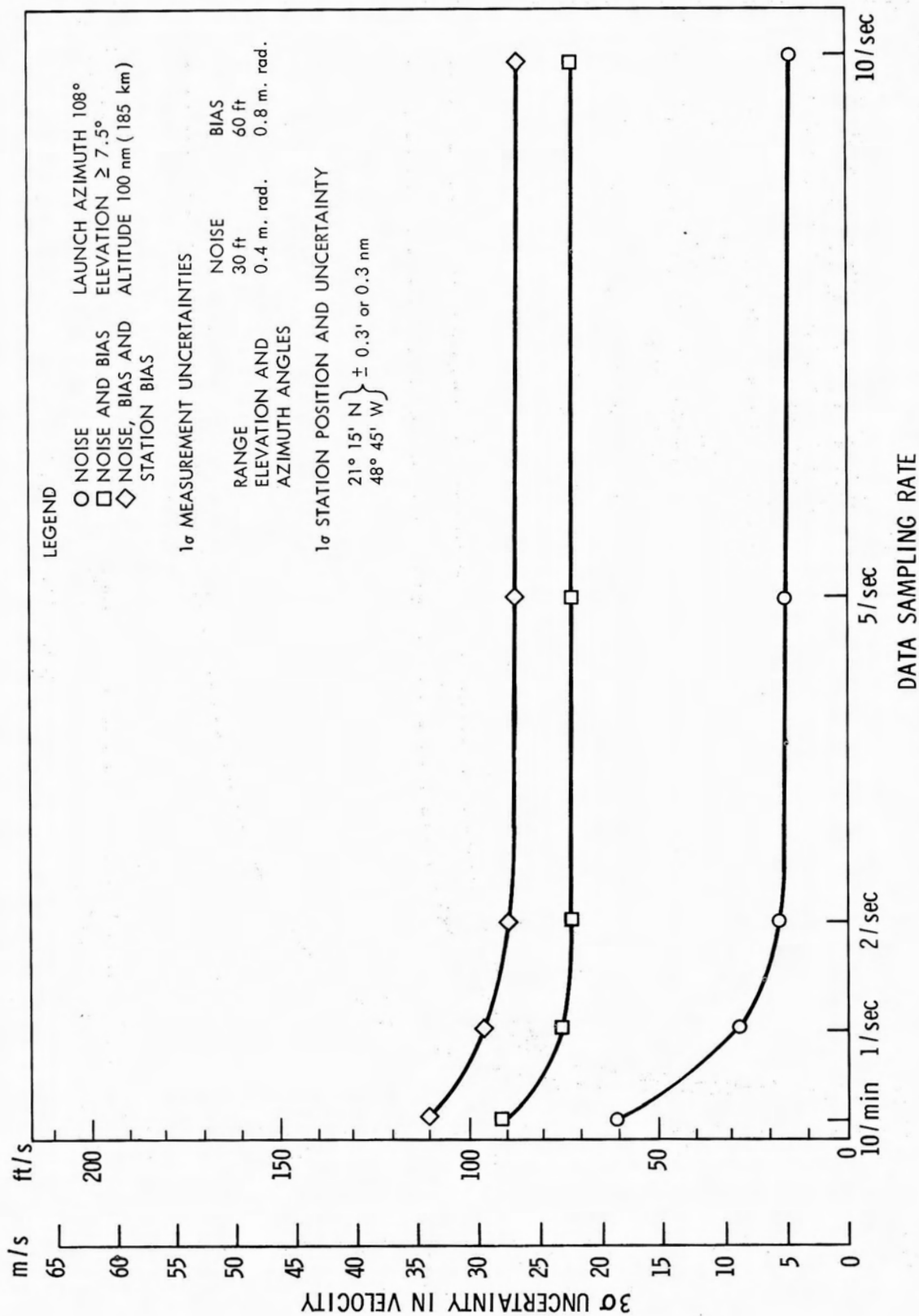


Figure 3.6c-Velocity uncertainty, 60 second tracking interval.

## 4.0 EARTH ORBIT PHASE

### 4.1 INTRODUCTION

The earth orbit phase as discussed below begins with the go decision to orbit and ends at the initiation of translunar injection.

During earth orbit, ground estimates of the orbit will be used to detect any deviations from the nominal or current flight plan. For unacceptable deviations, the S-IV-B guidance targeting may be updated. Onboard (S-IV-B and SC) knowledge of the orbit will be compared with the ground and the onboard values updated as necessary. Other earth orbit functions dependent on ground navigation are abort planning, site acquisition, and spacecraft platform alignment (Reference 1).

### 4.2 DESCRIPTION OF PHASE AND PROCEDURES

#### 4.2.1 Geometry

The nominal orbit is circular at 100 nm (185 km) altitude with a launch azimuth in the range from 72 to 108 degrees. The results of this report should not change for slightly elliptical orbits (85 perigee - 150 apogee).

The relationship of radar locations and the ground track for possible orbits is shown by Figure 4.1. The circles indicate the area in which a vehicle in a 100 nm (185 km) orbit has an elevation greater than five degrees to the radar. One revolution is covered on each plot.

It is noted that for azimuths between 85 and 95 degrees that Carnarvon, at about 45 minutes from insertion, is the first land based system to track. The Canary system tracks for azimuths less than 80 degrees and Ascension tracks when the azimuth is greater than 100 degrees. Tracking times are shown on Figure 4.2.

#### 4.2.2 Study Procedure

Tracking coverage plots (Figures 4.1) were used as a basis for the selection of orbits which would result in a representative sample of the variation in tracking coverage. Three orbits were chosen with launch azimuths of 72, 90, and 108 degrees.

Accuracies for 72 degree launch azimuth orbits are available from past postflight analysis (References 2, 3). These numbers would directly apply to Apollo C-band tracking if the venting uncertainty were very small and the same drag uncertainties were experienced.

A profile of orbit uncertainty was computed as a function of time from insertion for the three azimuths, including USBS tracking and the effect of venting uncertainties. Orbit accuracy was estimated with the use of statistical error analysis procedures based on the assumption that the error model biases were not accounted for in the orbit determination process. In actual orbit determination some of the systematic errors are accounted for through empirical weighting of the data. It would be optimistic to assume an error model and then to compute orbit accuracy based on the assumption that the biases of the assumed model were all properly accounted for, since this would be equivalent to assuming that all actual biases are properly accounted for in orbit determination. In general, assuming that the biases of the error model are not accounted for could be either pessimistic or optimistic. For example, if the error model included ten percent of the actual errors but only half of the effect of the actual errors were accounted for in the orbit determination process, then the results would be optimistic. If instead the error model included 90 percent of actual errors and half were accounted for in orbit determination, then assuming none were accounted for would be pessimistic. The method used in this study seems to provide fairly realistic results.

The overall procedure for checking the station error and other assumptions was to compute the expected orbit accuracy for the 72 degree launch azimuth orbit and to compare the results with actual Mercury and Gemini experience. The results for the three orbits were then computed with the influence of the venting uncertainty included.

#### 4.2.3 Data

The selection of data rates was based primarily on past Gemini and Mercury analysis and experience. When the results would be unaffected, less data was used in the study than would be processed during a mission, primarily to make the study easier and less costly. Uncertainties for the orbit based on data

from the first station and then from the first two stations were computed, after which the best set of three radars over the last one and a half revolutions was used to compute the uncertainties.

C-band data were used during earth orbit at the rate of one set of range, azimuth, and elevation every six seconds. Very little is gained by processing data at higher rates. USBS Doppler and angle data were used at six second intervals along with one range value per pass. Error analysis results seem to show that using frequent range values along with the Doppler and angles does not improve the orbit accuracy (Reference 4). The use of USBS Doppler and range for orbit determination should be studied further. When two tracking systems were available at a station, only one was used. Present results indicate that little is to be gained by using data from more than one radar at a station. Also, the predicted orbit accuracy for the USBS appears to be about the same as the realized accuracy for existing C-band radars (Reference 4, 5).

Onboard landmark angle sightings will likely be made for onboard check out purposes, but no onboard angle observations will be used in the ground orbit determination.

#### 4.2.4 Error Model

The noise and bias used on the observables along with values for the station position uncertainty are listed in Table 4.1 and were taken from Reference 6. The noise was adjusted to account for the smoothing effect obtained by accumulating Doppler count over six second intervals.

The observation bias values of Table 5-1, Reference 6, were used. For operational convenience, it was assumed that the bias values represent the composite effect of a number of sources including refraction, local vertical, and instrumentation, even though each source results in a differently behaved systematic error in the observable. This procedure has enough flexibility for generating useful earth orbit uncertainties. Very few, if any, error analysis programs are capable of properly handling the various sources of error individually. In general, the orbit errors experienced for actual flights over various tracking situations are in reasonable agreement with orbit uncertainties based on the above error model.

Prediction Model: The influence of the uncertainty in the earth's gravitational parameter,  $\mu$ , though small, was included for computing ground navigation uncertainty. The uncertainty due to drag for a 100 nm orbit is negligible. Uncertainties in venting thrust of 1.0 and 10.0 pounds were considered. During

Table 4-2  
STATION ERROR MODEL  $1\sigma$

SITE	System	RANGE		ANGLES		DOPPLER*		POSITION		
		Noise (ft)	Bias (ft)	Noise (m rad)	Bias (m rad)	Noise (ft/s)	Bias (ft/s)	Latitude (sec of arc)	Longitude (sec of arc)	Height (ft)
GTI	TPQ 18	30	60	.2	.4			1.	1.2	137
ANT	FPQ 6	20	40	.15	.3			1.	1.2	137
BDA	FPS 16	30	60	.2	.4			1.2	1.4	141
CYI	USB	60	120	.8	1.6	.04	.07	4.6	5.1	104
ASC	FPS 16	30	60	.2	.4			3.4	3.5	104
PRE	MPS 25	60	120	.2	.4			1.4	1.5	141
CRO	FPQ 6	20	40	.15	.3			1.9	2.2	216
GUA	USB	60	120	.8	1.6	.04	.07	6.4	6.6	104
HAW	FPS 16	30	60	.2	.4			1.4	1.6	141
WHS	FPS 16	30	60	.2	.4			1.0	1.2	131

\* Six second sampling



past Gemini and Mercury missions, the error in predicted position and velocity over several revolutions was due primarily to the error in the initial position and velocity. The contribution of earth gravitational and atmospheric drag uncertainties appeared small in comparison. In contrast, for Apollo earth parking orbits, a large S-IV-B venting uncertainty would have a significant influence on prediction accuracy. The present  $1\sigma$  value for the uncertainty is 0.65 pounds, which is ten percent of the total vent force. Therefore, a one pound uncertainty is about the correct size and ten pound uncertainty is pessimistic.

The S-IV-B computer uses its estimate of position and velocity at insertion and equations of motion to compute position and velocity during the earth orbit phase. The error in onboard navigation would be due to the error in the initial conditions and the error in the prediction equations. The largest part of the error in onboard knowledge of the orbit will likely be due to the initial conditions at the end of launch. Present estimates of these errors were used to compute onboard navigation uncertainties. The onboard system is not able to measure and account for deviations from nominal venting acceleration so that it suffers from the same venting uncertainty as the ground. It was assumed that the onboard system, when updated, would receive the components of the most recently computed position and velocity vectors. The onboard system then predicts forward to the time of injection.

### 4.3 RESULTS

The results based on a realistic venting uncertainty of one pound are discussed first and given for 72, 90, and 108 degree launch azimuths. The results for a pessimistic venting uncertainty of ten pounds for the 72 degree launch azimuth are then discussed. This is followed by a comparison of actual Mercury accuracy with statistical error analysis results and additional comments on the influence of a one pound venting error.

Figures 4.3 through 4.8 present  $3\sigma$  orbit uncertainties for the 72, 90, and 108 degree launch azimuth orbits. That is, the accuracy during the flight is expected to be well within the values presented in these figures. The influence of a one pound venting uncertainty was included. The vertical lines show the instantaneous improvement in the orbit as it is updated over each station. The lines which run across the page show how the initial errors propagate with time. For example, for the orbit computed 45 minutes after insertion, the  $3\sigma$  uncertainty in predicted position at 160 minutes from insertion would be 6 nm (11 km) (Figure 4.3). However, for the orbit computed at 140 minutes from insertion, the position uncertainty at 160 minutes would be 1.3 nm (2.4 km). These numbers are three times the root sum square of the  $1\sigma$  component errors in position and velocity.

The cross correlation between position and velocity should be accounted for when using the numbers in other work.

If the orbit is updated every 45 minutes, then the largest  $3\sigma$  orbit uncertainty any time after 45 minutes from insertion is 3.5 nm (6.5 km). This is true for all launch azimuths. The corresponding velocity values are 21 ft/s (6.4 m/s).

The results (Figure 4.4) indicate that for launch azimuths less than 80 degrees the orbit based on the Canary data can be used for an early comparison with onboard results. Present results indicate that the orbit based on Canary data is not useful for updating the onboard computers. For the 108 degree launch azimuth, the earliest time for a useful orbit is 15 minutes (Ascension). After 15 minutes, for the 108 degree azimuth, the orbit should always be known within  $3\sigma$  bounds of 4 km or 2 nm and 5 m/s or 15 ft/s (Figure 4.7).

Figures 4.9 and 4.10 show 72 degree launch azimuth orbit uncertainties, but with a ten pound venting uncertainty. For the one pound vent uncertainty, updating the orbit every 45 minutes meant that after 45 minutes from insertion, for all launch azimuths, the  $3\sigma$  uncertainty was less than 3.5 nm (6.5 km) and 21 ft/s (6.4 m/s). The corresponding values for a ten pound vent uncertainty are 30 nm (55 km) and 180 ft/s (55 m/s).

The actual errors for orbits computed during a typical Mercury flight (MA-6) are presented in Figures 4.11 and 4.12. For comparison, one sigma results from the statistical error analysis are also presented for a similar orbit and similar tracking. The straight lines merely connect local uncertainty or error points and do not represent propagated errors. The actual velocity errors are in good agreement with the estimated errors. The MA-6 position error of 0.23 nm (0.42 km) around 140 minutes is about three times the  $1\sigma$  estimate, but it should be noted that the tracking capabilities have improved since the MA-6 era. More recent results (Reference 7) indicate that for the first Gemini flight (GT-1) the error in this region was 0.08 nm (0.15 km).

Figures 4.13 and 4.14 show how the error in predicted position and velocity due to errors only in  $\mu$  or venting increase with time (perfect initial conditions). In actual practice the error due to  $\mu$  does not appear so dominant, possibly because the orbit determination program may adjust the semi-major axis slightly to account for the error in the orbit period due to  $\mu$ , or because the actual error in  $\mu$  may be less than the  $1\sigma$  value quoted. The results show that the one pound vent uncertainty becomes important after about one hour.

#### 4.4 CONCLUSIONS

For the expected tracking and venting uncertainties, the results indicate that the accuracy of the ground navigation is sufficient to perform the functions described in the introduction, i.e., updating of the onboard computer and flight plan verification.

Because of the expected rate of decline in the accuracy of the onboard navigation (Reference 8) and the rate of improvement of that of the ground, it is concluded that a ground update should be made 45 minutes from insertion if navigation accuracy is the sole consideration. Additional time before updating might be desired to obtain confidence in the orbit determination results. In this case, updating might be delayed until two land stations have tracked, for example, until over Hawaii, 70 minutes from insertion for the 90 degree azimuth orbit.

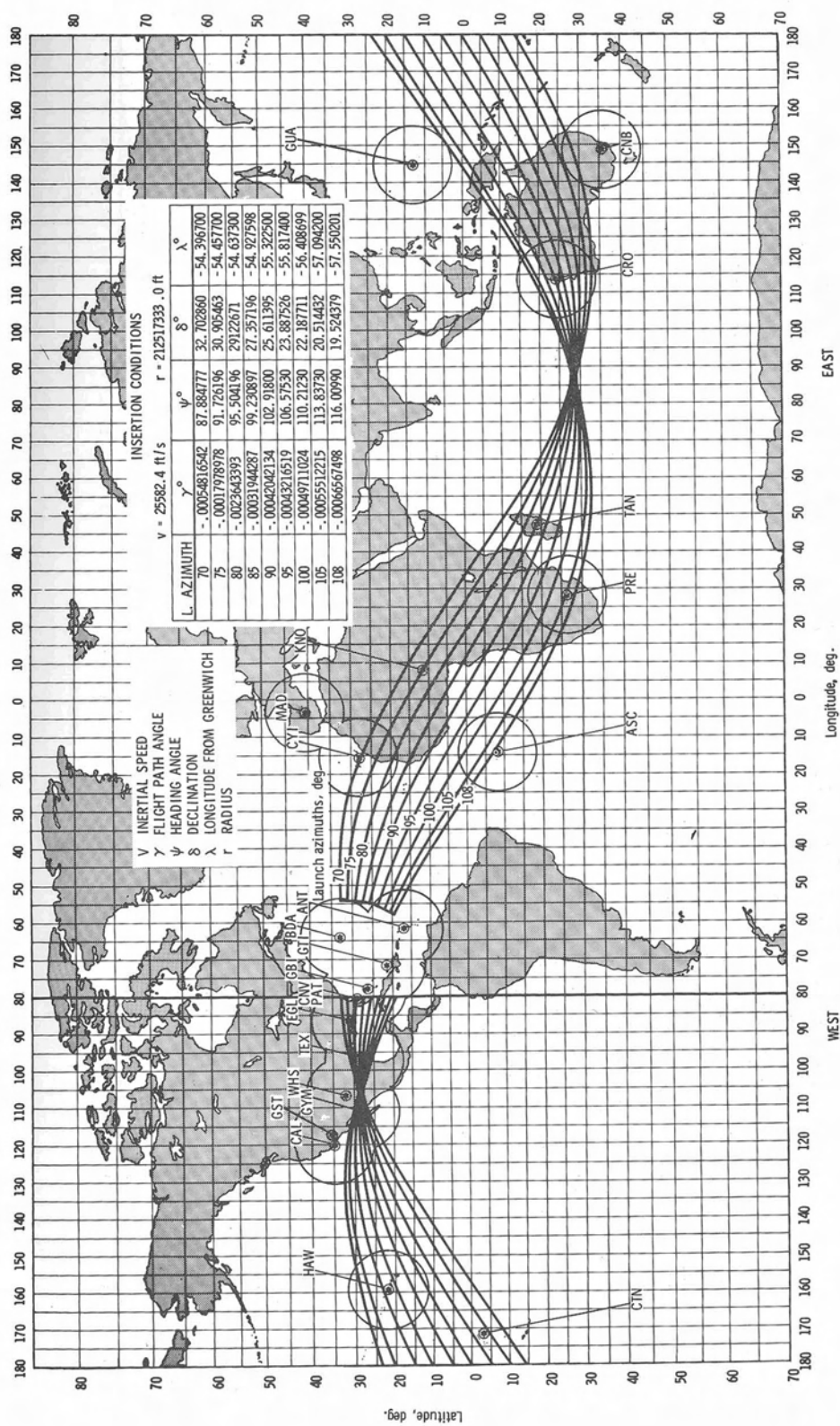
Furthermore, because of the time required to process the tracking data, compute the update, etc., it may not be desirable to track and update with the same station. The procedure in this case would be to track with two stations and update from the following station. For launch azimuths less than 100 degrees the first update would then occur at 80 minutes (near the end of the first revolution) and for launch azimuths greater than 100 degrees it would occur after 45 minutes over Carnarvon, assuming that Pretoria is available.

Mission plan verification can best be done with orbits computed during the second half of the first revolution. Rough verification will be possible from the ship results combined with either Canary or Ascension within 15 minutes from insertion, except for launch azimuths from 80 to 98 degrees where only ship tracking is available during the first half of the revolution.

The navigation update area is under consideration by many groups concerned with Apollo. The above discussion is meant only to serve as an aid to this planning. Further, the picture may change depending on the achieved accuracy for onboard and ground navigation. Future postflight analysis of early Apollo missions will provide valuable results needed for the evaluation of navigation updating procedures. The problem of updating guidance targeting may be considered in future revisions. Further, the effect on the midcourse fuel cost of performing injection with expected navigation error is an important part of the problem. Such work should be included in future revisions. For example, if the difference in required midcourse fuel is small for onboard versus ground navigation, the difference between the two systems is less interesting.

#### 4.5 REFERENCES

1. MSC Internal Note No. 64-FM-61, "Real Time Computer Requirements for Apollo Lunar Landing Missions," Mission Planning and Analysis Division (MPAD), Manned Spacecraft Center, Houston, Texas, 1964.
2. Schiesser, E., "Accuracy of the Mercury Tracking and Computing Complex," Manned Spacecraft Center (MSC) Memorandum, Houston, Texas, May 16, 1963.
3. Jackson, J. C., "Manned Spaceflight Network Performance Analysis for MA-9," Report No. X-551-63-108, Goddard Space Flight Center, Greenbelt, Maryland, June 6, 1963.
4. Pixley, P., "Comparison of USBS and C-Band Earth Orbit Tracking," Manned Spacecraft Center (MSC) Memorandum for Distribution, May 4, 1965.
5. Marlow, A., "Error Analysis for Apollo Earth Parking Orbits Using Range-Rate and Angle Measurements," Report No. X-513-65-42, Goddard Space Flight Center, Greenbelt, Maryland, January 1965.
6. MSC-GSFC, ANWG Report No. 65-AN-1.0, "Apollo Missions and Navigation Systems Characteristics," Feb. 5, 1965.
7. Corbett, B., "Accuracy of Earth Orbit Determination," Manned Spacecraft Center (MSC) Houston, Texas, Memorandum to Chief, MPAD Feb. 3, 1965.
8. Bissett-Berman Corporation, "Apollo Note Number C-6," October 23, 1964.
9. Cooley, J., "The Influence of Venting on the Apollo Earth Parking Orbit," Report No. X-513-64-359, Goddard Space Flight Center, Greenbelt, Maryland, November 24, 1964.





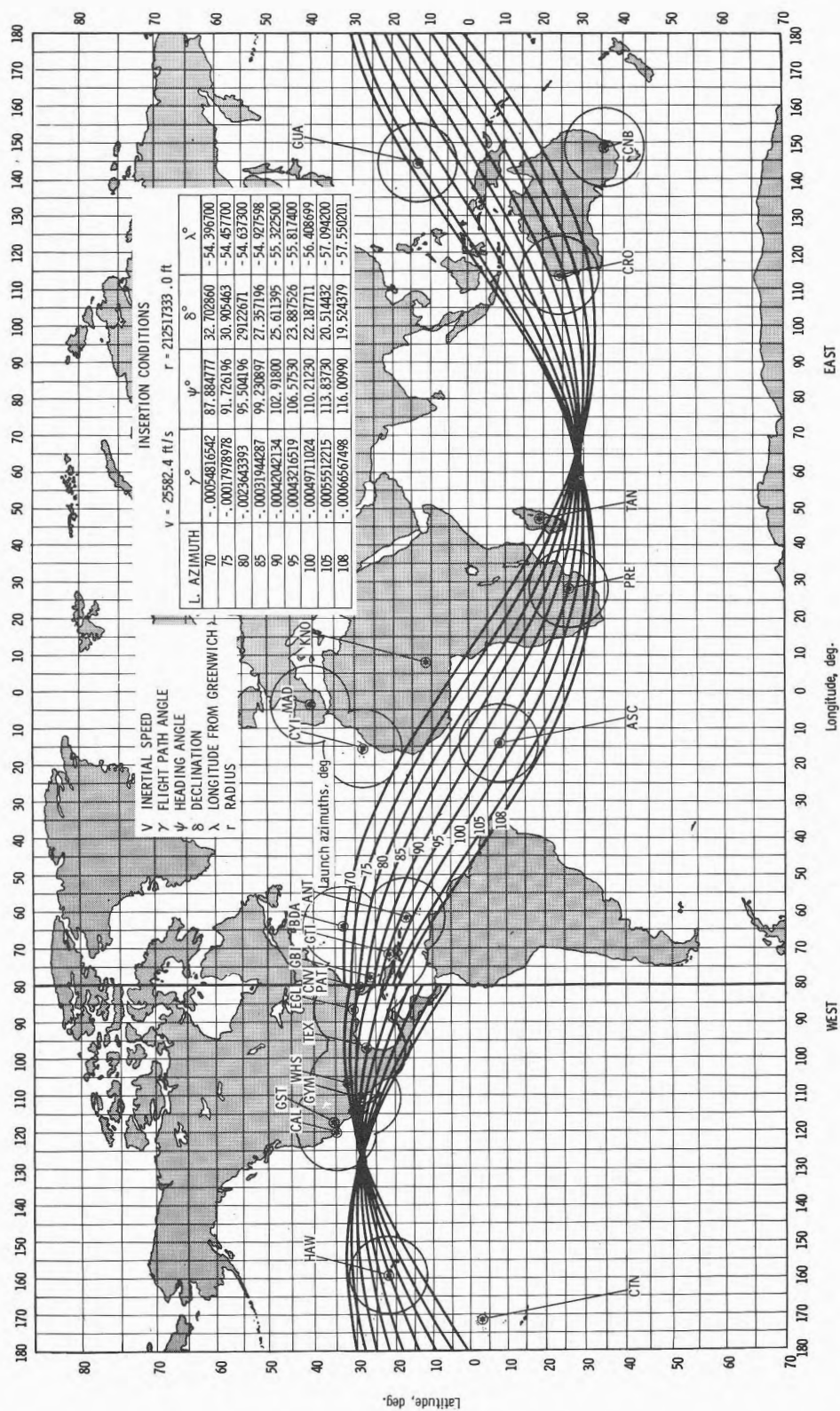


Figure 4.1b—Second revolution



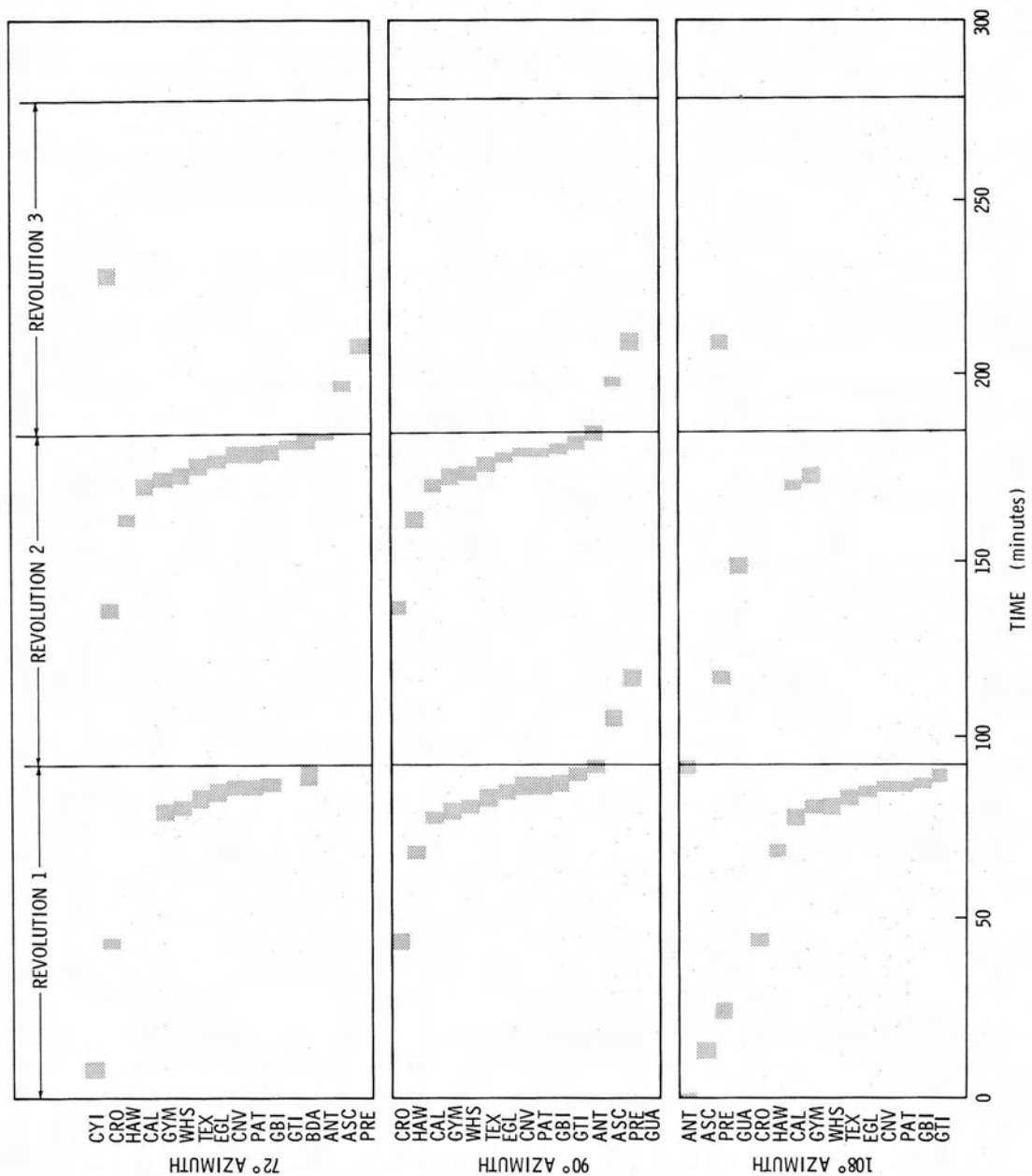


Figure 4.2—Earth parking orbit coverage



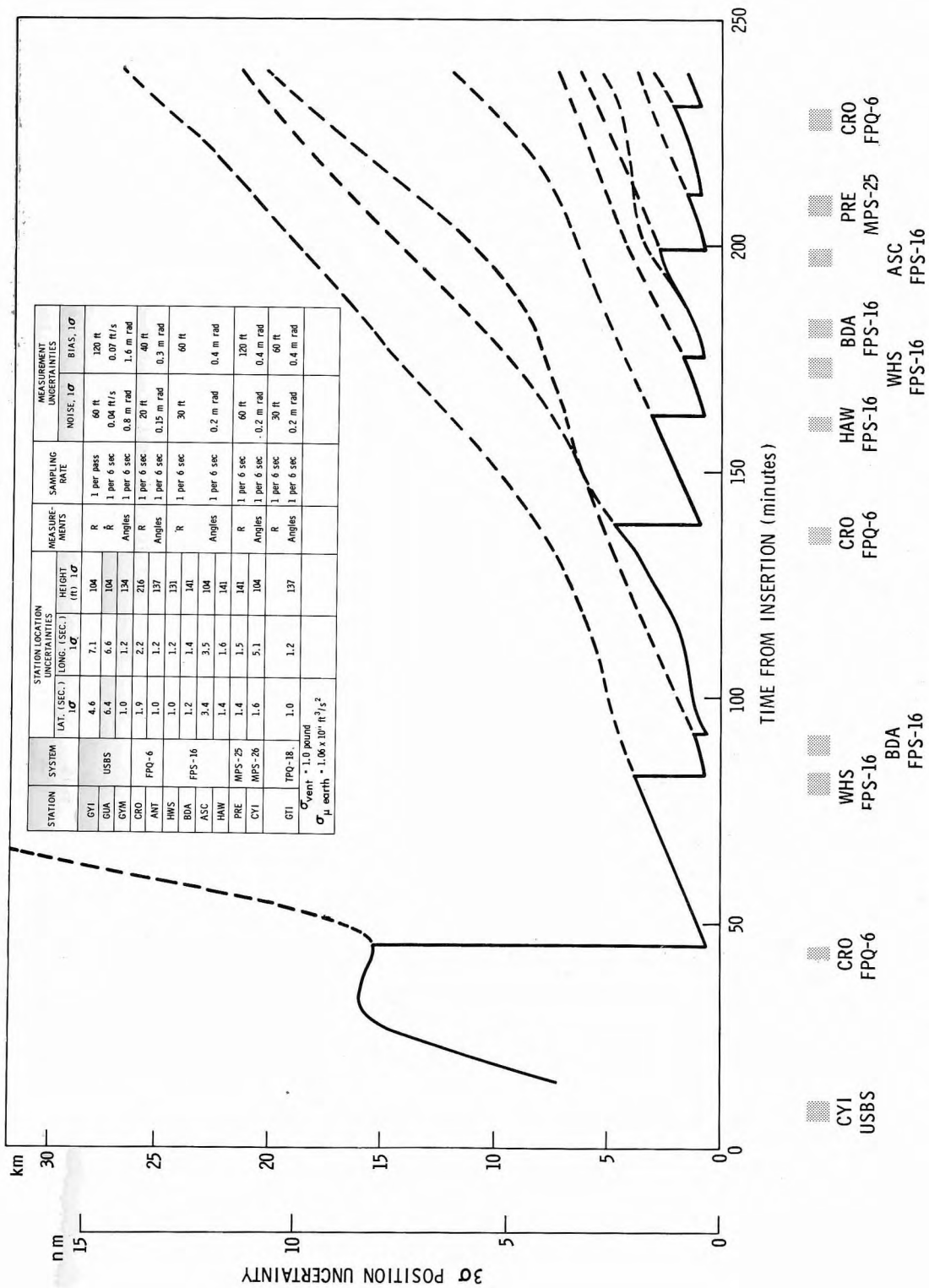


Figure 4.3-3  $3\sigma$  vehicle position uncertainty for a  $72^\circ$  launch azimuth earth parking orbit. One pound venting uncertainty.

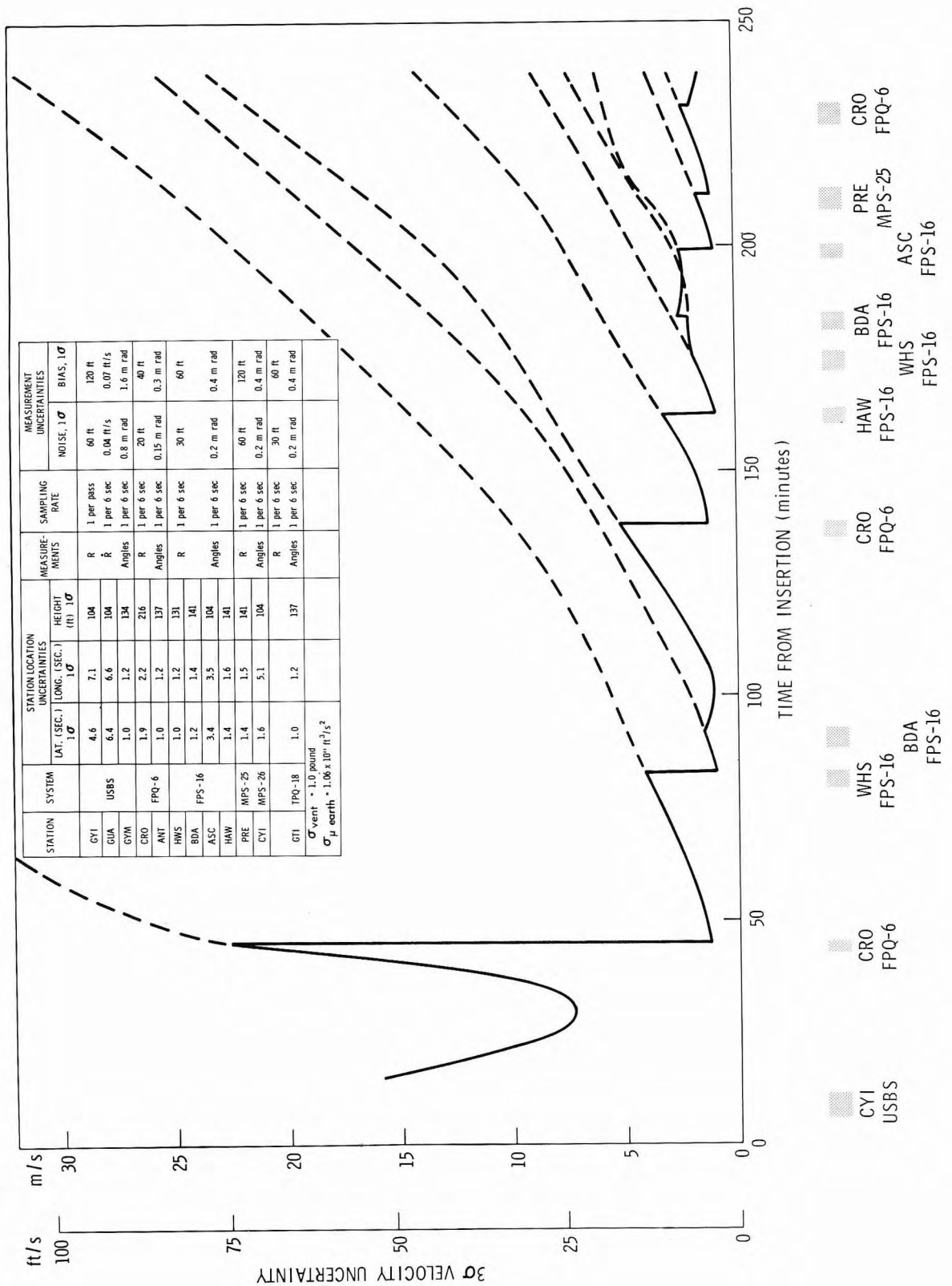


Figure 4.4-3  $\sigma$  vehicle velocity uncertainty for a 72° launch azimuth earth parking orbit. One pound venting uncertainty.

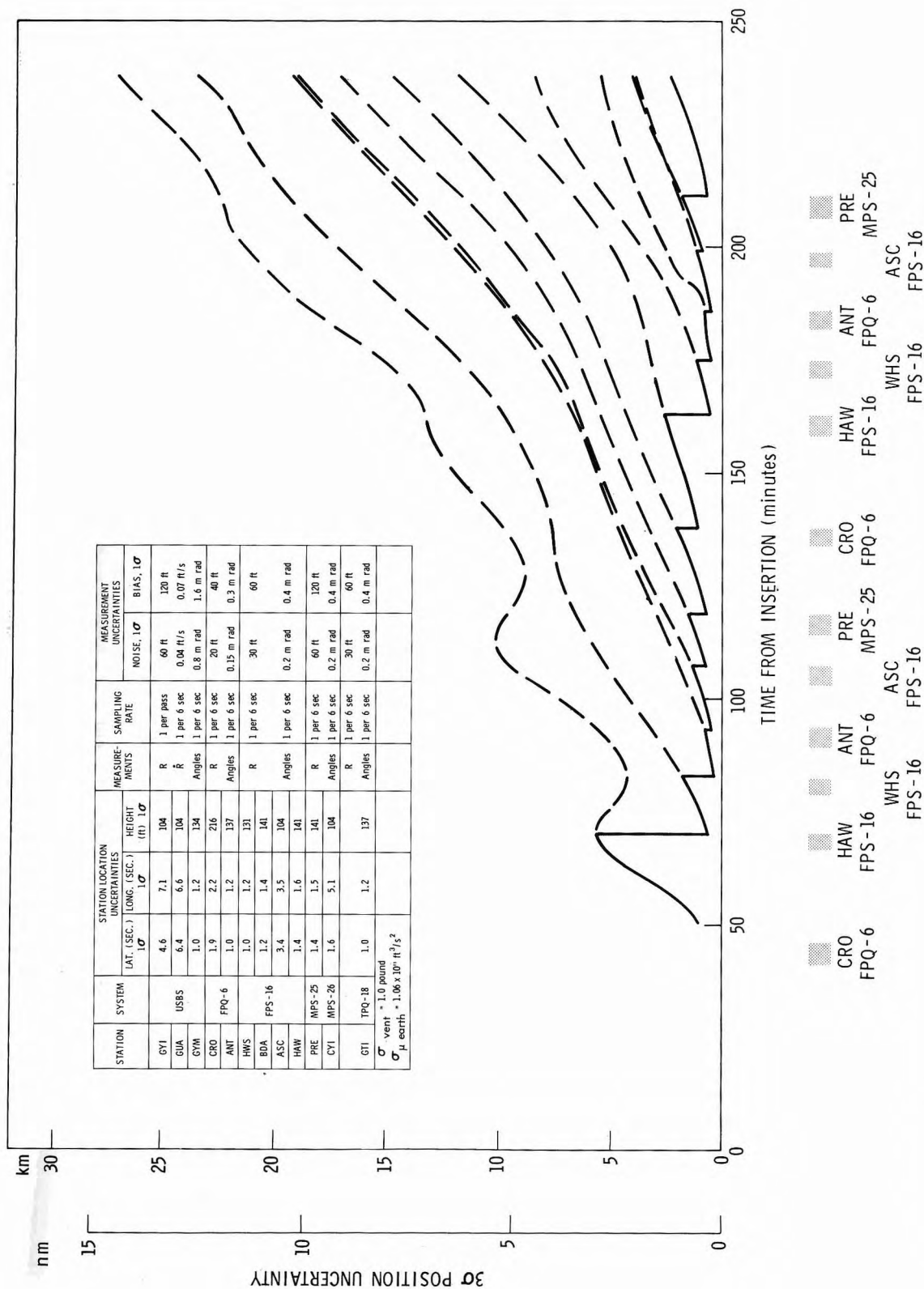


Figure 4.5-3  $3\sigma$  position uncertainty for a  $90^\circ$  launch azimuth earth parking orbit. One pound venting uncertainty.

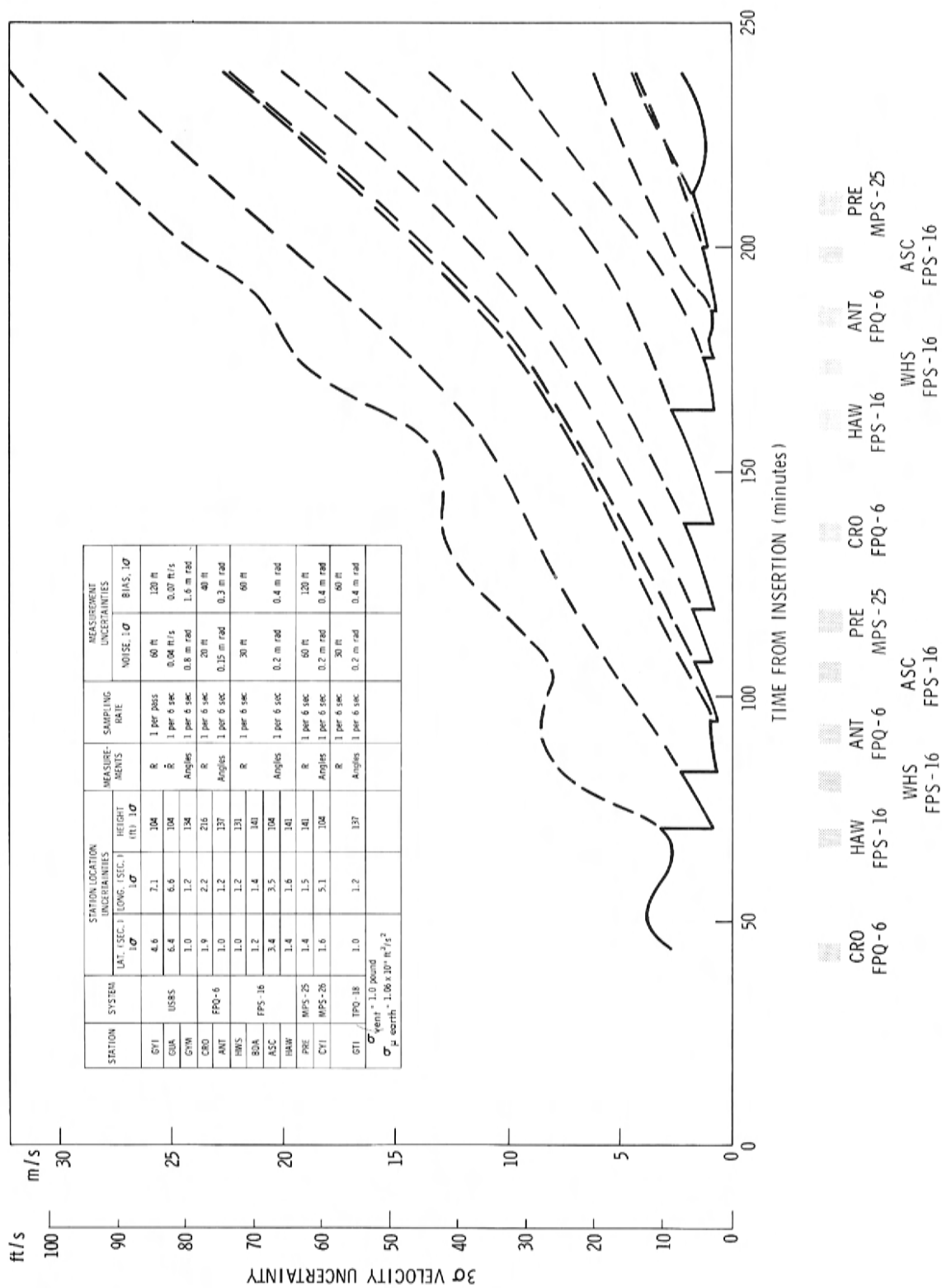


Figure 4.6-3  $\sigma$  velocity uncertainty for a  $90^\circ$  launch azimuth earth parking orbit. One pound venting uncertainty.





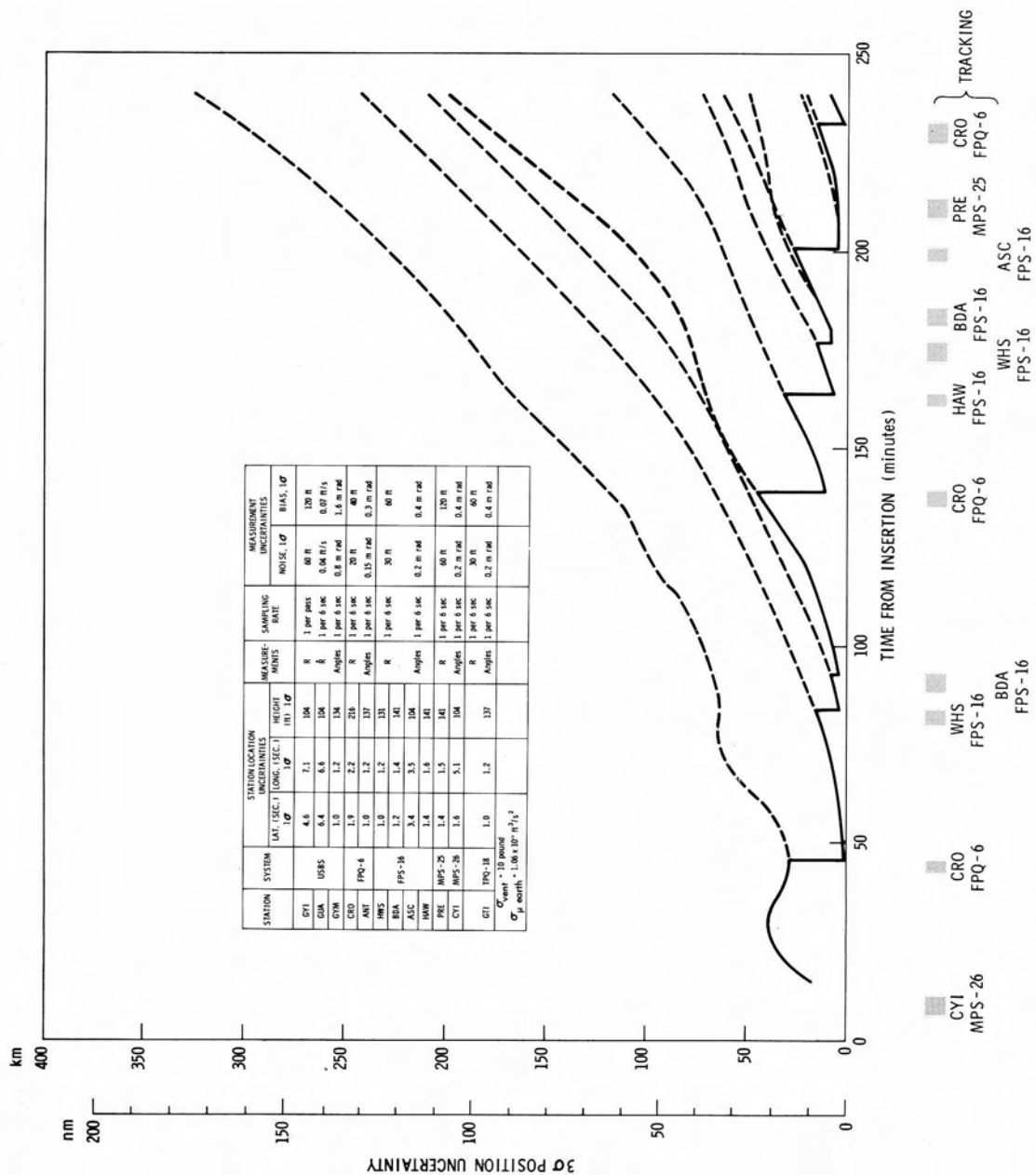


Figure 4.9—Position uncertainty at 72° launch azimuth 10 pound venting uncertainty.



Figure 4.10—Velocity uncertainty at  $72^\circ$  launch azimuth 10 pound venting uncertainty.



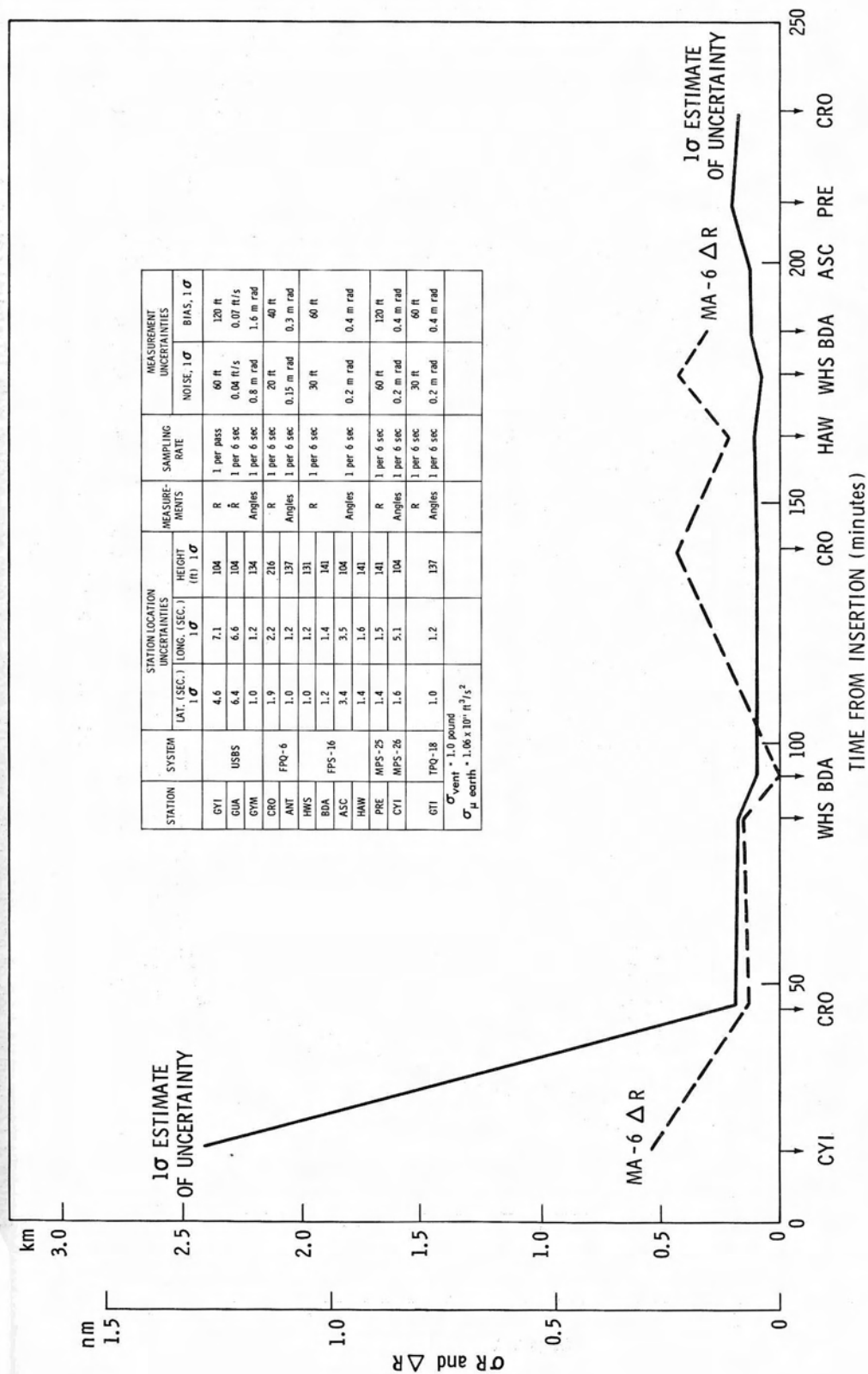


Figure 4.11—Comparison of actual Mercury orbit position errors  $\Delta R$  over each station with  $1\sigma$  statistical error analysis results ( $72^\circ$  launch azimuth). One pound venting uncertainty.

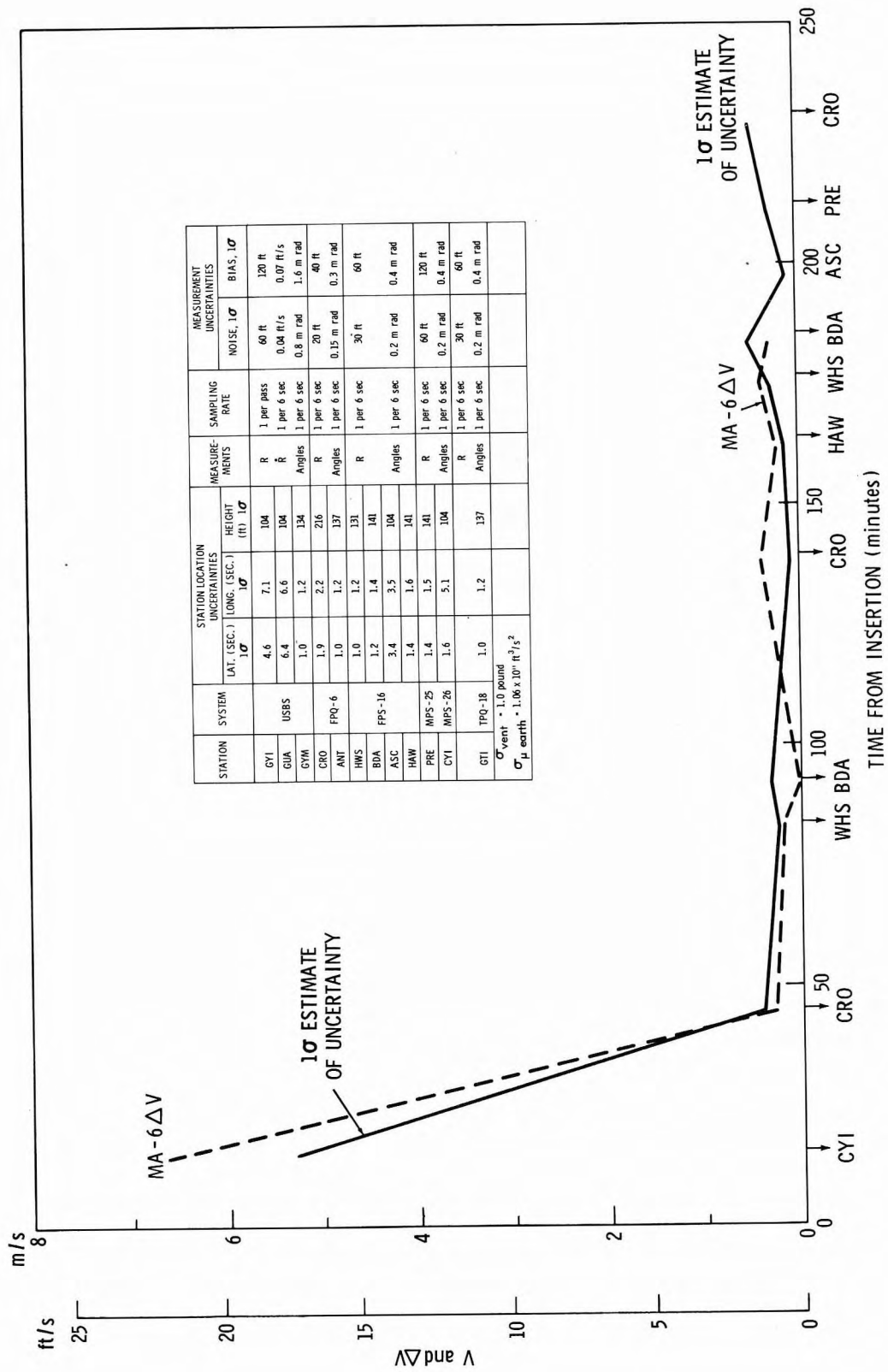


Figure 4.12—Comparison of actual Mercury velocity errors  $\Delta V$  over each station with  $1\sigma$  statistical error analysis results ( $72^\circ$  launch azimuth). One pound venting uncertainty.

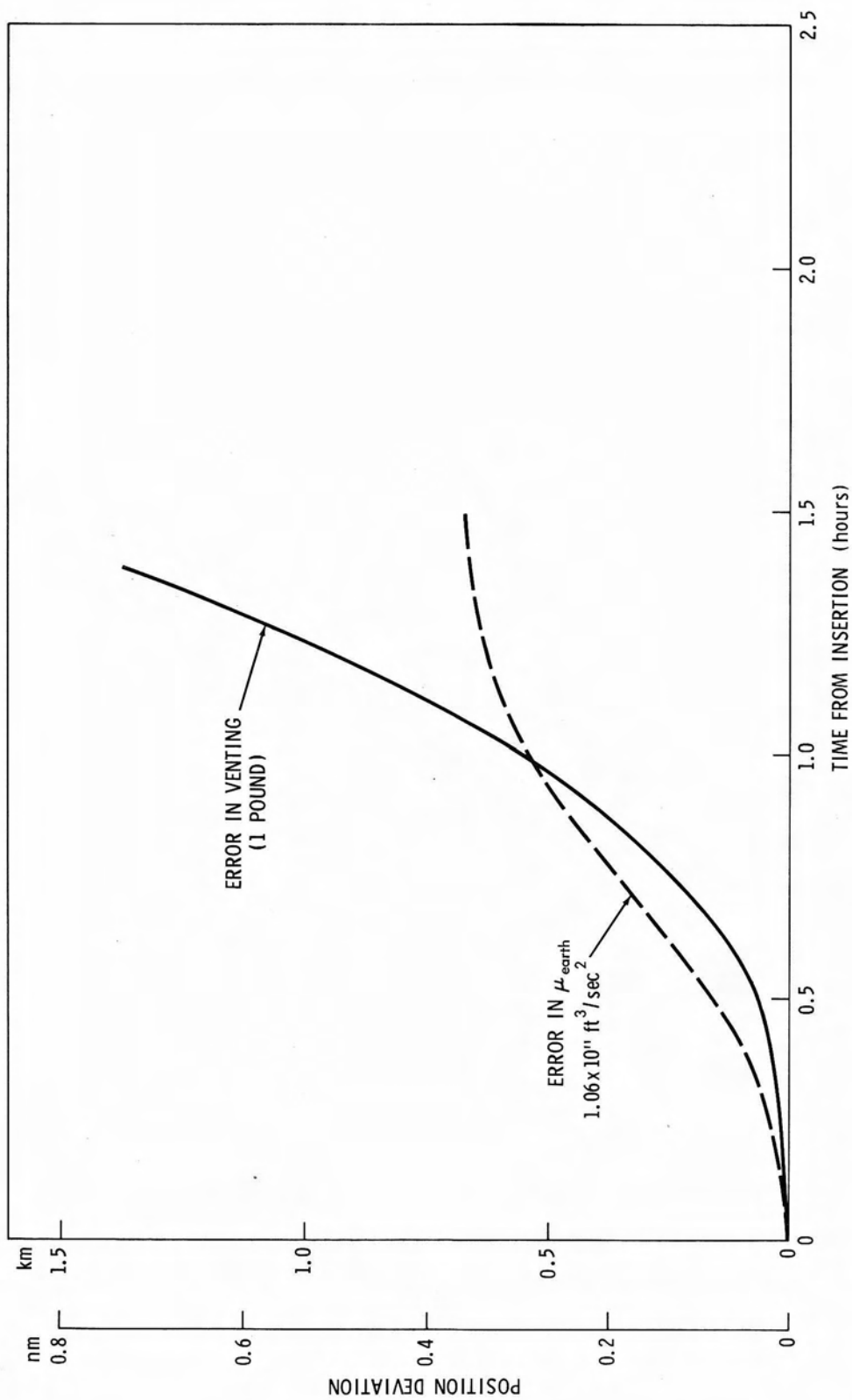


Figure 4.13—Deviation in vehicle position (root sum square of components) due to deviations in  $\mu$  and venting

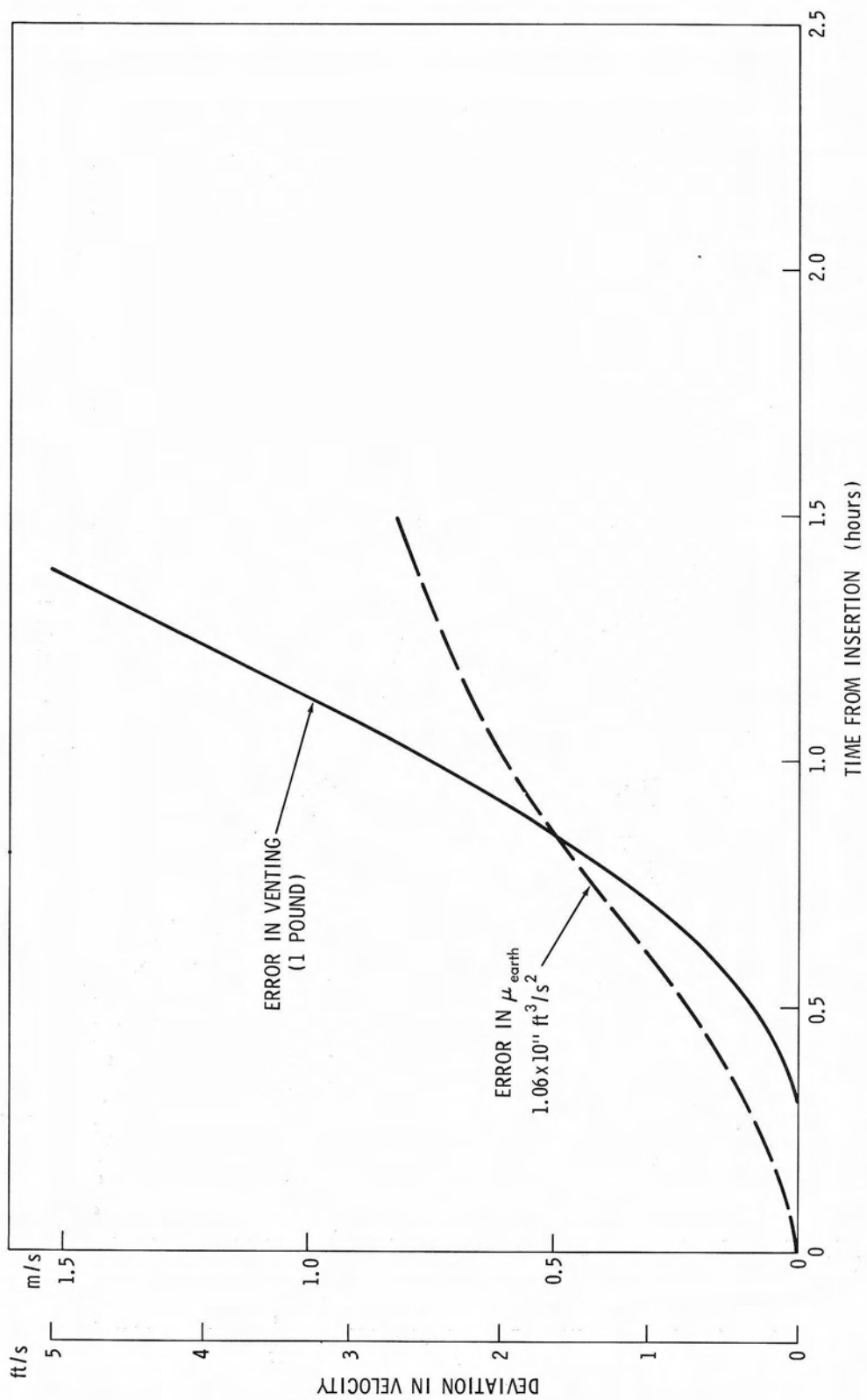


Figure 4.14—Deviation in vehicle velocity (root sum square of components) due to deviation in  $\mu$  and venting

## 5.0 TRANSLUNAR PHASE

### 5.1 INTRODUCTION

The translunar phase of the Apollo lunar mission is defined as beginning at the end of the injection burn and ending at the beginning of deboost into the lunar parking orbit. During this phase the MSFN (Manned Spaceflight Network) will be the prime source of navigation data. The purpose of the study presented in this chapter is to evaluate the capability of determining the translunar orbit using data from the MSFN.

Several operational modes (e.g., single and multiple station tracking) have been simulated in this study and some conclusions concerning the operational use of the MSFN have been reached.

The study was conducted with certain assumptions concerning the accuracy of the MSFN and with a linear error analysis program based on a weighted least squares filtering technique. (Reference 1) This error analysis program was used to evaluate the capability of determining an orbit with data of the assumed characteristics and with a filter which ignored the assumed biases. Further discussion of the assumed data characteristics is contained in the paragraph below. It should be noted that the Apollo real time orbit determination program will account for some bias effects by adjusting the measurement data weighting scheme or by solving for the known biases explicitly or, more probably, by using some combination of these two techniques. Consequently, the results reported below are considered to be conservative and are subject to change as further studies are conducted.

### 5.2 ASSUMPTIONS

The assumptions on which this study was based are consistent with Reference 2. For convenience, however, the uncertainties in station locations, gravitational constants of the earth and moon, and the noise and biases of the MSFN data are shown on each graph as they are applicable. Other assumptions which should be noted are:

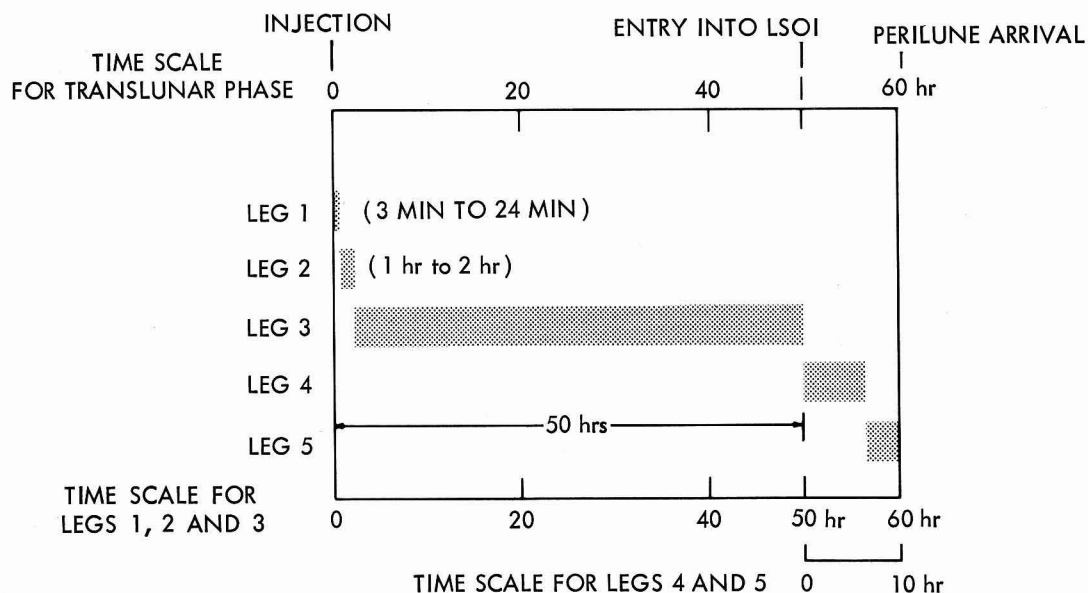
1. The translunar trajectory is of the free-return type with a perigee of 80 - 108 nm and a perilune of  $80 \pm 5$  nm. Figure 5.1 is an illustration of this trajectory showing the planned maneuvers.
2. The results for tracking ship capabilities assume two co-located ships at 20 degrees north, 130 degrees west with USB systems; the difference between them being in the level of uncertainty with which their locations are known and the noise and biases of their data.

### 5.3 RESULTS

To facilitate the studying and reporting of the MSFN performance, the translunar phase has been divided into five legs. These legs begin and end with one of the planned maneuvers (e.g., injection, transposition and docking, mid-course correction, and lunar deboost), and are defined as follows:

- Leg 1 - From end of injection burn to initiation of transposition and docking.
- Leg 2 - From end of transposition and docking to initiation of first mid-course correction.
- Leg 3 - From end of first midcourse correction to initiation of second midcourse correction.
- Leg 4 - From end of second midcourse correction to initiation of third midcourse correction.
- Leg 5 - From end of third midcourse correction to initiation of deboost into lunar parking orbit.

Each of these legs is nominally associated with a time from injection as shown by the upper scale of the schematic below. The lower scale of this schematic defines the time scale which is used in preparing the graphs of the results of this study.



The uncertainties that are depicted in the graphs are computed at various times in the legs and an explanation of the annotation of these computations is given on the following page.

- $t = 0$  This statement on a graph indicates that the uncertainties are of the orbit parameters at the beginning of the leg.
- $t + 30 \text{ min.}$  This statement indicates that uncertainties are of the orbit parameters at 30 minutes after the time against which they are plotted. This illustrates the accuracy with which an update of the onboard system can be made after a period of tracking, data processing etc.
- Entry into LSOI This statement indicates that the uncertainties are computed at the LSOI (Lunar Sphere of Influence).
- Perilune Arrival This statement indicates that the uncertainties are computed at the nominal time of arrival at the perilune.

In all of the above cases the uncertainties are plotted on the same time scale as the radar coverage periods and, thus, one can determine how the MSFN navigation capability varies with tracking time and with tracking coverage.

#### 5.3.1 Leg 1 – Navigational Accuracies at Injection

The results of the analysis for this leg illustrate the MSFN performance in the determination of position and velocity at injection and show the effects of these uncertainties in predicting the vehicle's position and velocity at the nominal time of entry into the LSOI.

The following eight cases (operational modes) were considered in the analysis.

- Case 1: Two C-band radars tracking; the first from three to seven minutes and the second from seven to 24 minutes.
- Case 2: The same as Case 1 with two USB Systems replacing the C-band radars.
- Case 3: Three C-band radars tracking; the first from three to seven minutes, the second from seven to fourteen minutes and the third from fourteen to 24 minutes.
- Case 4: The same as Case 3 with USB Systems replacing the C-band radars.
- Case 5: Ship A (USBS) tracking from three to 24 minutes.

Case 6: Ship B (USBS) tracking from three to 24 minutes.

Case 7: One USB System tracks from 10 to 24 minutes.

Case 8: Ship B tracks from three to ten minutes and the USB System of Case 7 tracks from 10 to 24 minutes.

The uncertainties in position and velocity for Cases 1 through 8 are referenced to  $t = 0$  (Figures 5.2a, 5.2b, 5.3c, and 5.3d, respectively).

The uncertainties in position and velocity for Cases 1, 2, and 5 through 8 are propagated to the LSOI where entry into the LSOI is assumed to occur 50 hours after injection (Figures 5.2e and 5.2f).

### 5.3.2 Leg 2 – Navigational Accuracies for the First Midcourse Correction

The results of the analysis for this leg of the translunar phase illustrate the accuracy with which the position and velocity of the vehicle can be predicted 30 minutes in advance and at the LSOI.

The following seven cases (operational modes) were considered in the analysis for this leg.

Case 1: Texas tracking with no a priori knowledge at the beginning of track.

Case 2: Case 1 with a priori knowledge.

Case 3: Texas and Antigua tracking simultaneously with no a priori knowledge at the beginning of track.

Case 4: Case 3 with a priori knowledge.

Case 5: Madrid, Ascension and Canary tracking simultaneously with no a priori knowledge at the beginning of track assumed.

Case 6: Madrid, Texas, and Ascension tracking simultaneously without a priori knowledge.

Case 7: Madrid and Ascension tracking simultaneously without a priori knowledge.

The uncertainties in position and velocity are propagated to  $t + 30$  minutes for all seven cases (Figures 5.3a and 5.3b) and propagated to the LSOI for cases 1, 3, and 5 through 7 (Figures 5.3c and 5.3d).



### 5.3.3 Leg 3 – Navigational Accuracies at the Second Midcourse Correction

The results of the analysis for this leg illustrate the accuracy in predicting the vehicles' state vector thirty minutes in advance of MSFN tracking and at the LSOI.

Three cases were simulated in the analysis for this leg and are as follows:

Case 1: Texas, Canberra, and Madrid alternating after each radar has tracked for several hours and with no a priori knowledge.

Case 2: The same as Case 1 with a priori knowledge.

Case 3: Texas, Antigua, and Hawaii alternate at the end of each hour and no a priori knowledge is assumed. The analysis for this case extended over a five hour interval which is sufficient to study the effects of a more frequent alternation of stations.

The uncertainties in position and velocity (Figures 5.4a and 5.4b) are propagated to  $t + 30$  minutes for all three cases and to the LSOI for Case 1 only.

### 5.3.4 Leg 4 – Navigational Accuracies for the Third Midcourse Correction

The results of the analysis for this leg illustrate the accuracy in predicting the vehicular position, velocity, and selenocentric radius 30 minutes in advance of MSFN tracking and at perilune.

Two cases were simulated in the analysis for this leg and are as follows:

Case 1: Three radars tracking simultaneously with no a priori knowledge.

Case 2: The same as Case 1 with a priori knowledge.

The uncertainties in position, velocity, and selenocentric radius are propagated to  $t + 30$  minutes (Figures 5.5a through 5.5c, respectively) and to perilune (Figures 5.5d through 5.5f). In all cases the orbital parameters are referenced to a selenocentric coordinate system.

#### 5.4.1 Leg 1

The first four cases (Figures 5.2a and 5.2c) represent multiple tracking. As might be expected, three stations are shown to be better than two. However, general conclusions concerning the relative merit of C-Band radar and USB Systems cannot be made because the errors vary so markedly with tracking time and period or propagation. The results from the next four cases (Figures 5.2b and 5.2d) are markedly poorer than for the first four.

It is interesting to compare Ship A, which is equivalent to a land station in tracking capability, with the HAW USBs at seven minutes. The only difference between these two solutions is their viewing angles (the vehicle is setting for HAW and rising for the ship). HAW yields a better local uncertainty (at  $t_0$ ) but a worse propagated uncertainty (at  $t_{LSOI}$ ).

Similarly, GST tracking from 10 minutes to 24 minutes yields a better solution at  $t_0$  than does Ship B, which tracks from 3 to 24 minutes, but at  $t_{LSOI}$  Ship B's solution is considerably better. This makes it difficult to determine which tracking situation yields the best solution since a great deal depends upon the propagating effects.

A USBS solution is greatly enhanced after a second station has viewed the vehicle. The GST and Ship B combination is better than Ship A alone and much better than either GST or Ship B alone. Notice also that the Ship A, Ship B, or GST solution does not improve significantly after ten minutes of tracking.

#### 5.4.2 Leg 2

In the hour to hour and a half following transposition and docking, the three station solution is clearly better (Figure 5.3a) than that of two station or a one station, even when the other two solutions use a priori knowledge. Within 25 minutes, the three station solution can predict the position at  $t_{LSOI}$  to within 486 nm (900 km). This is with no a priori knowledge at the beginning of track. Tracking an additional hour only improves position uncertainties to 270 nm (500 km). The corresponding velocity uncertainty at  $t_{LSOI}$  is less than 14 ft/s (4 m/s) after 25 minutes and less than 7 ft/s (2 m/s) after 1 hour and 25 minutes of tracking.

#### 5.4.3 Leg 3

Stations were alternated during the 48 hour period between first and second midcourse corrections. It is seen that by the time a second station tracks,

the effect of a priori information is overcome and the position uncertainties at  $t + 30$  varies between 13.5 nm (25 km) and 54 nm (100 km) all the way out to the LSOI (Figure 5.4a). For the last ten hours of the leg, the uncertainties at  $t + 30$  and the uncertainties propagated to LSOI are nearly the same.

The velocity uncertainties at  $t + 30$  show a slightly decreasing characteristic after two stations have tracked, going from 5 ft/s (1.5 m/s) to 0.7 ft/s (0.2 m/s) (Figure 5.4b).

If a more rapid reduction in the uncertainties of the orbital parameters is desired then at least three stations should track alternately with a period of approximately one hour.

#### 5.4.4 Leg 4

In this leg the uncertainty in knowledge of position and velocity at  $t + 30$  can be brought below 27 nm (50 km) and 20 ft/s (6 m/s), which implies an uncertainty of 73 nm (136 km), 295 ft/s (90 m/s) and 16 nm (30 km) in position, velocity, and altitude respectively at perilune arrival.

It is observed that the uncertainties for the case with poor a priori knowledge and the case with no a priori knowledge converge to the same level of uncertainty by the end of about four hours.

#### 5.4.5 Leg 5

In this leg after 2-1/2 hours of tracking the knowledge of position and velocity at perilune can be known to within 400 nm (720 km) and 3000 ft/s (900 m/s). Little of this uncertainty is in perilune altitude (uncertainty 2.7 nm (5 km)) and ground speed (uncertainty 16.5 ft/s (5 m/s)). The uncertainties in perilune conditions are very interesting because it is now likely that the third midcourse correction will be made one hour prior to perilune arrival and must guarantee a perilune altitude to within 5 nm (9.3 km) of nominal.

By the time of loss of sight, or 20 minutes before perilune arrival, the uncertainties in perilune conditions are less than 54 nm (100 km) in position, 197 ft/s (60 m/s) in velocity, 3.3 ft/s (1 m/s) in speed, and 0.5 nm (1 km) in altitude.

During the last four hours, the use of angular measurements speeds up the convergence. However, if a realistic a priori knowledge had been carried over from the previous 56 hours of tracking then angular measurements may not have been necessary.

## 5.5 CONCLUSIONS

The assumed noise, systematic biases, and uncertainties in location for the ship's tracking data (Ship B) degrades by a factor of 2 the accuracy with which position and velocity can be determined over the accuracy resulting from a ground station with a tracking geometry identical to the ship's.

In comparing the graphs of Figures 5.2a, 5.2d, 5.4a, and 5.4d, it is observed that alternating the tracking assignments of stations significantly reduces the uncertainties in the state vector.

The results for leg 5 (Figures 5.6a through 5.6d) show that angle measurements taken at lunar distance are useful for rapid convergence. However, the results depicted on these same figures show that all four operational modes (with and without angles, with and without a priori knowledge) converge to the same uncertainty level before perilune arrival.

After tracking from injection to initiation of transposition and docking the uncertainties in position and velocity at injection are 0.4 nm (0.74 km) and 10 ft/s (3.0 m/s) if data from land based USB Systems are used and 17 nm (31 km) and 300 ft/s (91 m/s) if ships data are used. These uncertainties, when projected to the LSOI, are 165 nm (306 km), 9 ft/s (2.7 m/s) and 1400 nm (2600 km), 30 ft/s (9.1 m/s) respectively.

The uncertainties in position and velocity for the first midcourse correction are 44 nm (82 km) and 20 ft/s (6.1 m/s) resulting in uncertainties of 270 nm (500 km) and 6 ft/s (1.8 m/s) when projected to the LSOI.

The uncertainties in position and velocity for the second midcourse correction are 13.5 nm (25 km) and 2 ft/s (0.6 m/s).

The uncertainties in position, velocity, and radius for the third midcourse correction are 25 nm (46 km), 22 ft/s (6.7 m/s), and 8.5 nm (15.7 km), respectively, and the corresponding uncertainties at perilune are 71 nm (130 km), 280 ft/s, (85 m/s) and 16.5 nm (31 km).

The uncertainties in position, velocity, radius, and lunar ground speed at perilune arrival, based on tracking up to 20 minutes before perilune arrival can be known to within 54 nm (100 km), 175 ft/s (53 m/s), 2 nm (3.7 km), and 7 ft/s (2.1 m/s).

## 5.6 APPENDIX A, COORDINATE SYSTEMS

### 5.6.1 Station Location Coordinate System

The coordinate system is earth centered with the X-axis through the prime meridian, the Z-axis in the direction of the earth's angular momentum vector, and the Y-axis such as to form a righthand orthogonal system.

### 5.6.2 Vehicular Coordinate System

The coordinate system is an earth or moon centered (depending on the reference body) non-rotating system with the X-axis pointing toward the vehicle at time  $t = 0$ , the Z-axis in the direction of the orbital angular momentum vector, and the Y-axis such as to form a right-hand orthogonal system.

## 5.7 APPENDIX B, TRAJECTORIES

### 5.7.1 Trajectory A (For analysis of Legs 1, 2, and 3)

This trajectory is an earth referenced conic section generated from the following initial conditions.

At Time	Inclination to earth equatorial plane	Radius (nm)	Tangential Velocity (ft/s)	Radial Velocity (ft/s)
0	32.47°	3613.15728	35325.436	4087.31952
	Subvehicle Point			
	Latitude		Longitude	
	14.16943°N		157.934°W	

The vehicle is ascending in its orbit at  $t = 0$ .

### 5.7.2 Trajectory B (For analysis of Legs 3 and 4)

This trajectory is a moon referenced conic section generated from the following initial conditions:

### Vehicle with Respect to Moon

At Time	Inclination to moon equatorial plane	Radius (nm)	Tangential Velocity (ft/s)	Radial Velocity (ft/s)
0	177°	27013.2246	-4154.373	318.935
	Subvehicle Point			
	Latitude		Longitude	
	2.26°N		54.2°W	

This trajectory will have a perilune latitude of 0.0°, a perilune radius of 1022.87556 nm, and a total flight time of 10 hours from LSOI to perilune arrival. The vehicle is ascending in its orbit at time  $t = 0$ .

### Moon with respect to the Earth

Earth-Moon Distance	Sublunar Point	Moon's Orbital Inclination to Earth's Equator
207,577.08 nm	15°N, 125°E	28.67°

The moon is ascending in its orbit about the earth.

## 5.8 APPENDIX C, COMPONENTS FOR ASSUMED A PRIORI KNOWLEDGE

Position (nm)			Velocity (ft/s)		
$\sigma_x$	$\sigma_y$	$\sigma_z$	$\sigma_{\dot{x}}$	$\sigma_{\dot{y}}$	$\sigma_{\dot{z}}$
Leg 2					
.51	.13	.51	3.84	3.64	5.54
Leg 3					
.66	.54	1.42	.34	.44	2.09
Legs 4 & 5					
10.8	10.8	21.6	6.56	6.56	13.12

## 5.9 APPENDIX D, CHECKOUT PROCEDURES

The error analysis program that was used to obtain the results presented in this chapter has been thoroughly checked out during the past two years. In addition, results from the program compare favorably with orbital accuracies based on real time data (Ranger and Gemini) for earth orbits. The same assumptions were made for this study as were made in the comparison and therefore the results presented in this chapter are considered to be conservative estimates of the capability of the MSFN.

## 5.10 REFERENCES

1. "Description of Orbit Error Analysis Program," Volumes 1 and 2, Bissett-Berman Corporation, Santa Monica, Calif., July and August, 1965.
2. MSC-GSFC, ANWG Report No. 65-AN-1.0, "Appolo Missions and Navigation Systems Characteristics," Feb. 5, 1965.

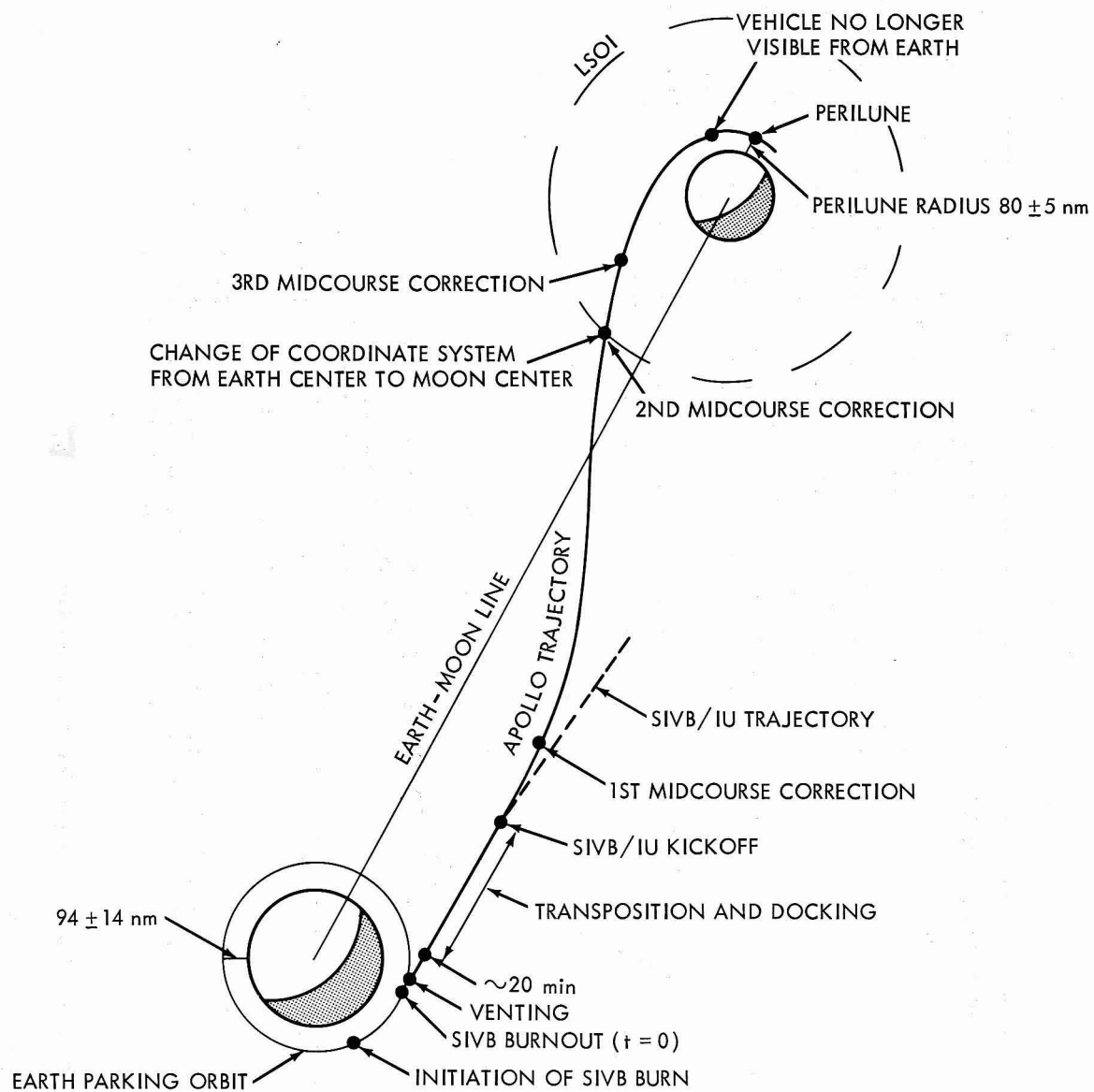


Figure 5.1



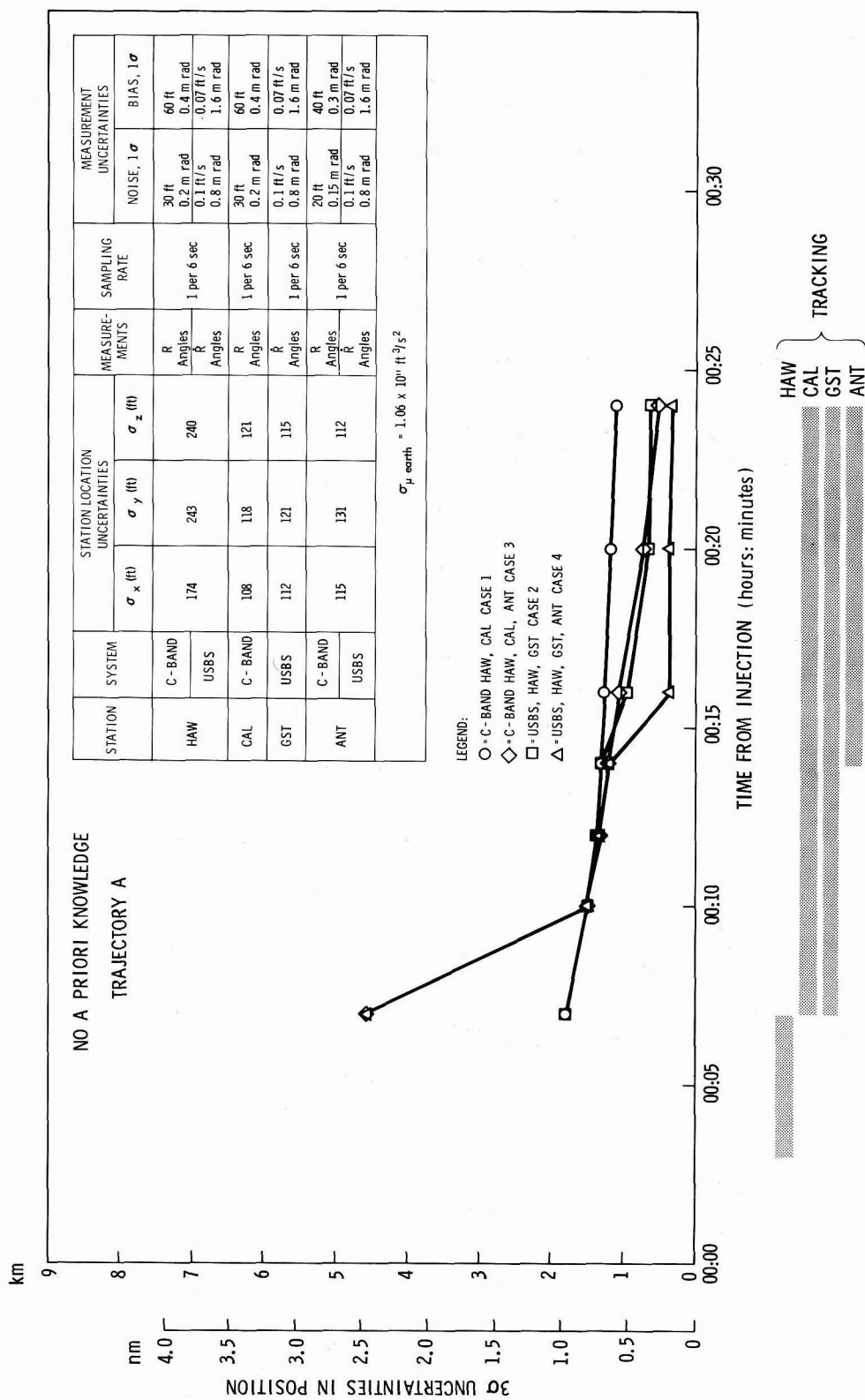


Figure 5.2a—Translunar Injection. Position Uncertainties (Referenced to time  $T = 0$  min), Leg 1.

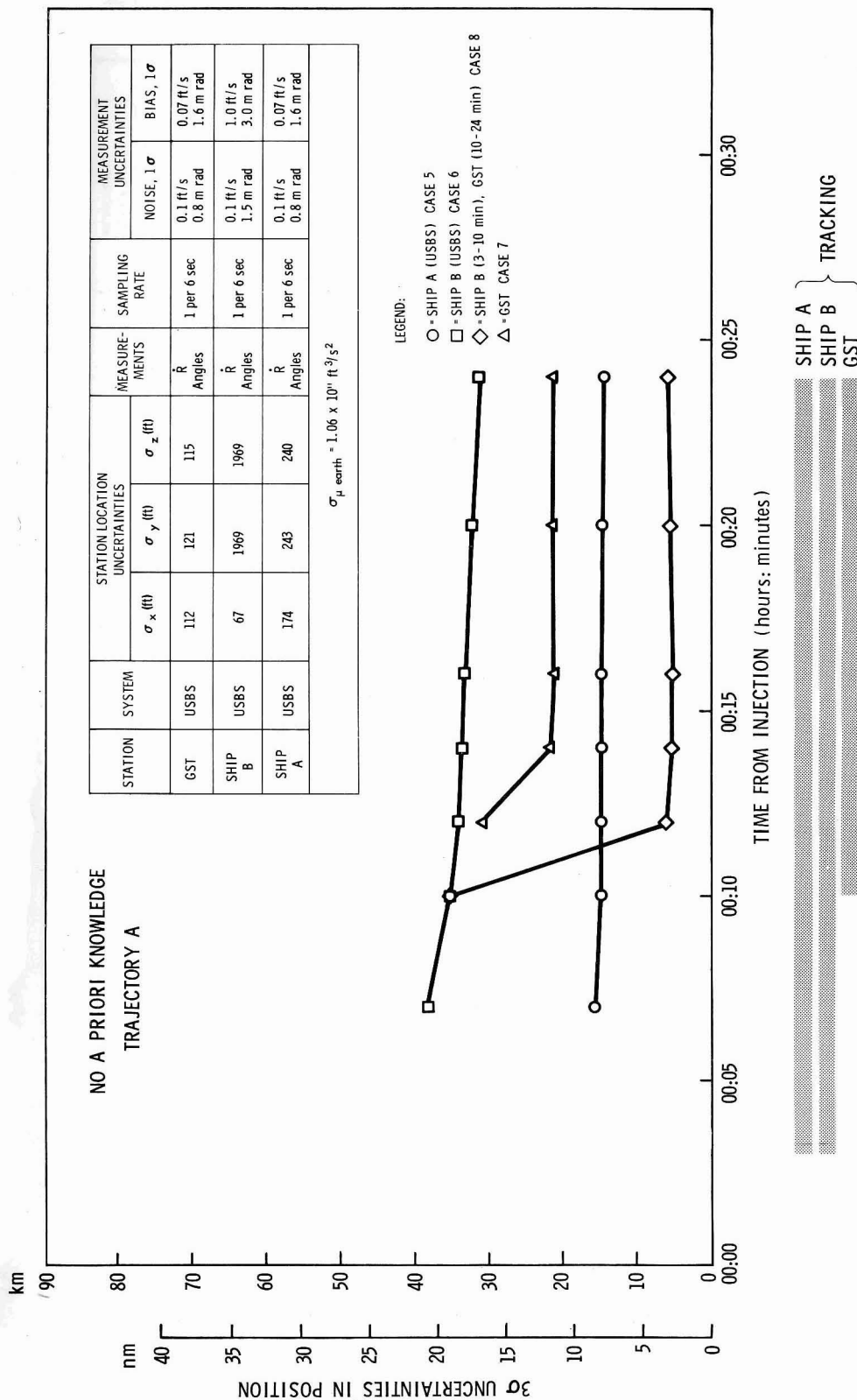


Figure 5.2b-Translunar Injection. Positions uncertainties (References to time  $T = 0$  min), Leg 1.

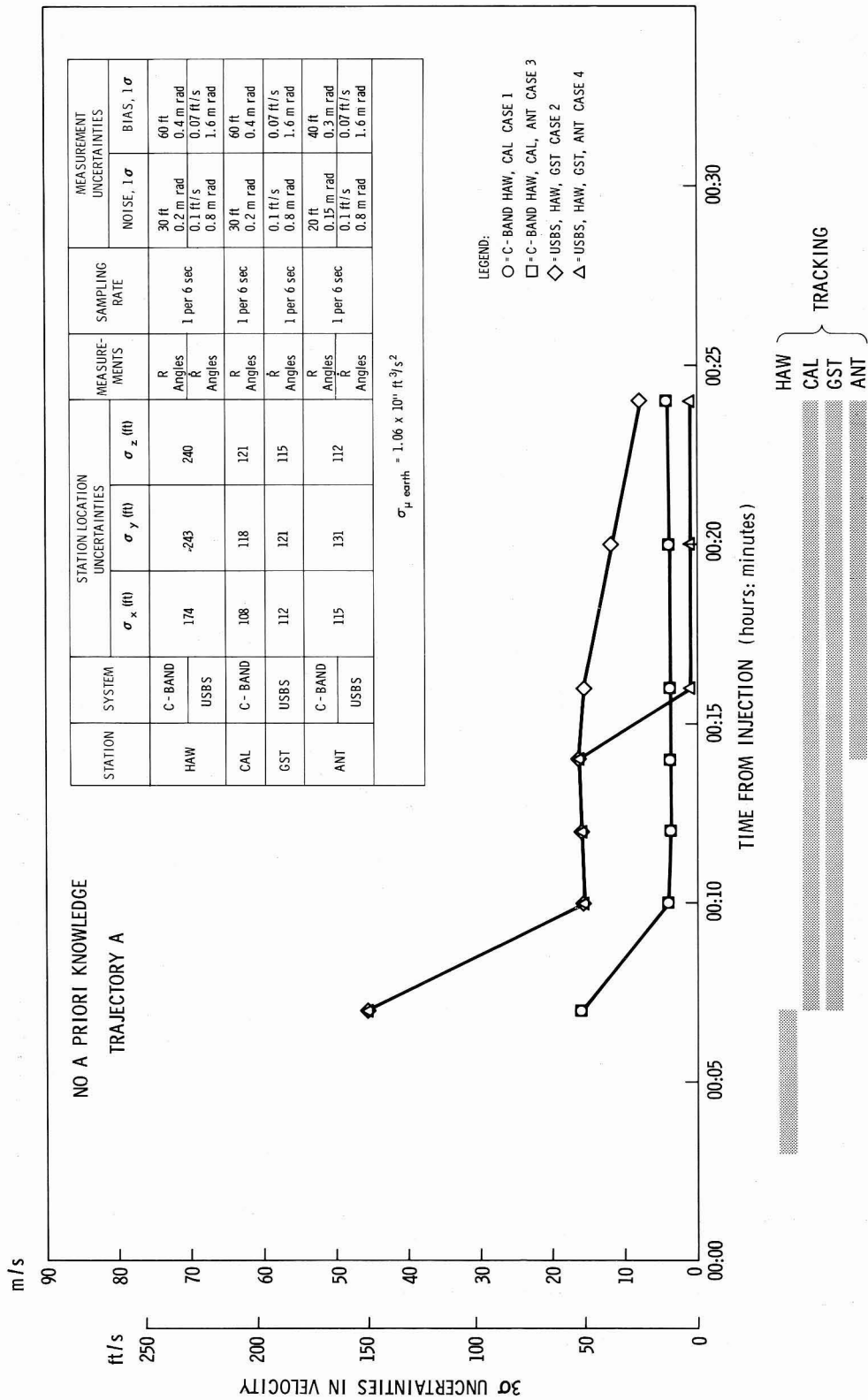


Figure 5.2c-Translunar Injection. Velocity uncertainties (Referenced to time  $T = 0$ ), Leg 1.

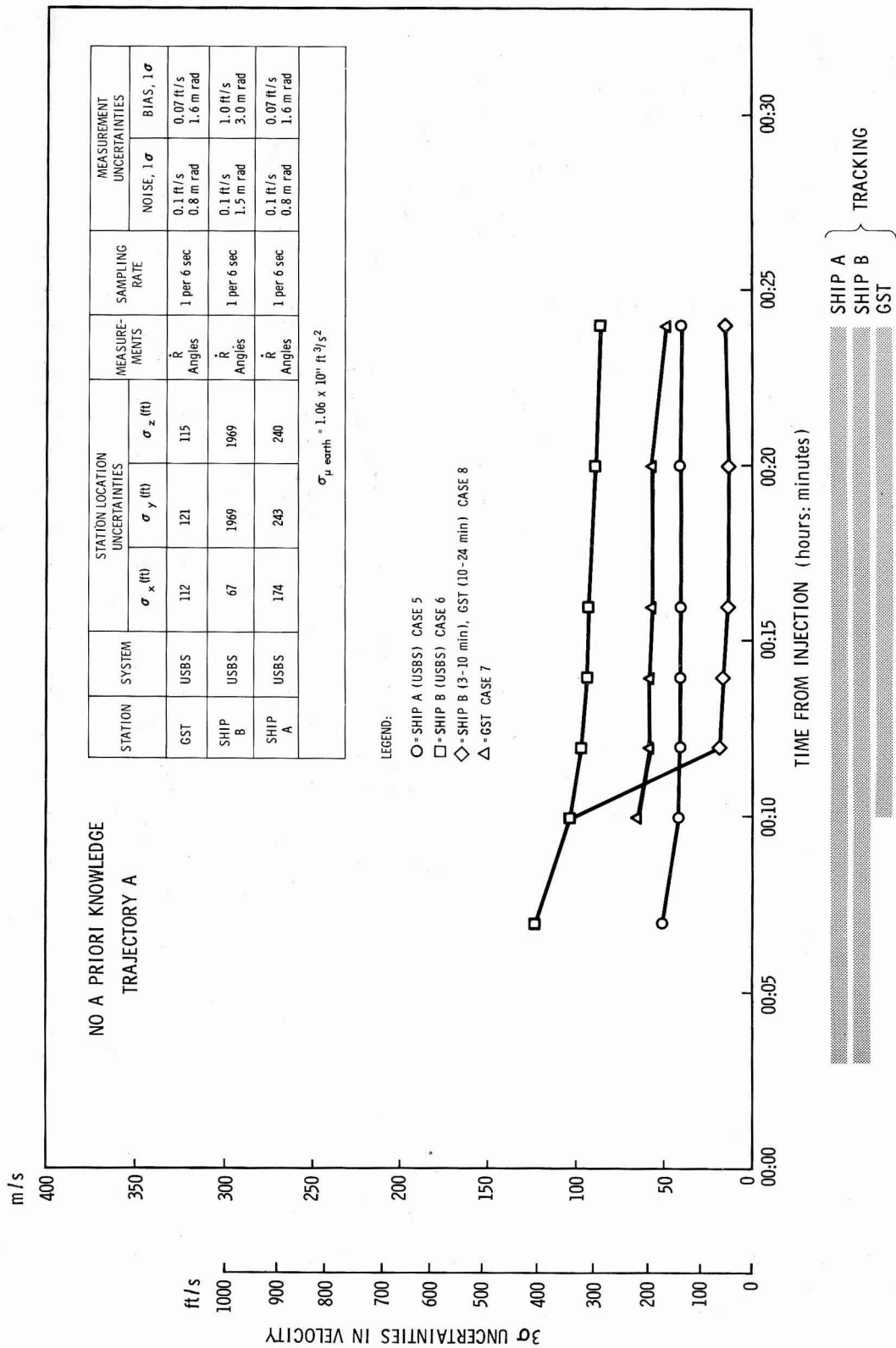


Figure 5.2d—Translunar Injection. Velocity uncertainties (Referenced to time  $T = 0$ ), Leg 1.

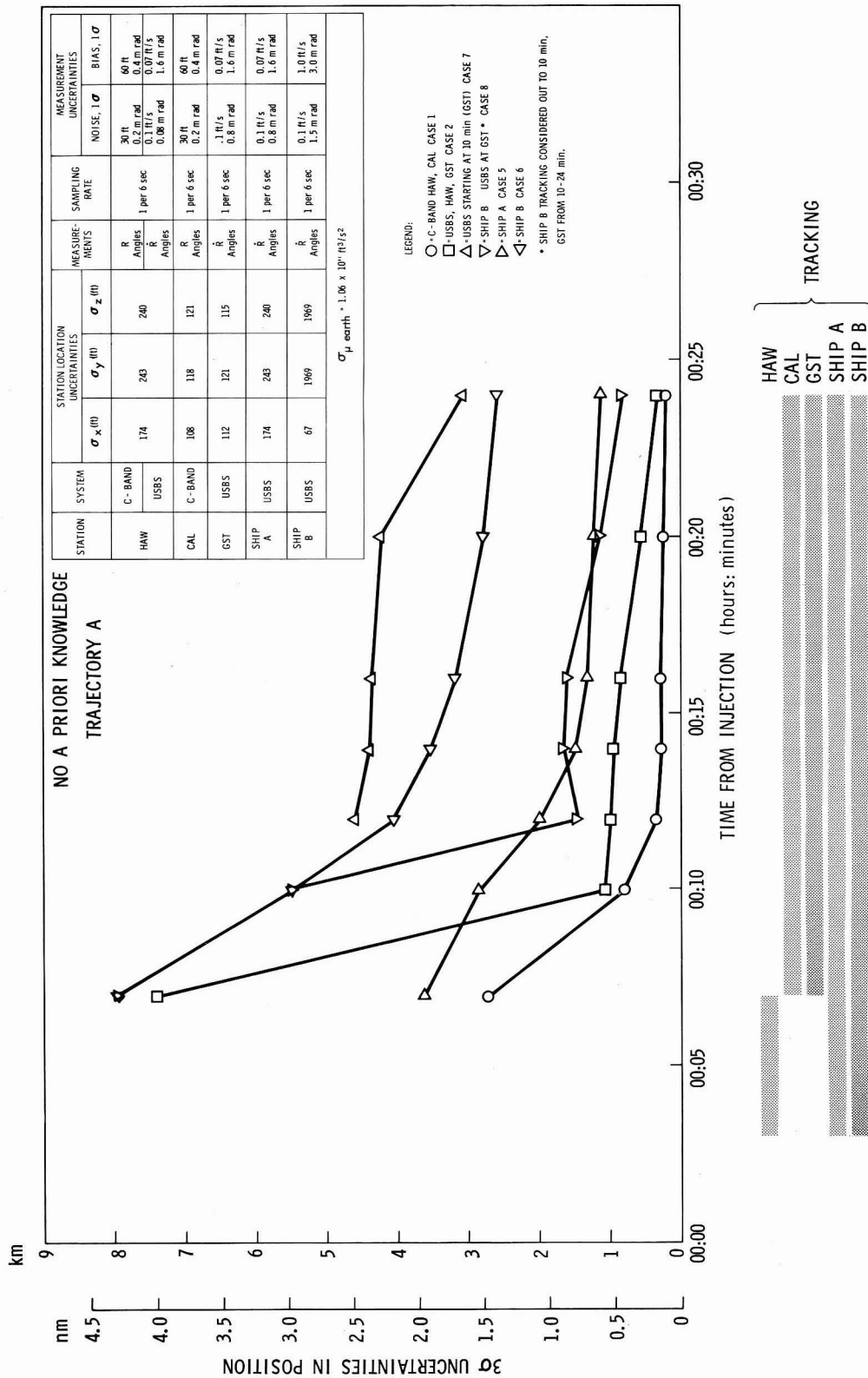


Figure 5.2e- Translunar Injection. Position uncertainties (Propagated to LSOI), Leg 1.

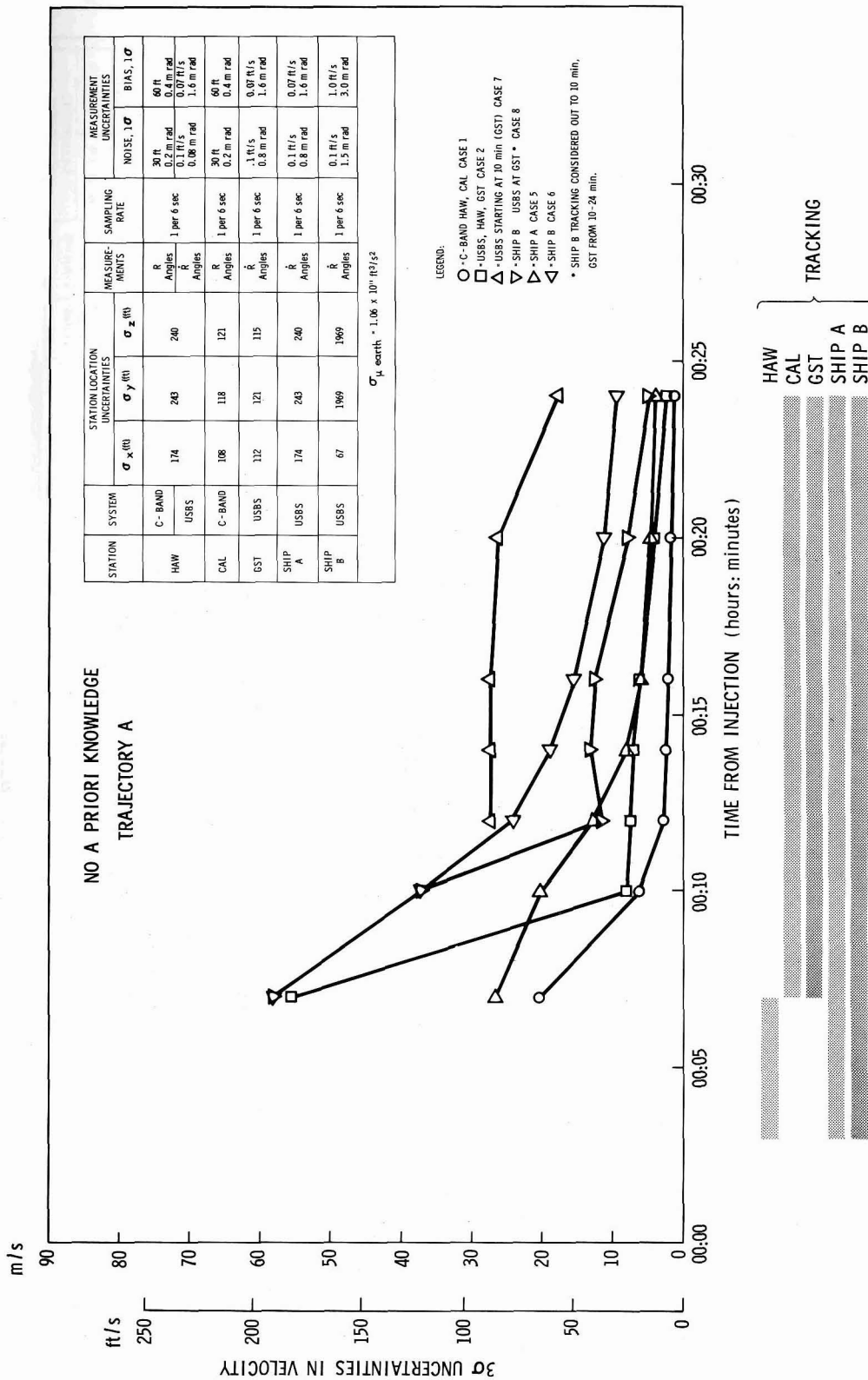


Figure 5.2f—Translunar Injection. Velocity uncertainties (Propagated to LSOI), Leg 1.

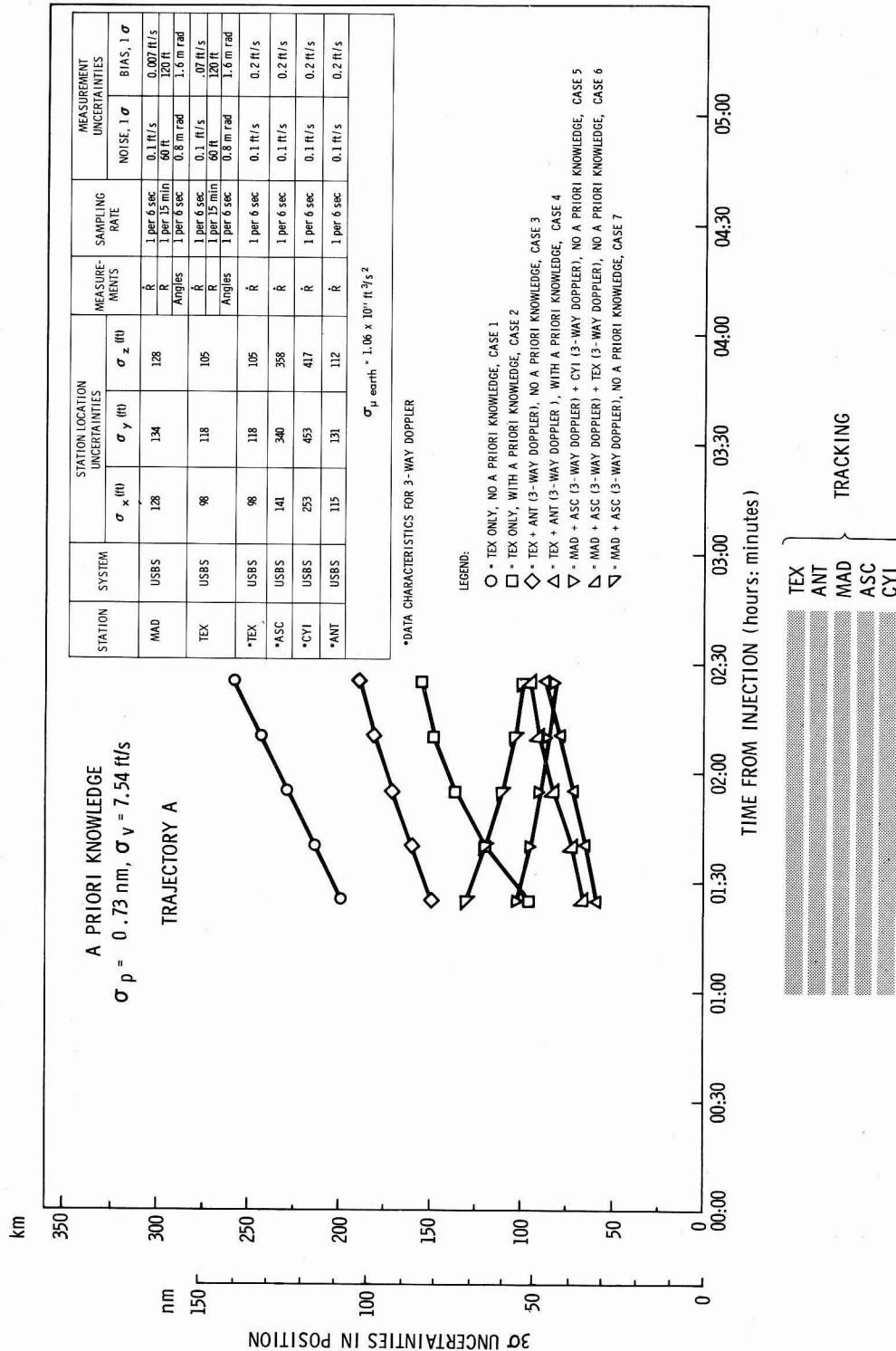


Figure 5.3a—First midcourse correction. Position uncertainties (Propagated to  $t + 30 \text{ min}$ ), Leg 2.

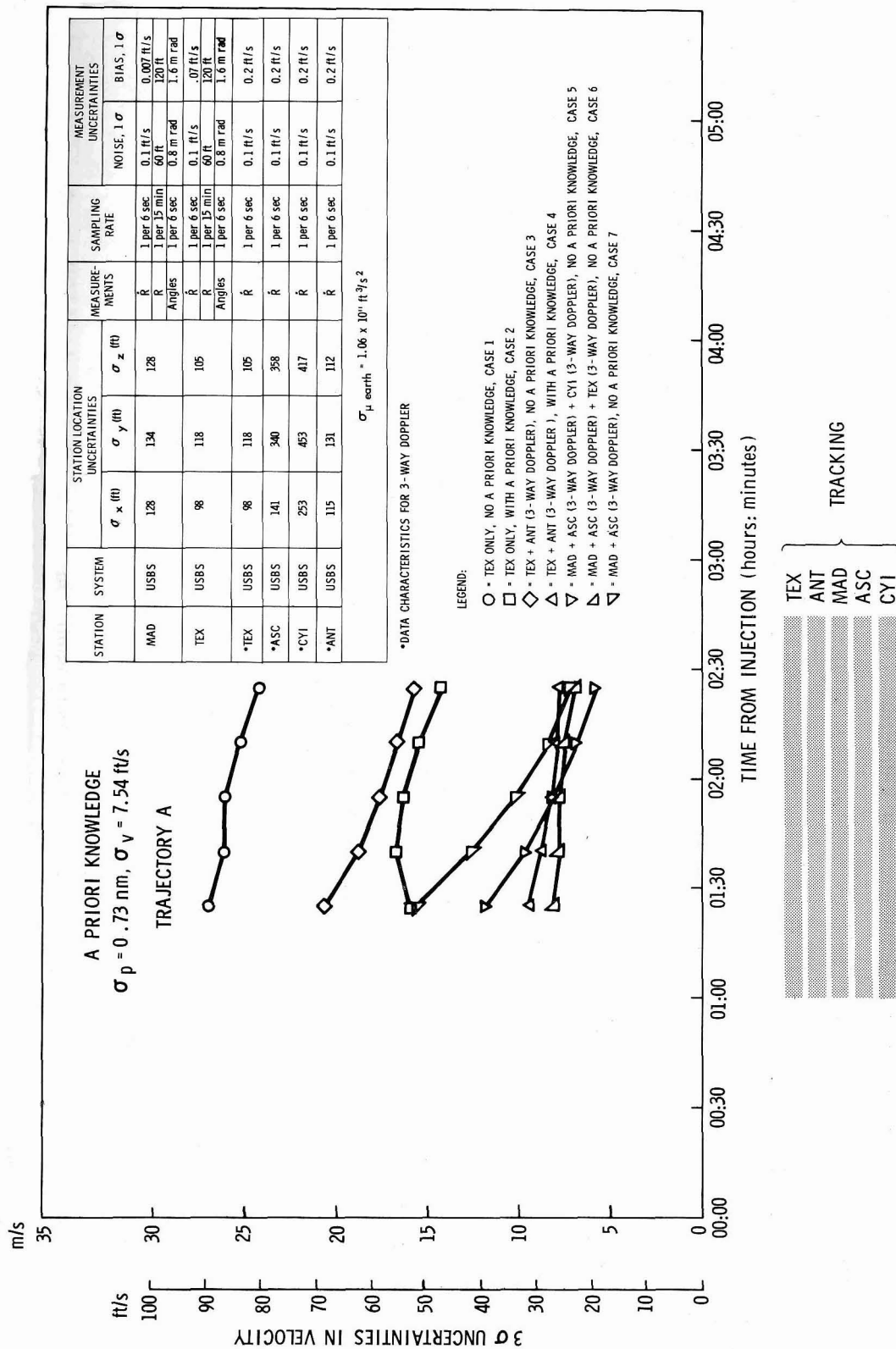


Figure 5.3b—First midcourse correction. Velocity uncertainties (Propagated to  $t + 30$ ), Leg 2.



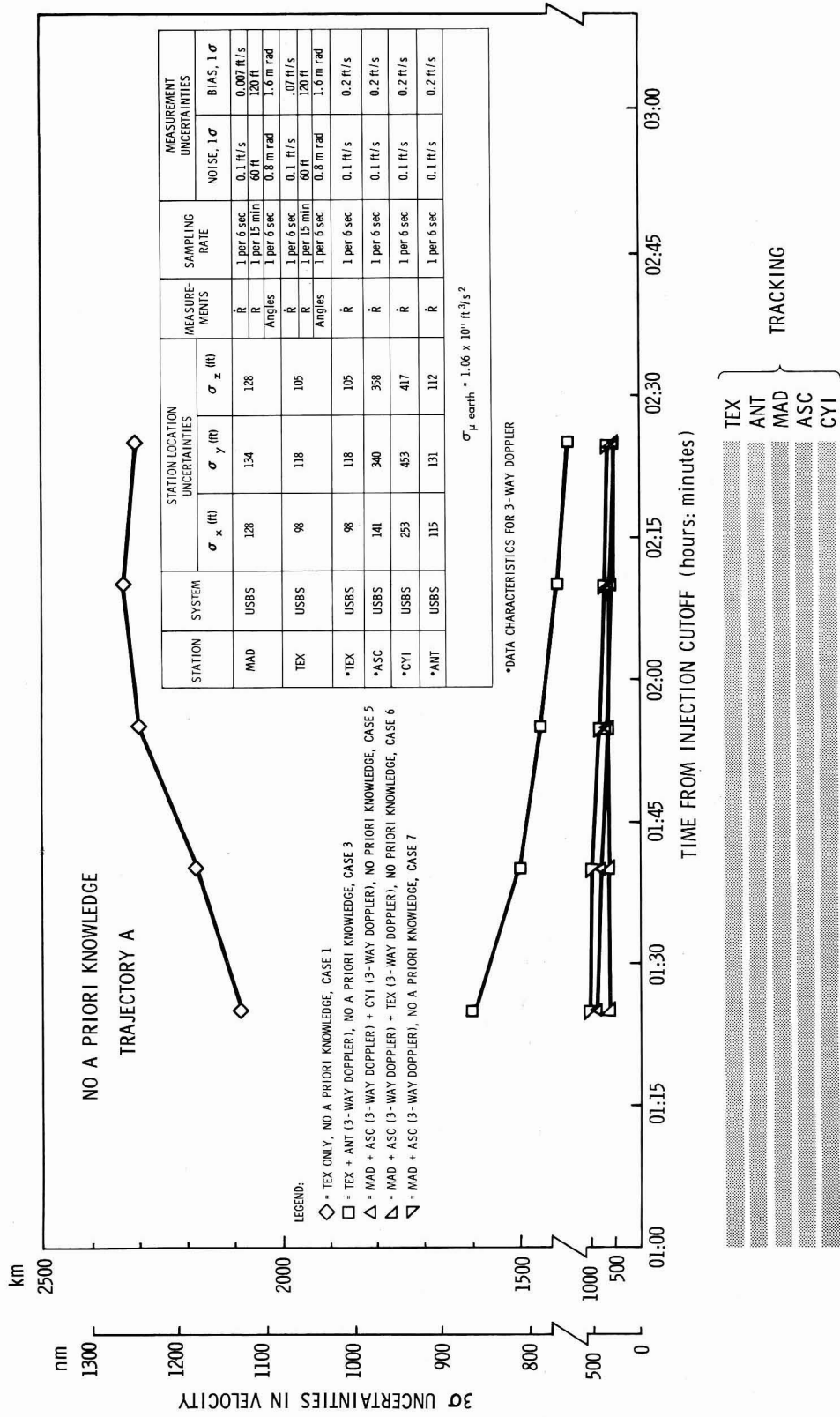


Figure 5.3c—First midcourse correction. Uncertainties in position (Propagated to LSOI), Leg 2.

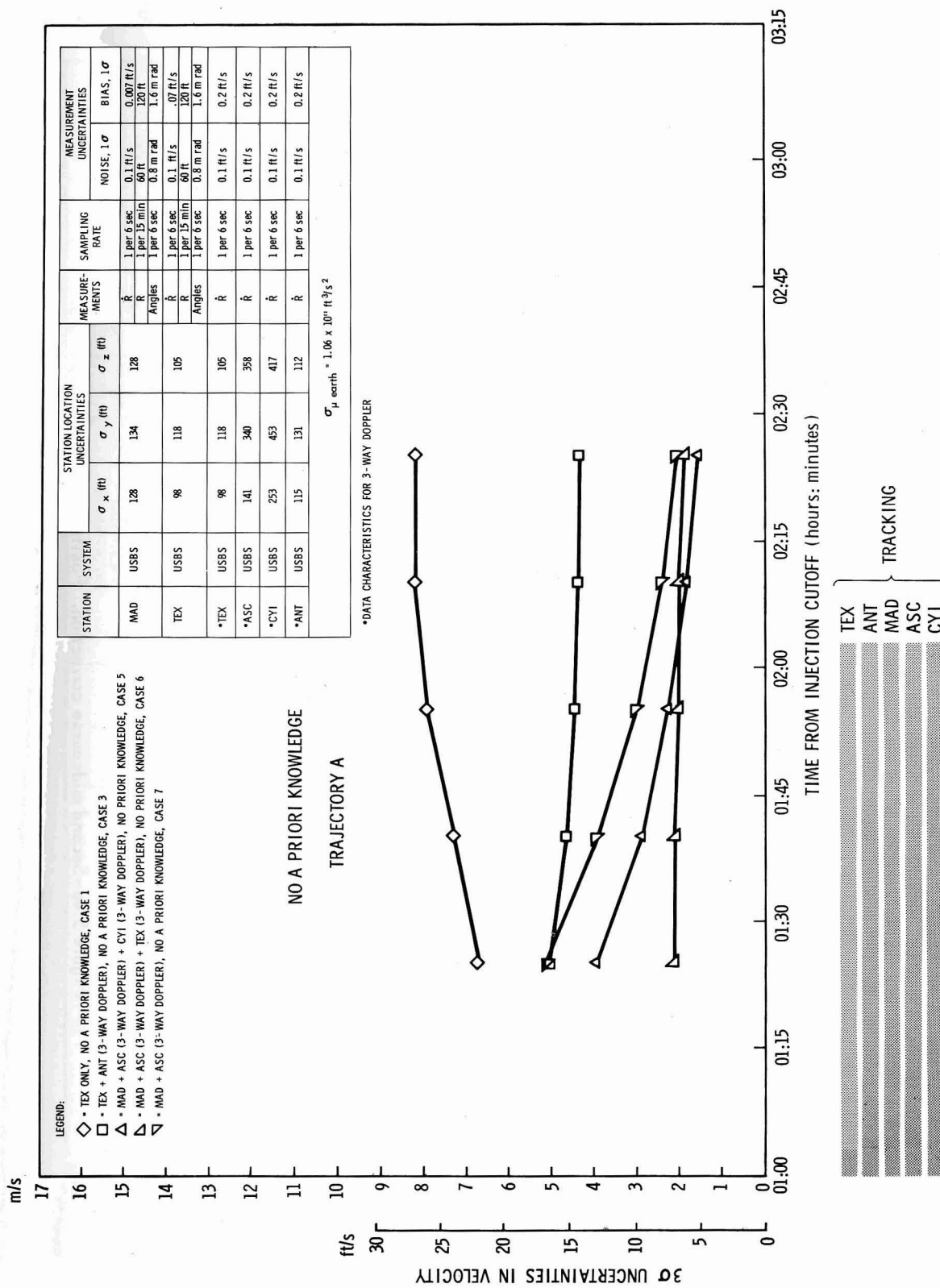


Figure 5.3d—First midcourse correction. Velocity uncertainties (Propagated to LSOI), Leg 2.

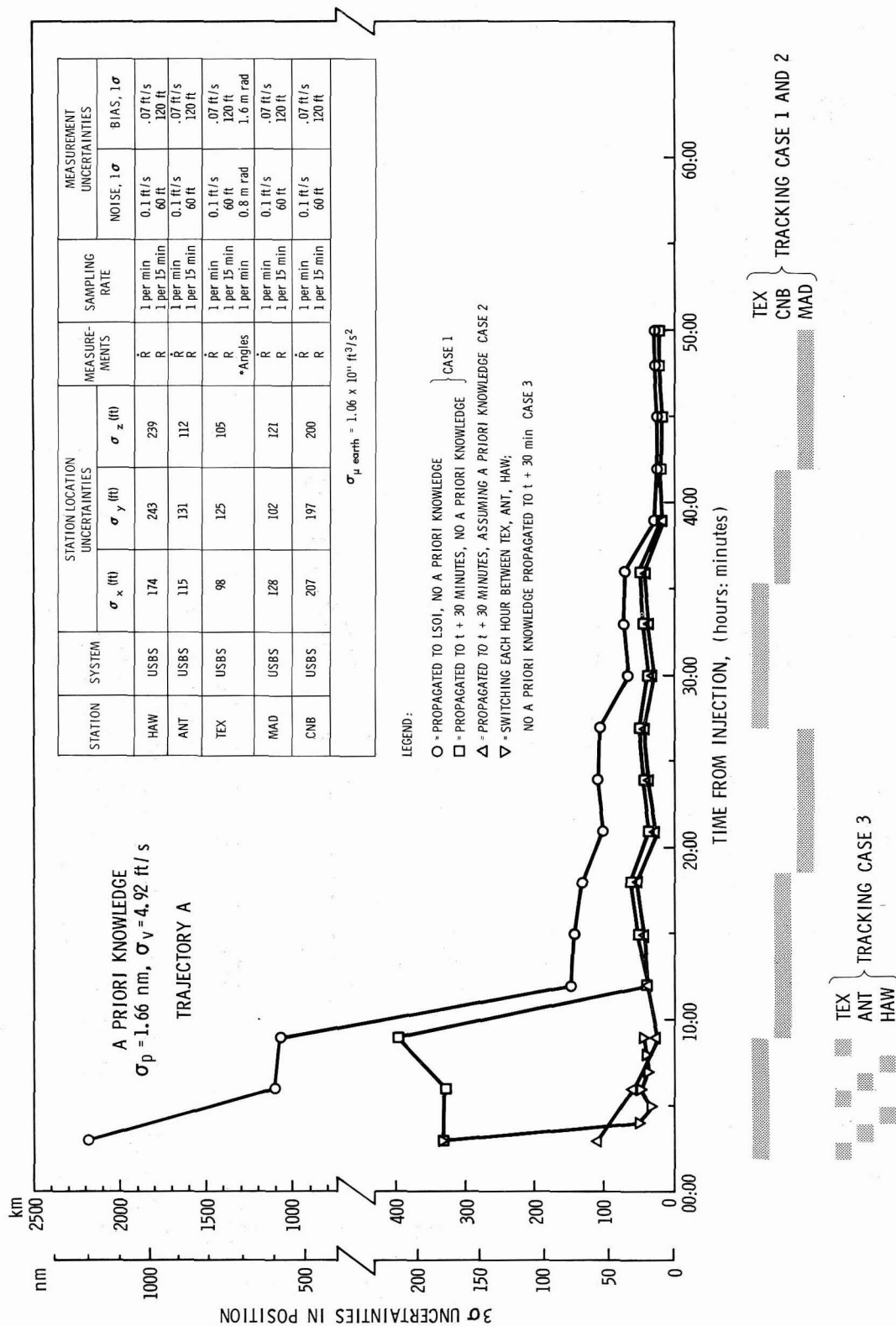


Figure 5.4a—Second midcourse correction. Position Uncertainties, Leg 3.

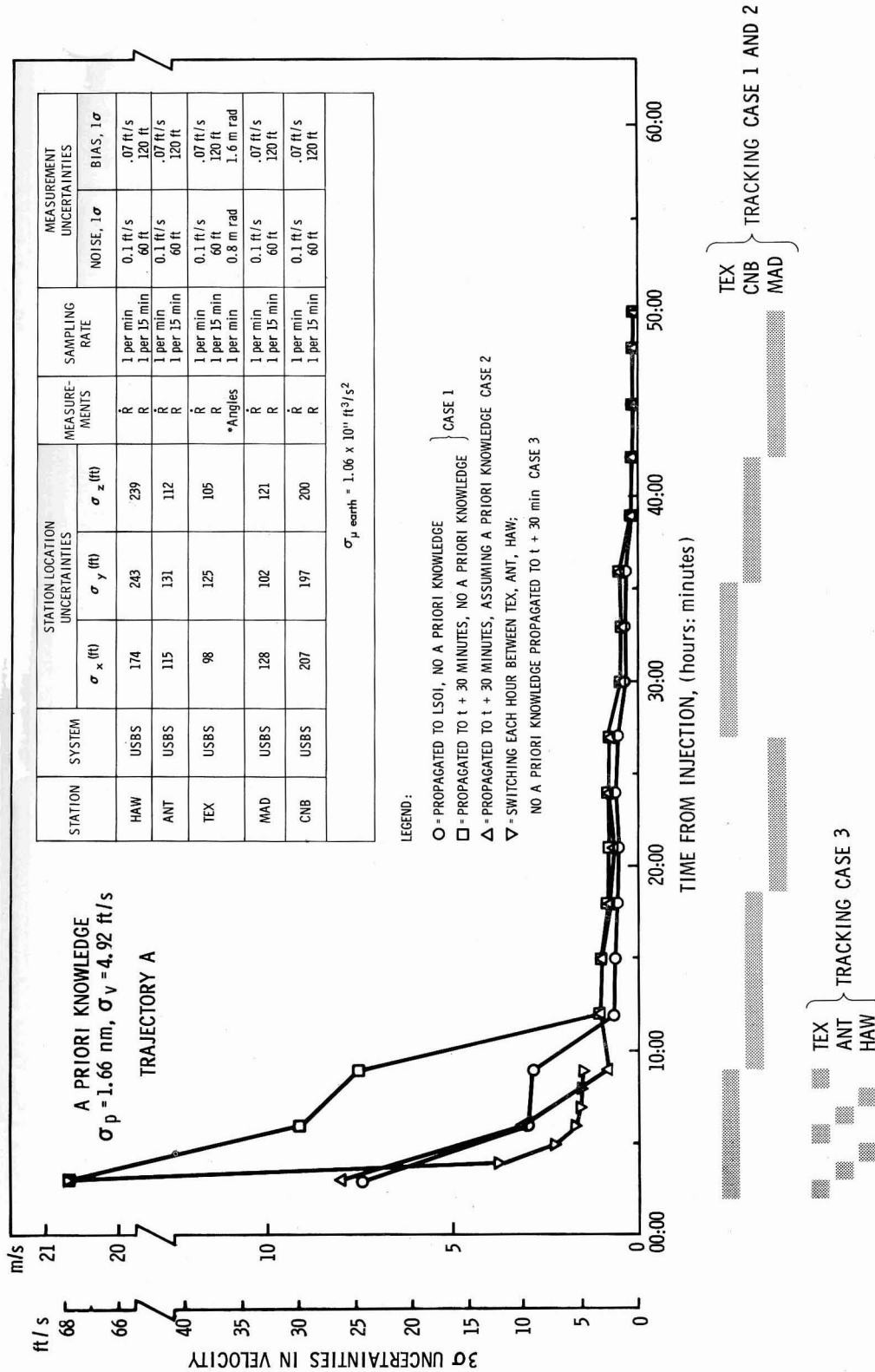


Figure 5.4b—Second midcourse correction. Velocity uncertainties, Leg 3.

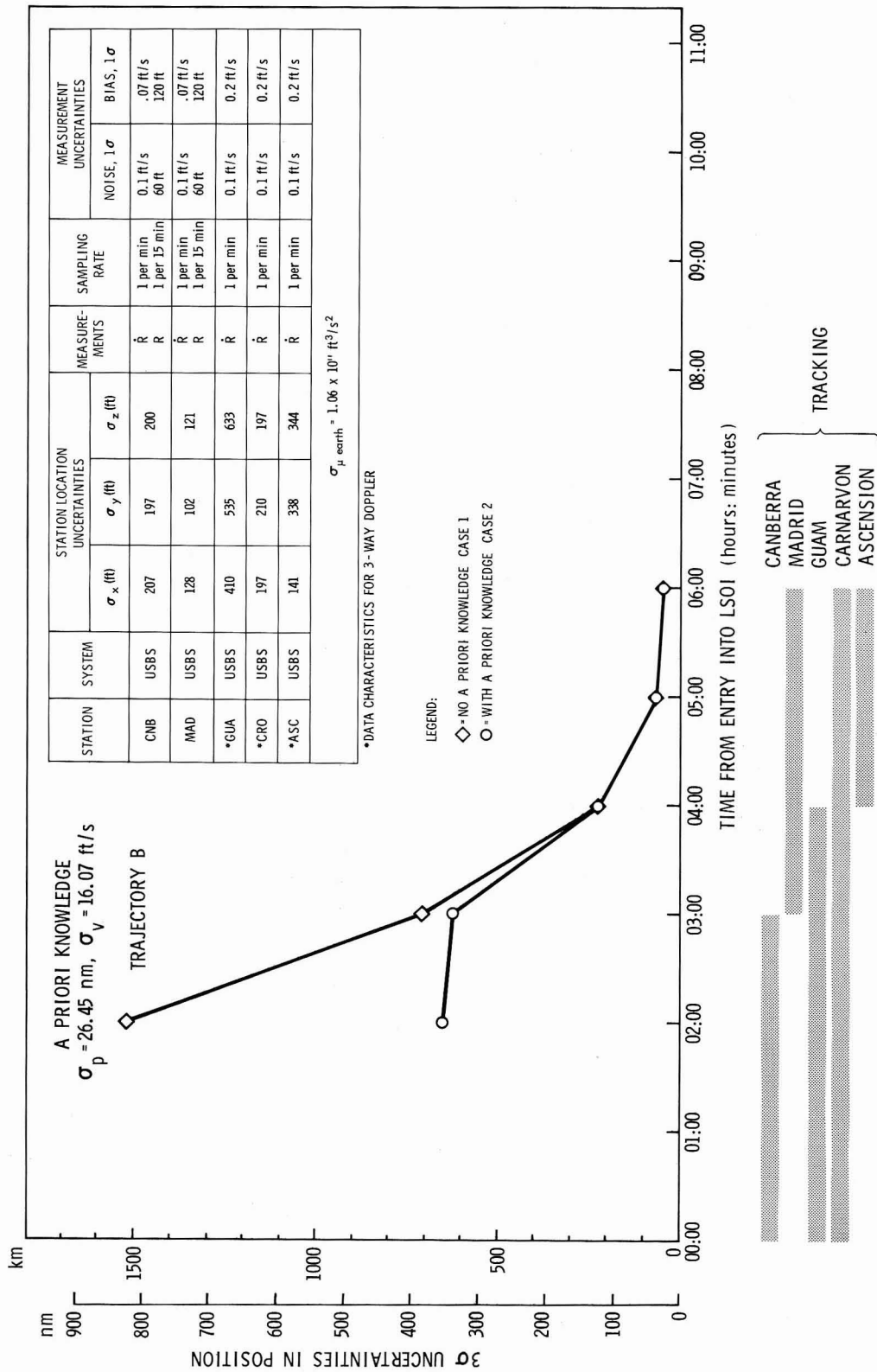


Figure 5.5a—Third midcourse correction. Position uncertainties (Propagated to  $t + 30 \text{ min}$ ), Leg 4.

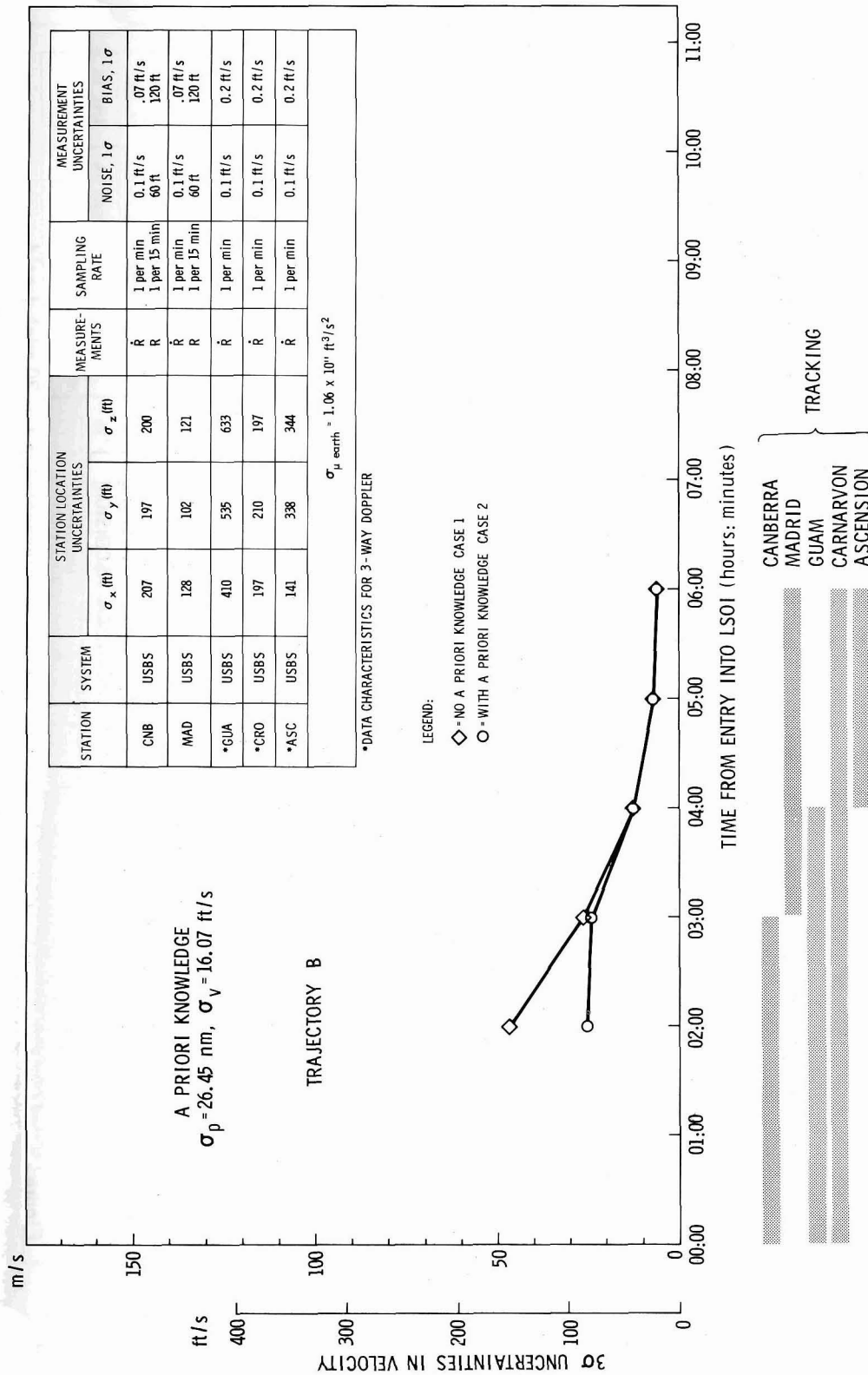


Figure 5.5b- Third midcourse correction. Velocity uncertainties (Propagated to  $t + 30 \text{ min}$ ), Leg 4.

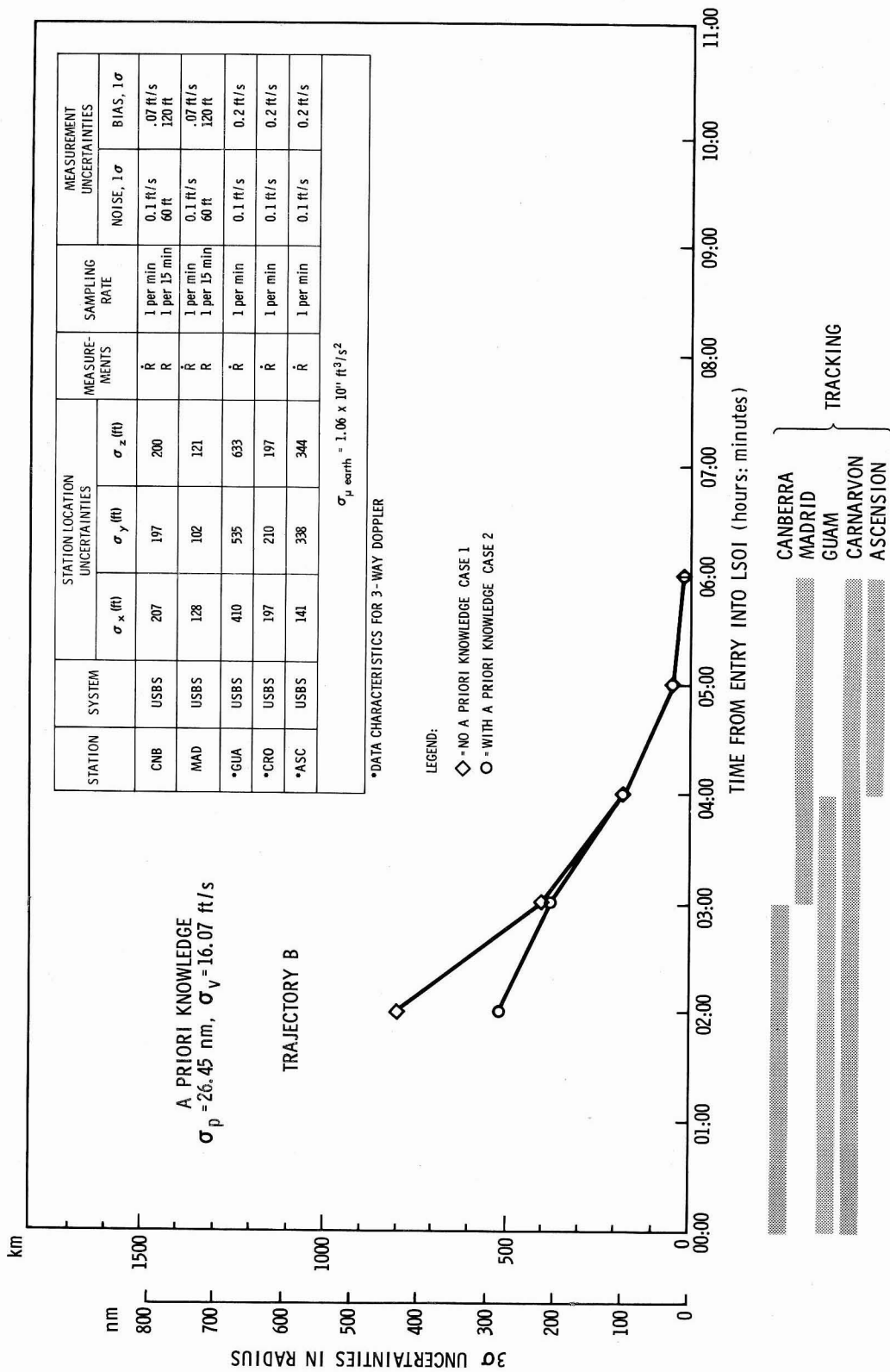


Figure 5.5c- Third midcourse correction. Radius uncertainties (Propagated to  $t + 30 \text{ min}$ ), Leg 4.

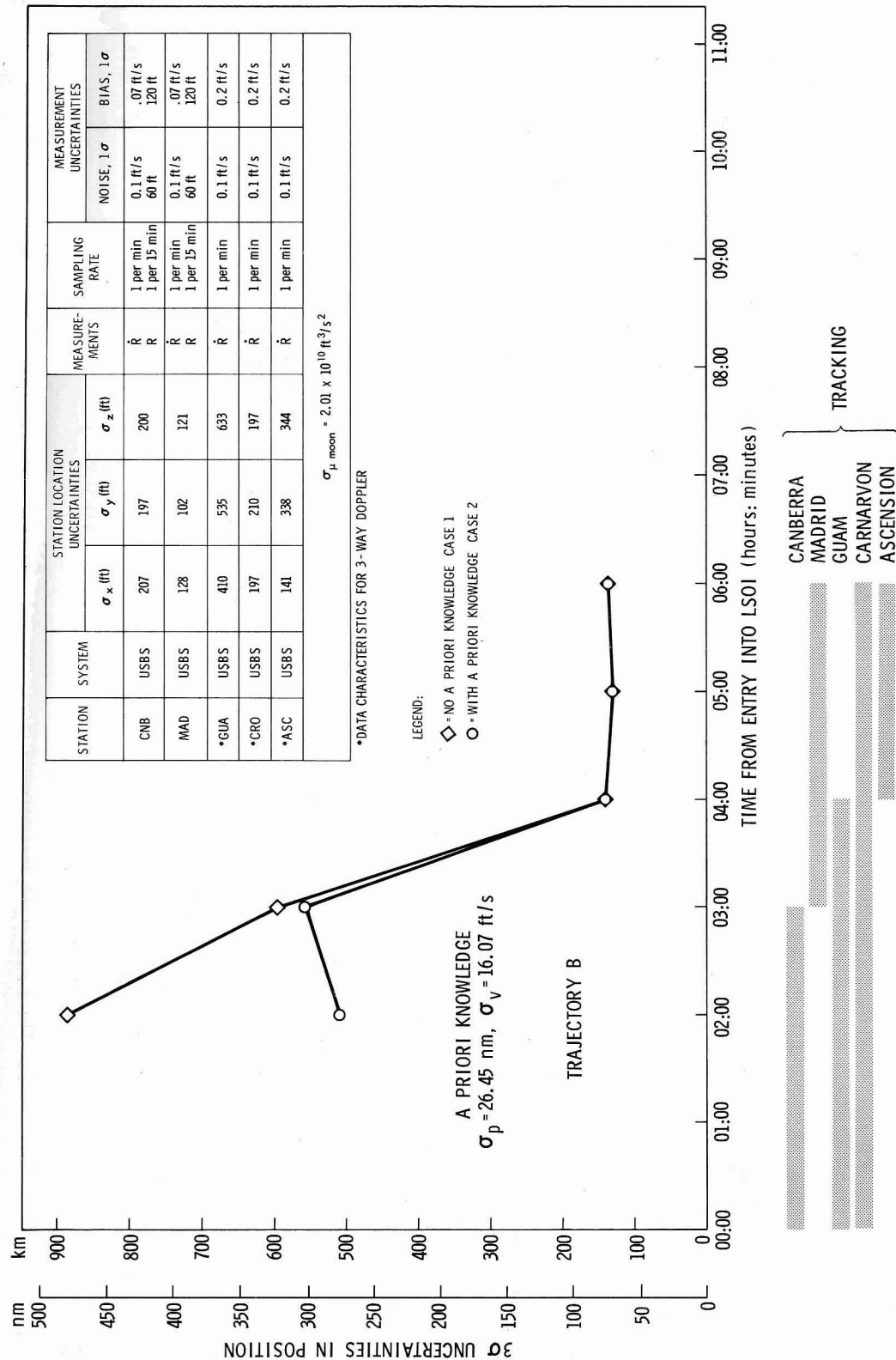


Figure 5.5d—Third midcourse correction. Position uncertainties (Propagated to perilune), Leg 4.



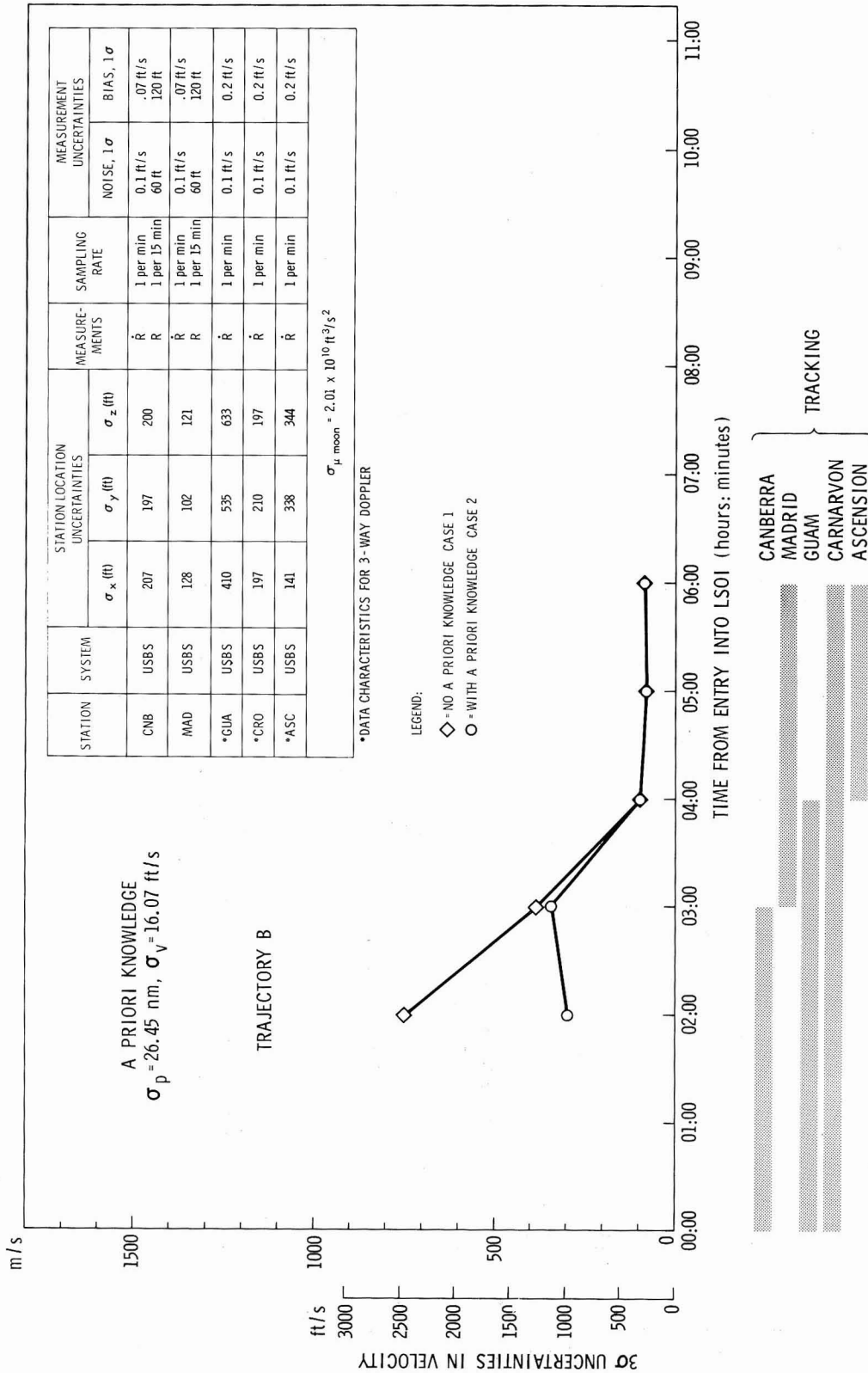


Figure 5.5e-Third midcourse correction. Velocities uncertainties (Propagated to perilune), Leg 4.

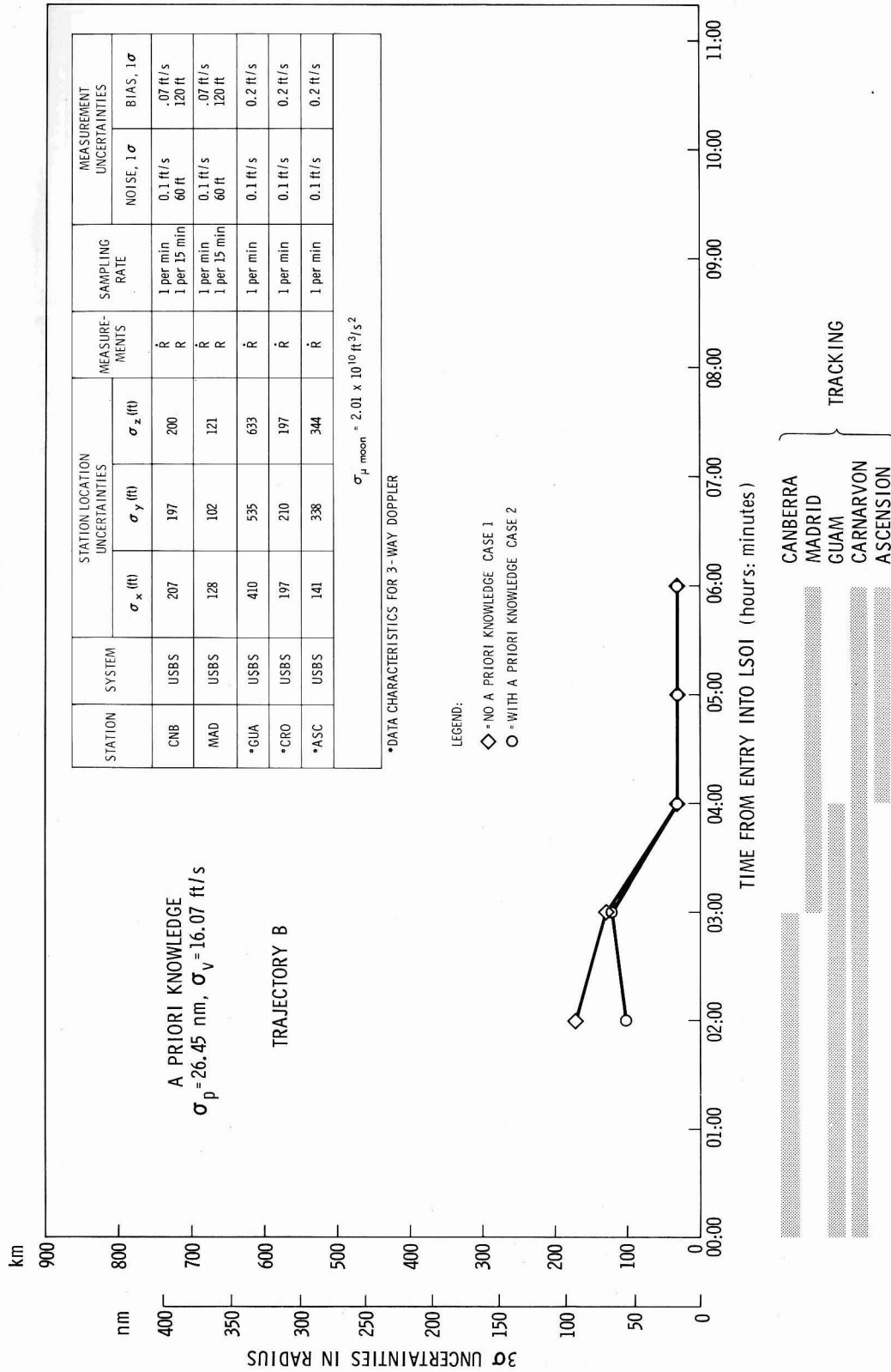


Figure 5.5f-Third midcourse correction. Radius uncertainties (Propagated to perilune), Leg 4.

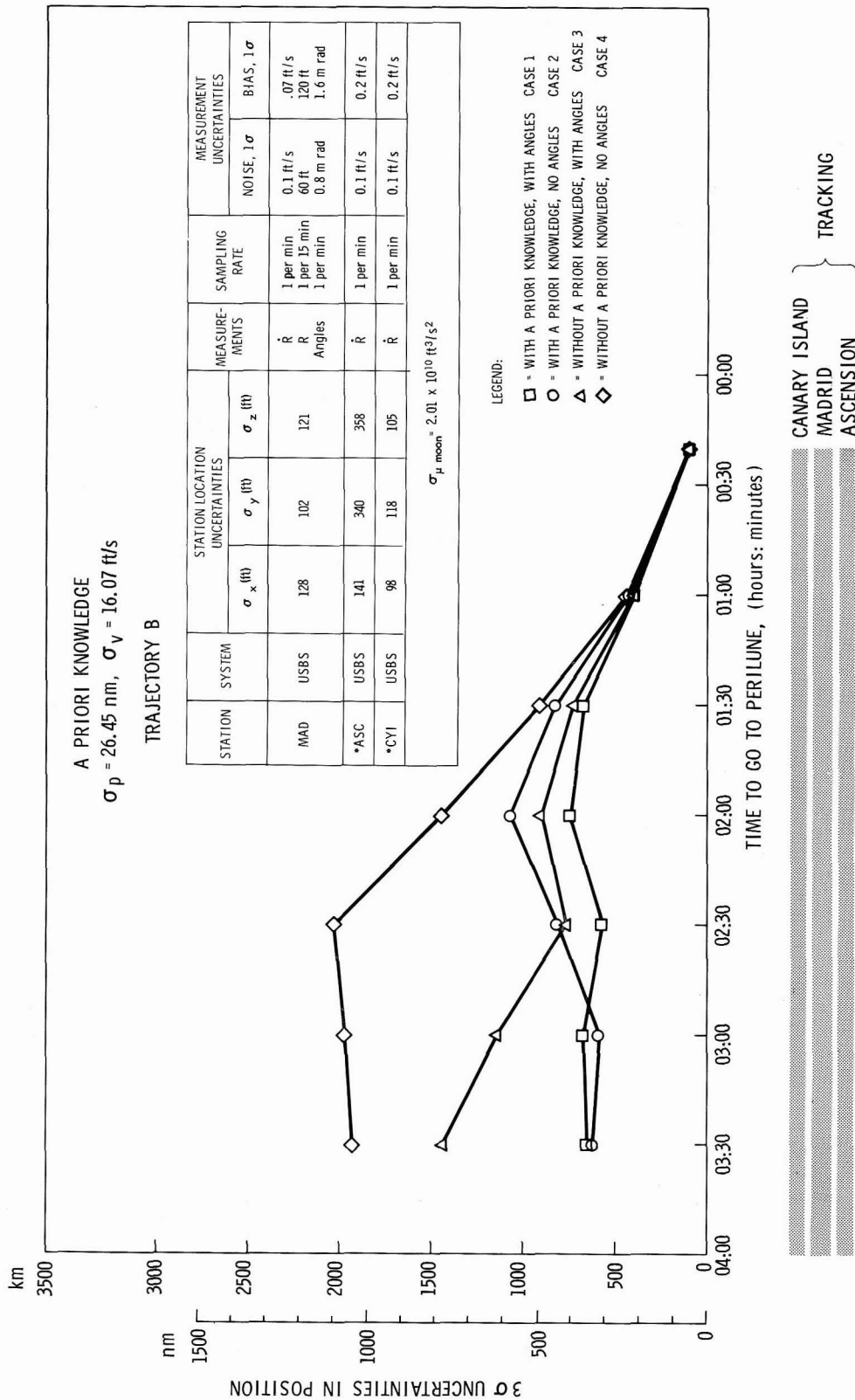


Figure 5.6a—Perilune. Position uncertainties (Propagated to perilune), Leg 5.

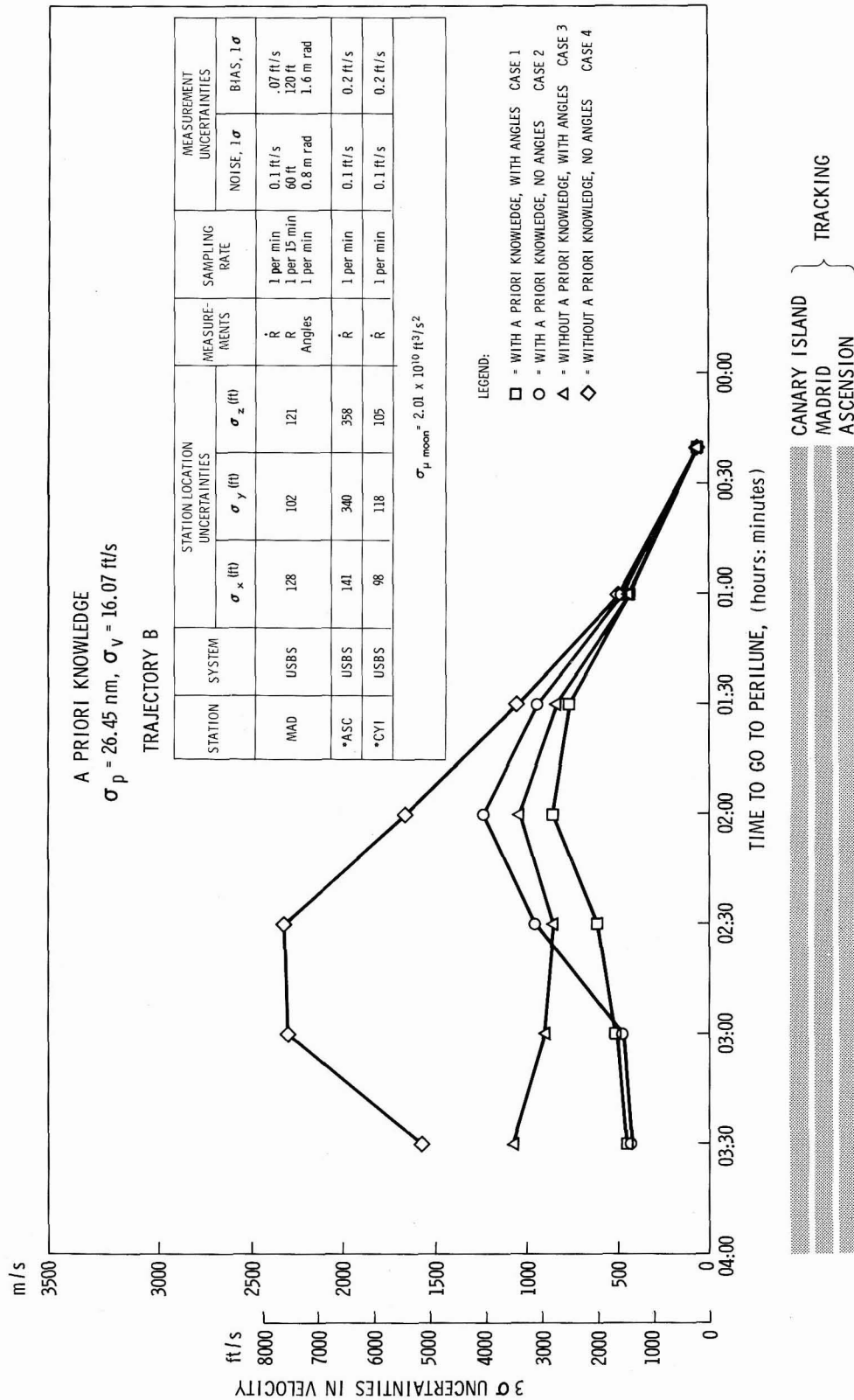


Figure 5.6b-Perilune. Velocity uncertainties (Propagated to perilune), Leg 5.

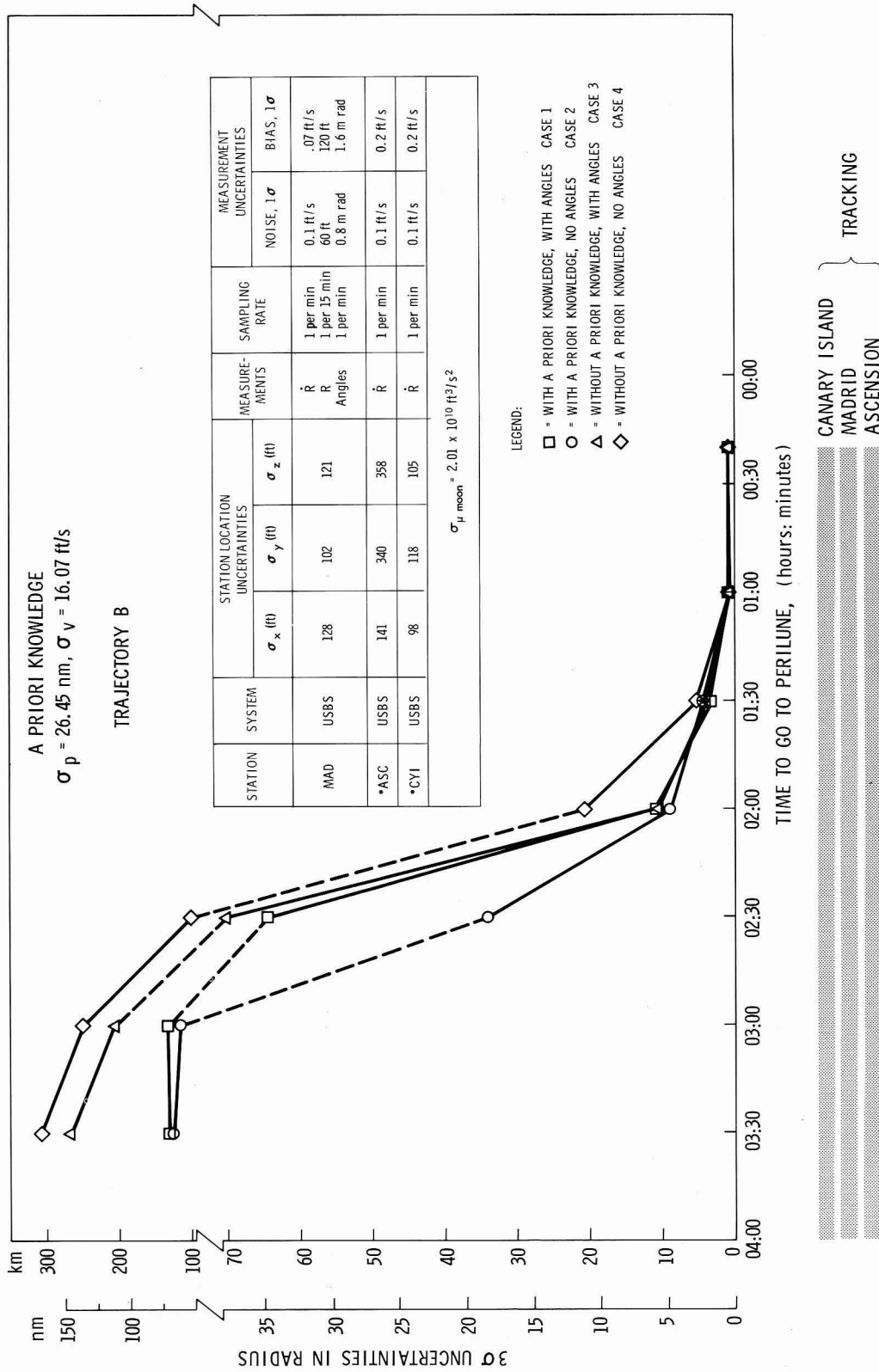


Figure 5.6c-Perilune. Radius Uncertainties (Propagated to perilune), Leg 5.

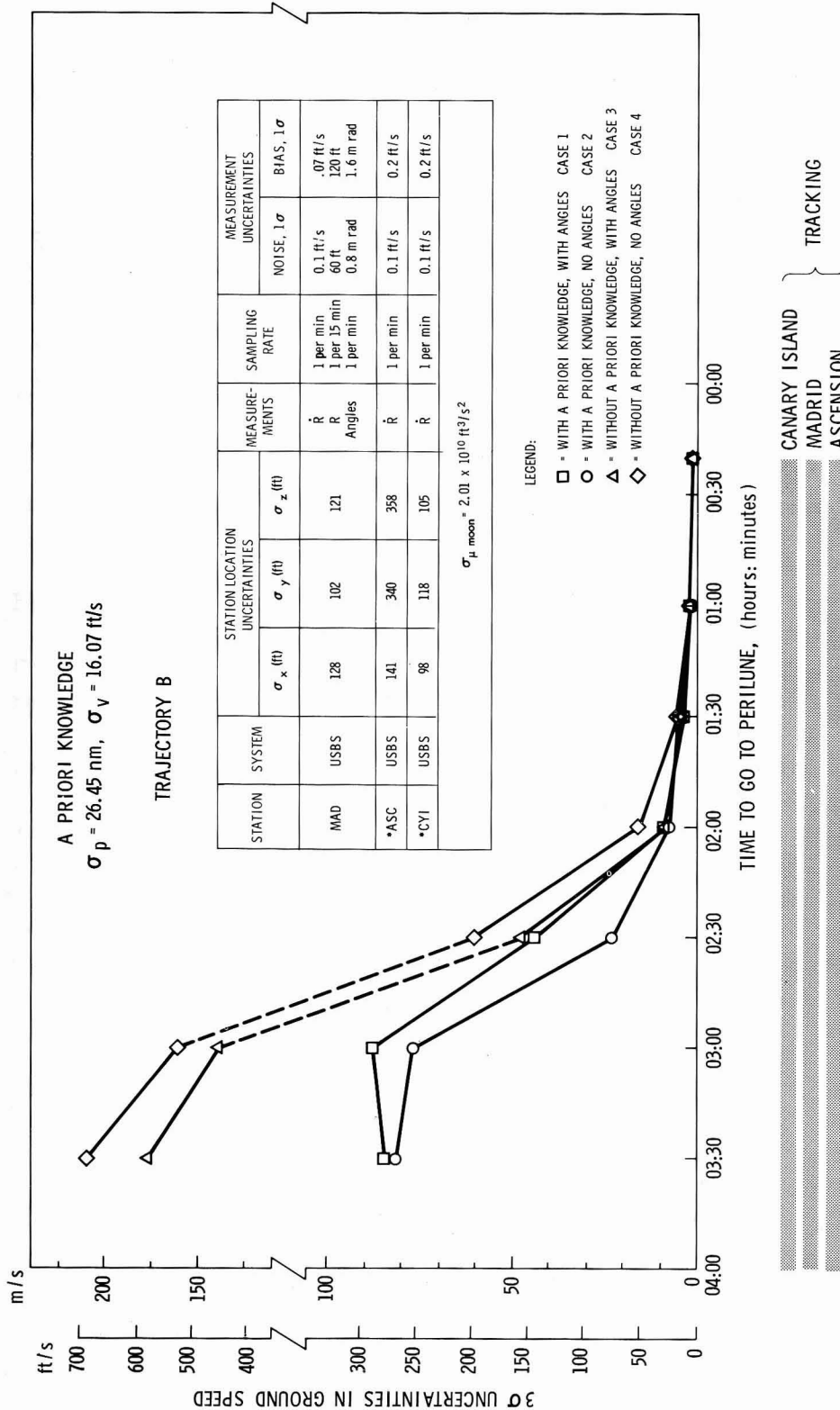


Figure 5.6d-Perilune. Ground speed uncertainties (Propagated to perilune), Leg 5.

## 6.0 CSM LUNAR PARKING ORBITS

### 6.1 INTRODUCTION

Error analysis studies were made for the CSM lunar parking orbit phase of the Apollo Mission for the purpose of evaluating the capabilities of the ground navigation system. This system makes use of the Manned Space Flight Network (MSFN). For the studies involving the ground navigation system, the Sept. 17, 1969 reference trajectory was used (Reference 1, page 3-11).

In order to evaluate the capabilities of the ground navigation system during the CSM lunar orbit phase, the following critical periods must be studied in detail:

1. From lunar parking orbit insertion to the beginning of CSM/LEM separation.
2. From the end of CSM/LEM separation to the beginning of CSM/LEM rendezvous
3. From the end of CSM/LEM rendezvous to transearth injection.

Although the present chapter emphasizes only the first period, the accuracies stated are indicative of those to be expected for any two orbits of the CSM. The first revision of this ANWG document will cover other portions of the CSM lunar orbit phase of the Apollo Mission in detail. Future studies will also consider the capabilities of the onboard navigation system which relies on an optical instrument much like a sextant to make sightings of lunar landmarks (References 5, 6, and 7).

### 6.2 DESCRIPTION OF THE LUNAR ORBIT PHASE

At the end of the burn of the Service Propulsion System, the spacecraft (CSM/LEM) is inserted into a lunar parking orbit. The inclination of the parking orbit is determined as a function of the landing site location, a region on the visible side of the moon bounded by selenographic longitude  $\pm 45^\circ$  and selenographic latitude  $\pm 5^\circ$ . The nominal parking orbit will be circular with an altitude above the moon's surface of  $80 \pm 5$  nm ( $148 \pm 9$  km). It is required that the vector from the moon's center through the chosen landing site lie in the lunar parking orbit plane during the period of time that the LEM lands on and lifts off the lunar surface.

The maximum allowable deviation of the landing site vector from the plane of the parking orbit is  $\pm 0.5^\circ$  (Reference 1, page 3-7).

The coordinates of the landing site chosen for the Sept. 17, 1969 reference trajectory are (Reference 4, pages 2-8 and 2-9):

Selenographic Latitude:  $2.24^\circ\text{N}$

Selenographic Longitude:  $13.00^\circ\text{W}$

For this reference trajectory, the CSM/LEM is inserted into a lunar parking orbit on the back side of the moon. The spacecraft will be occulted by the moon for approximately 22 minutes after insertion. Following this initial occultation period, the spacecraft will be visible to various tracking stations of the MSFN for a period of 77 minutes 18 seconds and occulted for a period of 45 minutes 42 seconds. Tracking coverage for the various tracking stations of the MSFN is given for the first 6 hours, 30 minutes after the spacecraft is inserted into the lunar parking orbit (Figure 6.1).

Near the end of the second lunar parking orbit, or approximately 3 hours 48 minutes after lunar orbit insertion, CSM/LEM separation occurs. Knowledge of the state vector at the time of CSM/LEM separation depends upon the tracking of the CSM during this first period. This state vector, when propagated through the thrusting period of the LEM, will then represent the a priori knowledge for the LEM descent transfer trajectory. The ability of various tracking station combinations of the MSFN to determine the state vector during this first critical phase of the CSM lunar orbit operations is investigated in detail.

### 6.3 THE GROUND NAVIGATION SYSTEM

The accuracy with which the state vector of the spacecraft is determined at the beginning of CSM/LEM separation is dependent on such factors as:

- a. Tracker – spacecraft geometry
- b. Types of measurements made
- c. The a priori knowledge about the condition of the state at the time of CSM/LEM lunar orbit insertion
- d. Frequency with which measurements are made



e. Errors due to:

- Measurement noise
- Measurement biases
- Station location biases
- Equations of motion biases.

It is assumed that linear filter theory can provide a statistical estimate of the state vector uncertainty which reflects the effects of the various error sources inherent in a measurement. One of the most commonly used linear estimators is the minimum variance filter (or Kalman - Schmidt filter). This linear estimator properly accounts for all the biases without updating and provides a (theoretically) optimal estimate of the state vector. This estimation procedure is recursive, i.e., data points are processed successively in their natural time order. The recursive procedure gives the optimal estimates at each data time.

Two error propagation computer programs using the minimum variance filter were used to generate all the error analysis studies in this chapter (References 3 and 8). Station location biases and the speed of light bias were accounted for in both programs, whereas measurement biases were accounted for in only one of these programs (Reference 8). The one sigma values of bias and noise used for the analysis, taken from Reference 1, are given on each graph presented. The present versions of these computer programs do not include the effects of errors in the equations of motion, such as the biases in the moon's gravitational constant and in the coefficients in the moon's gravitational potential function. Present plans call for these to be included in future studies.

### 6.3.1 Error Propagation in Spacecraft Position and Velocity Using One Tracking Station

Figures 6.2a and 6.2b show the three sigma errors in spacecraft position and velocity<sup>1</sup> with and without the assumption of a priori knowledge of the state at lunar orbit insertion. Without a priori knowledge the errors in the state vector are greater than when a priori knowledge is available. Range rate measurements from a single tracking station are used to improve estimates of the energy dependent variables such as velocity magnitude, semimajor axis, and orbital period. On the other hand, very little information about the orientation of the spacecraft's orbital plane can be extracted from these measurements. This information about the orientation is, however, implicitly contained in the a priori knowledge of the state. Therefore, the errors in the state vector will be smaller whenever a priori knowledge is available.

<sup>1</sup>These minimum variance error propagation computer programs require an initial statistical estimate of the state vector. Therefore, for analysis with no a priori knowledge, a very poor initial estimate is used.

If a single tracking station is used for determining the errors in the state vector at the time of CSM/LEM separation, the results depend on what initial a priori knowledge about the state is available. A summary of the three sigma errors at the time of CSM/LEM separation is given in Table 6.1.

Table 6.1  
3 $\sigma$  Errors of the State Vector at Time of CSM/LEM  
Separation Using Measurements From One Tracker

Type of Measurement	Was a Priori Knowledge Used?	3 Sigma Position Error	3 Sigma Velocity Error
$\dot{R}$	No	70,000 ft. (21 km)	30.0 ft/s (12.1 m/s)
$\dot{R}$	Yes <sup>2</sup>	50,000 ft. (15 km)	25.0 ft/s (7.6 m/s)

### 6.3.2 Error Propagation in Spacecraft Position and Velocity Using Three Tracking Stations

Wherever possible, a tracking station complex composed of three Unified S-Band Systems tracks the CSM/LEM up to CSM/LEM separation. The tracking station complex is composed of one 85-foot USBS which tracks the spacecraft in the two-way Doppler mode and two 30-foot USBS which track the spacecraft in the three-way (or passive) Doppler mode.

Figures 6.3a and 6.3b show how the tracker-spacecraft geometry influences the RMS errors in the state vector. The 85-foot USBS at Canberra tracks the spacecraft in the two-way Doppler mode and the 30-foot USBS at Carnarvon and another 30-foot USBS, either at Guam or at Hawaii, track the spacecraft in the three-way Doppler mode. Solutions are presented for both combinations.

Because of the better geometry of the Canberra – Carnarvon – Hawaii – combination, the three sigma errors in spacecraft position and velocity are smaller than for the Canberra – Carnarvon – Guam combination.

At the time of CSM/LEM separation, the three sigma errors in spacecraft position and velocity are as follows:

---

<sup>2</sup>A priori knowledge for study is:  
 Three sigma error in position: 51141.6 ft (15.5 km) } (see Reference 2)  
 Three sigma error in velocity: 102.3 ft/s (31 m/s) }

USBS Combination	3 Sigma Position Error	3 Sigma Velocity Error
Canberra - Carnarvon - Hawaii	28,000 ft. (8500 m)	20 ft/s (6.1 m/s)
Canberra - Carnarvon - Guam	35,000 ft. (10700 m)	26 ft/s (7.9 m/s)

The a priori knowledge which was assumed is

3 sigma position error: 51,141.6 ft (15500 m)

3 sigma velocity error: 102.3 ft/sec (31 m/s).

Figures 6.4a and 6.4b illustrate how the effect of measurement bias errors causes the errors in spacecraft position and velocity to increase. Using the tracker combination of Canberra - Carnarvon - Hawaii the three sigma errors at CSM/LEM separation are:

With/Without Measurement Bias	3 Sigma Position Error	3 Sigma Velocity Error
Without	1000 ft. (300 m)	0.7 ft/s (0.2 m/s)
With	28,000 ft. (8500 m)	20 ft/s (6.1 m/s)

As may be readily seen, the measurement bias errors are the major contributors to the errors in spacecraft position and velocity.

Increased sampling rates (Figures 6.5a and 6.5b) will not decrease the errors in spacecraft position and velocity for this case. Only measurement noise will decrease with an increased sampling rate; the measurement bias errors will remain unaffected. At the time of CSM/LEM separation, the three sigma errors in spacecraft position and velocity remain almost unchanged whether sampling rates of one measurement per minute or ten measurements per minute are used. The relatively close agreement between the curves of Figures 6.5a and 6.5b shows that increased sampling rates (for this tracking interval) cannot alone reduce errors in position and velocity in the presence of large bias errors.

For the results presented in Figures 6.6a and 6.6b, the spacecraft was tracked by the Canberra - Carnarvon - Hawaii complex of USBS tracking stations for the first tracking period of approximately 77 minutes 18 seconds. The resulting errors in spacecraft position and velocity propagated to the beginning of the second tracking period are the a priori knowledge of the state at this time.

Then two cases were compared. On one, the spacecraft was tracked by the same complex for the second tracking period. On the other, the spacecraft was tracked by only the Canberra tracking station for the second tracking period. The resulting errors in spacecraft position and velocity are practically the same for these two cases. Thus the number of tracking stations may be reduced on the second tracking period without degradation of the results.

#### 6.4 - LEVEL OF CONFIDENCE

A comparison of results between two different minimum variance error programs (References 3 and 8) has been made for the treatment of the effects of station location biases and the speed of light bias. For example, the two programs were in agreement on the results presented on the lower curves of Figures 6.4a and 6.4b to within 10 ft. and .01 ft/s, respectively, at all points. The error analysis studies for the ground navigation system for which the effects of measurement bias errors were evaluated have not been verified directly. However, the results are in general agreement with those obtained in other independent studies performed at GSFC and MSC.

#### 6.5 CONCLUSIONS

For the ground navigation system, the propagation of three sigma errors in spacecraft position and velocity during the first critical period of the CSM-lunar parking orbit phase of the Apollo Mission has been described. From all the results presented, it is quite evident that the measurement bias errors inherent in the data from the ground navigation system significantly influence the accuracy of the estimate of the spacecraft's position and velocity vectors. For example, the effect of measurement bias errors (Figures 6.4a and 6.4b) at the time of CSM/LEM separation (3 hours 48 minutes after lunar orbit insertion) has increased the error in spacecraft position and velocity by almost a factor of 30 (from 1,000 ft. to 28,000 ft. and from 0.7 ft/s to 20 ft/s respectively). One possible means of offsetting such effects could be the combining of data from the onboard navigation system with data from the ground navigation system.

In past error analysis studies it has been found that by solving for the measurement bias errors their effect on the knowledge of the state vector is decreased. This does not mean that such results can be obtained by a real time orbit determination program (ODP). Difficulty of uncoupling the effects of measurement bias errors might degrade rather than improve the knowledge of the state. Therefore, it is a qualified recommendation that some selected measurement bias errors should be solved for in order to reduce their effects on knowledge of the state vector, (subject to verification by simulating the processing of data with an operational ODP).

## 6 REFERENCES

MSC-GSFC, ANWG Report No. 65-AN-1.0 "Apollo Missions and Navigation Systems Characteristics," February 5, 1965.

Mayfield, S. O. and Bond, A. C., MSC Internal Note No. 65-FM-47, "Convergence and Non-convergence in Lunar Orbit Determination, Accuracy of Lunar Orbit Determination," April 20, 1965, page 10.

Philco Corporation, User's and Programmer's Manuals for Interplanetary Error Propagation Program prepared for Contract NAS5-3342.

Design Reference Mission - Apollo Mission Planning Task Force Vol. I Mission Description, October 30, 1964.

Sears, Norman E.; "Primary G&N System Lunar Orbit Operations," (U), MIT/IL, R446, Vol. I, April, 1964.

MSC Internal Note No. 65-ET-2, "Positional Uncertainties in Lunar Landmarks," NASA-MSC, Jan. 5, 1965.

Bond, V. R., MSC Internal Note EG-65-4, "Orbital Determination by Ill Defined Lunar Landmarks," February 1, 1965.

Woolston, D. C. and Mohan, J., "Program Manual for Minimum Variance Precision Tracking and Orbit Prediction Program," GSFC Report X-640-63-144, July 1, 1963.

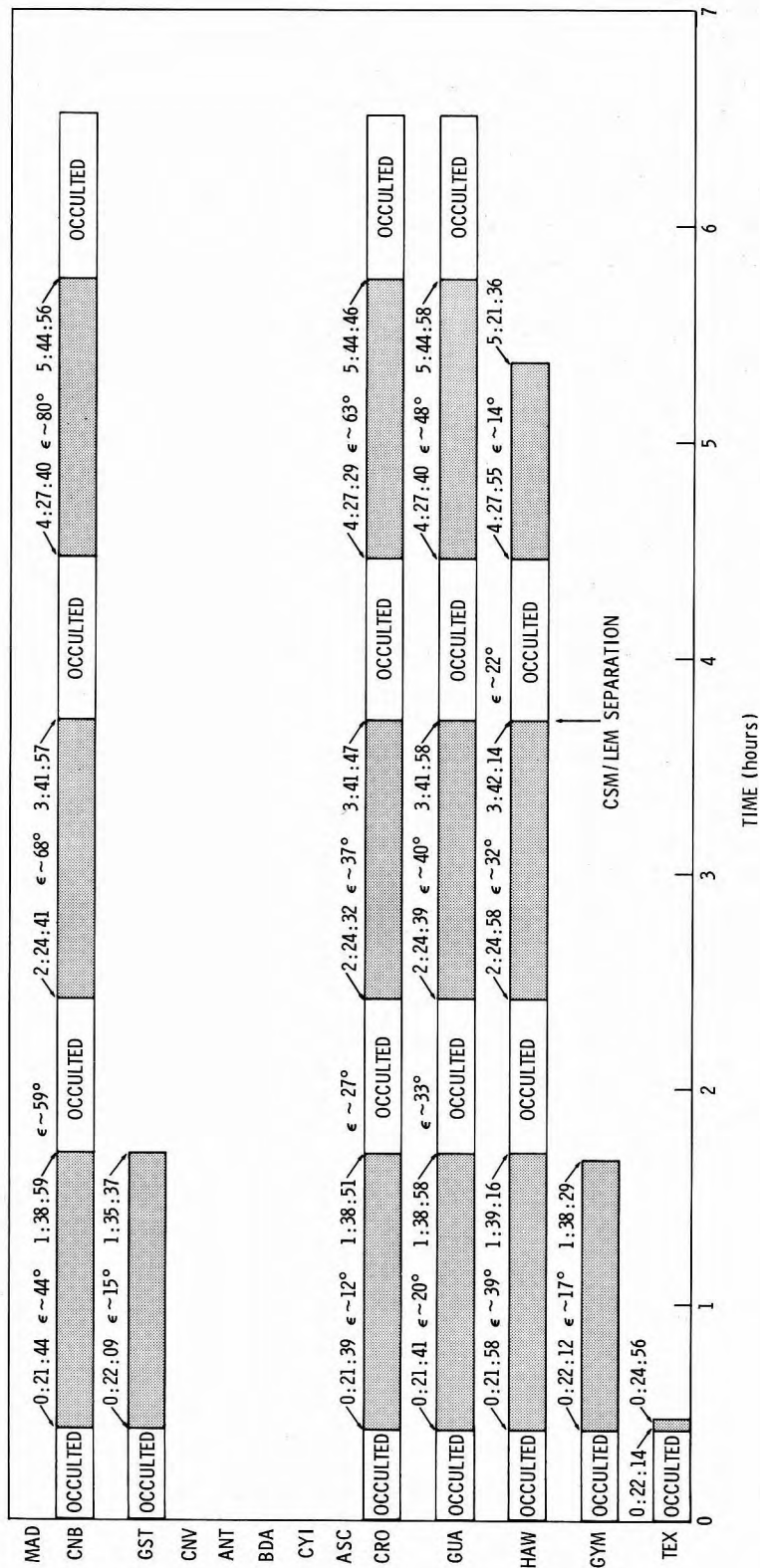


Figure 6.1—CSM station contact times for Sept. 20, 1969 trajectory



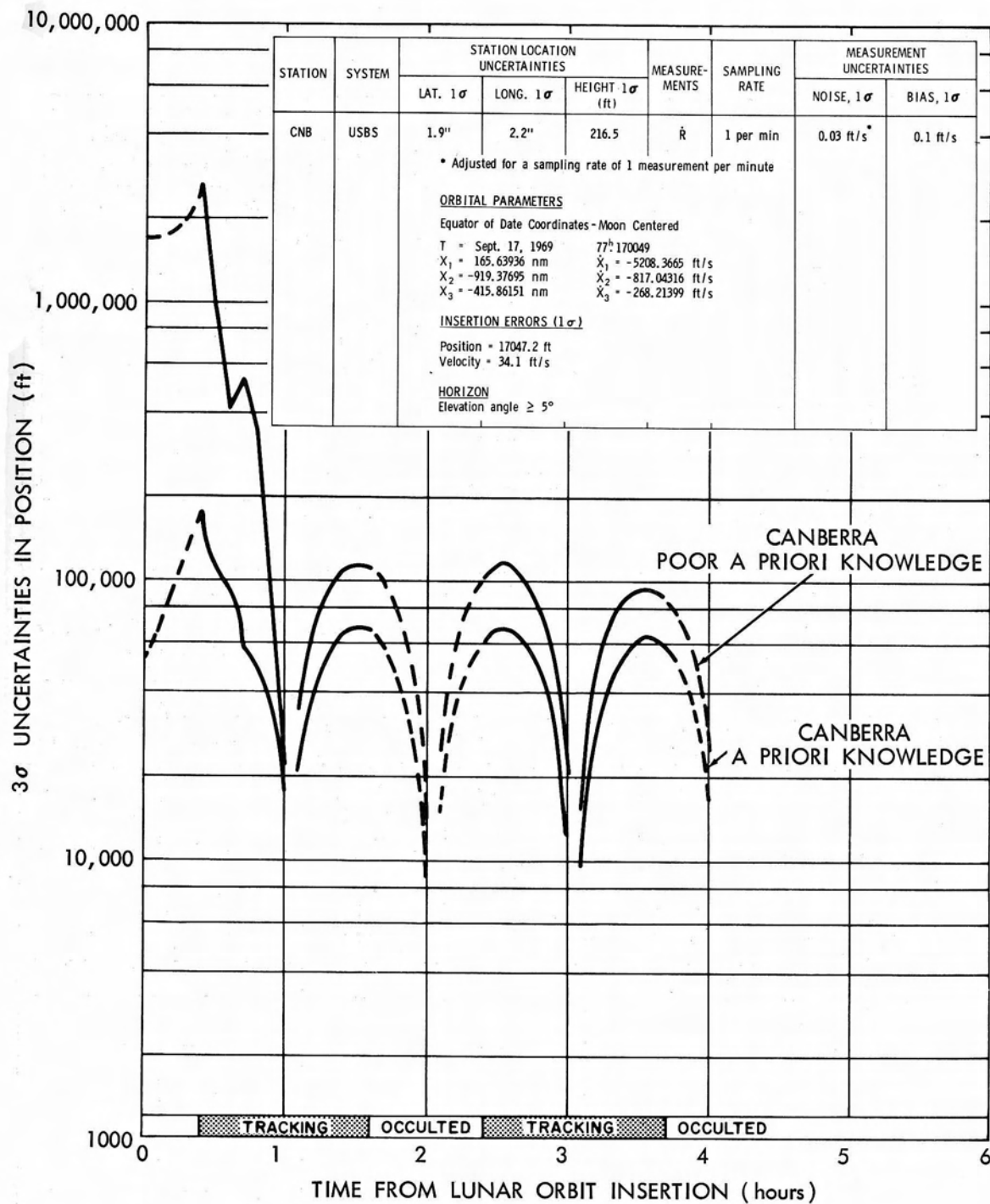


Figure 6.2a—Effects of a priori knowledge on error propagation in spacecraft position for a single station measuring range rate

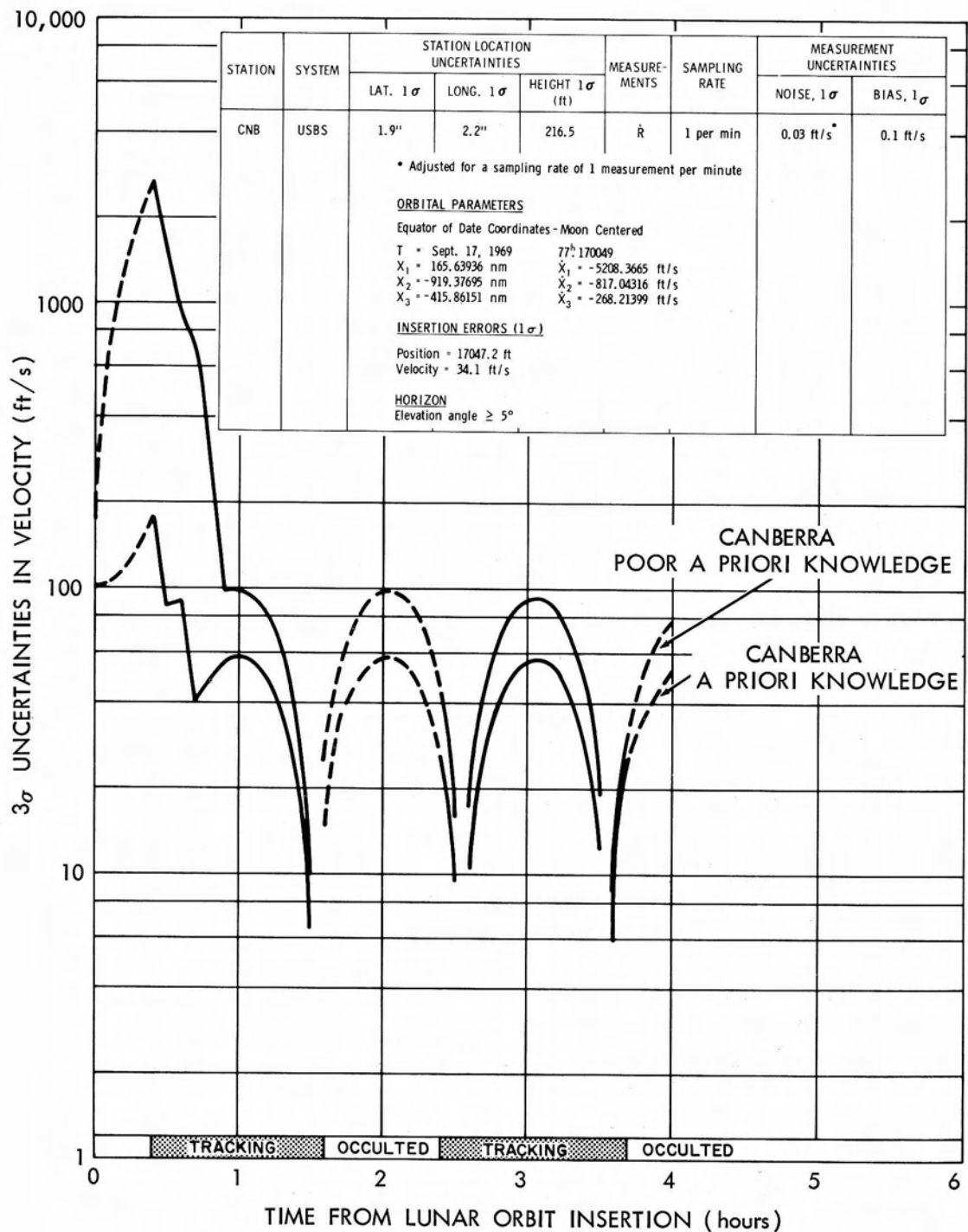


Figure 6.2b—Effects of a priori knowledge on error propagation in spacecraft velocity for a single station measuring range rate



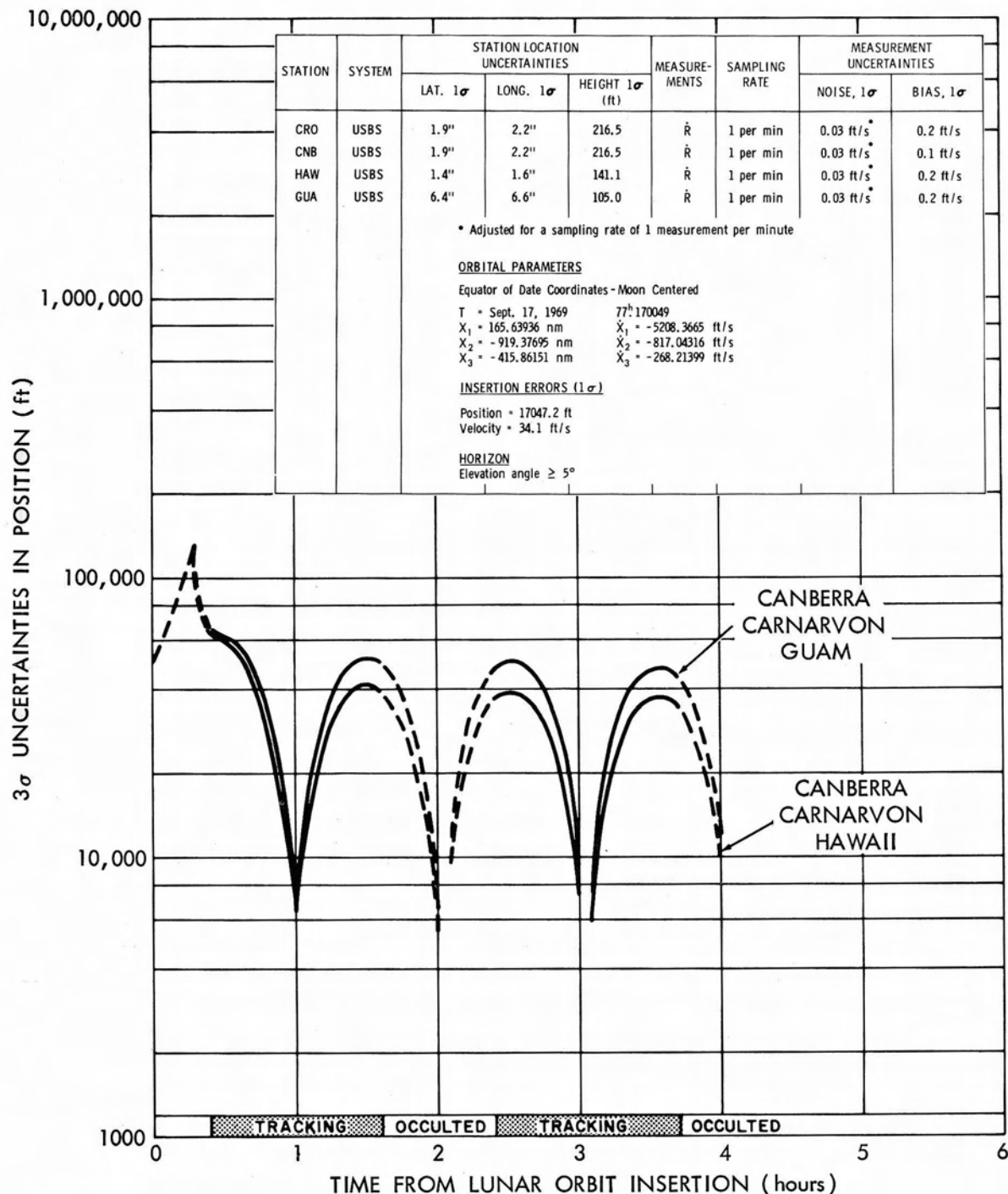


Figure 6.3a—Effects of tracker geometry on error propagation in spacecraft position for three trackers measuring range rate

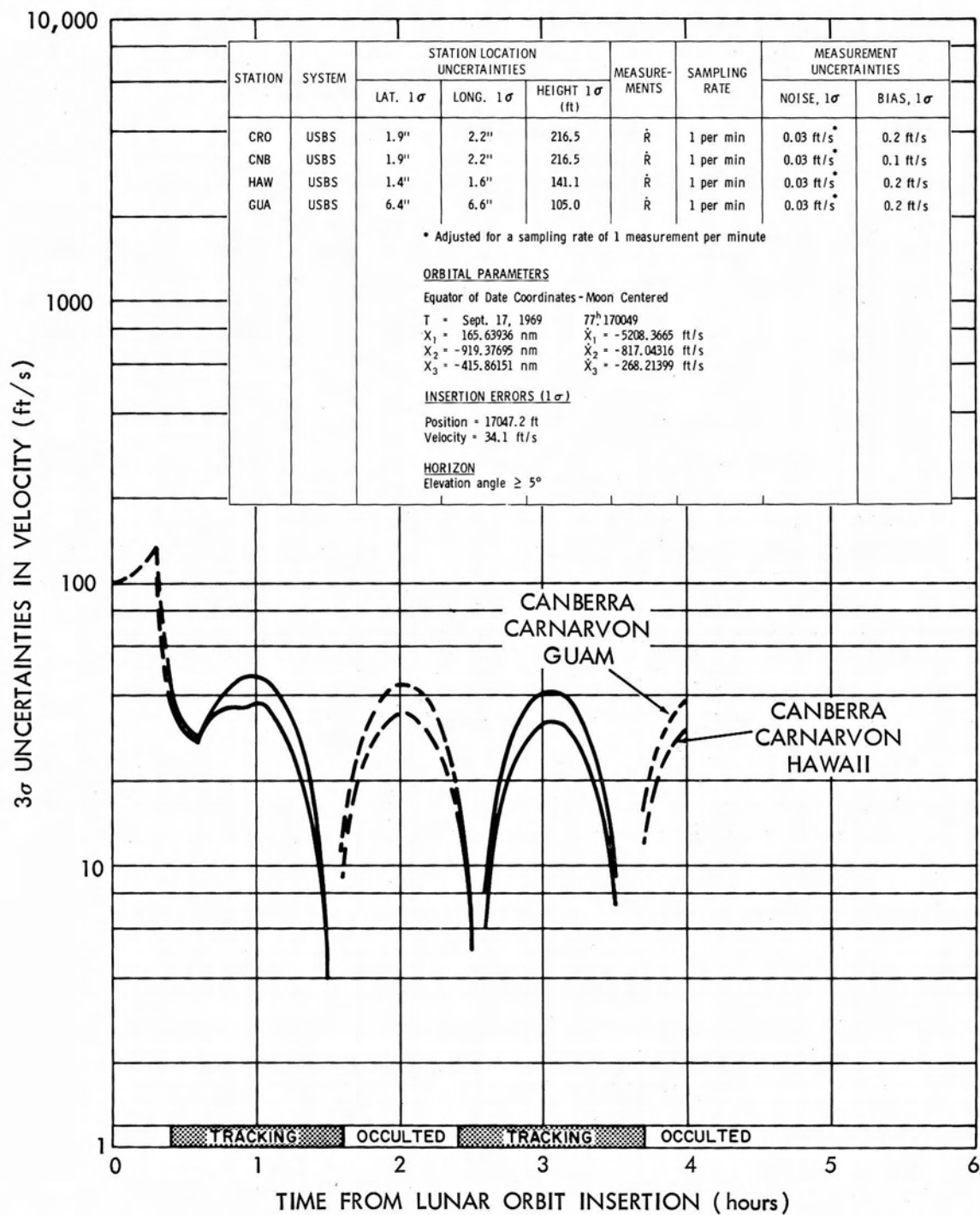


Figure 6.3b—Effects of tracker geometry on error propagation in spacecraft velocity for three trackers measuring range rate

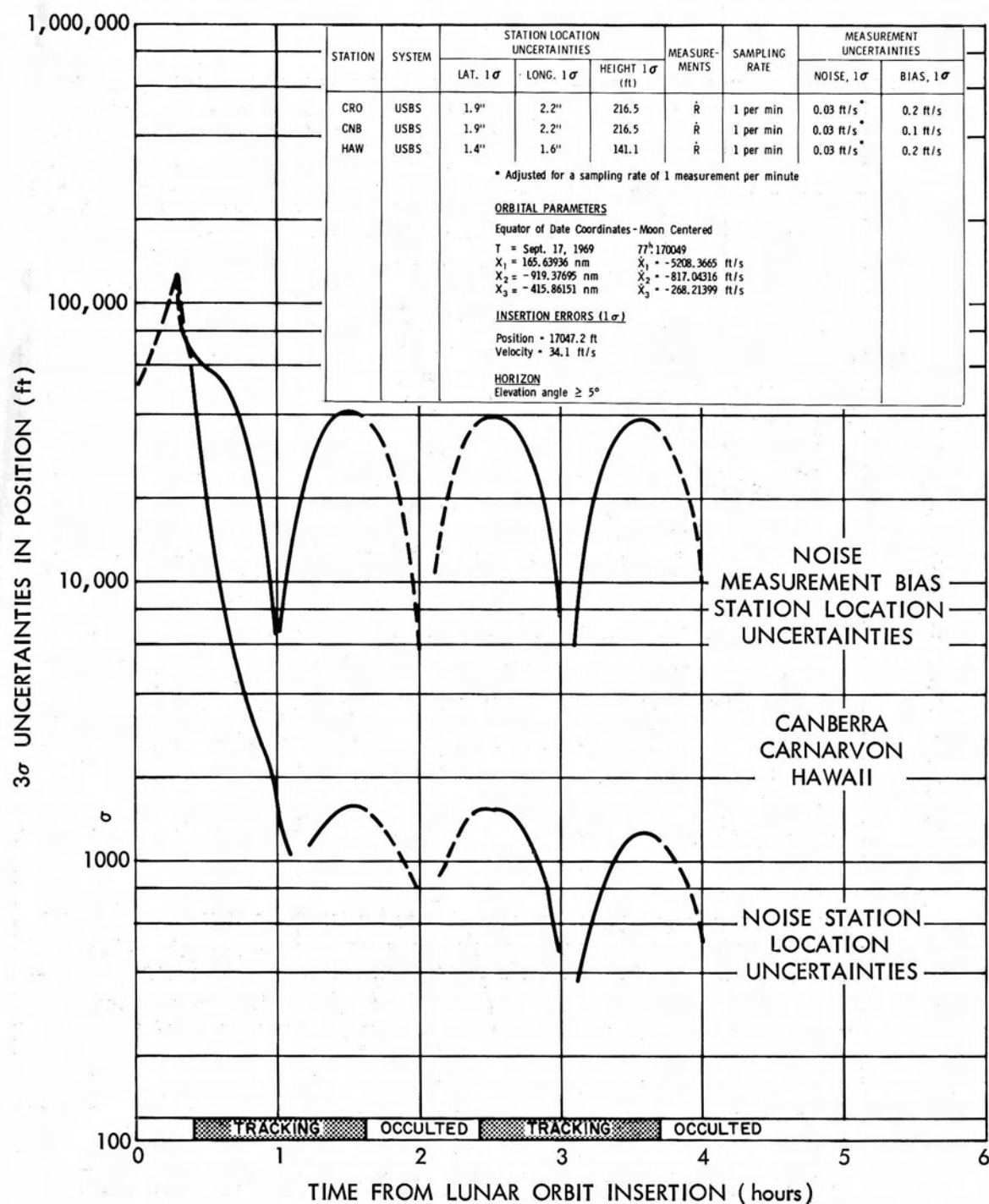


Figure 6.4a—Effects of measurement bias errors on propagation of errors in spacecraft position

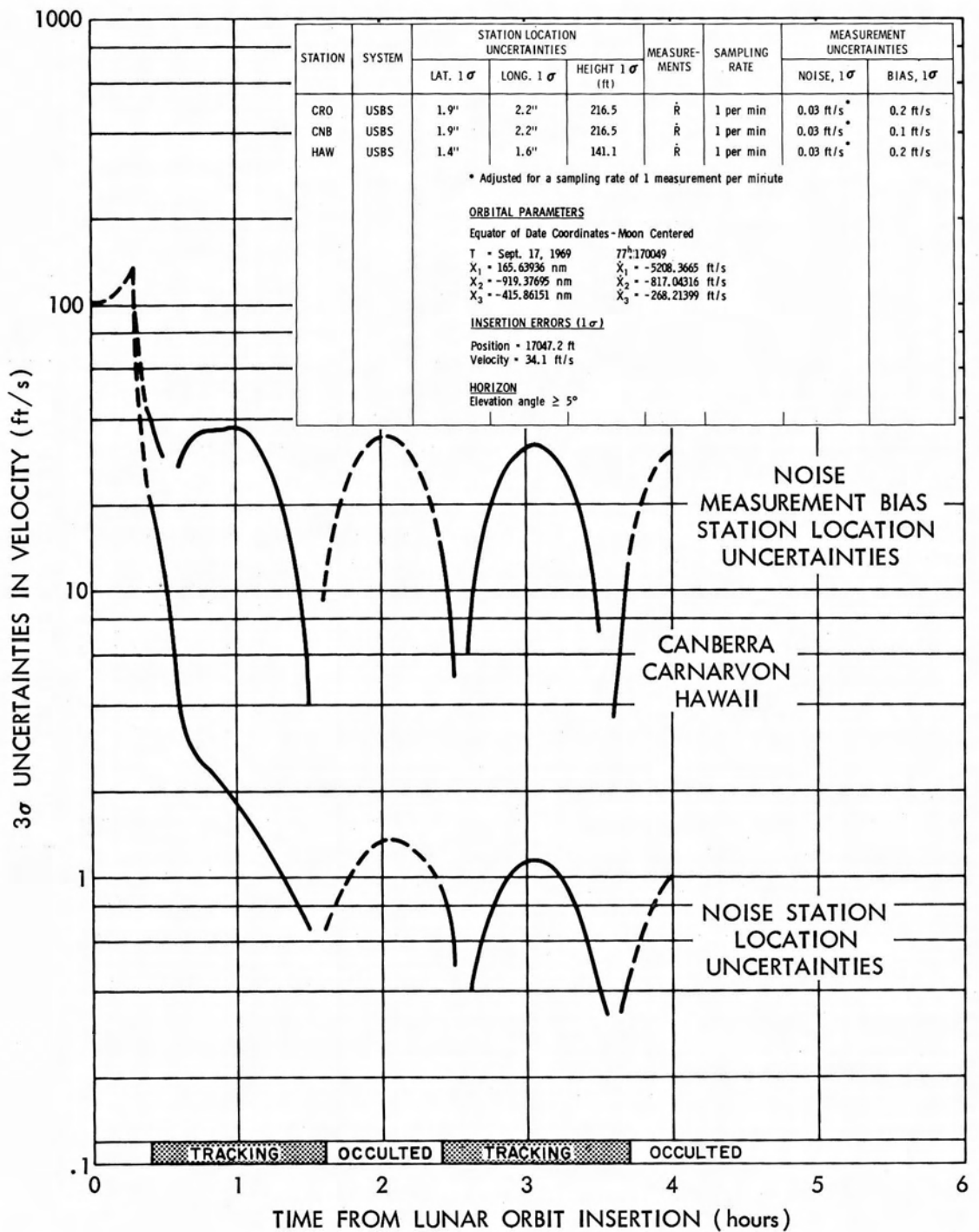


Figure 6.4b—Effects of measurement bias errors on propagation of errors in spacecraft velocity

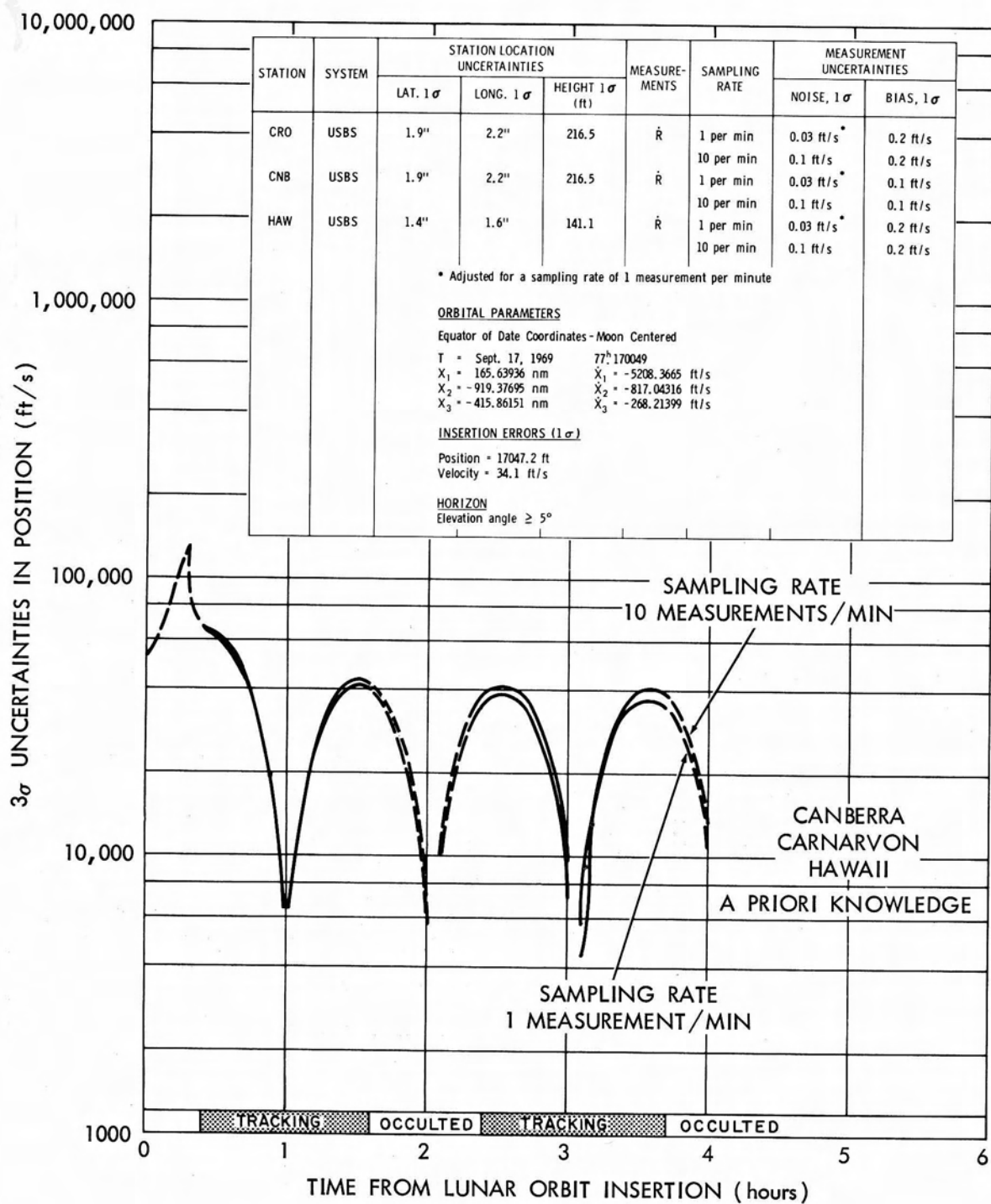


Figure 6.5a—Effects of sampling rates on propagation of errors in spacecraft position for three trackers measuring range rate

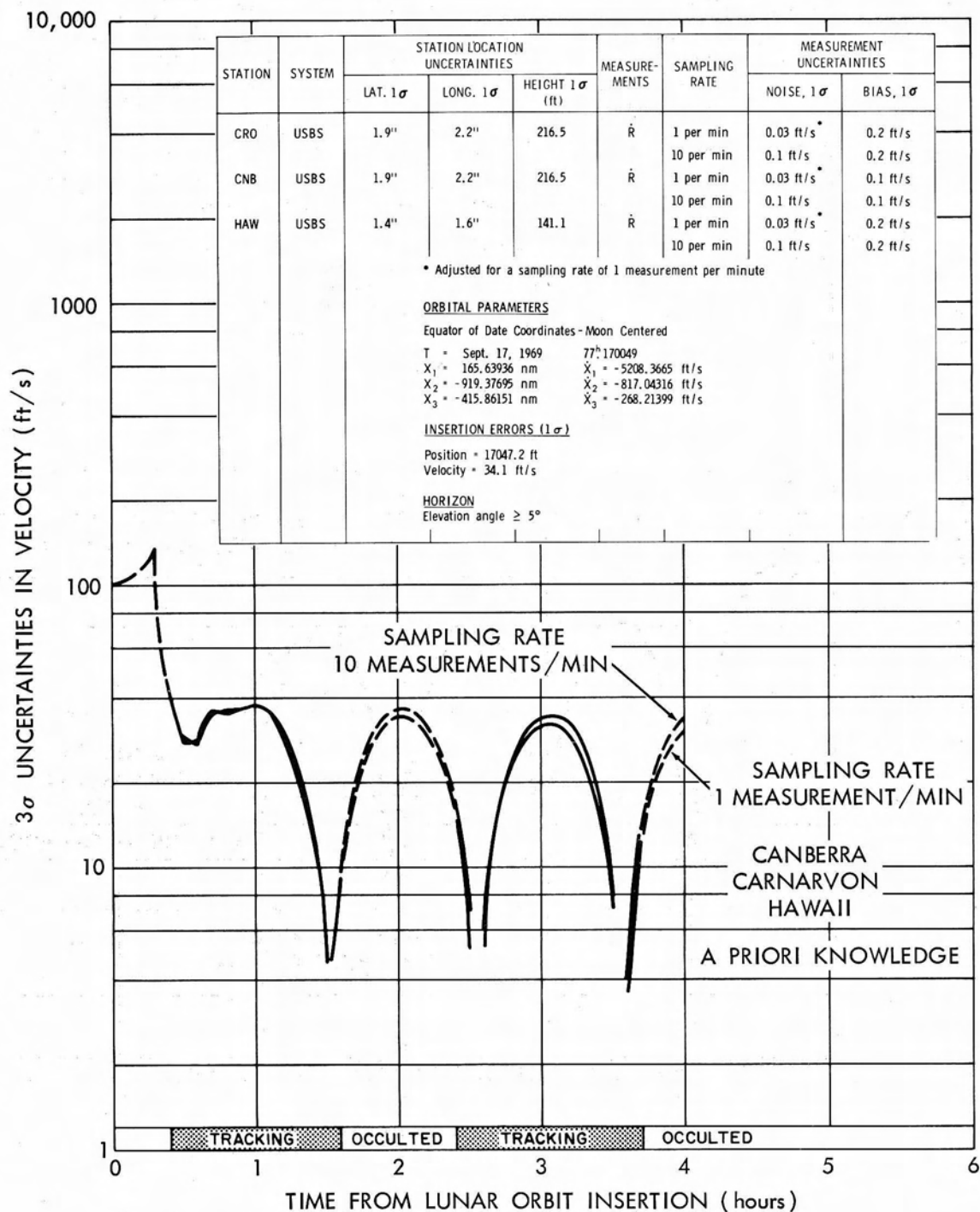


Figure 6.5b—Effects of sampling rates on propagation of errors in spacecraft velocity for three trackers measuring range rate

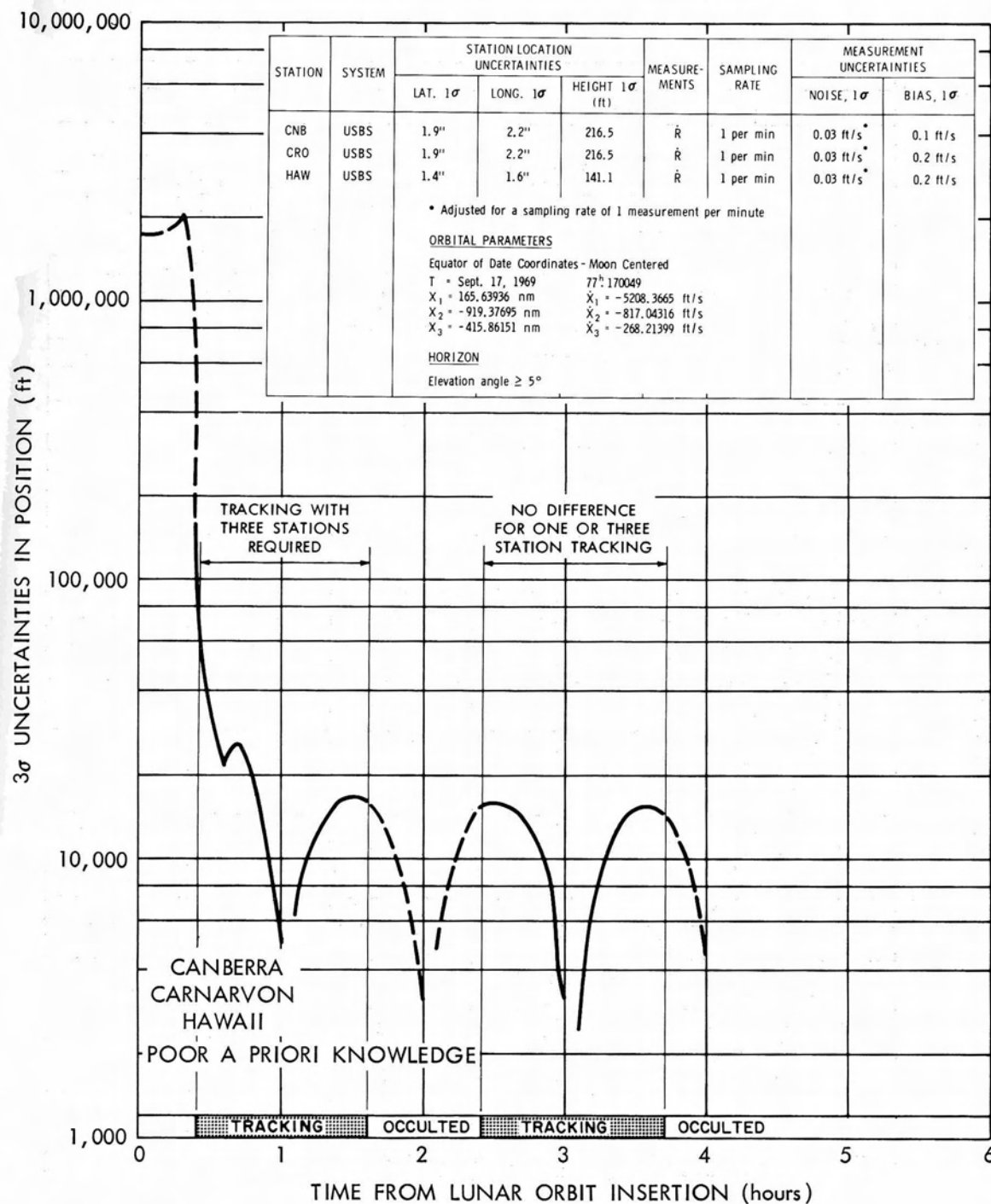


Figure 6.6a—Error propagation in spacecraft position when tracking the spacecraft with one or three trackers after the first complete occultation period

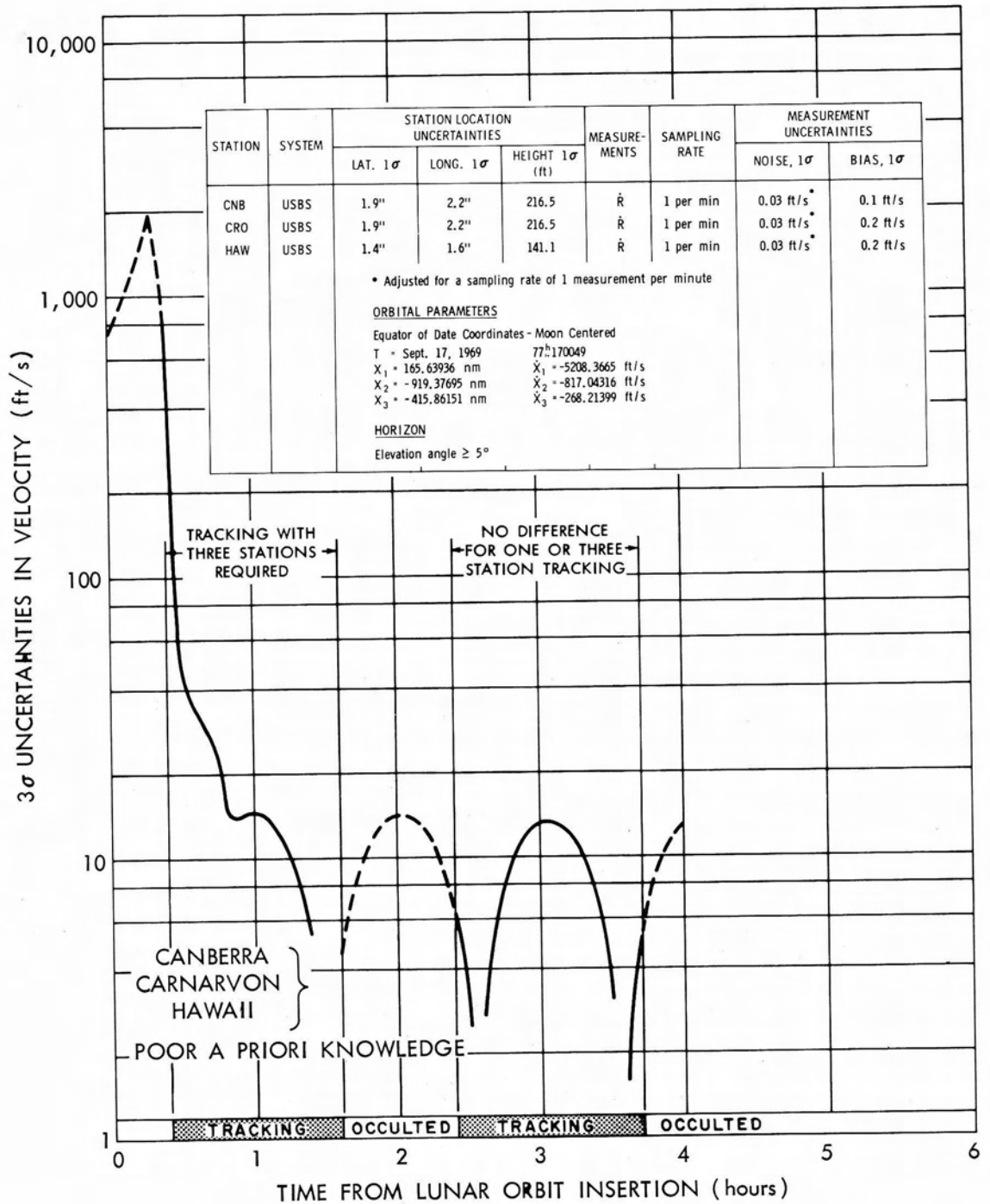


Figure 6.6b—Error propagation in spacecraft velocity when tracking the spacecraft with one or three trackers after the first complete occultation period



## 7.0 LEM OPERATIONS PHASE

### 7.1 INTRODUCTION

The LEM operation phase is defined for this study as beginning with the separation of the LEM from the CSM and terminating with the docking of the LEM with the CSM. For the present, this study investigates only the free fall portions of both the descent and ascent trajectories and makes no utilization of onboard data concerning the position and velocity of the LEM. All results are based on data obtained by the MSFN (Manned Spaceflight Network) alone.

The study concerning the descent trajectory starts immediately subsequent to insertion into the descent trajectory and ends at perilune arrival.

The study concerning the ascent trajectory starts immediately subsequent to ascent burnout and ends at the nominal time of rendezvous. The thrusting maneuvers that occur subsequent to ascent burnout and prior to rendezvous are taken into account only insofar as execution errors are assumed for each maneuver.

#### 7.1.2 Use of the MSFN

During periods when tracking occurs, it is assumed that three USBS stations are simultaneously tracking the LEM. One station is the transmitting station (master) and the other two are passive trackers (slave 1 and slave 2). The transmitting station obtains two-way Doppler while the passive trackers obtain three-way doppler. All of the observations are taken at a rate of one observation per six seconds. Angular data, due to its geometric dilution at lunar distances, was not used. The predominate procedure for this study was to not use range measurements. Data reliability is assumed to be 100 percent, i.e., no data is assumed lost due to loss of lock, station failures, or transmission troubles. Noise and biases on the data, uncertainty in the gravitational constant of the moon, and station location uncertainties that were assumed for this study are presented on the figures in which they are applicable, and are consistent with Reference 1. When results are presented in tabular form, reference will be made to the data characteristics that were assumed for those results.

### 7.1.3 Areas of Investigation

#### A. USBS tracking station geometry relative to the LEM's orbit

In this study three different sets of three stations were chosen to track the LEM in order to investigate the influence that the different station geometries have on the results. These three sets and their geometry relative to the LEM's orbit plane are:

1. Goldstone (master), Antigua (slave 1), and Hawaii (slave 2). These stations have a very good east-west separation but a poor north-south separation. The sublunar point (the point where the earth-moon line pierces the earth) at the epoch time for each trajectory for which these stations are tracking the vehicle was assumed to be  $20^{\circ}\text{N}$  latitude and  $90^{\circ}\text{W}$  longitude. The LEM's orbit plane (which is assumed for this entire study to be in the earth-moon plane) is in approximately the plane of the stations.
2. Madrid (master), Canary (slave 1), and Ascension (slave 2). These stations have a good north-south separation but a poor east-west separation. The sublunar point at the epoch time for each trajectory, for which these stations are tracking the vehicle, was assumed to be  $20^{\circ}\text{N}$  latitude and  $40^{\circ}\text{E}$  longitude. The LEM's orbit plane is approximately perpendicular to the plane containing these stations.
3. Canberra (master), Carnarvon (slave 1), and Guam (slave 2). These stations have both a fairly good east-west and north-south displacement. The sublunar point at the epoch time for each trajectory for which these stations are tracking the vehicle was assumed to be  $20^{\circ}\text{N}$  latitude and  $165^{\circ}\text{E}$  longitude.

#### B. Landing sites

The longitude of the landing site determines the length of the tracking interval previous to perilune arrival and subsequent to ascent burnout. Therefore, descent to and ascent from three different landing sites were investigated in this study. They are  $45^{\circ}\text{W}$  longitude,  $0^{\circ}$  longitude, and  $45^{\circ}\text{E}$  longitude in the selenographic coordinate system. Varying the latitude of the landing site has little effect on the tracking, and, hence, it was kept fixed at  $0^{\circ}$ .

### C. Error Analysis Techniques

This study was conducted with certain assumptions concerning the accuracy of the MSFN and with a linear error analysis program (Reference 2) based on a weighted least squares filtering technique. This error analysis program was used to evaluate the capability of determining an orbit with data of the assumed characteristics and with a filter which makes certain assumptions concerning the biases.

Most of the study was conducted to evaluate the capability of determining an orbit with data containing noise and biases and with a filter which ignored the assumed biases. This filter will henceforth be referred to as Filter-1. In making this evaluation the error analysis program computed the uncertainties in the orbital parameters taking into account that there are biases on the data which are being ignored by the filter. It should be noted that the Apollo real time orbit determination program will account for some bias effects by adjusting the measurement data weighting scheme or by solving for some biases explicitly or, most probably, by using some combination of these two techniques. Consequently, the results obtained with Filter-1 are considered to be conservative and subject to change as future studies are conducted.

The concluding portion of the study was conducted to evaluate orbital accuracies with two other filters which assume:

1. The MSFN measurements are corrupted by random noise and biases, and, in this case, the biases are solved for in the same manner as the position and velocity. This procedure, **referred to** as an optimum filter, should produce the smallest residuals in the orbit determination. It will hereafter be referred to as Filter-2.

2. The MSFN measurements are corrupted by random noise and biases. In this case, selected biases are solved for in the same manner as the position and velocity, but the remaining biases are ignored. This procedure will be referred to as Filter-3. This filter offers a compromise between filters 1 and 2.

3. Filter-3 was studied for a case such that the data it processed actually was bias free. The results which this case produces serve as a gauge by which to measure the results obtained from the other filters.

## 7.2 PROCEDURES AND ASSUMPTIONS

### 7.2.1 Geometry of the Descent and Ascent Trajectories (Figure 1)

The LEM will separate from the CSM and initiate its Hohmann descent trajectory (80 nm apolune to an 8 nm perilune) as it reaches a point a little more than  $180^\circ$  from the chosen lunar landing site in the second lunar orbit of the CSM. The chosen landing site will lie between  $\pm 5^\circ$  latitude and  $\pm 45^\circ$  longitude in the selenographic coordinate system. The period of the trajectory is approximately two hours so that, depending upon the landing site, the LEM will come into view of the earth 15 to 45 minutes prior to perilune arrival. At perilune the vehicle begins initiation of the powered descent. The plane of the LEM's orbit will be the same as the CSM's lunar orbital plane, which will lie within  $15^\circ$  of the earth-moon plane.

The following description of the ascent trajectory represents the type that is likely to be chosen when navigational aid, either in a primary or back up role, is to be based on MSFN data. The LEM ascends to an orbit having a perilune of 8 nm and an apolune of 30 to 70 nm. At apolune the LEM initiates a maneuver to circularize the orbit. Approximately 20 to 30 minutes after the LEM reappears from behind the moon (allowing time for an update of the LEM's position and velocity, based on MSFN navigation) it initiates a rendezvous transfer maneuver. Rendezvous with the CSM occurs at an 80 nm. altitude and approximately  $150^\circ$  from the transfer maneuver. A midcourse correction will probably be made between the transfer maneuver and rendezvous.

## 7.3 RESULTS

### 7.3.1 Outline of Results

#### A. Descent Phase - 4 Figures, 2 Tables.

Figures 7.2 - 7.4 present the position and velocity uncertainties at perilune arrival, as a function of tracking time, that result from different tracking geometries and different landing sites.

Figure 7.5 presents the position and velocity uncertainties at perilune arrival, as a function of tracking time, that result from an analysis with Filter-1, Filter-2, Filter-3, and Filter-3 for which the data contain no biases.

Table 7.1 breaks down the position uncertainties at perilune arrival into the components altitude, range, and track. Altitude is in the direction of the radius vector; track is parallel to the orbit angular momentum vector; and range completes a right-hand orthogonal system.

Each row in Tables 7.1, 7.3, 7.4, and 7.5 and each curve on a figure represents a particular set of assumptions labeled by case numbers. These cases are defined in Table 7.6.

Table 7.2 shows the one sigma uncertainties of the biases, as a function of tracking time, that result when the biases are solved for in the same manner as the position and velocity.

#### B. Ascent Phase - 3 Tables

Table 7.3 presents the uncertainties in the LEM's position and velocity vectors at four key points along the ascent trajectory. These points are:

1.  $t_0$  (ascent burnout)
2.  $t_{\text{circulation}}$  (the time of the circularization maneuver)
3.  $t_{\text{transfer}}$  (the time of the rendezvous transfer maneuver)
4.  $t_{\text{rendezvous}}$  (the nominal time of rendezvous)

Points 1 and 2: Columns 1-2 and 3-4 show how well insertion conditions can be known and circularization conditions can be predicted. These uncertainties are based on tracking data obtained between ascent burnout and 5 minutes prior to loss of sight (the 5 minutes being allowed for updating the LEM computer and verification of this update). Points 2 and 3: Columns 5-6 and 7-8 show how well the circularization conditions can now be known and how well the transfer conditions can be predicted. These uncertainties are based on the additional tracking data obtained between the time the LEM is reacquired after being occulted by the moon and up to 5 minutes prior to the transfer maneuver. Points 3 and 4: Columns 9-10, 13-14, 17-18, and 11-12, 15-16, 19-20, respectively, show how well conditions at transfer can be determined and how well rendezvous conditions can be predicted. Execution errors were taken into account for each maneuver.

Table 7.4 presents a regrouping of selected cases from Table 7.3 in order to facilitate a comparison.

Table 7.5 presents uncertainties in the LEM's position and velocity after the transfer maneuver, assuming that the LEM guidance computer has been updated with MSFN navigation data prior to transfer.



### 7.3.2 Discussion of Results

#### A. Descent Phase

The configuration of Goldstone, Antigua, and Hawaii represents the poorest station geometry of the three tracking station sets that were considered for this study, provided the tracking interval is at least 10 minutes. Figures 7.2 through 7.4 show that the uncertainties in position and velocity that were computed from the data obtained by Goldstone, Antigua, and Hawaii are consistently greater than the uncertainties that were computed from the data obtained by the other two station sets. As these stations lie approximately in the LEM's orbit plane, little knowledge of the out-of-plane component can be obtained from their data. An inspection of Table 7.1, cases 1, 4, 7, 10, and 13 (see Table 7.6) will verify that the uncertainty in the track (out-of-plane) component of position is not reduced as significantly as the in-plane components with increased tracking time.

The configuration of Madrid, Canary, and Ascension represents the poorest station geometry for a tracking interval of 5 minutes. Table 7.1, cases 2, 5, 8, and 11 will show that the uncertainty in the range component of position constitutes a large part of the total position uncertainty that is computed from 5 minutes of tracking data. The range component, during these 5 minutes, is approximately perpendicular to the plane containing the stations. These stations have very little east-west separation, and, consequently, the data they obtain in 5 minutes contain very little information concerning this component. However, after about 10 minutes the earth's rotation plus the LEM's motion offsets the lack of east-west separation and the uncertainty in the range component is significantly reduced.

Table 7.1, cases 1-9, all without a priori knowledge, show that the uncertainty in the track component of position is not significantly reduced with increased tracking time. In an effort to reduce the uncertainty in this component, cases 10, 11, and 12 were investigated assuming a priori knowledge of the LEM's position and velocity. A comparison of cases 1, 2, and 3 with cases 10, 11, and 12, respectively, will show that, the respective cases give approximately the same results.

In addition, case 13 was investigated to ascertain the significance of range measurements. It is the same as case 7 except the data from the master station includes range measurements at a frequency of one observation every 15 minutes. A comparison of these two cases will show that range measurements offered very little additional information regarding the track component.

Figure 7.5 is presented in order to allow a comparison of the results obtained from the three filters that were explained in section 7.2.3 C. The uncertainties that result when Filter-1 processes data that contain biases represent the upper bound in this comparison. The uncertainties that result from the data processing of Filter-2 show that, as the knowledge of the biases is improved, they approach the minimum case, i.e. Filter-3 with no biases on the data. If only the 3-way doppler biases are solved for with Filter-3, the improvement over Filter-1 is as much as 50 per cent of the improvement of Filter-2 over Filter-1.

The question may arise as to why special emphasis was placed on three-way doppler biases. Table 7.2 gives the one sigma uncertainties of the biases as a function of tracking time. This table shows that the uncertainties in the biases of the gravitational constant of the moon, two-way doppler bias, and three-way doppler bias are significantly reduced with increased tracking time. The uncertainties in the biases of station location showed little or no improvement and therefore the station location biases need not be solved for. Furthermore, it is not necessary to solve for the bias of the gravitational constant of the moon because it will be significantly reduced as a result of missions prior to the Apollo lunar missions. As seen from the preceeding paragraph, the 3-way doppler biases have a predominating effect, and, therefore, it was logical to place emphasis on them.

## B. Ascent Phase

The position uncertainties presented in Table 7.3 and referenced to the time of rendezvous are of particular interest. These uncertainties represent the predicted rendezvous miss that results from MSFN navigation and the execution errors assumed for each maneuver. It should be noted, however, that these uncertainties are inertially referenced and are based on the knowledge of the LEM's position and velocity alone. The uncertainty in the relative range of the LEM and CSM is a subject for future studies.

Table 7.3, cases 17, 18, and 19 give the position and velocity uncertainties that result when ascent is from  $45^{\circ}$ W longitude. No a priori knowledge of the LEM's position and velocity at ascent burnout was assumed. The execution errors for the circularization maneuver and the transfer maneuver were assumed to be 9.8 ft/s in each component of the velocity vector. Cases 20, 21, and 22 give the position and velocity uncertainties that result when ascent is from  $0^{\circ}$  longitude. Cases 23, 24, and 25 give the position and velocity uncertainties that result when ascent is from  $45^{\circ}$ E longitude. The assumptions concerning a priori knowledge and execution errors for cases 20-25 are the same as those for cases 17, 18, and 19.

The importance of the tracking station geometry relative to the geometry of the LEM's orbit plane was noted in the results presented for the descent trajectories. The same trend can be noted for the ascent trajectories. Comparing cases 17, 20, and 23 with either cases 18, 21, and 24 or cases 19, 22, and 25, respectively, will verify that the data obtained from Goldstone, Antigua, and Hawaii yield larger uncertainties in the LEM's position and velocity than those that were computed from the data obtained by either of the other two station sets.

Cases 26, 27 and 28 are the same respectively as cases 23, 24, and 25 except that the execution errors for the maneuvers were reduced from 9.8 ft/s to 0.1 ft/s in each component of the velocity vector. A comparison of the results will show that the uncertainties, presented at times after a maneuver has been performed, are larger for the cases with larger execution errors, as one would expect.

Cases 29, 30, and 31 are the same respectively as cases 26, 27, and 28, except that a priori knowledge of the LEM's position and velocity at ascent burnout was assumed for the former cases. The a priori covariance matrix used was assumed to represent the LEM's launch cutoff conditions; however, it is felt to be optimistic. A comparison of the results will show that the a priori knowledge that was assumed did not significantly reduce the uncertainties at rendezvous, in spite of the optimism.

Case 32 is the same as case 29 except that range measurements from Goldstone were included. A comparison of the results will show that range measurements add very little to the knowledge of the LEM's position and velocity at the nominal time of rendezvous.

Cases 33 and 34 are the same, respectively, as 17 and 19, except that Filter-3 was used in the former cases. Also, cases 35 and 36 are the same, respectively, as 17 and 19, except that Filter-2 was used in the former cases. A comparison of case 33 with cases 17 and 35 and a comparison of case 34 with cases 19 and 36 (refer to Table 7.4) will illustrate the advantages of solving for the 3-way doppler biases.

### C. Confidence Level

The results of this analysis were checked against the results obtained from a previous analysis in which the Jet Propulsion Laboratory's Orbit Determination Program was used (Reference 3). The LEM rendezvous flight plans and the data assumptions for each of the analyses were somewhat different, but, when tracking intervals and propagating times were similar, the results were in close agreement.



#### 7.4 CONCLUSIONS

The results of this study indicate that north-south station separation is more beneficial than east-west separation.

A combination of range measurements with the Doppler data obtained by the master station, in those cases for which the combination was made, gave no additional information concerning the position and velocity of the LEM.

Because using Filter-2 resulted in a 50 percent decrease in two-way doppler bias, study of the effect of this bias needs to be made to determine whether or not it should be solved for in the real time Apollo ODP.

#### 7.5 REFERENCES

1. MSC - GSFC, ANWG Report No. 65-AN-1.0 "Apollo Missions and Navigation Systems Characteristics," February 5, 1965.
2. "Description of Orbit Error Analysis Program," Volumes 1 and 2, Bissett - Berman Corporation, Santa Monica, Calif., July and August, 1965.
3. J. D. Alexander, A. C. Bond, and S. O. Mayfield: MSC Internal Note No. 65-FM-6, January 25, 1965.

Table 7.1  
Descent  
Three Sigma Uncertainties in Altitude, Range, and Track as a Function of Tracking Time  
Propagated to Perilune

Case No.	5 min.			10 min.			15 min.			20 min.			25 min.			30 min.			35 min.			40 min.		
	A (nm)	R (nm)	T (nm)	A (nm)	R (nm)	T (nm)	A (nm)	R (nm)	T (nm)	A (nm)	R (nm)	T (nm)	A (nm)	R (nm)	T (nm)	A (nm)	R (nm)	T (nm)	A (nm)	R (nm)	T (nm)	A (nm)	R (nm)	T (nm)
1	3.9	31.4	32.4	1.6	8.6	34.7	1.2	0.9	25.9	0.9	0.2	25.3	0.9	0.1	27.2	0.4	0.1	28.0	0.3	0.1	29.2	0.2	0.1	29.6
2	13.3	107.5	9.4	0.8	3.8	9.1	0.4	0.3	9.7	0.4	0.2	10.5	0.4	0.1	11.2	0.3	0.1	11.7	0.3	0.1	12.0	0.2	0.1	12.0
3	6.3	45.0	10.9	1.5	8.7	12.0	1.1	0.9	11.7	0.9	0.3	12.2	0.9	0.2	12.8	0.3	0.2	12.8	0.3	0.2	13.1	0.2	0.2	13.3
4	8.0	19.1	49.1	1.2	6.0	32.1	0.3	1.1	25.9	0.3	0.5	25.1	0.3	0.5	23.3									
5	26.4	59.9	10.9	.5	2.6	10.4	0.1	0.3	10.0	0.1	0.3	9.6	0.1	0.2	9.1									
6	10.9	25.0	12.3	1.2	5.8	12.5	0.3	1.0	12.0	0.3	0.5	11.3	0.2	0.5	9.6									
7	6.5	5.7	41.8	1.0	1.4	18.1																		
8	17.2	15.1	11.0	0.4	0.5	6.8																		
9	7.9	6.8	12.3	0.9	1.4	11.2																		
10	3.9	30.9	31.4	1.6	8.4	33.5	1.1	1.0	25.8	0.8	0.2	25.3	0.8	0.1	27.1	0.3	0.1	28.0	0.3	0.1	29.2	0.2	0.1	29.6
11	12.8	102.6	9.2	0.8	3.7	9.1	0.5	0.3	9.7	0.4	0.2	10.5	0.5	0.1	11.2	0.3	0.1	11.7	0.3	0.1	12.0	0.2	0.1	12.0
12	6.3	44.9	10.5	1.5	8.7	12.0	1.1	1.0	11.7	1.0	0.3	12.2	1.0	0.2	12.8	0.3	0.2	12.8	0.3	0.2	13.0	0.2	0.1	13.3
13	6.2	5.5	38.4	0.8	0.8	18.0																		
14	2.1	13.4	11.8	0.5	1.0	11.2	0.5	0.3	9.7	0.3	0.2	6.6	0.2	0.1	8.3	0.2	0.1	9.7	0.2	0.1	9.2	0.2	0.1	7.8
15	1.9	13.0	10.9	0.5	1.0	9.7	0.5	0.3	8.4	0.3	0.1	5.7	0.1	0.05	3.9	0.05	0.05	3.1	0.05	0.05	1.9	0.05	0.05	1.3
16	0.6	3.1	6.0	0.1	0.6	1.8	0.1	0.1	0.8	0.1	0.3	0.5	0.1	0.01	0.3	0.05	0.1	0.3	0.02	0.01	0.3	0.01	0.005	0.3

Table 7.2  
Descent  
One Sigma Uncertainty in Biases as a Function of Tracking Time.  
(Biases solved for)

Station Sets	$\sigma_{f_{\text{moon}}} \text{ (ft}^3/\text{s}^2)$					2-Way Doppler Bias (ft/s)					3-Way Doppler Slave 1 Bias (ft/s)					3-Way Doppler Slave 2 Bias (ft/s)				
	0	10	20	40		0	10	20	40		0	10	20	40		0	10	20	40	
ANT, GST, HAW	Min.	Min.	Min.	Min.		Min.	Min.	Min.	Min.		Min.	Min.	Min.	Min.		Min.	Min.	Min.	Min.	
MAD, CYL, ASC	20x10 <sup>9</sup>	20x10 <sup>9</sup>	15x10 <sup>9</sup>	6x10 <sup>9</sup>		.10	.06	.06	.05		.20	.14	.12	.11		.20	.18	.13	.11	
CNB, CRO, GUA	20x10 <sup>9</sup>	20x10 <sup>9</sup>	14x10 <sup>9</sup>	6x10 <sup>9</sup>		.10	.08	.07	.05		.20	.12	.12	.11		.20	.19	.14	.11	
	20x10 <sup>9</sup>	20x10 <sup>9</sup>	16x10 <sup>9</sup>	6x10 <sup>9</sup>		.10	.07	.06	.06		.20	.14	.12	.11		.20	.19	.13	.11	

STATION LOCATION UNCERTAINTIES

Tracking Time Min.	GST (Master)				ANT (Slave 1)				HAW (Slave 2)			
	$\sigma_x$ , ft.	$\sigma_y$ , ft.	$\sigma_z$ , ft.		$\sigma_x$ , ft.	$\sigma_y$ , ft.	$\sigma_z$ , ft.		$\sigma_x$ , ft.	$\sigma_y$ , ft.	$\sigma_z$ , ft.	
0	112	121	115		115	131	112		174	243	240	
10	112	121	115		115	131	112		174	243	240	
20	112	121	115		115	131	112		174	243	240	
40	112	121	115		115	131	112		174	243	240	

Tracking Time Min.	MAD (Master)				CYI (Slave 1)				ASC (Slave 2)			
	$\sigma_x$ , ft.	$\sigma_y$ , ft.	$\sigma_z$ , ft.		$\sigma_x$ , ft.	$\sigma_y$ , ft.	$\sigma_z$ , ft.		$\sigma_x$ , ft.	$\sigma_y$ , ft.	$\sigma_z$ , ft.	
0	128	102	121		253	453	417		141	340	358	
10	128	102	121		253	453	417		141	340	358	
20	128	102	121		253	450	417		141	340	358	
40	128	102	121		253	447	417		141	340	358	

Tracking Time Min.	CNB (Master)				CRO (Slave 1)				GUA (Slave 2)			
	$\sigma_x$ , ft.	$\sigma_y$ , ft.	$\sigma_z$ , ft.		$\sigma_x$ , ft.	$\sigma_y$ , ft.	$\sigma_z$ , ft.		$\sigma_x$ , ft.	$\sigma_y$ , ft.	$\sigma_z$ , ft.	
0	207	197	200		197	210	197		410	535	633	
10	207	197	200		197	210	197		410	535	633	
20	204	197	200		197	210	197		410	532	633	
40	201	197	200		197	210	197		410	529	633	

Table 7.3  
Ascent  
Three Sigma Uncertainties in Position and Velocity

Case No.	After tracking from ascent burnout to 5 min. prior to loss of sight Referenced to				After tracking from acquisition to transfer Referenced to						After tracking from transfer to											
					Transfer +5 min. Referenced to						Transfer +10 min. Referenced to						Transfer +20 min. Referenced to					
	t <sub>0</sub>		t <sub>circularization</sub>		t <sub>circularization</sub>		t <sub>transfer</sub>		t <sub>rendezvous</sub>		t <sub>transfer</sub>		t <sub>rendezvous</sub>		t <sub>transfer</sub>		t <sub>rendezvous</sub>		t <sub>transfer</sub>		t <sub>rendezvous</sub>	
	R (nm)	V (ft/s)	R (nm)	V (ft/s)	R (nm)	V (ft/s)	R (nm)	V (ft/s)	R (nm)	V (ft/s)	R (nm)	V (ft/s)	R (nm)	V (ft/s)	R (nm)	V (ft/s)	R (nm)	V (ft/s)	R (nm)	V (ft/s)	R (nm)	V (ft/s)
	Col. 1	Col. 2	Col. 3	Col. 4	Col. 5	Col. 6	Col. 7	Col. 8	Col. 9	Col. 10	Col. 11	Col. 12	Col. 13	Col. 14	Col. 15	Col. 16	Col. 17	Col. 18	Col. 19	Col. 20		
17	37.9	183.0	43.3	194.8	22.7	54.1	9.9	124.0	8.1	124.0	15.2	150.6	7.3	126.0	13.0	135.8	8.4	100.4	16.7	64.0		
18	4.3	58.4	6.7	61.0	3.7	65.9	12.2	20.7	11.0	66.9	8.1	94.5	7.9	72.8	4.7	89.5	1.9	65.9	7.5	52.2		
19	9.7	70.8	18.1	100.4	5.0	66.9	12.3	27.6	11.7	73.8	16.2	128.9	9.4	75.8	14.3	112.2	7.1	60.0	10.7	43.3		
20	16.0	163.3	17.2	158.4	12.6	91.5	3.3	104.3	8.6	107.3	17.7	81.7	6.3	101.4	14.6	74.8	12.0	96.4	17.0	71.8		
21	7.6	48.2	8.1	47.2	3.1	72.8	9.6	54.1	9.1	53.1	13.4	30.5	7.3	51.2	11.3	29.5	6.6	51.2	10.7	29.5		
22	7.3	63.0	8.1	62.0	4.1	79.7	11.0	56.1	13.1	62.0	16.5	64.9	12.5	61.0	14.3	61.0	10.2	53.1	12.6	37.4		
23	27.2	113.2	28.5	108.2	22.7	249.9	30.9	222.4	29.6	89.5	36.3	63.0	28.2	65.9	31.4	39.4	21.1	74.8	23.7	56.1		
24	11.5	27.6	12.2	27.6	11.2	128.9	15.4	116.1	15.2	53.1	22.0	74.8	14.9	41.3	17.8	30.5	13.0	33.5	14.7	11.8		
25	11.8	46.2	12.3	45.3	9.9	124.0	13.9	112.2	13.8	58.1	19.1	56.1	13.4	50.2	16.5	31.5	12.2	51.2	14.3	33.5		
26	27.2	113.2	28.5	108.2	16.5	185.0	22.4	165.3	19.0	131.9	29.0	64.0	15.9	113.2	24.3	58.1	12.5	101.4	19.8	59.0		
27	11.5	27.6	12.2	27.6	6.6	67.9	8.9	60.0	8.7	58.1	13.3	25.6	8.4	55.1	12.8	24.6	7.8	53.1	11.8	23.6		
28	11.8	46.2	12.3	45.3	8.4	77.7	10.7	69.9	10.7	65.9	15.2	34.4	10.2	62.0	14.4	33.5	9.6	58.1	13.3	34.4		
29	10.9	112.2	11.3	107.3	8.3	151.5	13.1	141.7	11.8	121.0	21.7	71.8	10.5	109.2	19.4	66.9	9.4	102.3	17.5	64.0		
30	9.4	30.5	9.7	29.5	5.7	65.9	7.9	59.0	7.8	57.1	12.3	27.6	7.5	55.1	12.0	27.6	7.1	53.1	11.3	25.6		
31	9.4	45.3	9.9	44.3	7.1	73.8	9.4	66.9	9.4	64.0	13.9	35.4	9.1	61.0	13.3	34.4	8.9	58.1	12.6	34.4		
32	11.0	113.2	11.5	108.2	8.3	151.5	13.2	140.7	11.8	120.0	21.5	71.8	10.7	109.2	19.6	66.9	9.9	101.4	17.7	64.9		
33	5.8	150.6	6.5	144.6	3.7	16.7	3.1	19.7	4.1	51.2	5.5	57.1	2.8	16.7	6.2	36.4	5.0	57.1	2.1	61.0		
34	4.5	67.9	5.3	66.9	1.6	13.8	2.6	8.9	4.7	30.5	5.2	13.4	2.6	15.7	4.2	30.5	3.1	36.4	1.3	38.4		
35	5.8	134.8	6.5	128.9	3.7	16.7	3.1	19.7	2.7	16.1	4.2	25.6	2.3	14.8	2.9	19.4	1.4	10.8	1.6	10.5		
36	4.1	59.0	4.9	58.1	1.6	13.8	2.4	8.9	2.3	10.5	3.9	24.6	1.6	9.8	2.3	16.4	0.8	6.9	0.9	6.6		

Table 7.4  
Ascent7-13

Table 7.5  
Ascent  
Resulting Three Sigma Position and Velocity Errors if the Lem Guidance Computer is Updated  
at the Transfer Maneuver Based on MSFN Navigation (Execution Errors are Included)

Case No.	REFERENCED TO:											
	End of Transfer Maneuver		Transfer Maneuver + 10 Min.		Transfer Maneuver + 15 Min.		Transfer Maneuver + 25 Min.		Transfer Maneuver + 50 Min.*			
	R (nm)	V (ft/s)	R (nm)	V (ft/s)	R (nm)	V (ft/s)	R (nm)	V (ft/s)	R (nm)	V (ft/s)	R (nm)	V (ft/s)
17	9.9	133.8	18.1	110.2	22.0	71.8	27.4	97.4	45.4	259.8		
18	12.2	55.1	13.1	56.1	13.3	66.9	15.4	104.3	45.0	236.2		
19	12.4	58.1	13.9	55.1	14.3	65.9	15.9	104.3	45.0	238.1		
20	8.7	116.1	8.1	121.0	12.6	116.1	22.2	109.2	47.1	242.1		
21	9.6	74.8	6.0	89.5	7.8	94.5	15.9	107.3	46.2	232.2		
22	11.0	75.8	7.3	93.5	8.4	98.4	16.0	111.2	46.5	232.2		
23	30.9	228.3	8.6	281.4	12.0	280.4	36.0	232.2	65.3	255.8		
24	15.4	126.0	5.7	151.5	9.1	152.5	22.4	139.7	50.7	239.1		
25	13.9	123.0	5.5	144.6	9.6	143.7	22.0	131.9	49.7	239.1		
26	22.4	165.3	5.5	203.7	7.8	200.7	24.8	157.4	35.5	83.6		
27	8.9	60.0	2.3	75.8	2.1	76.8	8.9	62.0	13.9	30.5		
28	10.7	69.9	4.7	87.6	4.4	87.6	10.4	71.8	15.9	37.4		
29	13.1	141.7	3.6	157.4	10.2	148.6	22.5	103.3	24.9	86.6		
30	7.9	59.0	1.5	72.8	2.6	71.8	8.9	56.1	13.0	32.5		
31	9.4	66.9	3.9	81.7	4.4	80.7	10.2	64.0	14.4	38.4		
32	13.3	140.7	3.7	156.8	10.2	148.6	22.5	103.3	24.9	85.6		
33	3.1	55.1	5.5	57.1	8.1	62.0	14.4	88.6	44.4	232.2		
34	2.6	52.2	5.5	54.1	7.9	59.0	14.1	87.6	44.2	231.2		
35	3.1	55.1	5.5	57.1	8.0	62.0	14.4	88.2	44.3	231.9		
36	2.4	52.2	5.5	54.1	7.9	59.0	14.1	87.2	44.2	231.2		

\*Nominal time of rendezvous

Table 7.6  
Data Characteristics and Definition of Cases

Data Characteristics					Station Location Uncertainties		
Station	Measurement	Sampling Rate	Noise $1\sigma$	Bias $1\sigma$	$\sigma_x$ (ft)	$\sigma_y$ (ft)	$\sigma_z$ (ft)
GST	$\dot{R}$ R (when applicable)	1 per 6 sec 1 per 15 min	0.1 ft/s 60 ft	0.1 ft/s 120 ft	112	121	115
ANT	$\dot{R}$	1 per 6 sec	0.1 ft/s	0.2 ft/s	115	131	121
HAW	$\dot{R}$	1 per 6 sec	0.1 ft/s	0.2 ft/s	174	243	240
MAD	$\dot{R}$	1 per 6 sec	0.1 ft/s	0.1 ft/s	128	102	121
CYI	$\dot{R}$	1 per 6 sec	0.1 ft/s	0.2 ft/s	253	453	417
ASC	$\dot{R}$	1 per 6 sec	0.1 ft/s	0.2 ft/s	141	340	358
CNB	$\dot{R}$	1 per 6 sec	0.1 ft/s	0.1 ft/s	207	197	200
CRO	$\dot{R}$	1 per 6 sec	0.1 ft/s	0.2 ft/s	197	210	197
GUA	$\dot{R}$	1 per 6 sec	0.1 ft/s	0.2 ft/s	410	535	633

#### CASE DEFINITIONS

- Case 1 - Descent to perilune of 45°W longitude; ANT, GST, and HAW tracking; no a priori knowledge assumed; Filter-1.
- Case 2 - Descent to perilune of 45°W longitude; MAD, CYI, and ASC tracking; no a priori knowledge assumed; Filter-1.
- Case 3 - Descent to perilune of 45°W longitude; CNB, CRO, and GUA tracking; no a priori knowledge assumed; Filter-1.
- Case 4 - Descent to perilune of 0° longitude; ANT, GST, and HAW tracking; no a priori knowledge assumed; Filter-1.
- Case 5 - Descent to perilune of 0° longitude; MAD, CYI, and ASC tracking; no a priori knowledge assumed; Filter-1.
- Case 6 - Descent to perilune of 0° longitude; CNB, CRO, and GUA tracking; no a priori knowledge assumed; Filter-1.
- Case 7 - Descent to perilune of 45° E longitude; ANT, GST, and HAW tracking; no a priori knowledge assumed; Filter-1.

- Case 8 - Descent to perilune of 45° E longitude; MAD, CYI, and ASC tracking; no a priori knowledge assumed; Filter-1.
- Case 9 - Descent to perilune of 45° E longitude; CNB, CRO, and GUA tracking; no a priori knowledge assumed; Filter-1.
- Case 10 - Descent to perilune of 45° W longitude; ANT, GST, and HAW tracking; a priori knowledge assumed:

$$\begin{array}{ll} \sigma_x = 8.1 \text{ nm} & \sigma_{\dot{x}} = 49.2 \text{ ft/s} \\ \sigma_y = 8.1 \text{ nm} & \sigma_{\dot{y}} = 49.2 \text{ ft/s} \\ \sigma_z = 8.1 \text{ nm} & \sigma_{\dot{z}} = 49.2 \text{ ft/s} \end{array}$$

x - altitude, y - range, z - track; Filter-1.

- Case 11 - Descent to perilune of 45° W longitude; MAD, CYI, and ASC tracking; a priori knowledge assumed (same as in Case 10); Filter-1.
- Case 12 - Descent to perilune of 45° W longitude; CNB, CRO, and GUA tracking; a priori knowledge assumed (same as in Case 10); Filter-1.
- Case 13 - Descent to perilune of 45° E longitude; ANT, GST, and HAW tracking; no a priori knowledge assumed; GST takes range measurements in addition to doppler data; Filter-1.
- Case 14 - Descent to perilune of 45° W longitude; CNB, CRO, and GUA tracking; no a priori knowledge assumed; Filter-3, three-way doppler biases are solved for.
- Case 15 - Descent to perilune of 45° W longitude; CNB, CRO, and GUA tracking; no a priori knowledge assumed; Filter-3.
- Case 16 - Descent to perilune of 45° W longitude; CNB, CRO, and GUA tracking; no a priori knowledge assumed; Filter-3, data contain no biases.
- Case 17 - Ascent from 45° W longitude; ANT, GST, and HAW tracking; no a priori knowledge assumed; execution errors assumed to be 9.8 ft/s in each component of the velocity vector; Filter-1.
- Case 18 - Ascent from 45° W longitude; MAD, CYI, and ASC tracking; no a priori knowledge assumed; execution errors same as for case 17; Filter-1.



- Case 19 - Ascent from 45° W longitude; CNB, CRO, and GUA tracking; no a priori knowledge assumed; execution errors same as for case 17; Filter-1.
- Case 20 - Ascent from 0° longitude; ANT, GST, and HAW tracking; no a priori knowledge assumed; execution errors same as for case 17; Filter-1.
- Case 21 - Ascent from 0° longitude; MAD, CYI, and ASC tracking; no a priori knowledge assumed; execution errors same as for case 17; Filter-1.
- Case 22 - Ascent from 0° longitude; CNB, CRO, and GUA tracking; no a priori knowledge assumed; execution errors same as for case 17; Filter-1.
- Case 23 - Ascent from 45° E longitude; ANT, GST, and HAW tracking; no a priori knowledge assumed; execution errors same as for case 17; Filter-1.
- Case 24 - Ascent from 45° E longitude; MAD, CYI, and ASC tracking; no a priori knowledge assumed; execution errors same as for case 17; Filter-1.
- Case 25 - Ascent from 45° E longitude; CNB, CRO, and GUA tracking; no a priori knowledge assumed; execution errors same as for case 17; Filter-1.
- Case 26 - Ascent from 45° E longitude; ANT, GST, and HAW tracking; no a priori knowledge assumed; execution errors assumed to be 0.1 ft/sec in each component of the velocity vector; Filter-1.
- Case 27 - Ascent from 45° E longitude; MAD, CYI, and ASC tracking; no a priori knowledge assumed; execution errors same as for case 26; Filter-1.
- Case 28 - Ascent from 45° E longitude; CNB, CRO, and GUA tracking; no a priori knowledge assumed; execution errors same as for case 26; Filter-1.
- Case 29 - Ascent from 45° E longitude; ANT, GST, and HAW tracking; a priori knowledge assumed is:

$$\sigma_x^2 = 3.39 \times 10^6 \text{ ft}^2$$

$$\sigma_y^2 = 1.8 \times 10^6 \text{ ft}^2$$

$$\sigma_x^2 = 43.8 \text{ ft}^2/\text{s}^2$$

$$\sigma_y^2 = 13.6 \text{ ft}^2/\text{s}^2$$

$$\sigma_z = 3.05 \times 10^6 \text{ ft}^2$$

$$\sigma_z^2 = 40.3 \text{ ft}^2/\text{s}^2$$

x - altitude, y - range, z - track; execution errors same as for case 26; Filter-1.

- Case 30 - Ascent from 45° E longitude; MAD, CYI, and ASC tracking; a priori knowledge assumed (same as for case 29); execution errors same as for case 26; Filter-1.
- Case 31 - Ascent from 45° E longitude; CNB, CRO, and GUA tracking; a priori knowledge assumed (same as for Case 29); execution errors same as for case 26; Filter-1.
- Case 32 - Ascent from 45° E longitude; ANT, GST, and HAW tracking; a priori knowledge assumed (same as for case 29); execution errors same as for case 26; Filter-1.
- Case 33 - Ascent from 45° W longitude; ANT, GST, and HAW tracking; no a priori knowledge assumed; execution errors same as for case 17; Filter-3, three-way doppler biases are solved for.
- Case 34 - Ascent from 45° W longitude; CNB, CRO, and GUA tracking; no a priori knowledge assumed; execution errors same as for case 17; Filter-3.
- Case 35 - Ascent from 45° W longitude; ANT, GST, and HAW tracking; no a priori knowledge assumed; execution errors same as for case 17; Filter-2.
- Case 36 - Ascent from 45° W longitude; CNB, CRO, and GUA tracking; no a priori knowledge assumed; execution errors same as for case 17; Filter-2.

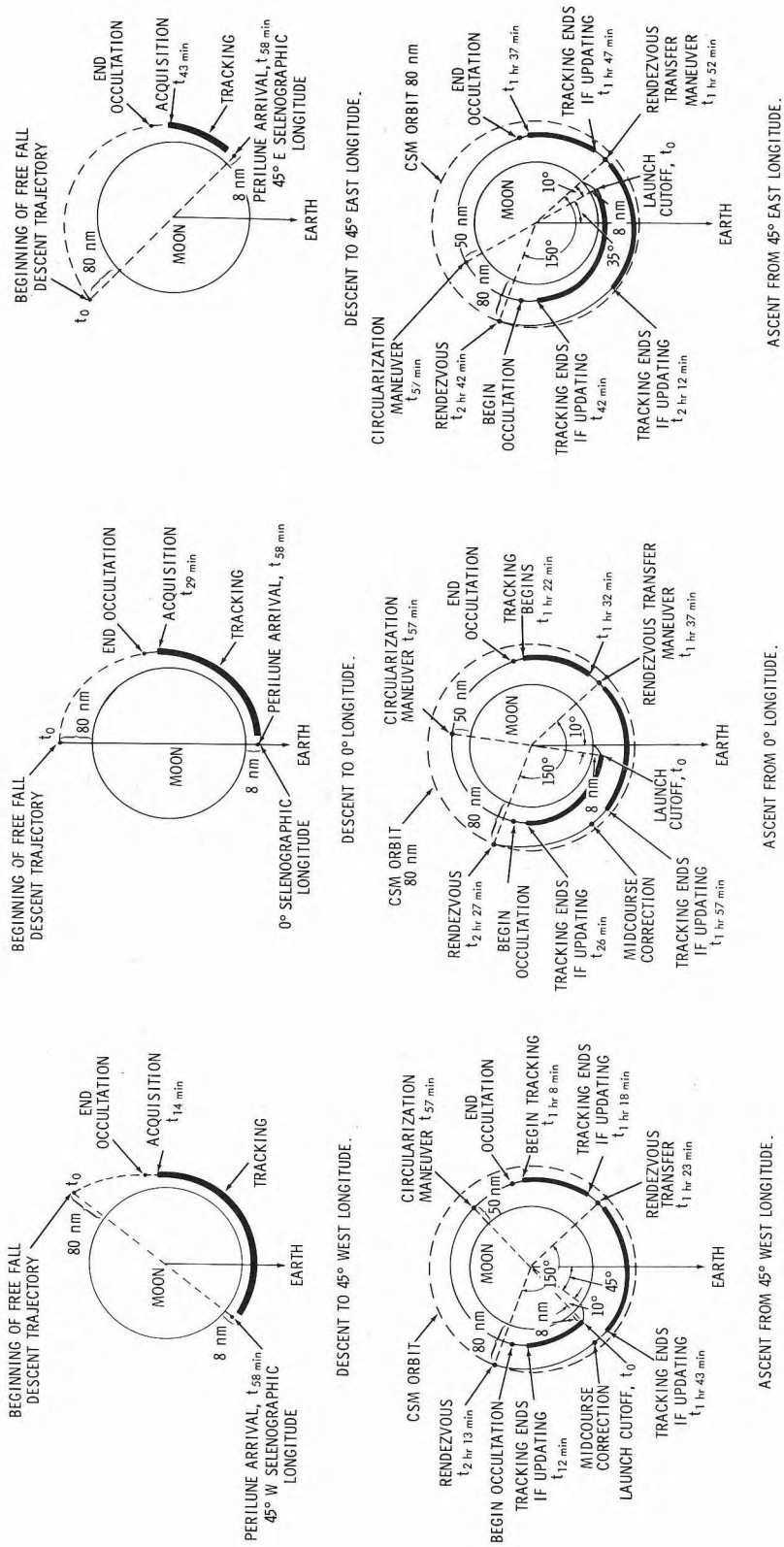


Figure 7.1

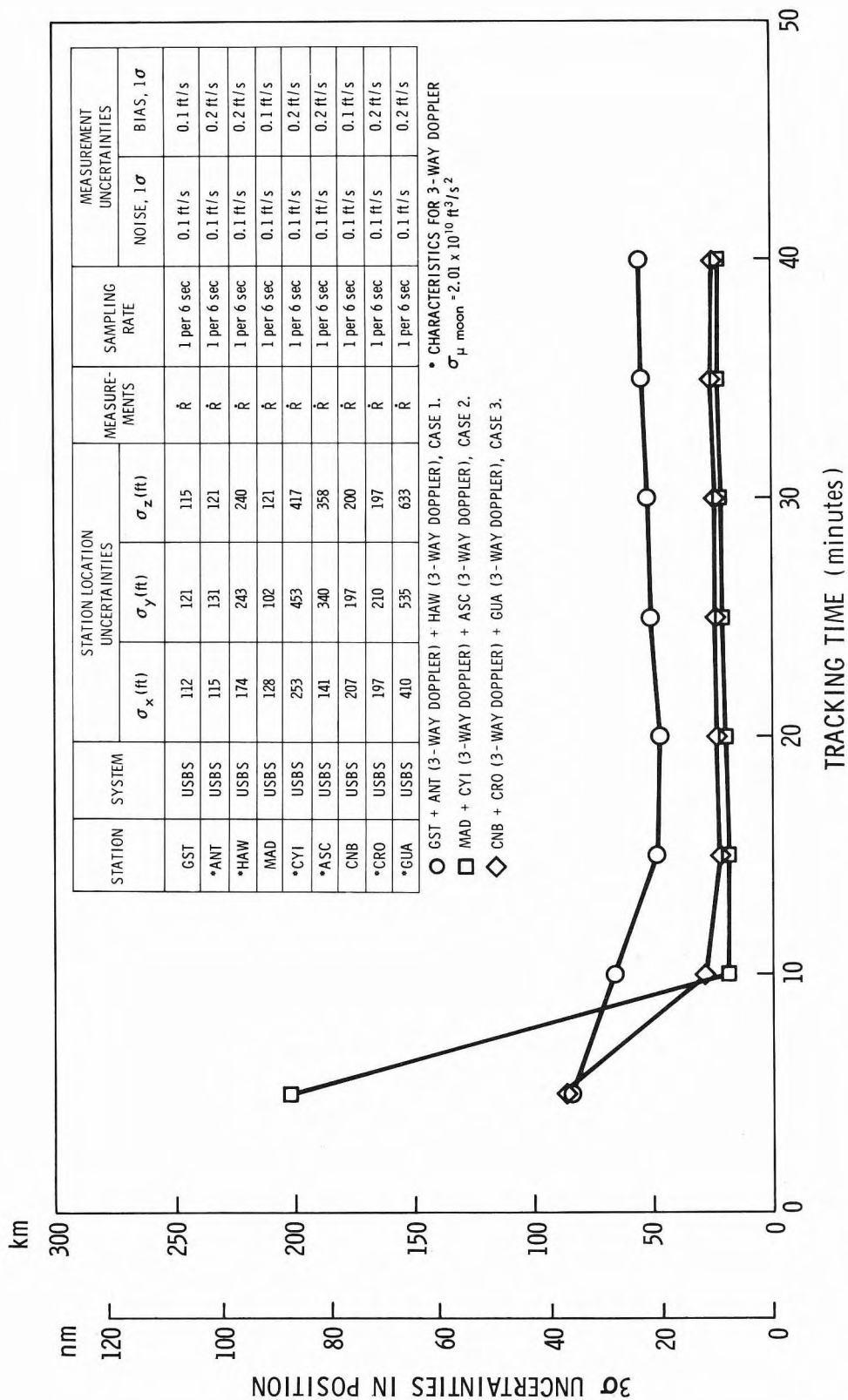


Figure 7.2a—3 $\sigma$  position uncertainties (Filter=1) at perilune of 45° W. longitude. Tracking starts 14 minutes after insertion into the descent trajectory.

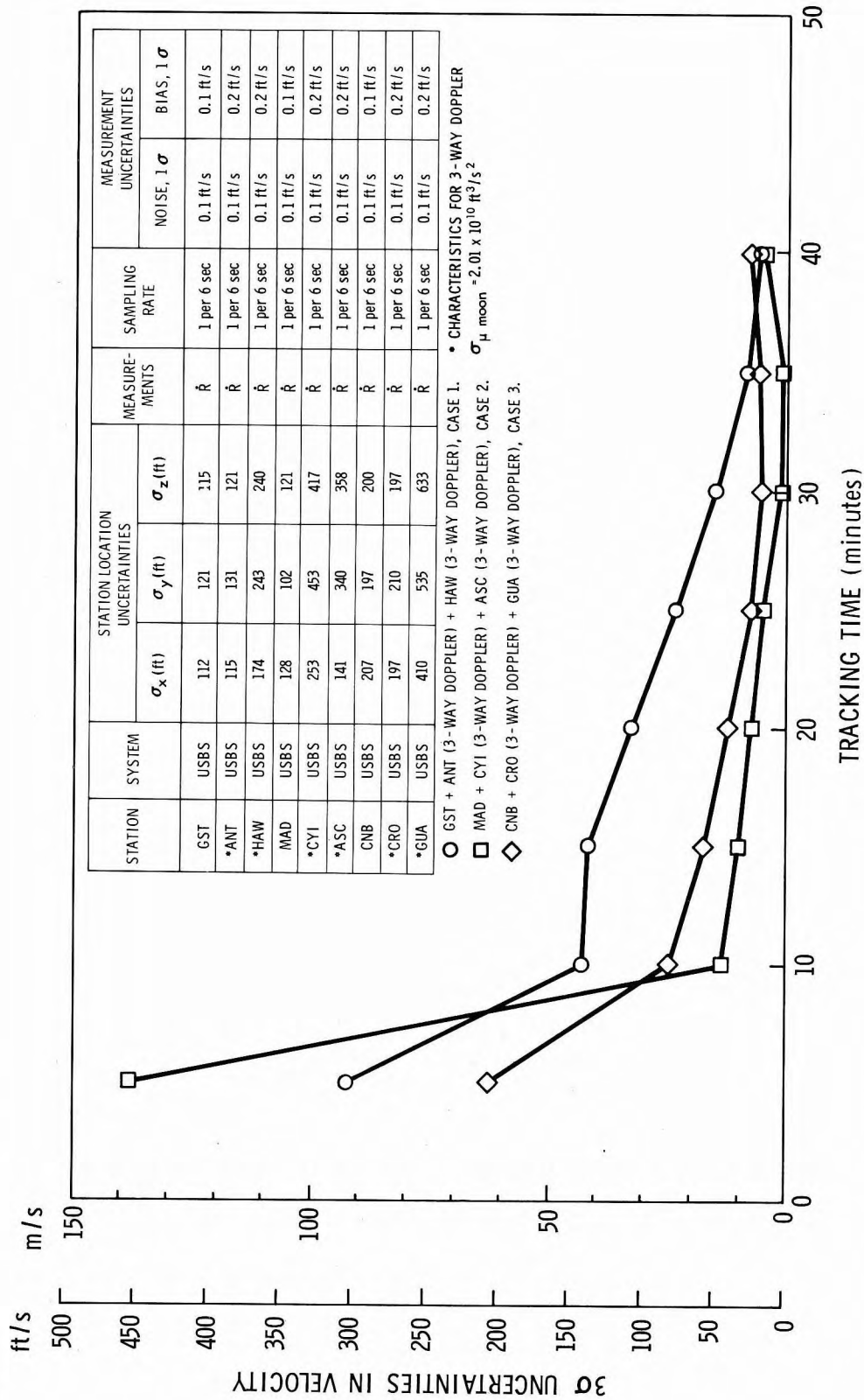


Figure 7.2b-3 $\sigma$  velocity uncertainties (Filter-1) at perilune of 45° W. longitude. Tracking starts 14 minutes after insertion into the descent trajectory.

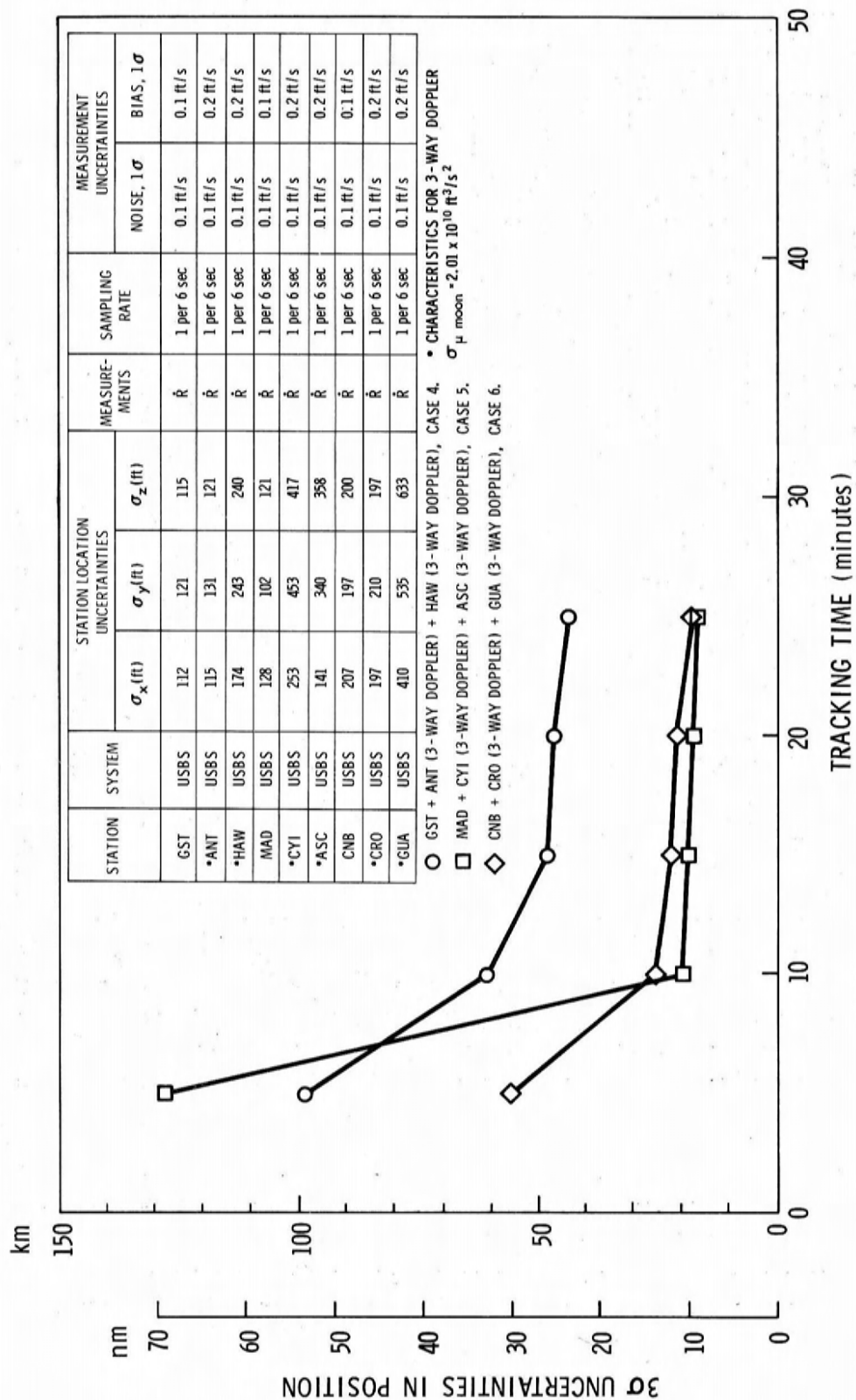


Figure 7.3a—3 $\sigma$  position uncertainties (Filter—1) at perilune of 0° longitude. Tracking starts 29 minutes after insertion into the descent trajectory.

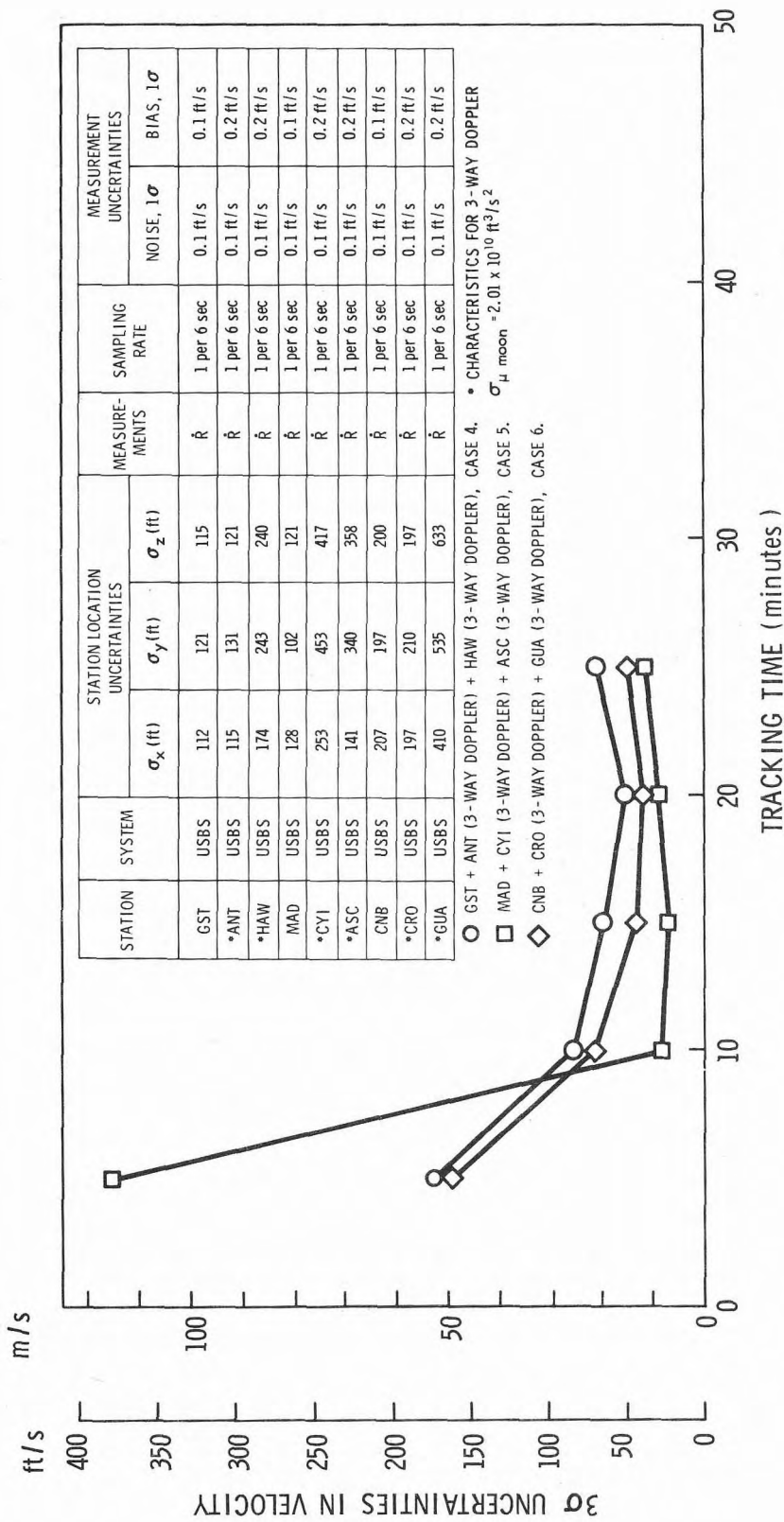


Figure 7.3b-3 $\sigma$  velocity uncertainties (Filter-1) at perilune of 0° longitude. Tracking starts 29 minutes after insertion into the descent trajectory.

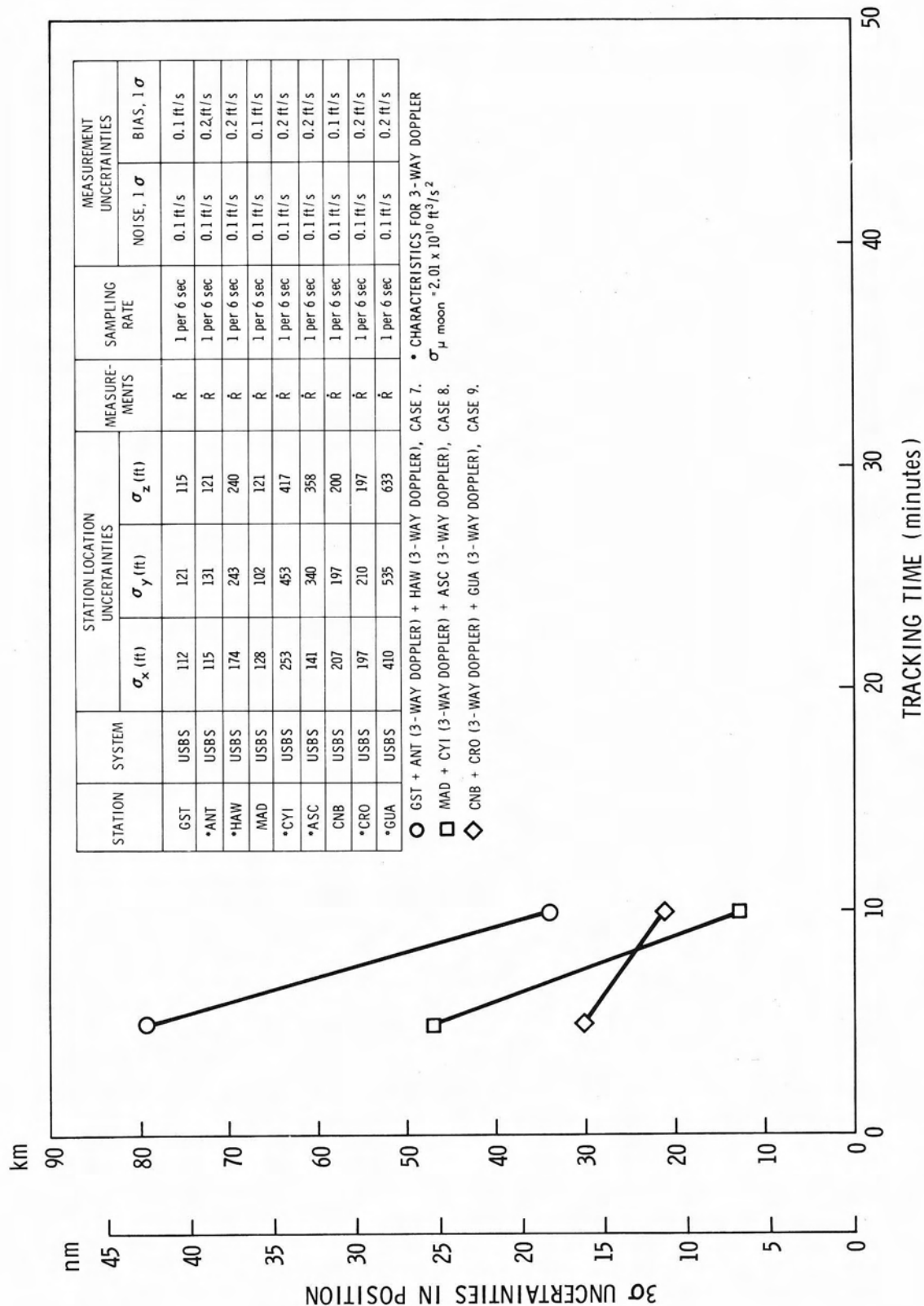


Figure 7.4a-3 $\sigma$  position uncertainties (Filter-1) at perilune of 45° E. longitude. Tracking starts 43 minutes after insertion into descent trajectory.



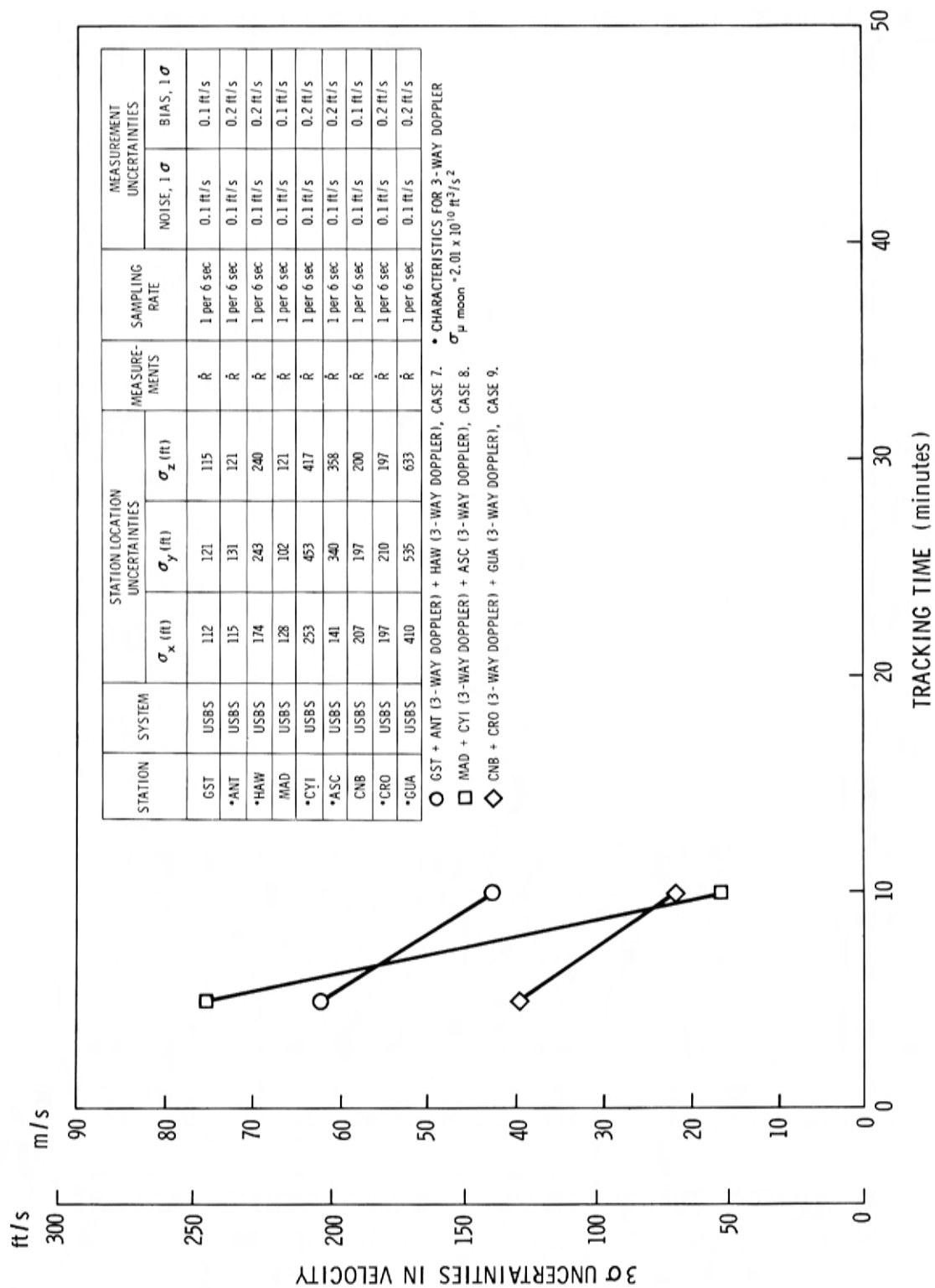


Figure 7.4b-3 $\sigma$  velocity uncertainties (Filter-1) at perilune of 45° E. longitude.  
Tracking starts 43 minutes after insertion into descent trajectory.

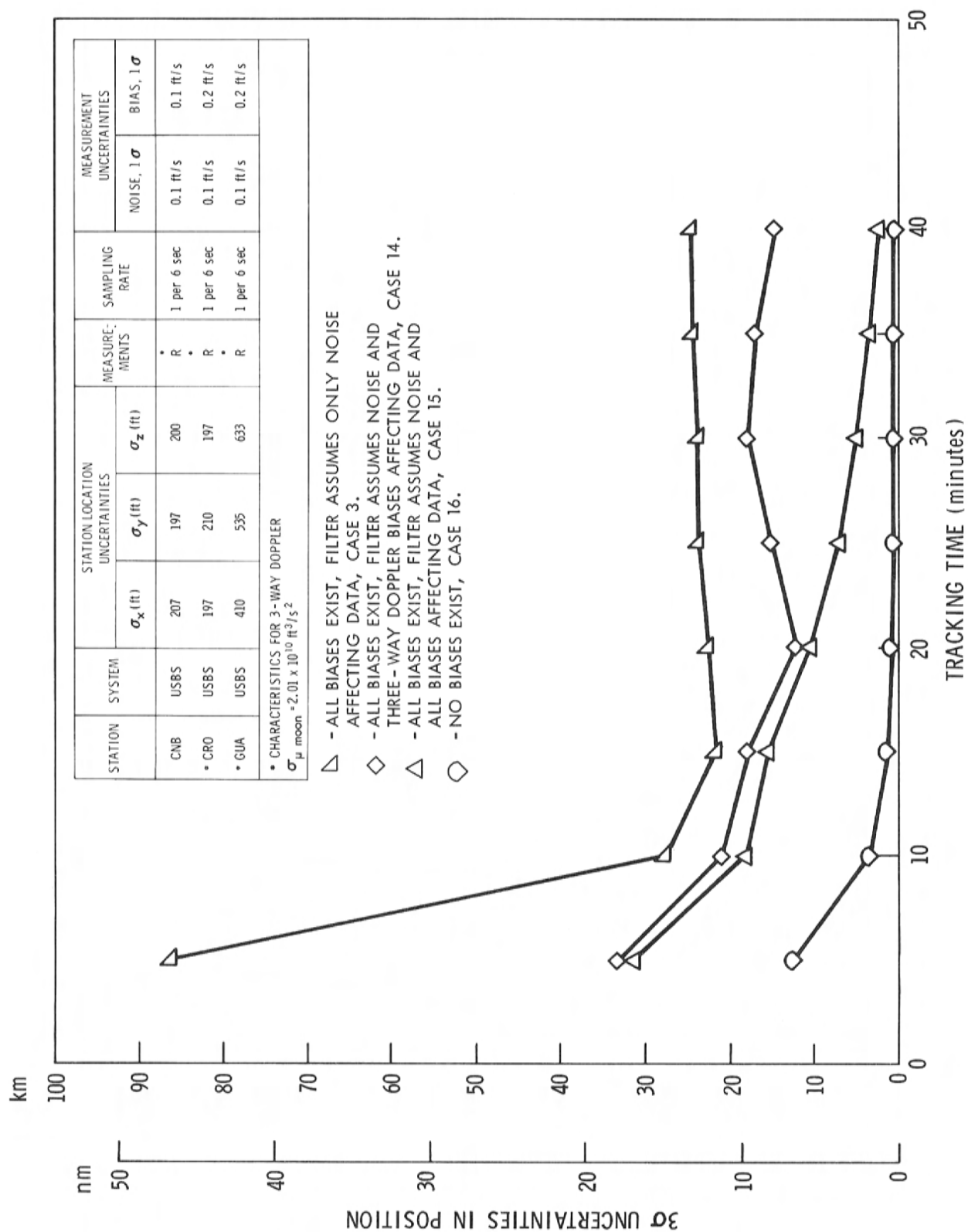


Figure 7.5a—3σ position uncertainties at perilune of 45° W. longitude, resulting from different assumptions made concerning an orbit determination scheme.

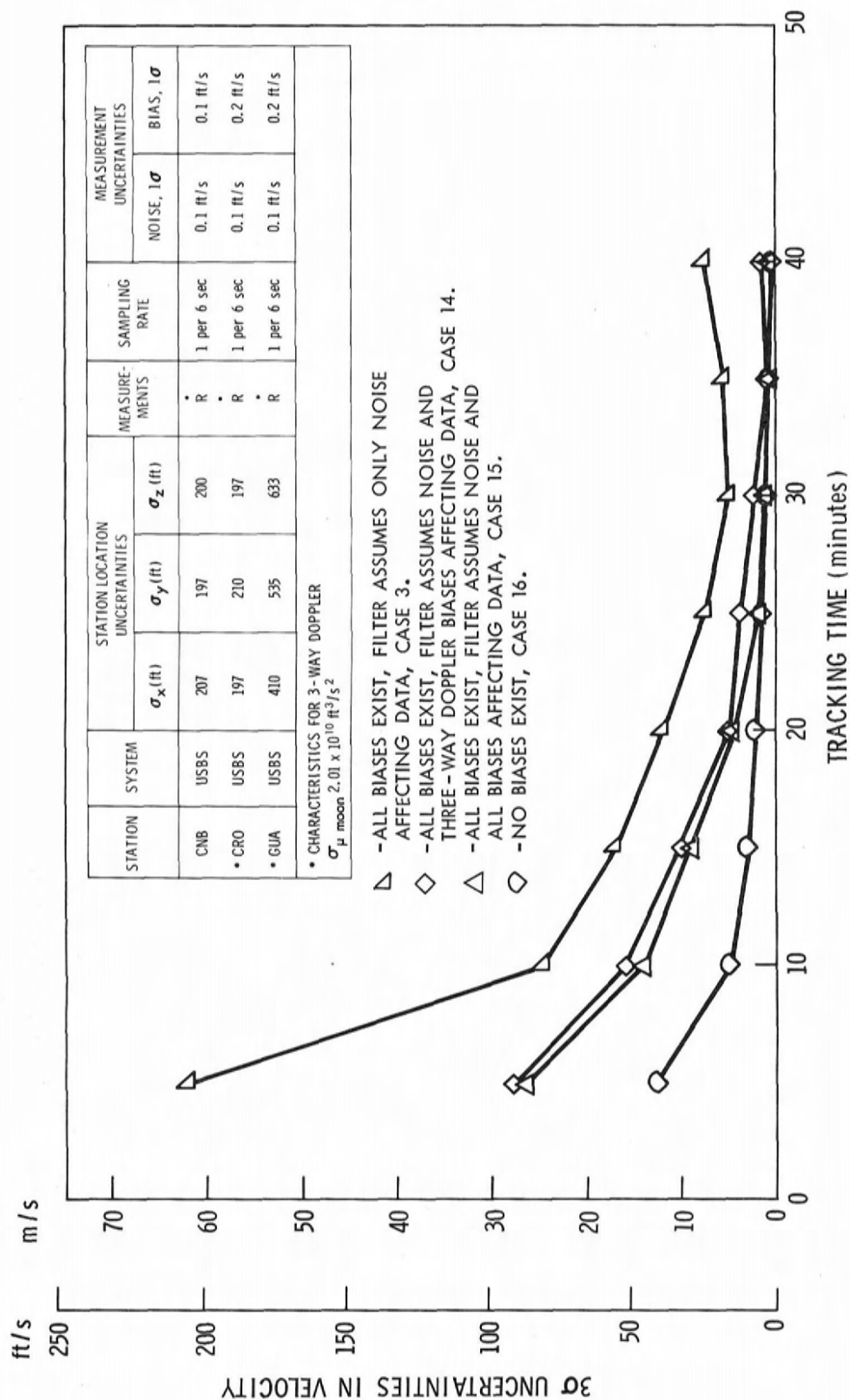


Figure 7.5b-3 $\sigma$  velocity uncertainties of 45° W. longitude, resulting from different assumptions made concerning an orbit determination scheme.

## 8.0 TRANSEARTH PHASE

### 8.1 INTRODUCTION

The transearth phase of the Apollo lunar missions is defined as beginning at the end of the injection burn and ending at the reentry into the earth's atmosphere. During this phase the MSFN (Manned Spaceflight Network) will be the prime source of navigation data. The purpose of the study presented in this chapter is to evaluate the capability of determining the transearth orbit by using data from the MSFN.

Several operational modes (e.g., single and multiple station tracking) have been simulated in this study and some conclusions concerning the operational use of the MSFN have been reached.

The study was conducted with certain assumptions concerning the accuracy of the MSFN and with a linear error analysis program (Reference 1) based on a weighted least squares filtering technique. This error analysis program was used to evaluate the capability of determining an orbit with data of the assumed characteristics and with a filter which ignored the assumed biases. Further discussion of the assumed data characteristics is contained in the paragraph below. It should be noted that the Apollo real time orbit determination program will account for some bias effects by adjusting the measurement data weighting scheme or by solving for the known biases explicitly or, most probably, by using some combination of these two techniques. Consequently, the results reported below are considered to be conservative and are subject to change as further studies are conducted.

### 8.2 ASSUMPTIONS

The assumptions on which this study was based are consistent with Reference 2. For convenience, however, the uncertainties in station locations, gravitational constants of the earth and moon, and the noise and biases of the MSFN data are shown on each graph as they are applicable. Other assumptions which should be noted are:

(1) Injection will occur from an  $80 \pm 5$  nm. lunar parking orbit and on the back side of the moon. Figure 1 is an illustration of a transearth trajectory showing the planned maneuvers.

(2) The vehicle is occulted by the moon for the first 20 minutes after injection, and each midcourse correction burn causes the loss of 5 minutes of tracking data.

### 8.3 RESULTS

To facilitate the studying and reporting of the MSFN performance, the transearth phase has been divided into five legs with the exception of leg 2; these legs begin and end with one of the planned maneuvers (e.g., injection and midcourse corrections). Leg 2 ends at entry into ESOI (earth's sphere of influence) which is an artificial break established for the purpose of analysis and should logically be considered a part of leg 3.

The legs of the transearth phase are defined as follows:

Leg 1 - From end of injection burn to initiation of first midcourse correction.

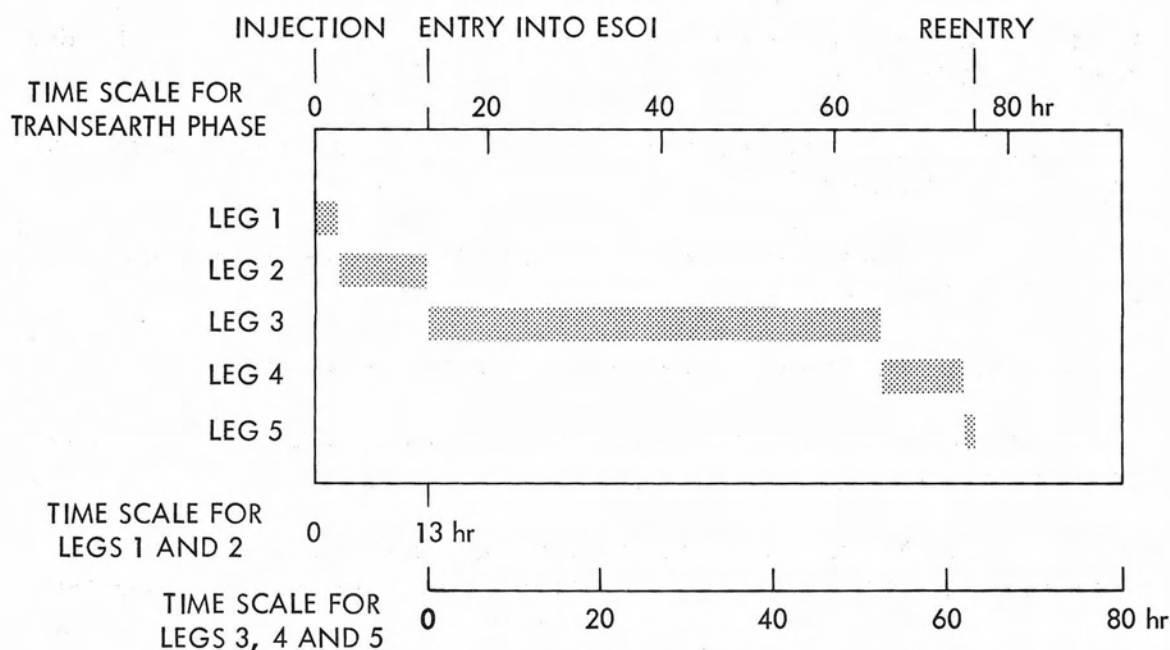
Leg 2 - From end of first midcourse correction to entry into ESOI.

Leg 3 - From entry into ESOI to initiation of second midcourse correction.

Leg 4 - From end of second midcourse correction to initiation of third midcourse correction.

Leg 5 - From end of third midcourse correction to reentry (400,000 feet altitude).

Each of these legs is nominally associated with a time from injection as shown by the upper scale of the schematic below. The lower scale of this schematic defines the time scale which is used in preparing the graphs of the results of this study.



The uncertainties that are depicted in the graphs are computed at various times in the legs and an explanation of the annotation of these computations is given below.

- $t = 0$  This statement on a graph indicates that the uncertainties are of the orbit parameters at the beginning of the leg.
- $t + 30 \text{ min.}$  This statement indicates that the uncertainties are of the orbit parameters at 30 minutes after the time against which they are plotted. This illustrates the accuracy with which an update of the onboard system can be made after a period of tracking, data processing, etc.
- Reentry This statement indicates that the uncertainties are computed at the nominal time of reentering the earth's atmosphere.

In all of the above cases the uncertainties are plotted on the same time scale as the station coverage periods and, thus, one can determine how the MSFN navigation capability varies with tracking time and tracking coverage.

### 8.3.1 Leg 1 - Navigational Accuracies at Injection

The results of the analysis for this leg illustrate the MSFN performance in the determination of position and velocity at transearth injection and the effects

of the uncertainties in predicting the vehicle's position and velocity 30 minutes in advance of MSFN tracking.

Five cases (operational modes) were simulated in the analysis for this leg and are as follows:

Case 1: Range, range rate, and angular measurements are used and a priori knowledge is assumed.

Case 2: The same as case 1 without a priori knowledge.

Case 3: The same as case 2 except that angle measurements are taken for only the first 15 minutes.

Case 4: Madrid and Ascension tracking simultaneously with angle measurements from Madrid for the first 15 minutes and no a priori knowledge assumed.

Case 5: Same as case 4 with Texas added.

The uncertainties in position and velocity are referenced to  $t = 0$  (Figures 8.2a and 8.2b) and propagated to  $t + 30$  minutes (Figures 8.2c and 8.2d).

### 8.3.2 Leg 2 - Navigational Accuracies for Entry into the ESOI

The results of the analysis illustrate the uncertainties in position and velocity at  $t + 30$  min. (Figures 8.3a and 8.3b).

Two cases were simulated for the analysis for this leg and are as follows:

Case 1: Three stations tracking simultaneously and a priori knowledge is assumed.

Case 2: The same as case 1 without a priori knowledge.

### 8.3.3 Leg 3 - Navigational Accuracies at the Second Midcourse Correction

The results of the analysis illustrate the uncertainties in position and velocity at  $t + 30$  min. (Figures 8.4a and 8.4b).

Two cases were simulated:

Case 1: Goldstone, Canberra, and Madrid alternately tracking in the 2-way doppler mode and no a priori knowledge is assumed.

Case 2: Same as case 1 with a priori knowledge assumed.

#### 8.3.4 Leg 4 - Navigational Accuracies for the Third Midcourse Correction

The results of the analysis show the uncertainties in the spacecraft's position, velocity, and geocentric radius at  $t + 30$  min. (Figures 8.5a through 8.5c).

Two cases were simulated:

Case 1: Three stations tracking simultaneously and a priori knowledge is assumed. Because of its long viewing period, the USBS at Guam was used in the two-way doppler mode.

Case 2: Same as case 1 with no a priori knowledge assumed.

#### 8.3.5 Leg 5 - Navigational Accuracies at Reentry

The results of the analysis illustrate the uncertainties in position, velocity, geocentric radius, and ground speed at reentry. (Figures 8.6a through 8.6d). It should be noted that, although the trajectory assumed for this analysis can be viewed from ground located stations up to five minutes before reentry, it is entirely possible for reentry to occur such that the vehicle cannot be viewed from the ground for the last 30 minutes or more before reentry.

Two cases were simulated:

Case 1: Madrid tracks the vehicle for the first 17 minutes and Guam tracks the vehicle up to five minutes before reentry. No a priori knowledge of the vehicle's position and velocity is assumed.

Case 2: Same as case 1 with a priori knowledge assumed.



## 8.4 DISCUSSION OF RESULTS

The results, presented below, represent how well the MSFN can do for a likely station and data utilization plan and suggest means for improving this utilization plan. Where improvement in navigational accuracy seems desirable, there are many avenues open which were not explored such as:

- (1) Utilization of onboard data
- (2) A more rigorous use of a priori knowledge
- (3) Solving for the three-way doppler biases
- (4) Utilization of more multiple station tracking data
- (5) Alternating assignments more frequently between the stations using two-way doppler.

### 8.4.1 Leg 1

The reason the one station solution with a priori knowledge information is so accurate is that the a priori knowledge accounts only for injection errors and not for the uncertainties prior to the injection burn. The case was run for the purpose of determining the value of a priori knowledge for the one station tracking situation. Leg 1 also demonstrates that with the filter used the processing of angles, after fifteen minutes, is a detriment rather than an aid.

### 8.4.2 Leg 2

The last 11 hours in the lunar sphere of influence are interesting in that they exhibit the possible fluctuations in solution accuracy due to station geometry. ANT, HAW, and GST offered a good geometrical view of the vehicle. The switch from ANT to CNB at 8 hr. and 30 min. resulted in an increase in position uncertainty because the vehicle was effectively in the same plane as CNB, GST, and HAW. (Figure 8.3a).

A corresponding change in the slope of the velocity uncertainty curves can be seen in Figure 8.3b. These figures also show that the difference between the assumed and no a priori knowledge has little effect after about two hours of tracking.

#### 8.4.3 Leg 3

This leg was separated from leg 2 for computational reasons only. In the long span of time available, the effect of a priori knowledge decreases. Because of the excessive amount of data available, the three station solution procedure was dropped in favor of sequential one station solutions. A more rapid reduction of uncertainty could be effected by use of simultaneous tracking or more rapid switching between stations. For results see Figures 8.4a and 8.4b.

#### 8.4.4 Leg 4

During this ten hour span, the three station solution procedure was resumed. A comparison of the uncertainties in position and radius (Figures 8.5a and 8.5c) show that the major uncertainty is in the orientation of the radius vector.

#### 8.4.5 Leg 5

There is little choice in selection of stations during this leg. For the analysis all available data was used. Even without a priori information the uncertainties in position, velocity, radius, and speed at reentry are less than 0.54 nm. (1 km), 7 ft/s (2 m/s), 0.3 nm (0.5 km) and 2 ft/s (0.5 m/s), respectively. This accuracy was achieved by 40 minutes of tracking in the last hour, and little improvement was achieved during the last twenty minutes. However, continuous coverage for the first 40 minutes may not always be available for all incoming trajectories. This, and its effect, must be investigated.

### 8.5 SUMMARY

By the time of the first, second and third midcourse corrections and by the time of reentry the ground will know the position and velocity uncertainties to:

	Position Uncertainty	(Out-of plane position com- ponent uncertainty)	Velocity Uncertainty
By time of first midcourse correction	49 nm (90 km)	47.5 nm (88 km)	39 ft/s (12 m/s)
By time of second midcourse correction	11 nm (20 km)	7.3 nm (13.5 km)	0.82 ft/s (0.25 m/s)
By time of third midcourse correction	22 nm (40 km)	21 nm (39 km)	7 ft/s (2 m/s)
By time of reentry	0.8 nm (1.5 km)	0.75 nm (1.4 km)	10 ft/s (3 m/s)

For the midcourse corrections the answers are referenced to the time of the maneuver and tracking was terminated 30 minutes prior to each maneuver to allow time for the ground to compute and execute an update and time for the vehicle to align for the maneuver.

## 8.6 CONCLUSIONS

The results that are presented in this study represent how well the MSFN can do for a likely station and data utilization plan and suggest means for improving this utilization plan.

The results for leg 1 (Figures 8.2a and 8.2b) indicate that three stations, tracking in the 3-way doppler mode, are no better than two in determining the orbit subsequent to injection and prior to the first midcourse correction. This leads to the conclusion that the biases on the data (being ignored by the ODP) are cancelling the usefulness of the data from the third radar. Therefore, the following table is presented to show that when the biases are accounted for, in the ODP, three stations are much better than two, as expected.

Time After injec- tion (hr:min)	Orbit Determination Program			
	Ignores biases (Figure 8.2a)		Solves for all Biases Listed on Figure 8.2a	
	MAD, ASC $3\sigma_p$ (nm)	MAD, ASC, TEX $3\sigma_p$ (nm)	MAD, ASC $3\sigma_p$ (nm)	MAD, ASC, TEX $3\sigma_p$ (nm)
00:35	15.1	40.4	14.1	10.4
2:35	14.0	14.6	5.3	2.6

A priori information is not a critical factor in determining the orbit when several hours of tracking is available (based upon the results for legs 2 through 5).

The uncertainties in position and velocity for the first midcourse correction are 54 nm (100 km) and 39 ft/s (11.5 m/s), assuming no a priori knowledge.

The uncertainties in position and velocity for the second midcourse correction are 11 nm (20 km) and 0.9 ft/s (0.3 m/s).

The uncertainties in position, velocity, and radius for the third midcourse correction are 23 nm (43 km), 6 ft/s (1.8 m/s), and 1.2 nm (2.2 km), respectively.

Based upon the first 40 minutes of tracking, the uncertainties in position, velocity, radius, and ground speed at reentry are 0.8 nm (1.5 km), 10 ft/s (3.1 m/s), 0.25 nm (0.46 km), and 2 ft/s (0.6 m/s), respectively.

## 8.7 APPENDIX A - COORDINATE SYSTEMS

### 8.7.1 Coordinate System for Station Location

The coordinate system is earth centered with the x-axis passing through the prime meridian, the z-axis in the direction of the earth's angular momentum vector and the y-axis such as to form a right-hand orthogonal system.

### 8.7.2 Vehicular Coordinate System

The coordinate system is an inertial earth or moon centered (depending upon the reference body) coordinate system with the x-axis pointing toward the vehicle, at time  $t = 0$ , the z-axis in the direction of the orbital angular momentum vector and the y-axis such as to form a right-hand orthogonal system.

## 8.8 APPENDIX B - TRAJECTORIES

### 8.8.1 Trajectory A

This trajectory is a conic section generated from the following initial conditions.

#### Moon Referenced

AT TIME	Radius (nm)	Inclination to Moon's Equator	Subvehicle Point	
			Latitude	Longitude
0	1022.973	175.95°	1.44°S	149.48°W
			Velocity (ft/s)	
			Tangential 8008.566	Radial 202.4777

The vehicle is ascending in its lunar orbit.

#### Moon with Respect to Earth

E-M Distance (nm)	Inclination of Moon's Orbit to Earth's Equator	Sublunar Point at $t = 0$
207577.08	28.67°	10°N, 15°W

The moon is ascending in its orbit.

### 8.8.2 Trajectory B

This trajectory is a conic section generated from the following initial conditions

Earth Referenced				
AT TIME	Radius (nm)	Inclination to Earth's Equator	Subvehicle Point Latitude	Longitude
0	178,762.8906	37.92°	25.781°N	123.4°
	Velocity (ft/s)			
	Tangential		Radial	
	703.01224		-1897.105752	

And the vehicle is ascending in its orbit.

### 8.9 APPENDIX C - COMPONENTS OF ASSUMED A PRIORI KNOWLEDGE

Position (nm)			Velocity (ft/s)		
$\sigma_x$	$\sigma_y$	$\sigma$	$\sigma_{\dot{x}}$	$\sigma_{\dot{y}}$	$\sigma_{\dot{z}}$
0.06	0.09	0.42	2.21	.95	1.48
Leg 2					
1.62	1.62	4.32	6.56	6.56	16.40
Leg 3					
.59	8.35	41.94	0.39	1.44	6.89
Leg 4					
2.16	2.70	4.32	3.28	3.28	16.40
Leg 5					
14.04	14.04	8.64	6.56	6.56	13.12

#### 8.10 APPENDIX D - CHECK OUT PROCEDURES

The error analysis program that was used to obtain the results presented in this chapter has been thoroughly checked out during the past two years.

In addition, results from the program have been compared to orbital accuracies based on real time data (Ranger and Gemini) for earth orbits and were found to compare favorably therewith. The same assumptions were made for this study as were made in the comparison and, therefore, the results as presented are considered to be conservative estimates of the capability of the MSFN.

#### 8.11 REFERENCES

1. "Description of Orbit Error Analysis Program," Volumes 1 and 2, Bissett-Berman Corporation, Santa Monica, Calif., July and August, 1965.
2. MSC-GSFC, ANWG Report No. 65-AN-1.0, "Apollo Missions and Navigation Systems Characteristics," February 5, 1965.

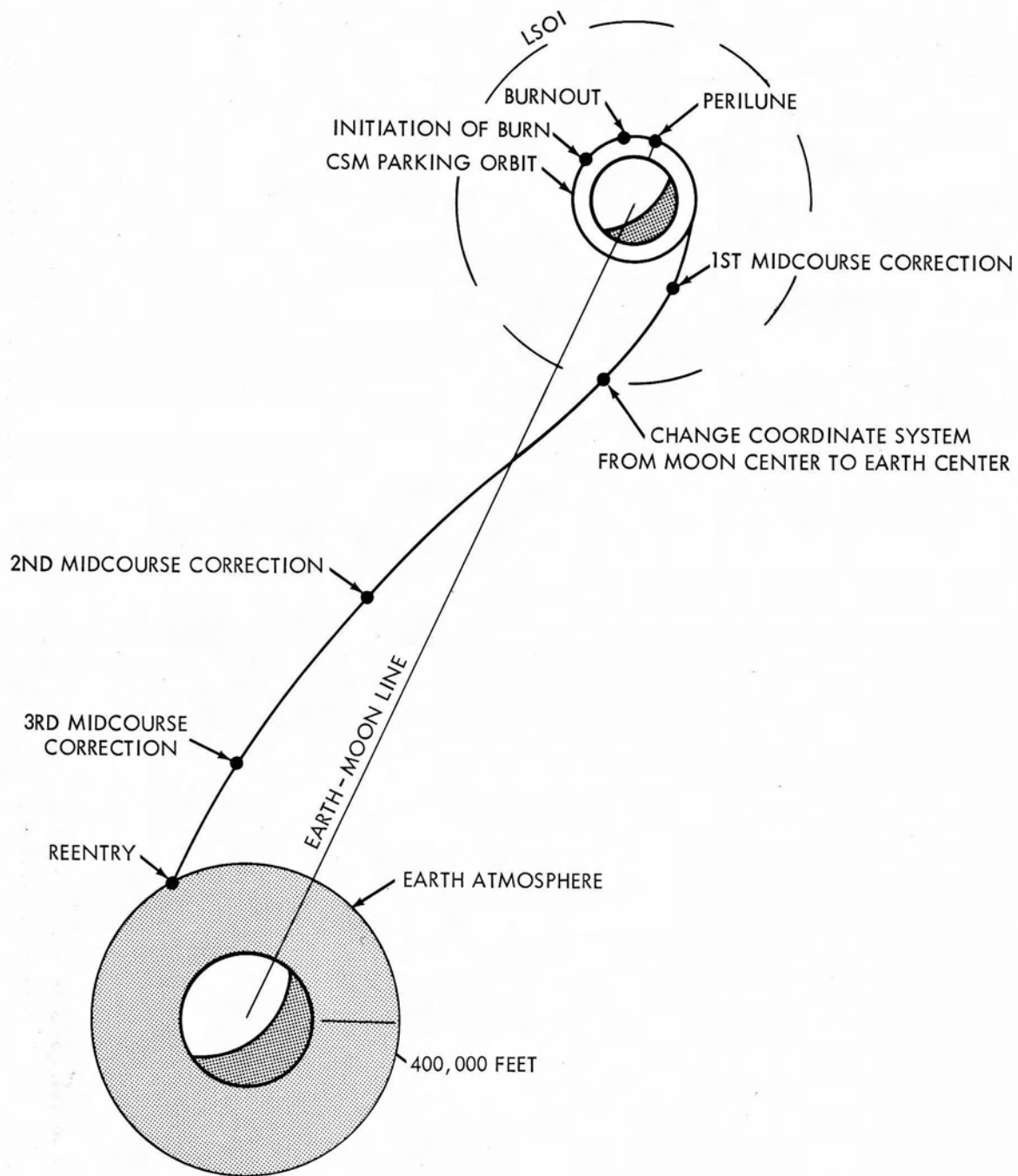


Figure 8.1—Geometry for earth transfer orbit



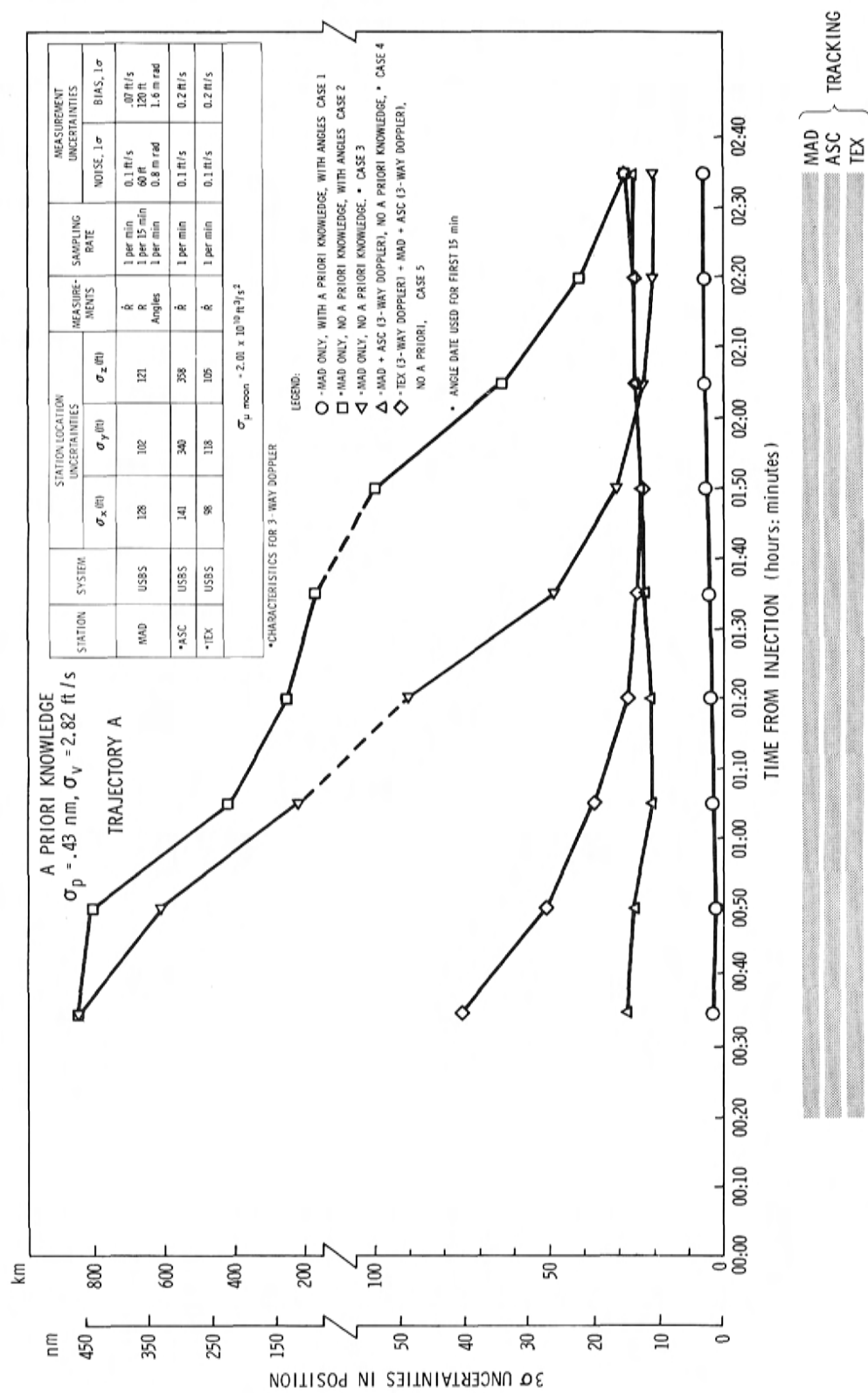


Figure 8.2a-Navignational accuracies for transearth injection. Position uncertainties (reference to t=0 min.) leg 1.

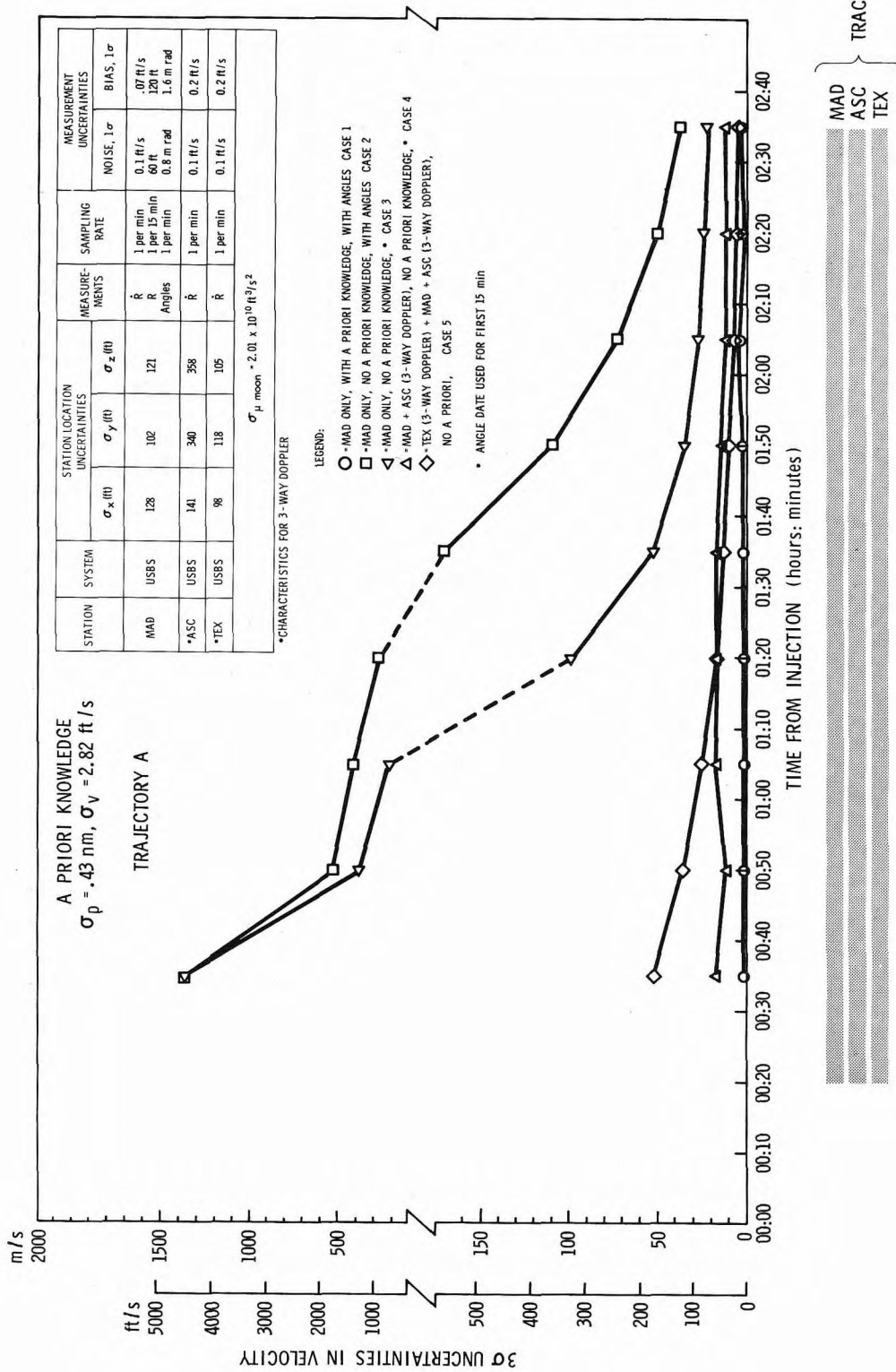


Figure 8.2b-Velocity uncertainties (reference to  $t = 0 \text{ min.}$ ) leg 1

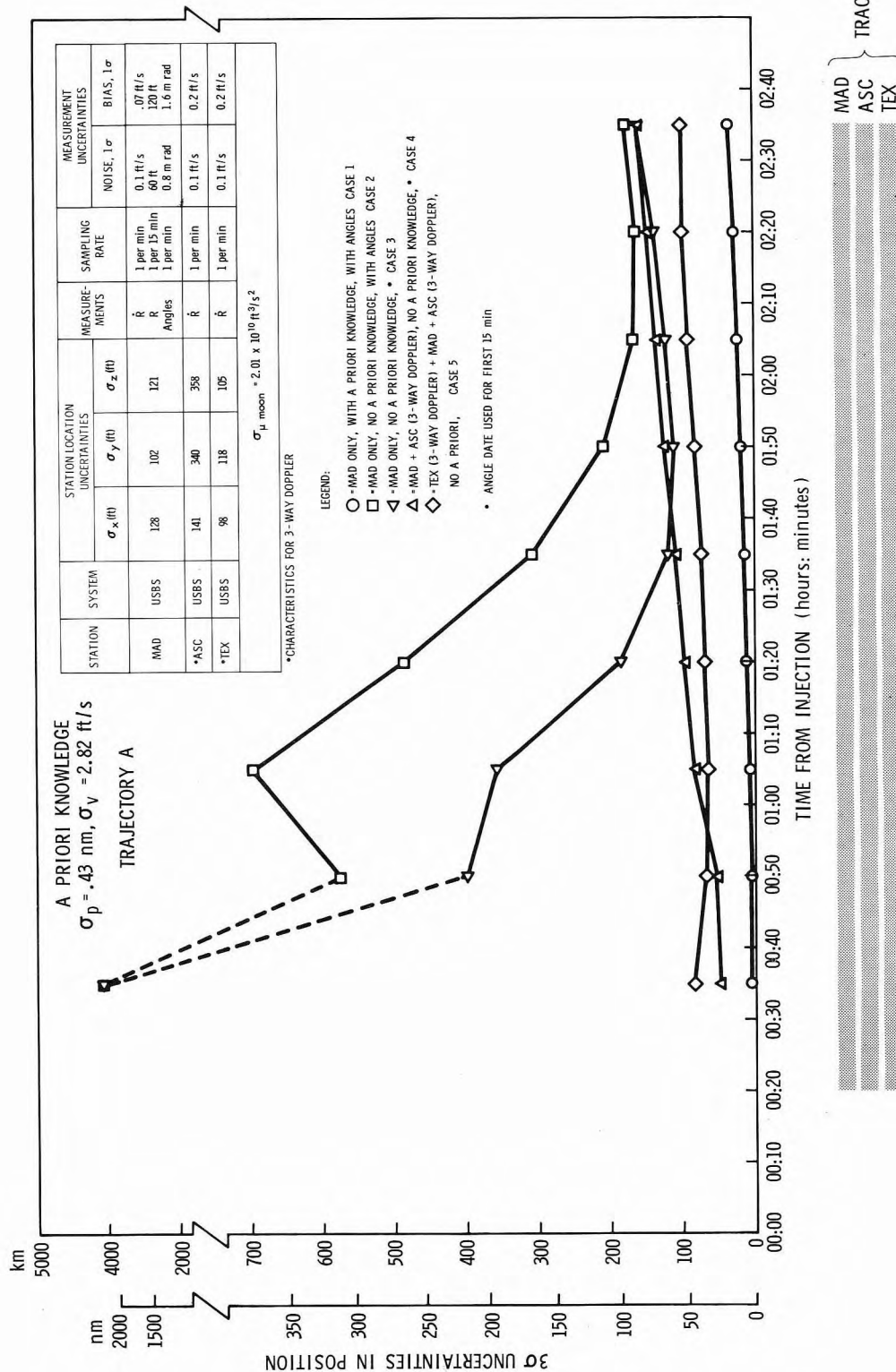


Figure 8.2c-Position uncertainties (propagated to  $t + 30 \text{ min.}$ ) leg 1

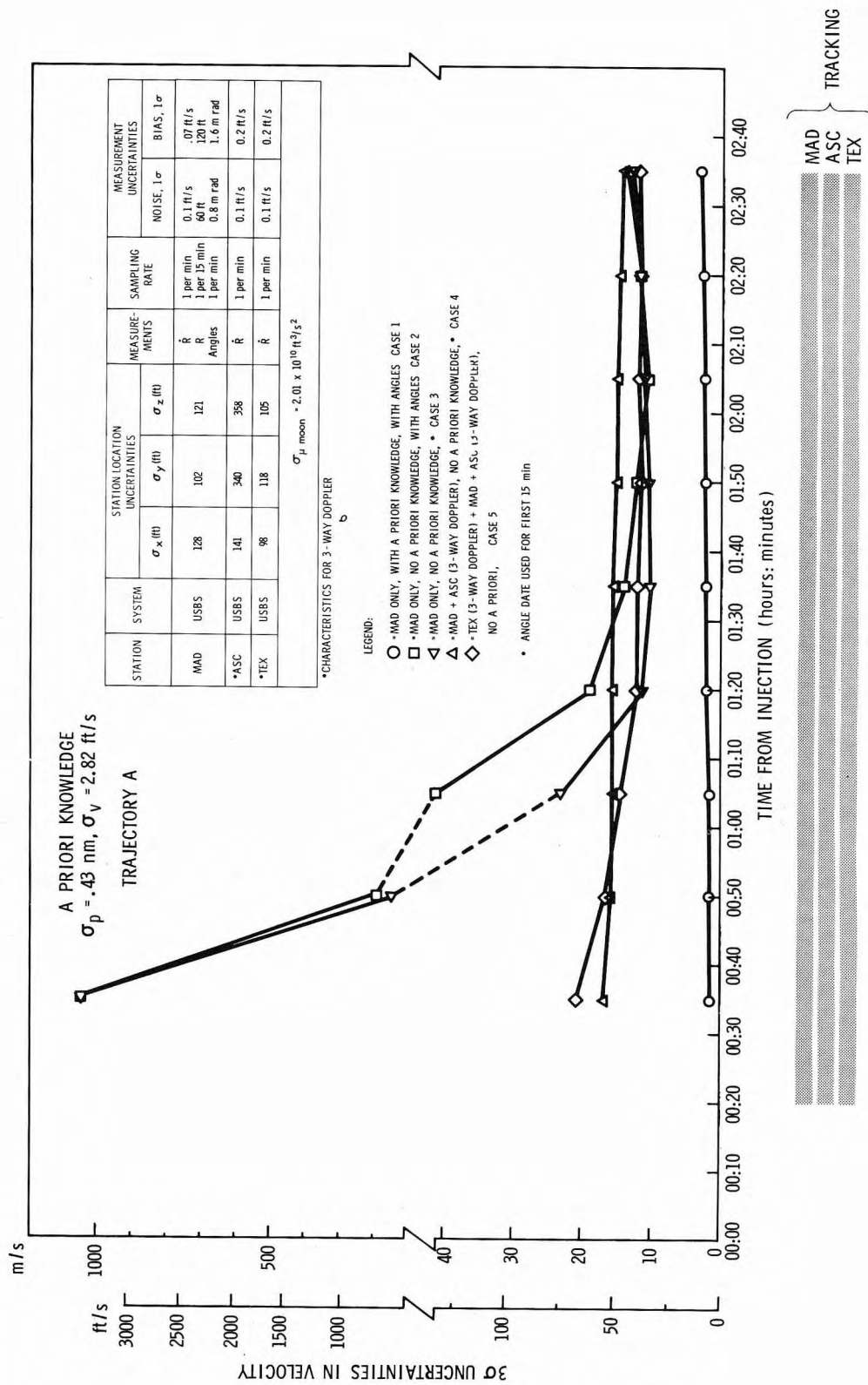


Figure 8.2d - Velocity uncertainties (propagated to  $t + 30 \text{ min.}$ ) leg 1

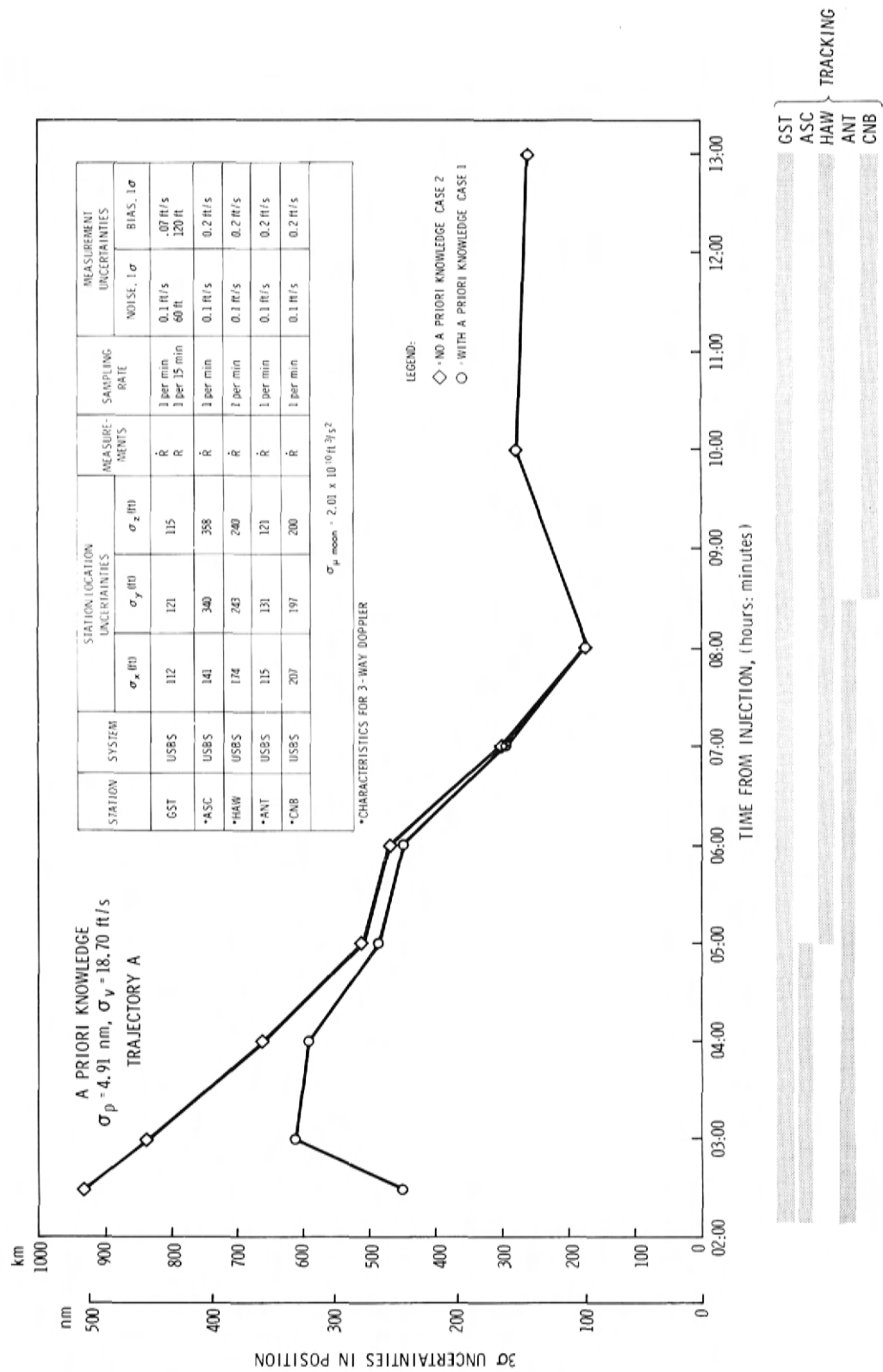


Figure 8.3a-Position uncertainties (propagated to  $t + 30 \text{ min.}$ ) leg 2.  
 Navigational accuracies for entry into ESOI.

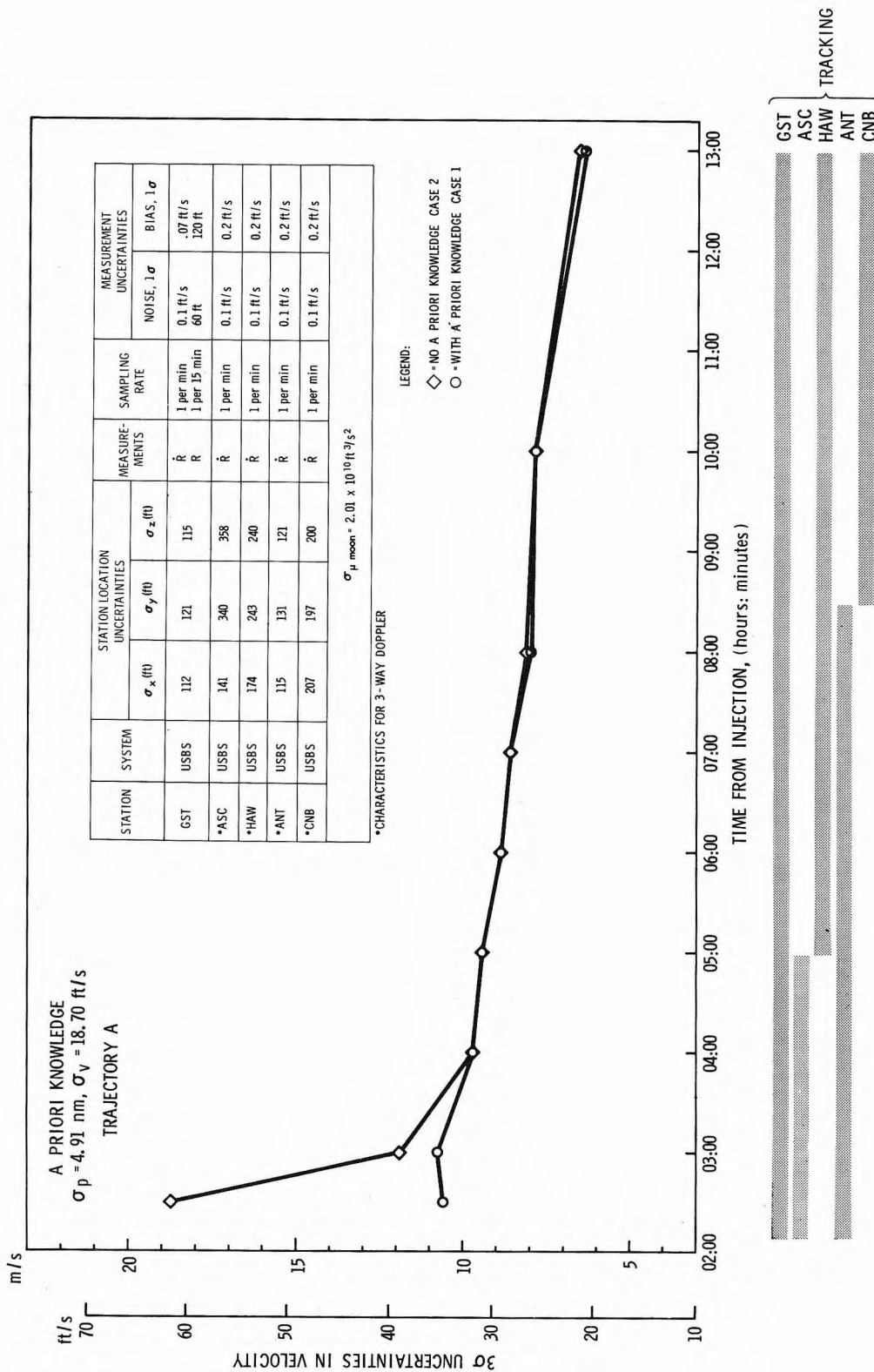


Figure 8.3b-Velocity uncertainties (propagated to  $t + 30 \text{ min.}$ ) leg 2.

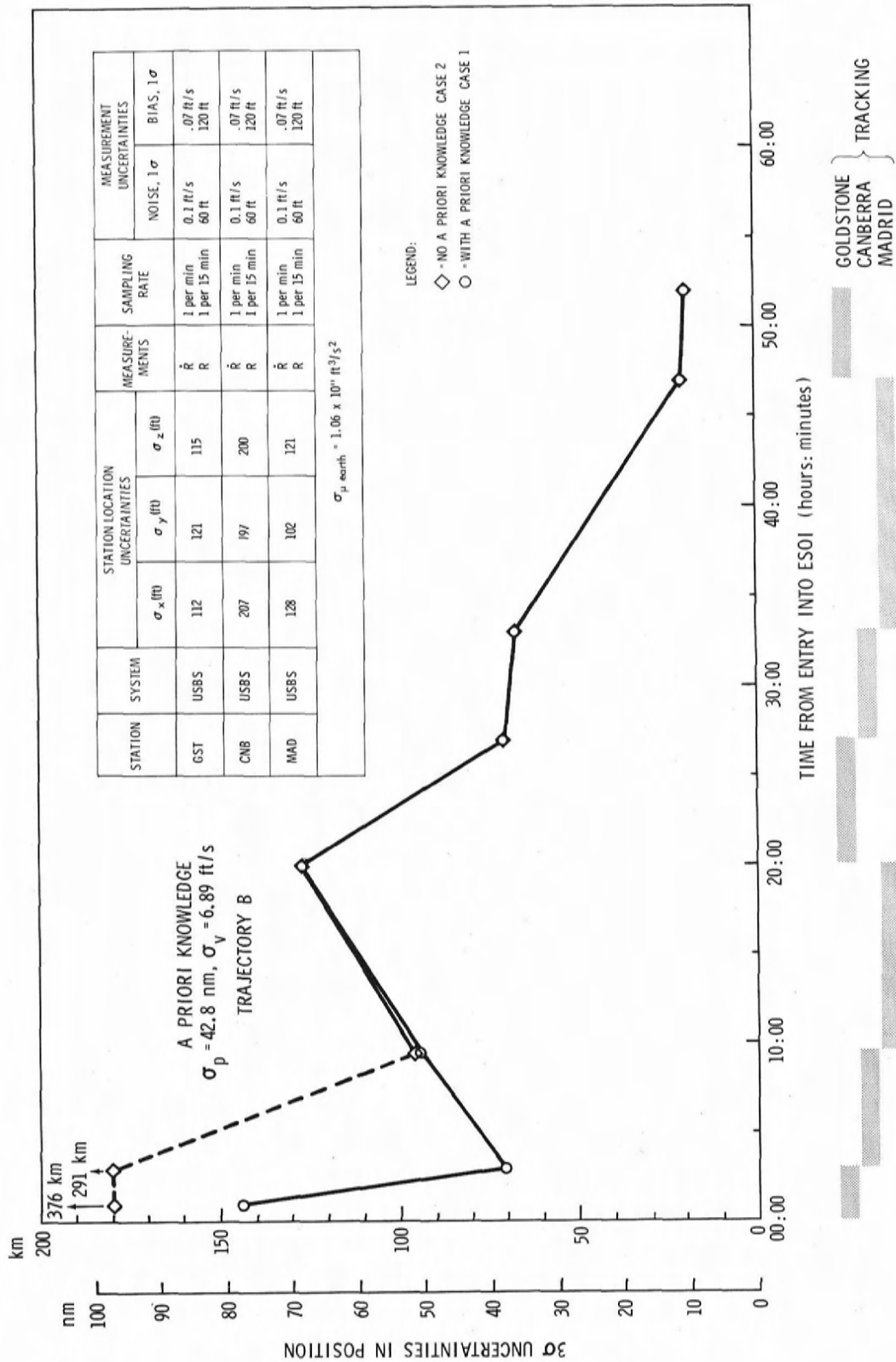


Figure 8.4a—Navigational accuracies for second midcourse corrections. Position uncertainties (propagated to  $t + 30 \text{ min.}$ ) leg 3.

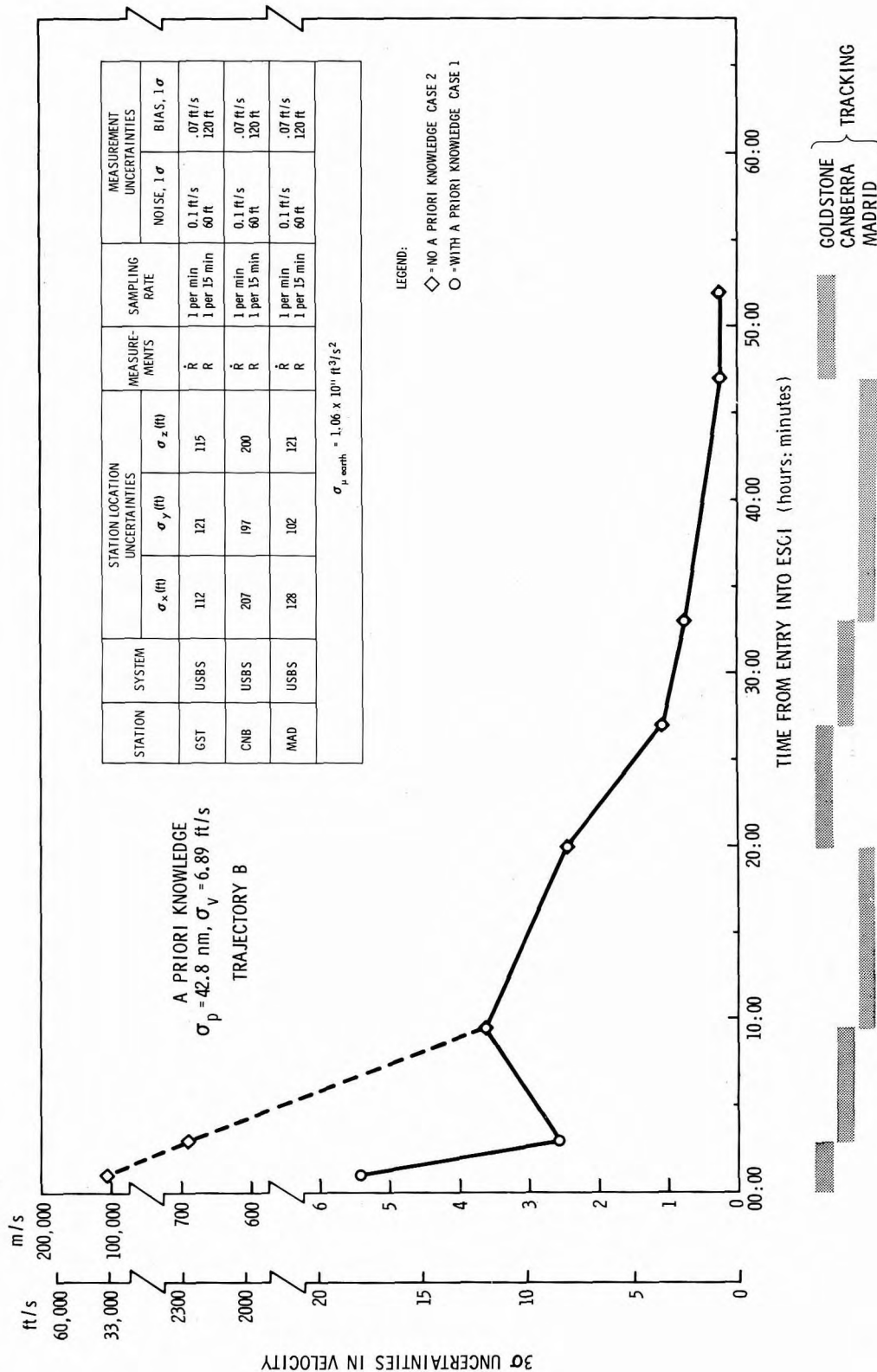


Figure 8.4b—Velocity uncertainties (propagated to  $t + 30 \text{ min.}$ ) lea 3.



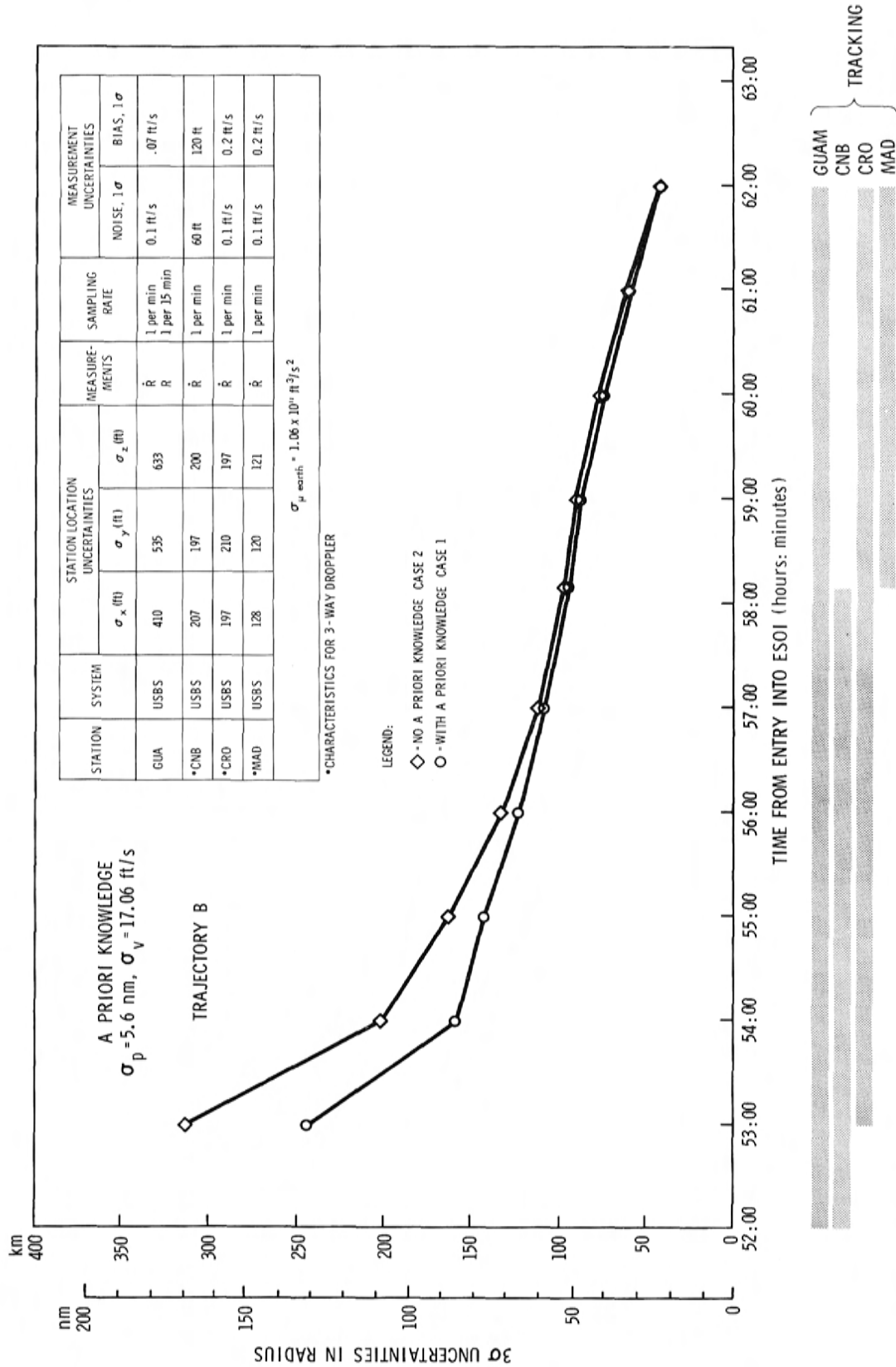


Figure 8.5a—Navigational accuracies for third midcourse correction. Position uncertainties (propagated to  $t + 30 \text{ min.}$ ) leg 4.

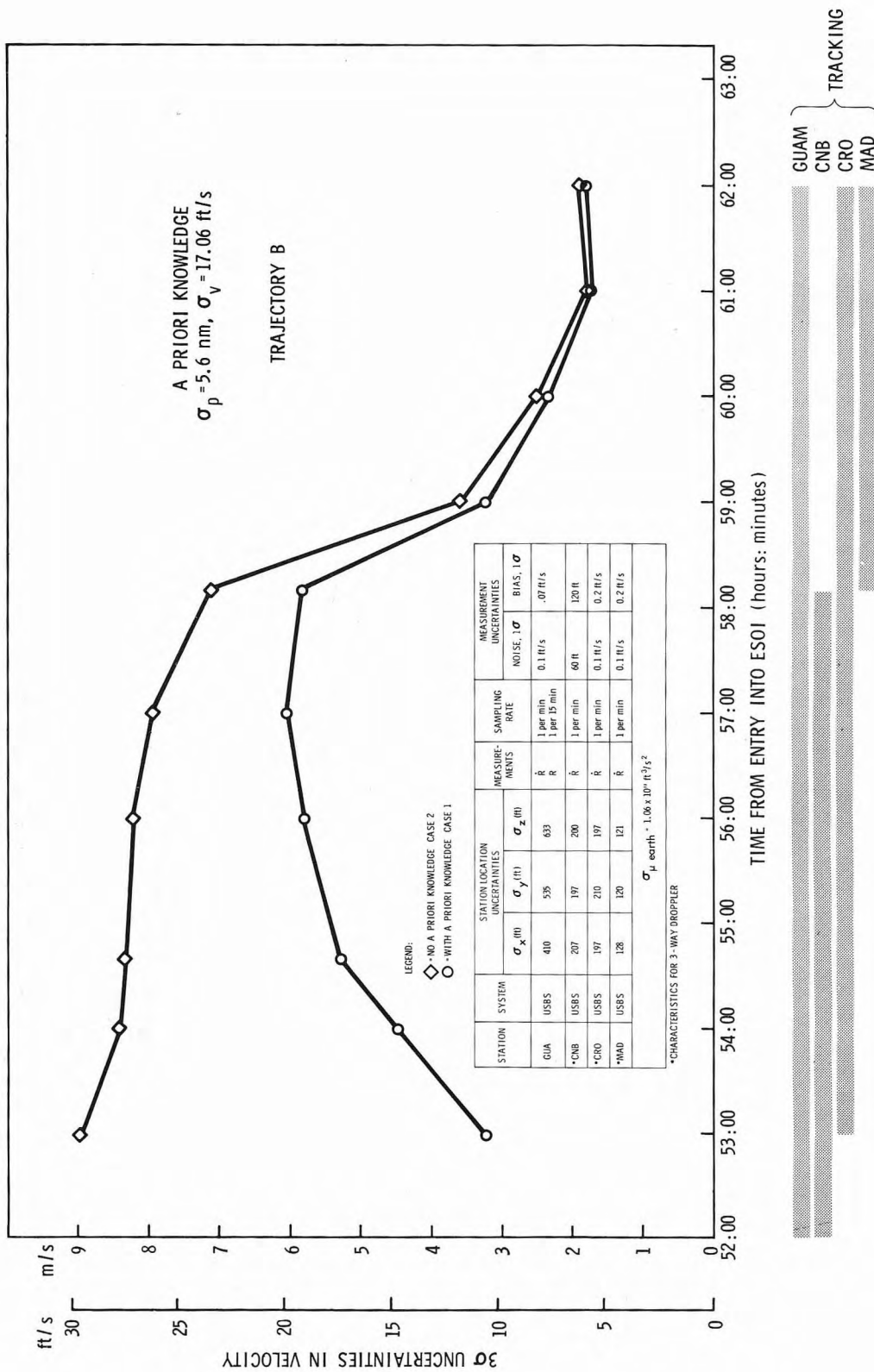


Figure 8.5b—Velocity uncertainties (propagated to  $t + 30 \text{ min.}$ ) leg 4.

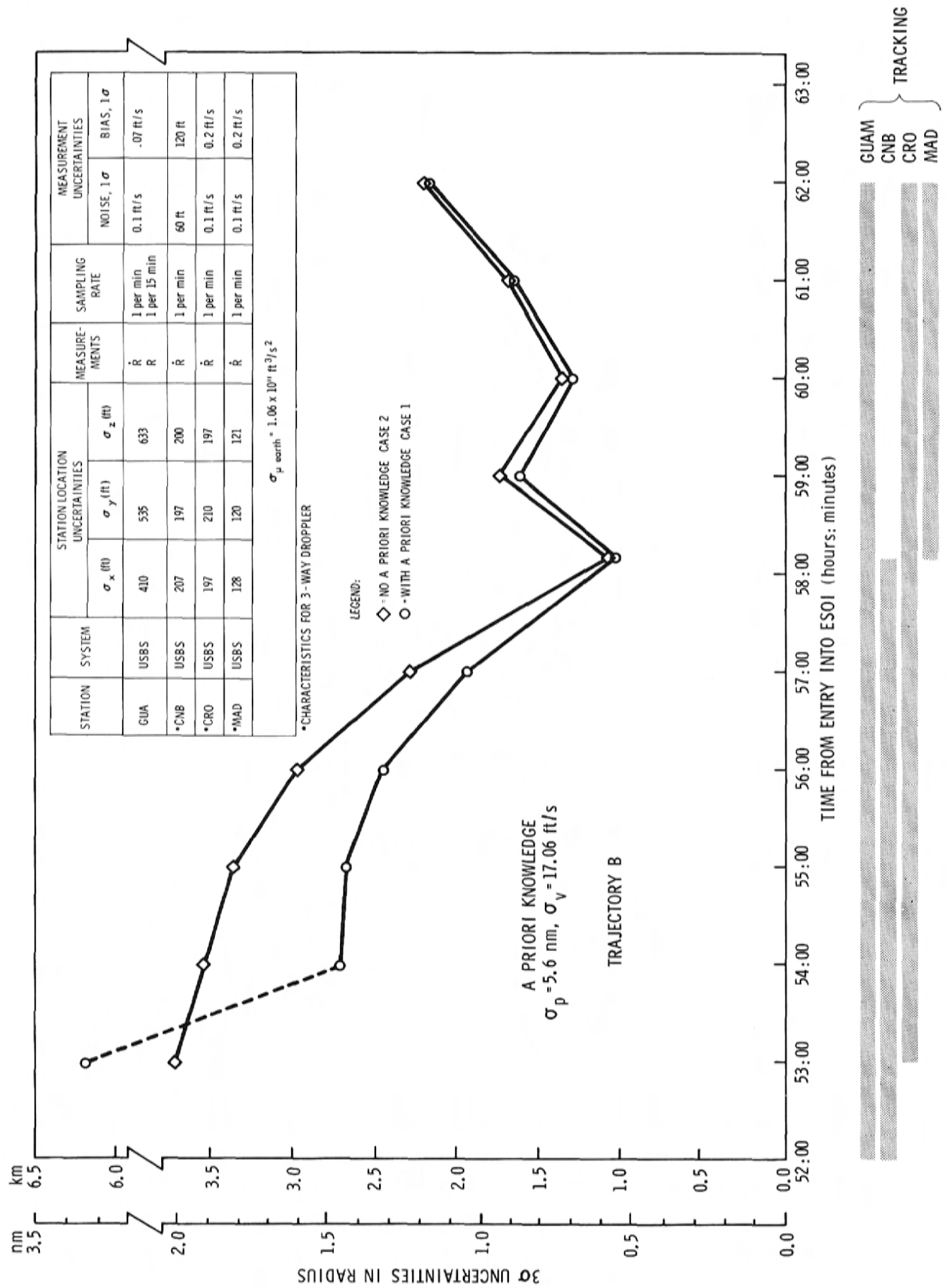


Figure 8.5c—Navigational accuracies for third midcourse correction. Radius uncertainties (propagated to  $t + 30 \text{ min.}$ ) leg 4.

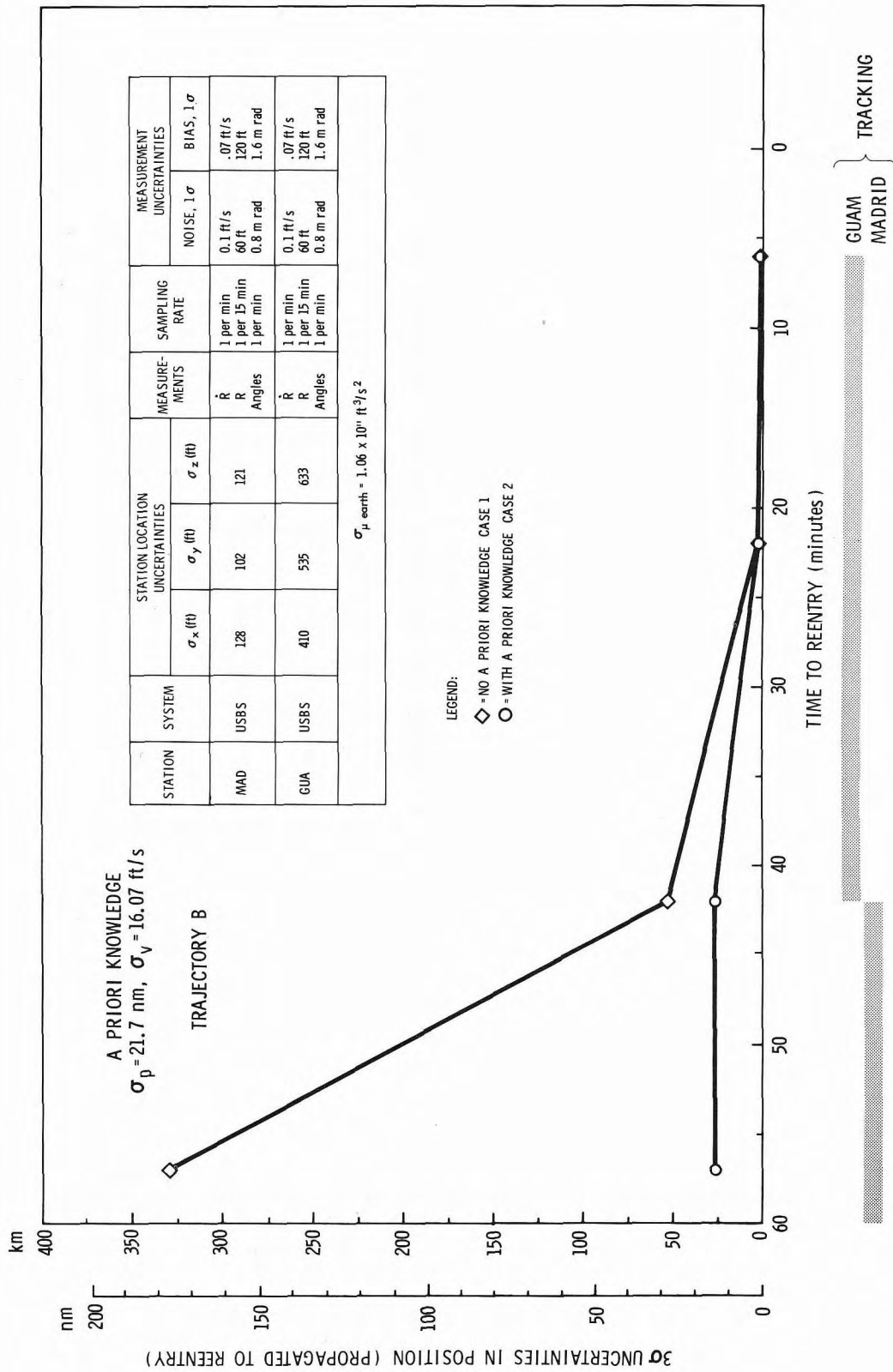


Figure 8.6a—Navigational accuracies for reentry. Position uncertainties (propagated to reentry) leg 5.

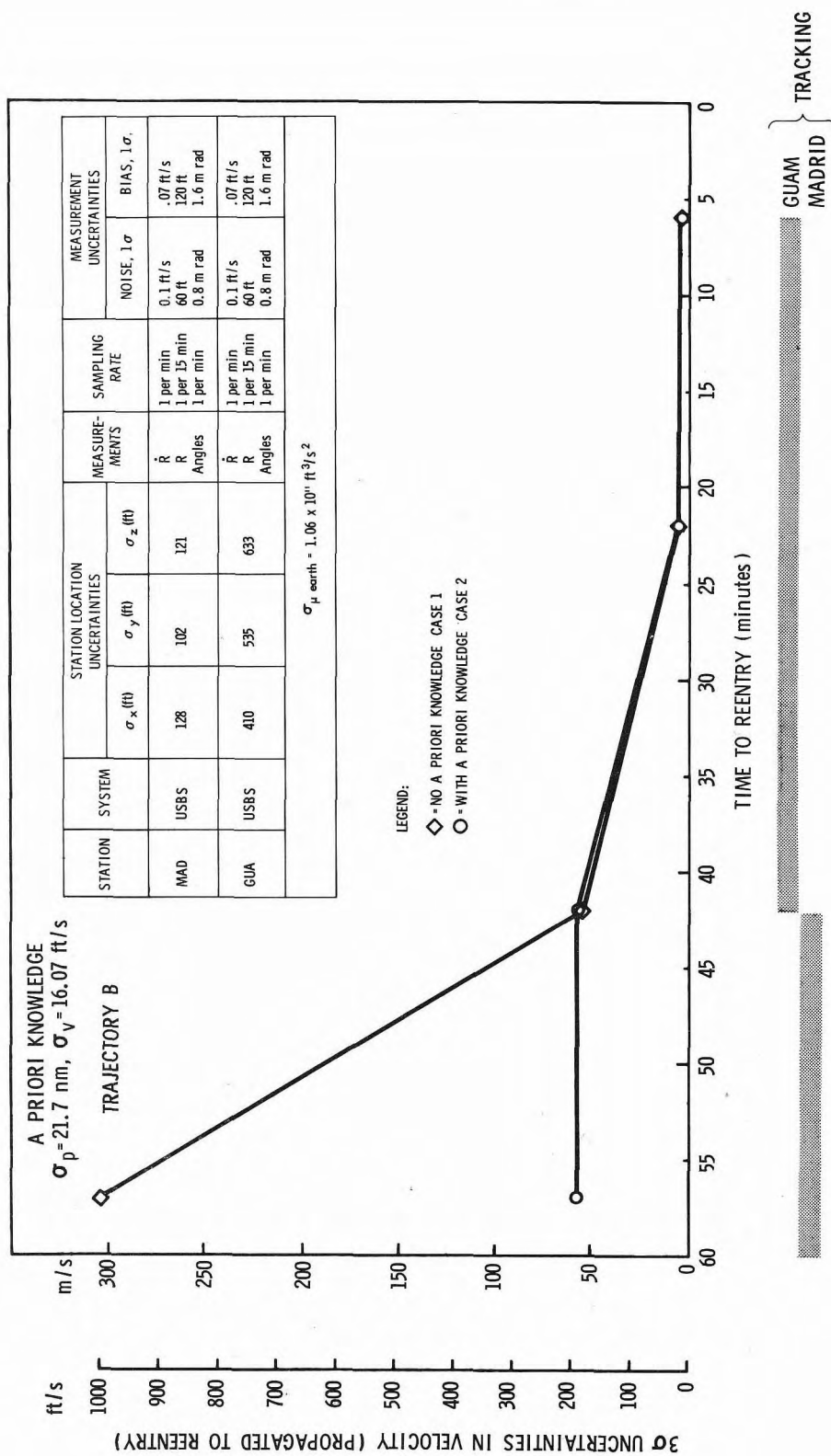


Figure 8.6b—Velocity uncertainties (propagated to reentry) leg 5.

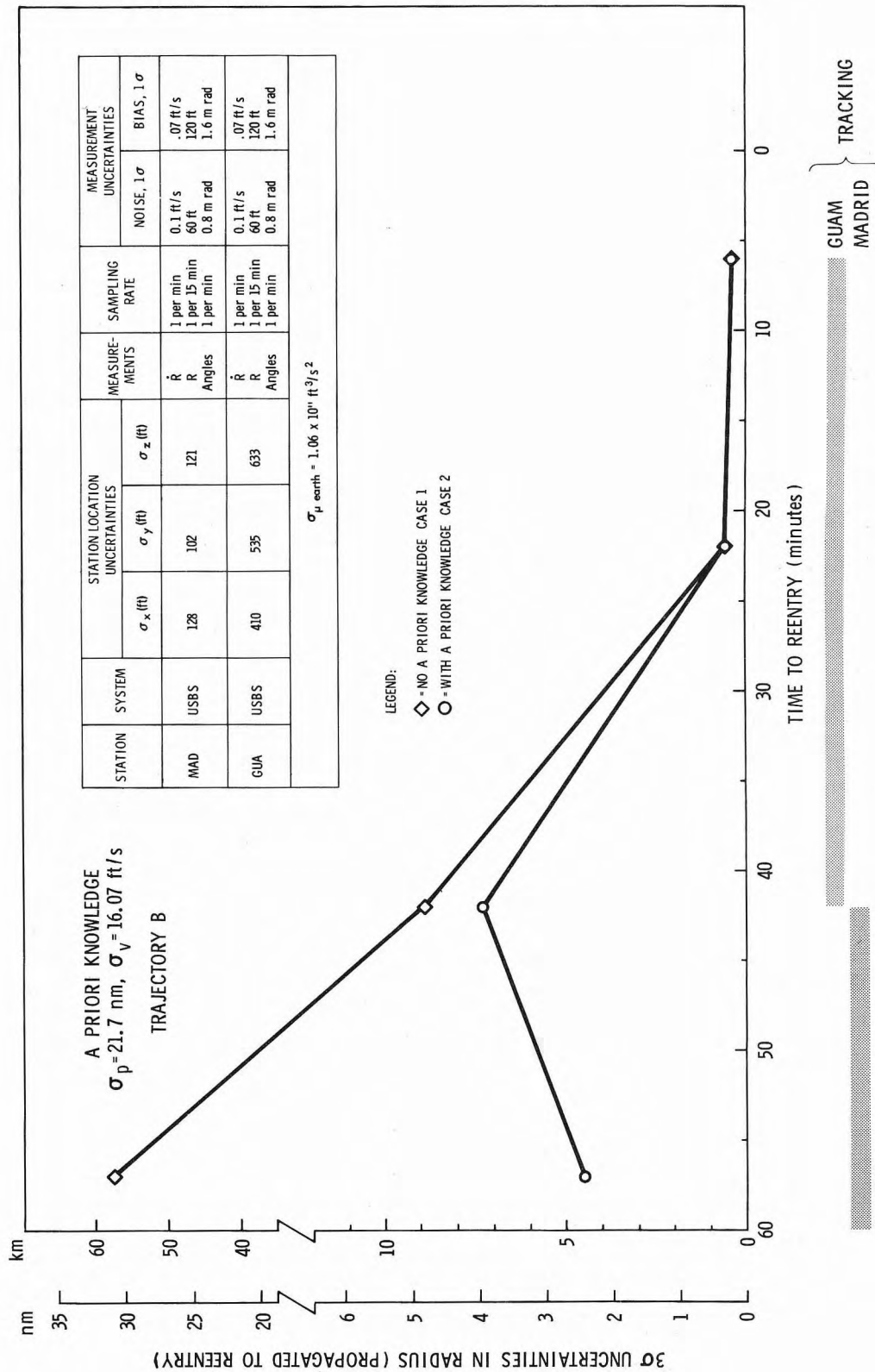


Figure 8.6c--Radius uncertainties (propagated to reentry) leg 5.

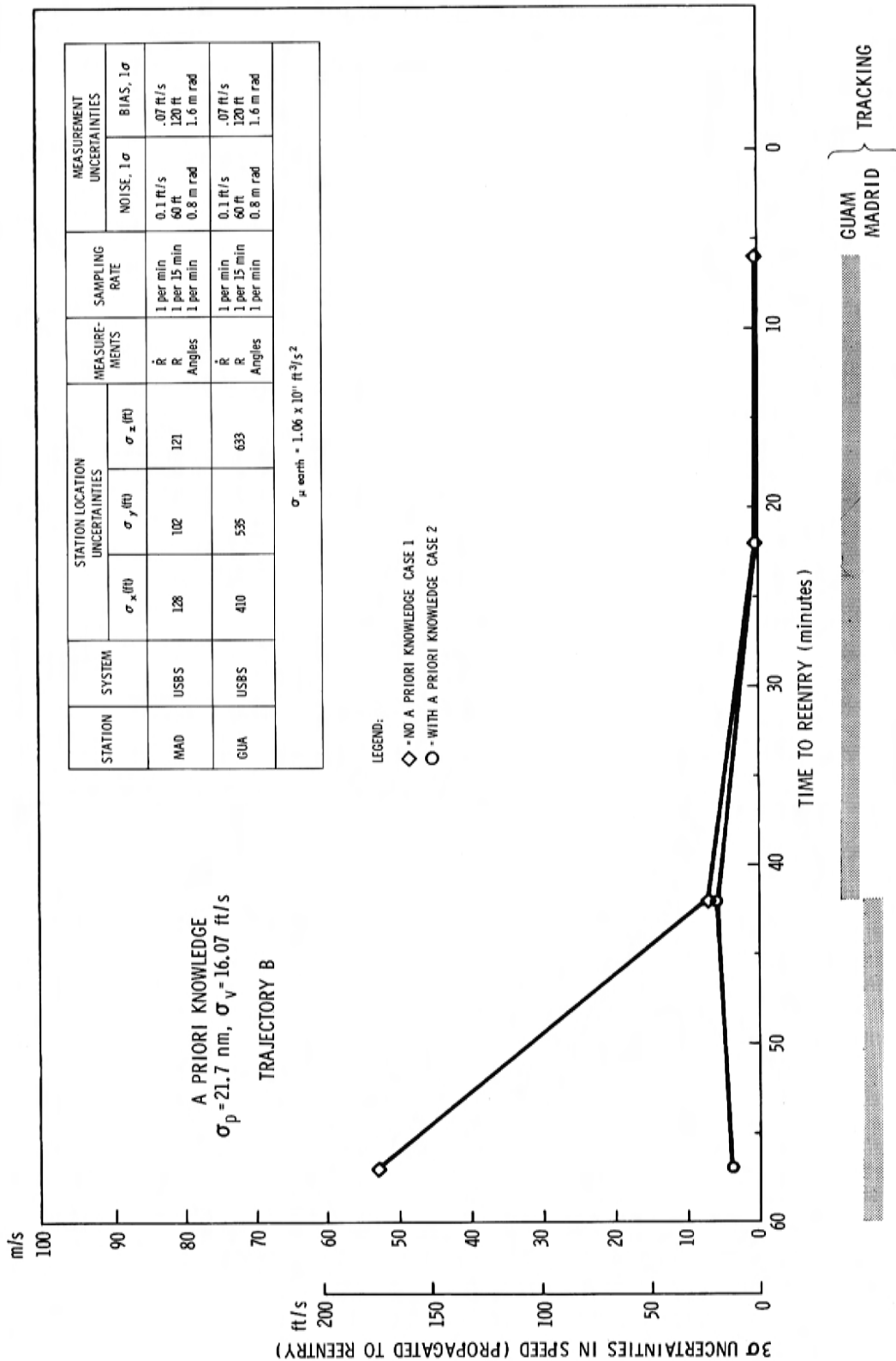


Figure 8.6d—Ground speed uncertainties (propagated to reentry) leg 5.

## 9.0 REENTRY PHASE

### 9.1 INTRODUCTION

The purpose of this chapter is to discuss the navigational problems encountered during the earth reentry phase of an Apollo lunar mission. The navigational accuracies at the point of atmospheric reentry that are required to complete a safe single pass reentry are defined by a reentry corridor. It will be the function of the midcourse navigation and guidance system to steer to a point in this corridor that will ensure a safe reentry. Safe reentry will be defined to mean a reentry within a corridor that prevents undershoot and its accompanying excess aerodynamic loads or overshoot and an uncontrolled exit back into space.

Throughout the reentry phase, the onboard inertial navigation system will be the primary method of navigation. In addition, operational requirements on the lunar mission specify that the Command Module be tracked by radar during a skip-out portion of the reentry trajectory (Reference 1). However, the tracking system to be used has not been specified at this time; therefore, no tracking errors are presented for this phase. Emphasis will be placed on the capabilities of the onboard inertial system and the Manned Space Flight Network will be discussed in future revisions to this document. The problems associated with positioning the ship and tracking during reentry are discussed from the point of view of the Command Module range capabilities and communications "blackout" during reentry.

### 9.2 ASSUMPTIONS AND PROCEDURES

#### 9.2.1 Definition of Reentry Phase

The aerodynamic portion of the phase is assumed to begin when the Command Module reaches an altitude of 400,000 feet (122 km). This phase is assumed to terminate at an altitude of 24,000 feet (15 km). The reentry trajectory that the Command Module will follow is a function of the steering commands that are generated by the onboard guidance system which in turn are a function of the onboard navigational measurements combined with the targeting data in the Apollo Guidance Computer.



### 9.2.2 Reentry Corridor

The reentry corridor is defined by the conditions at the beginning of the earth's atmosphere (assumed 400,000 feet altitude) that will allow a safe reentry of the Command Module. It is the function of the midcourse guidance system to steer to a point within the reentry corridor such that the estimates of the position and velocity combined with the uncertainties in these quantities are still within the corridor.

The concept of the reentry corridor was discussed by Chapman (Reference 2) and is presented pictorially by Figure 9.1. The numerical values that define the corridor for the Apollo Command Module are presented in Figures 9.3a to 9.3h. The technique that was used to compute the reentry corridor is described in Reference 3 which was the source of the information presented here.

The reentry corridor is formed by overshoot and undershoot boundaries, as the lower and upper limits, respectively. The overshoot boundary as used in this report is formed by the reentry conditions (inertial velocity and flight path angle) that will enable the spacecraft to be captured by the earth's gravitational field and atmosphere on the first attempt. Both positive and negative lift overshoot boundaries are shown on the figures. The use of negative lift has the effect of increasing the corridor width to allow for more flexibility at the reentry interface. The conditions on both of these overshoot boundaries result in equilibrium glide conditions when the flight path angle passes through zero. Equilibrium glide is defined to be the condition when the time rate of change of flight path angle equals zero ( $\dot{\gamma} = 0$ ). Thus, with an equilibrium condition at the point when the flight path angle equals zero, it is possible to prevent the altitude from increasing and thus an uncontrolled skip out.

The negative lift overshoot boundary is defined by a lift vector down attitude from reentry to the point when the flight path angle equals zero. The positive lift overshoot boundary is based on a lift vector up orientation from the reentry interface until zero flight path angle, but with lift vector instantaneously re-oriented to 15 degrees from the lift vector down attitude at zero flight path angle. This approximate lift vector down attitude is required to maintain an equilibrium glide condition. The 15 degree orientation from the lift vector down position is to compensate for the finite time required to roll from the lift vector up (positive lift) to the lift vector down attitude (negative lift).

The undershoot boundary is defined as the reentry conditions that will not exceed a specified "g" limit between the reentry interface and the point that the flight path angle equals zero.

To account for atmospheric density deviations from the 1962 U. S. Standard Atmosphere, the effect of density deviation was evaluated using the change of density defined in Reference 7. This density deviation is also presented in Figure 9.2 of this report. The effect of a negative deviation of the atmosphere on the overshoot boundaries is to reduce the width of the corridor. For the undershoot boundaries, however, the corridor is reduced by either a positive or negative density deviation depending on the reentry velocity.

The reentry corridors are shown in Figures 9.3a through 9.3d, in terms of reentry inertial flight path angle for lift-to-drag ratios ( $L/D$ ) of 0.2, 0.3, 0.34, and 0.4, respectively. An alternate means of describing the reentry corridors is vacuum perigee altitude. The corridors are presented in Figures 9.3e to 9.3h for the same values of lift-to-drag ratio.

### 9.2.3 Unusual Problems During Reentry

There are two unique problem areas in the acquisition and tracking of the Command Module from the ground during the reentry phase.

1. The Command Module will have the capability to move in a lateral direction as well as down range.
2. There will be communications blackout during a significant portion of the flight.

The lateral capability of the Command Module is desirable from a guidance point of view but adds to the difficulty of placing a tracking ship along the flight path. The lateral capabilities of the Command Module for lift-to-drag ratios of 0.3 to 0.4 as a function of range are presented in Figures 9.4a to 9.4g. These results also show the predicted communications blackout boundaries that can be expected during the flight. It should be noted that the problem of predicting the onset and termination of communications blackout has not been completely resolved at present (Reference 4); therefore, these curves should be used with caution. Furthermore, the lateral capabilities of the Command Module are based on current estimates of the spacecraft aerodynamic characteristics which are also subject to revision. However, these curves may be used for present planning purposes and will be updated as more current information becomes available. Lift-to-drag ratios of 0.3 and 0.4 were chosen because they bound the nominal ratio of 0.34.

There is a requirement for the Command Module to be tracked during a skip-out phase of the reentry trajectory. However, the equipment to be used by the tracking ship during reentry has not been specified at the present time. Consequently, the discussion of the tracking ship will be deferred until future revisions of this document.

#### 9.2.4 Capabilities of the Onboard Inertial Navigation System

Throughout the reentry phase the primary means of navigation will be the self-contained, onboard inertial navigation system. It is the purpose of this section to discuss the errors in indicated position at the termination of the reentry trajectory. In order to prevent the necessity of a classified appendix to this volume, the results of the inertial guidance system error analysis will not be presented here. The reader is referred to Reference 6 for the absolute values of the system performance. Position errors have been computed separately for each hardware error source and are tabulated in Reference 6 for reentry trajectories of 1500 and 5000 nautical mile total range. A discussion of the results will be presented here, however.

##### Assumptions and Method of Analysis

The following assumptions are pertinent to the analysis and interpretation of data contained in Reference 6.

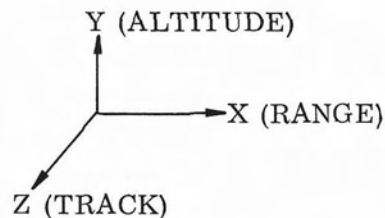
1. The position and velocity uncertainties due to the various Inertial Measurement Unit error terms are predicted uncertainties. No steering errors were assumed. The uncertainties in position were computed separately for each sensor error term using an array of error equations and the input position and acceleration profile from the trajectory data. These equations take into account the effect of the position error on the gravity vector computation.
2. The Inertial Measurement Unit was aligned prior to reentry.
3. The data in the error tables (Reference 6) are given relative to local vertical axis (altitude, track, range) at an altitude of 50,000 feet.
4. An "open loop" method of analysis was used to propagate inertial system errors to termination of a reentry trajectory. "Open loop" in this case means that the errors in position and velocity were not propagated through the guidance equations which would cause erroneous steering commands. Reference 5 gives a description of the type of analysis used. A comparison of this technique with a complete flight simulation computer program indicated a difference of about 20 percent, item for item, and about 10 percent for the total root-sum-square.

The onboard inertial navigation system consists of the following components.

1. Inertial Measurement Unit
2. Display and Control Unit
3. Digital Guidance Computer

The navigational uncertainties due to hardware errors in the Inertial Measurement Unit will be discussed in this chapter.

The following local coordinate system is defined for the termination of the reentry trajectory and is applicable to the following discussion of the onboard system.



The X-axis is in the local horizontal along the velocity vector, Y is the local vertical (up) and Z completes the right-hand triad.

The accuracy of the onboard inertial system is a function of the components in the system. The component error sources considered in the analysis are accelerometer errors and gyro errors and are tabulated below.

#### Accelerometers

1. Bias
2. Scale Factor
3. Non-Orthogonality
4. Acceleration Squared Sensitive Indication

#### Gyros

1. Null Bias Drift
2. Acceleration Sensitive Drift
3. Acceleration Squared Sensitive Drift

The following generalized error models were used for the study:

1. Accelerometer Error Model

$$\Delta A_I = B + (SF)A_I + (GSEN) A_I^2 + (NO)A_J$$

where

$A_I$  = Sensed acceleration along accelerometer input axis

$A_J$  = Sensed acceleration along  $J^{th}$  axis normal to  $A_I$

$B$  = Accelerometer bias error

$SF$  = Accelerometer scale factor error

$GSEN$  = Accelerometer sensitivity to input acceleration squared

$NO$  = Accelerometer input axis misalignments

2. Gyro Drift Model

$$\dot{\phi} = BIAS + (ADIA)A_I + AD_{(IA) (IA)} A_I^2$$

where

$BIAS$  = Null bias drift

$ADIA$  = Acceleration sensitive drift

$AD_{(IA) (IA)}$  = Acceleration squared sensitive drift

3. Initial Platform Misalignment

### 9.3 RESULTS AND CONCLUSIONS

It was found that the errors in the components of the inertial system themselves contribute little to the final position errors as compared with the initial condition errors or the initial platform misalignment error. The misalignment about the vertical propagates primarily into track errors; the misalignment about the downrange axis propagates into track errors; and the misalignment about the track axis propagates into altitude and range errors.

The seven inertial component error sources that were considered (see page 9-6) were assumed to be uncorrelated. The accelerometer with the input axis along the vertical does not propagate any of the accelerometer error sources into a track error, whereas the accelerometer with the input axis normal to the trajectory plane does not propagate any of the accelerometer error sources into altitude or range errors at touchdown. The accelerometer with its input axis along the range axis does not propagate any of its error sources into track errors at final touchdown. The gyro with its input axis normal to the trajectory plane does not propagate any of its error sources into track errors at final touchdown.

The accelerometer bias errors cause the largest final position errors of the inertial components with the null bias drift and the gyro acceleration sensitive drift the next largest error sources, respectively.

#### 9.4 LEVEL OF CONFIDENCE

The error analysis technique that was described is termed an "open-loop" error analysis. The errors are integrated based on a pre-stored guided reentry trajectory that is generated with a perfect stable platform and initial conditions. This technique had been compared with what is termed a "closed loop" error analysis. The "closed loop" error analysis uses a guided reentry with an imperfect stable platform and initial conditions to generate steering commands. Hence, the steering commands are based on indicated position and velocity. The difference between the two analyses is about 20 percent, item for item, and better than 10 percent for the total root-sum-square.

#### 9.5 ACKNOWLEDGMENT

The editor wishes to acknowledge the contributions to this chapter by Messrs. James Adams and Aaron Cohen of the Manned Spacecraft Center, Houston, Texas. They contributed the data on the reentry corridors and Inertial Guidance System error analysis, respectively.

## 9.6 REFERENCES

1. Program Support Requirements — Apollo/Saturn V, Vol. 1, General Information (p. 1410.01), April, 1965.
2. Chapman, D.R., "An Analysis of the Corridor and Guidance Requirements for Supercircular Entry into Planetary Atmospheres," NASA Technical Report R-55, 1960.
3. Adams, J.H., "Apollo Rentry Corridors," Manned Spacecraft Center Memorandum 65-FM5-32, June 29, 1965.
4. Lehnert, R. and Rosenbaum, B., "Plasma Effects on Apollo Reentry Communication," NASA Technical Note D-2732, March, 1965.
5. Harter, G. A., "Inertial Guidance," (Chapter 12) edited by G. R. Pitman, Jr., J. Wiley and Sons, Inc., 1962.
6. Cohen, A., "Apollo Reentry Guidance Requirements," Manned Spacecraft Center, Apollo Spacecraft Program Office, 1965.
7. Smith, O. E. and Chenoweth, H. B., "Range of Density Variation from Surface to 120 km Altitude," NASA Technical Note D-162, July, 1961.



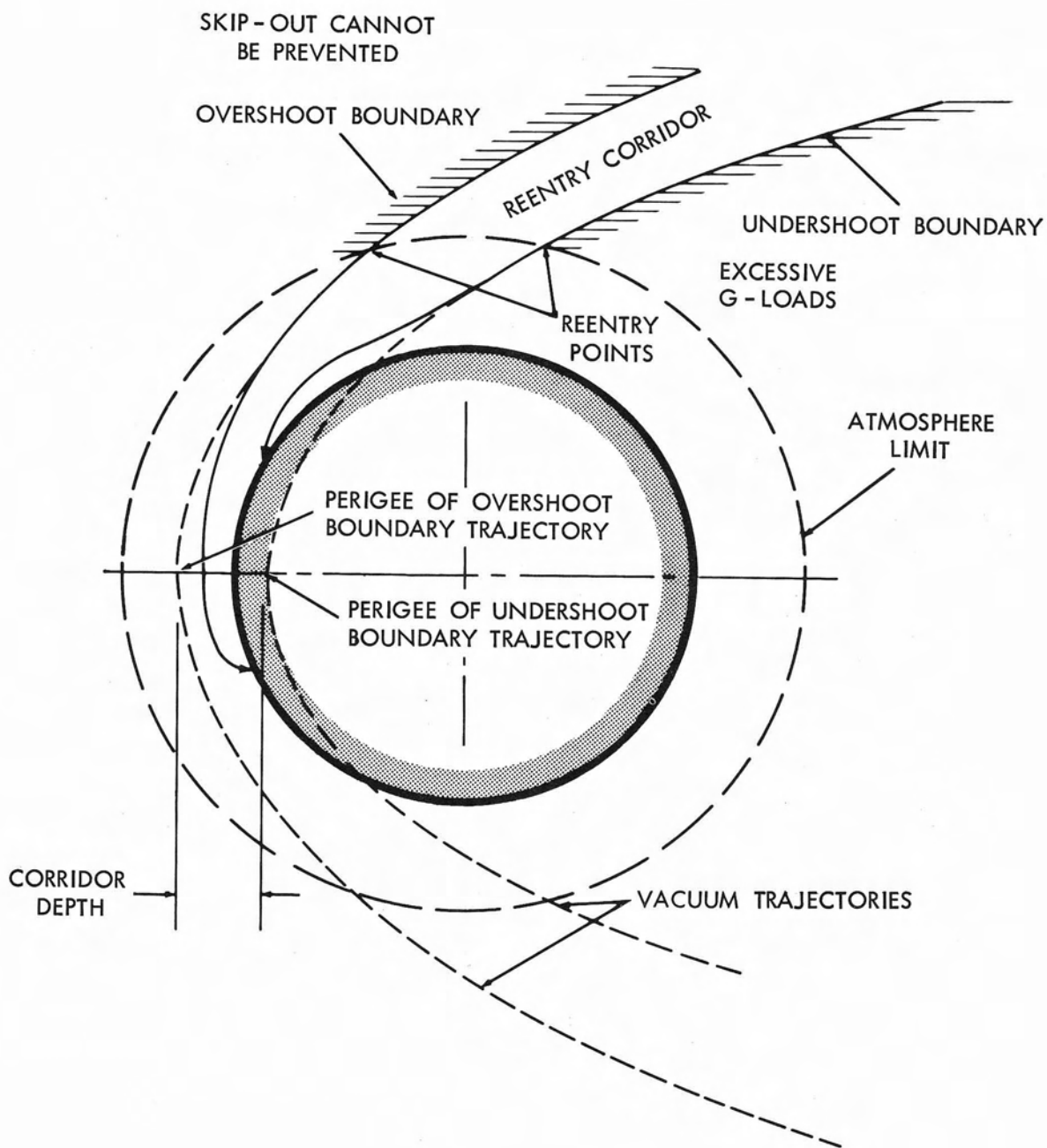


Figure 9.1—Reentry corridor.



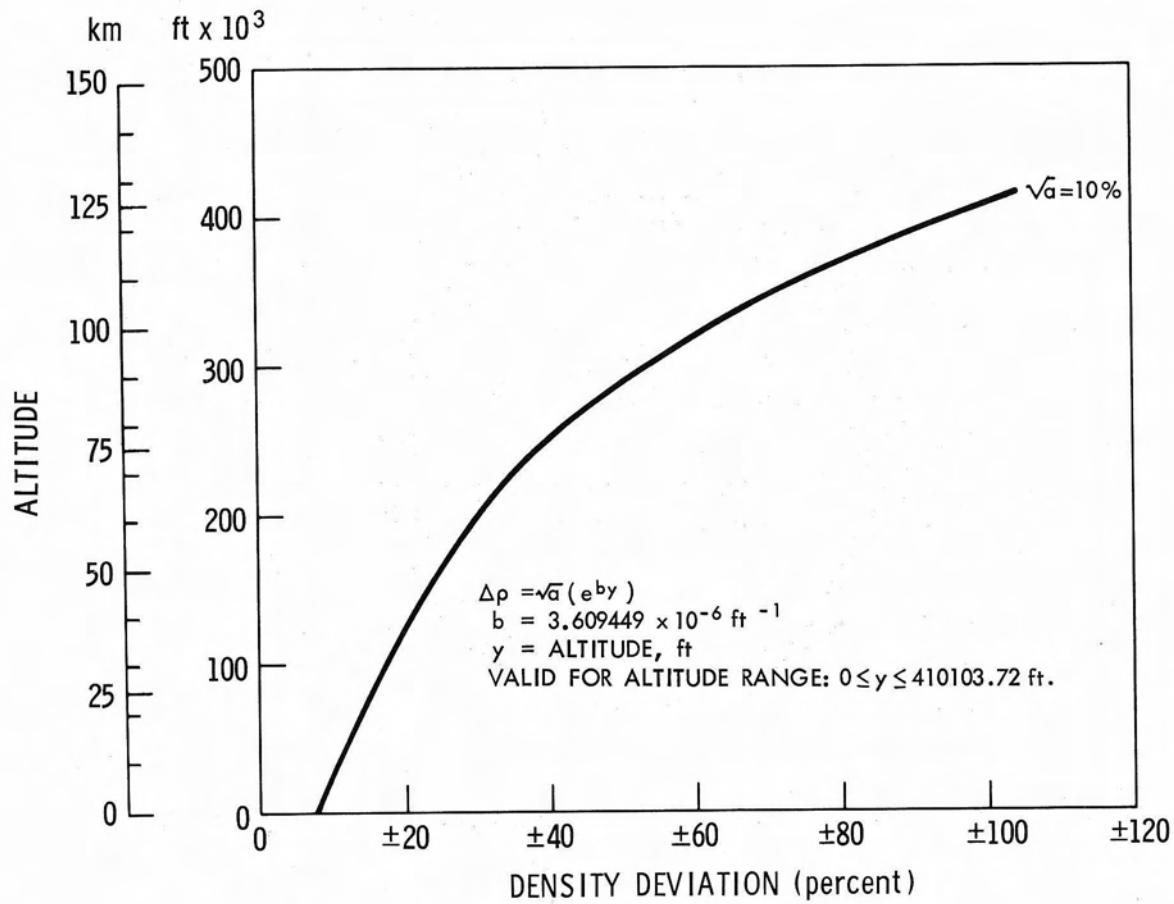


Figure 9.2—Altitude versus density deviation

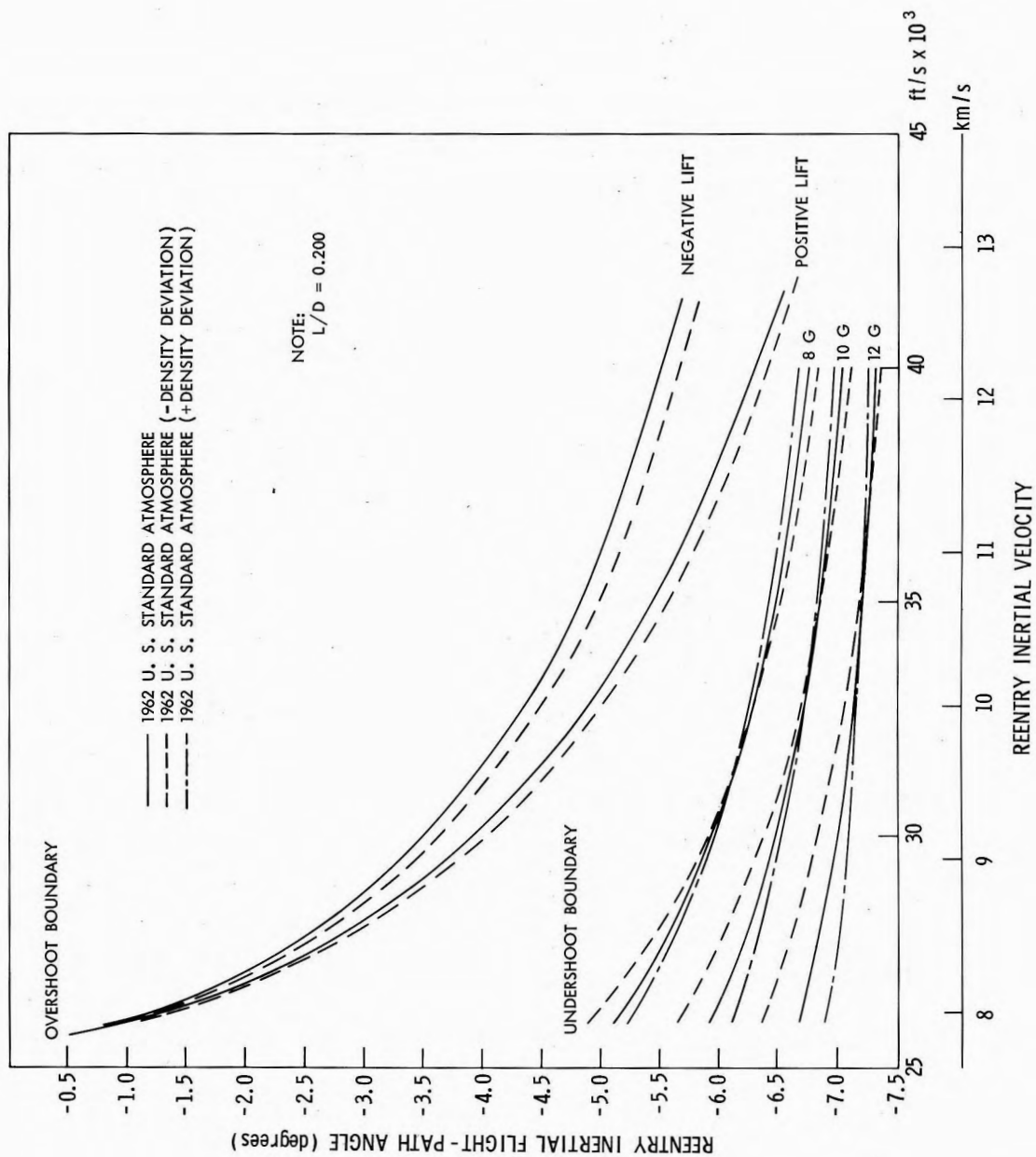


Figure 9.3a—Reentry corridor as a function of reentry inertial velocity,  $L/D = 0.200$ .

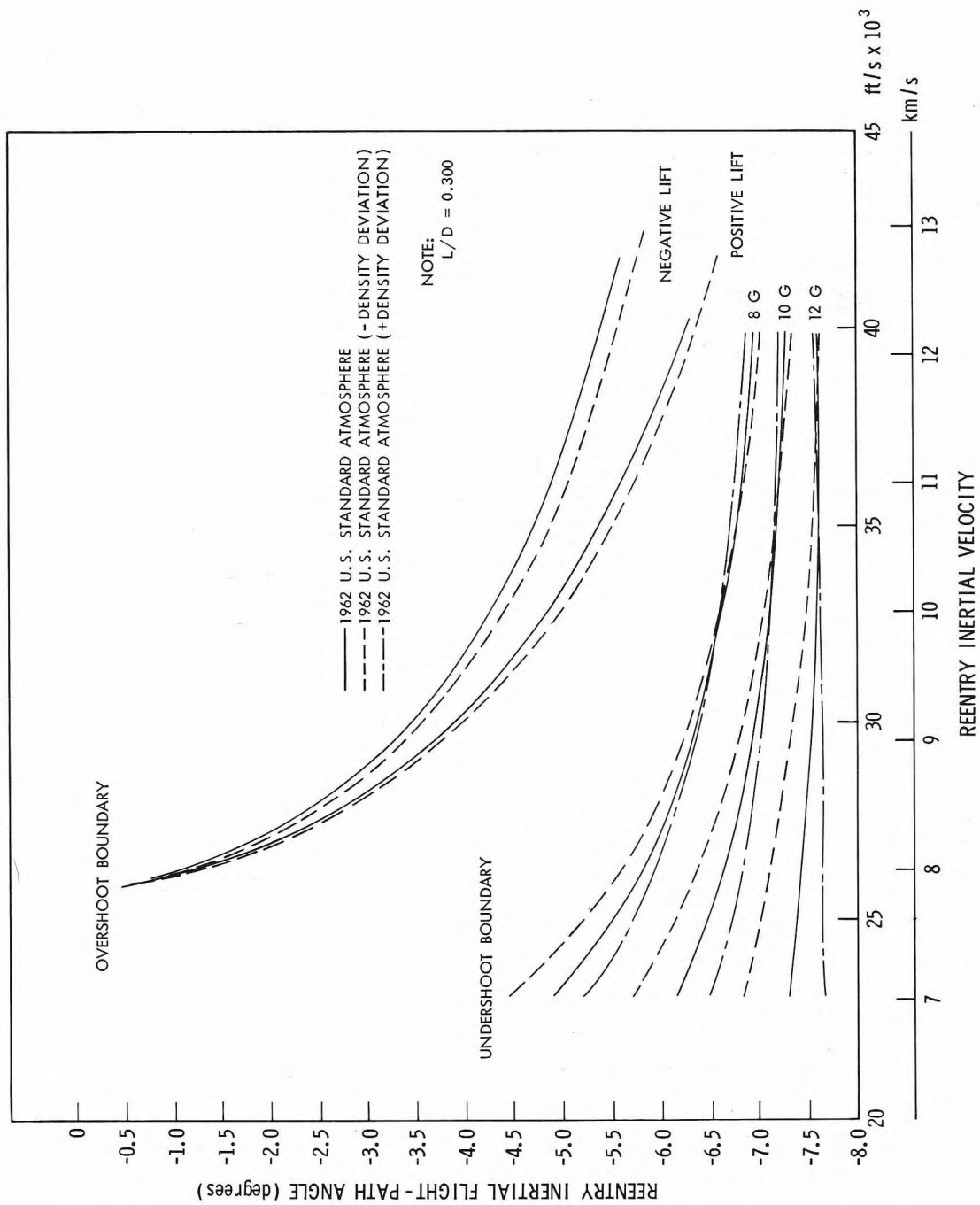


Figure 9.3b—Reentry corridor as a function of reentry inertial velocity,  $L/D = 0.300$ .

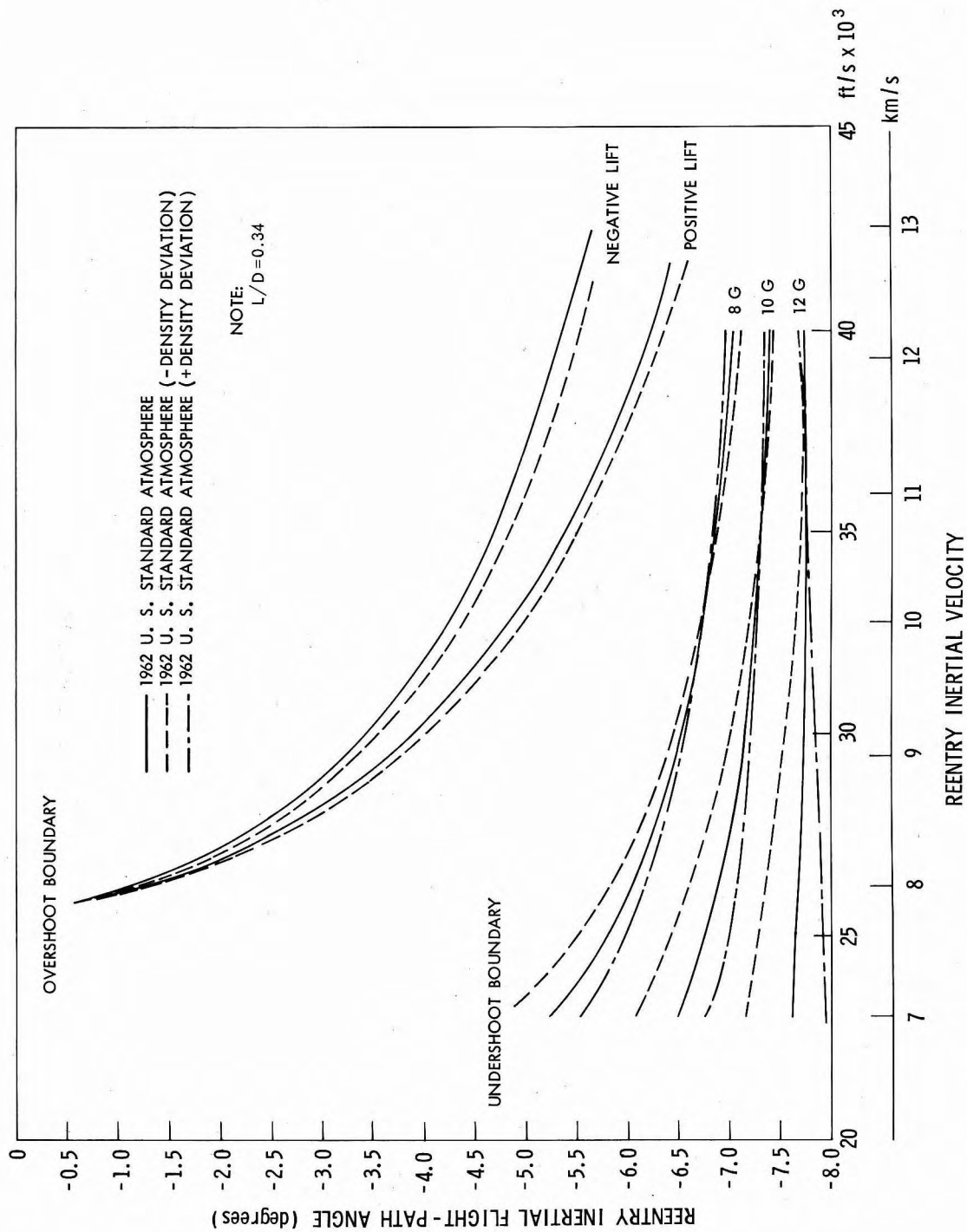


Figure 9.3c--Reentry corridor as a function of reentry inertial velocity,  $L/D = 0.340$ .

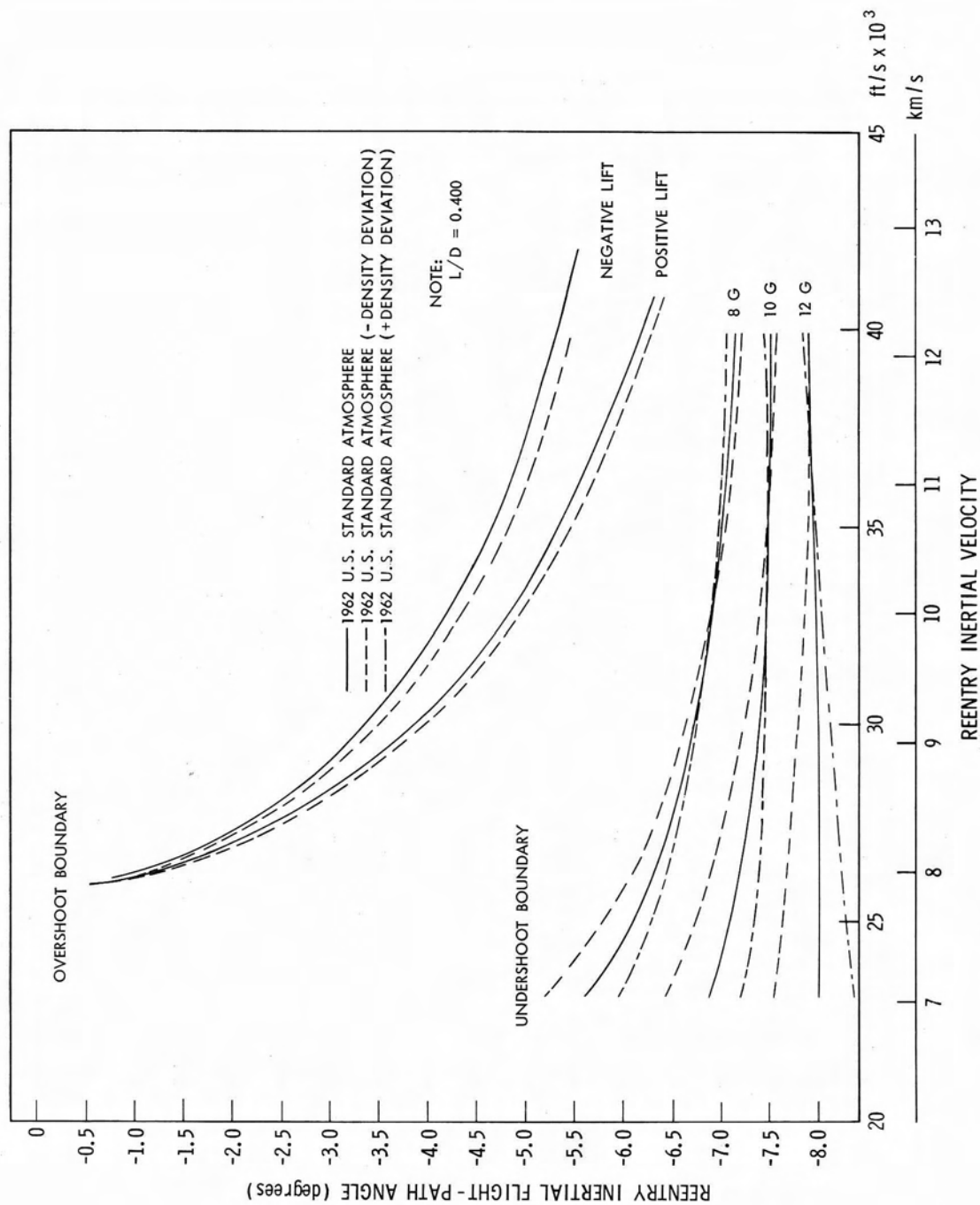


Figure 9.3d—Reentry corridor as a function of reentry inertial velocity,  $L/D = 0.400$ .

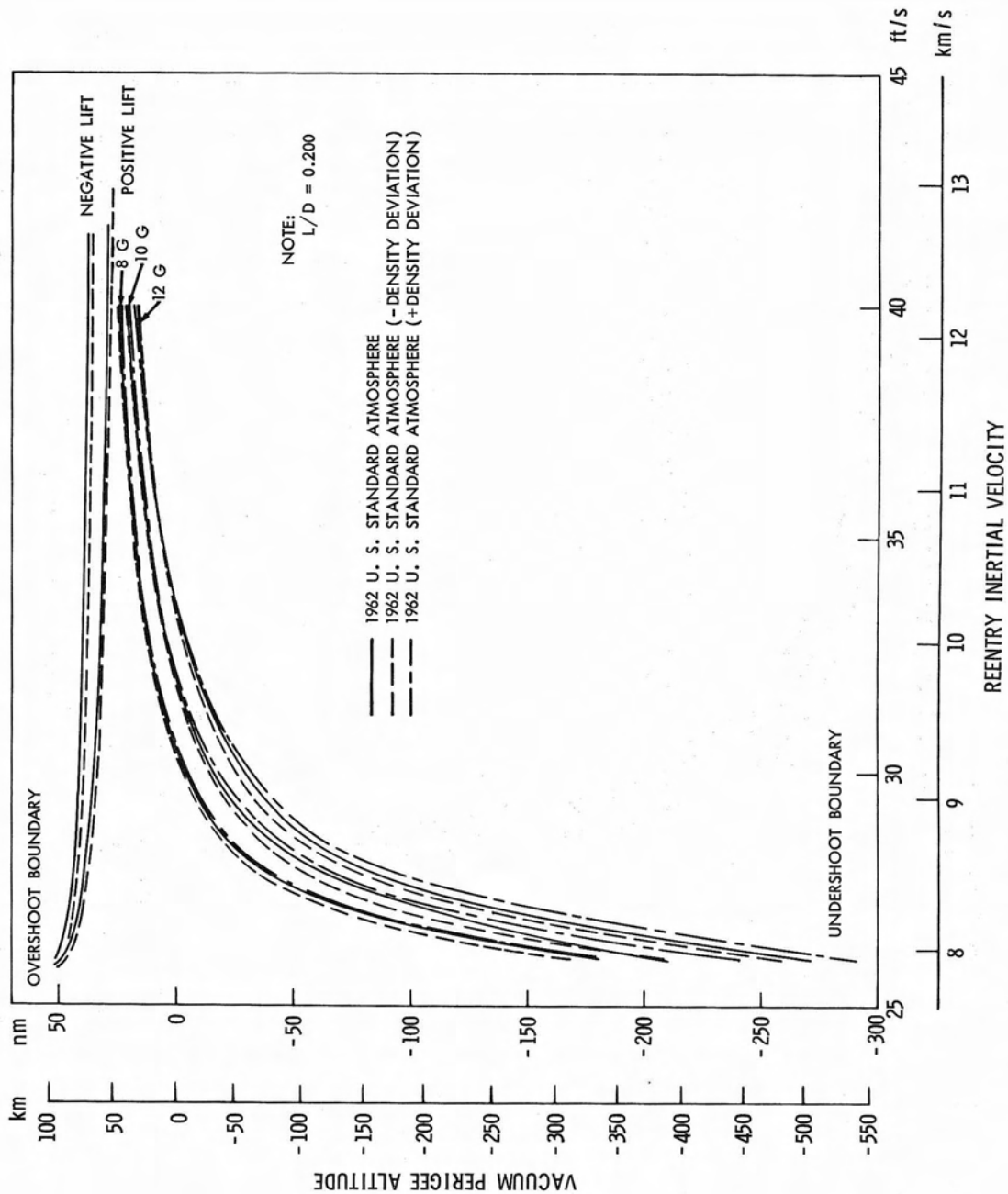


Figure 9.3e—Reentry corridor as a function of vacuum perigee altitude,  $L/D = 0.200$ .

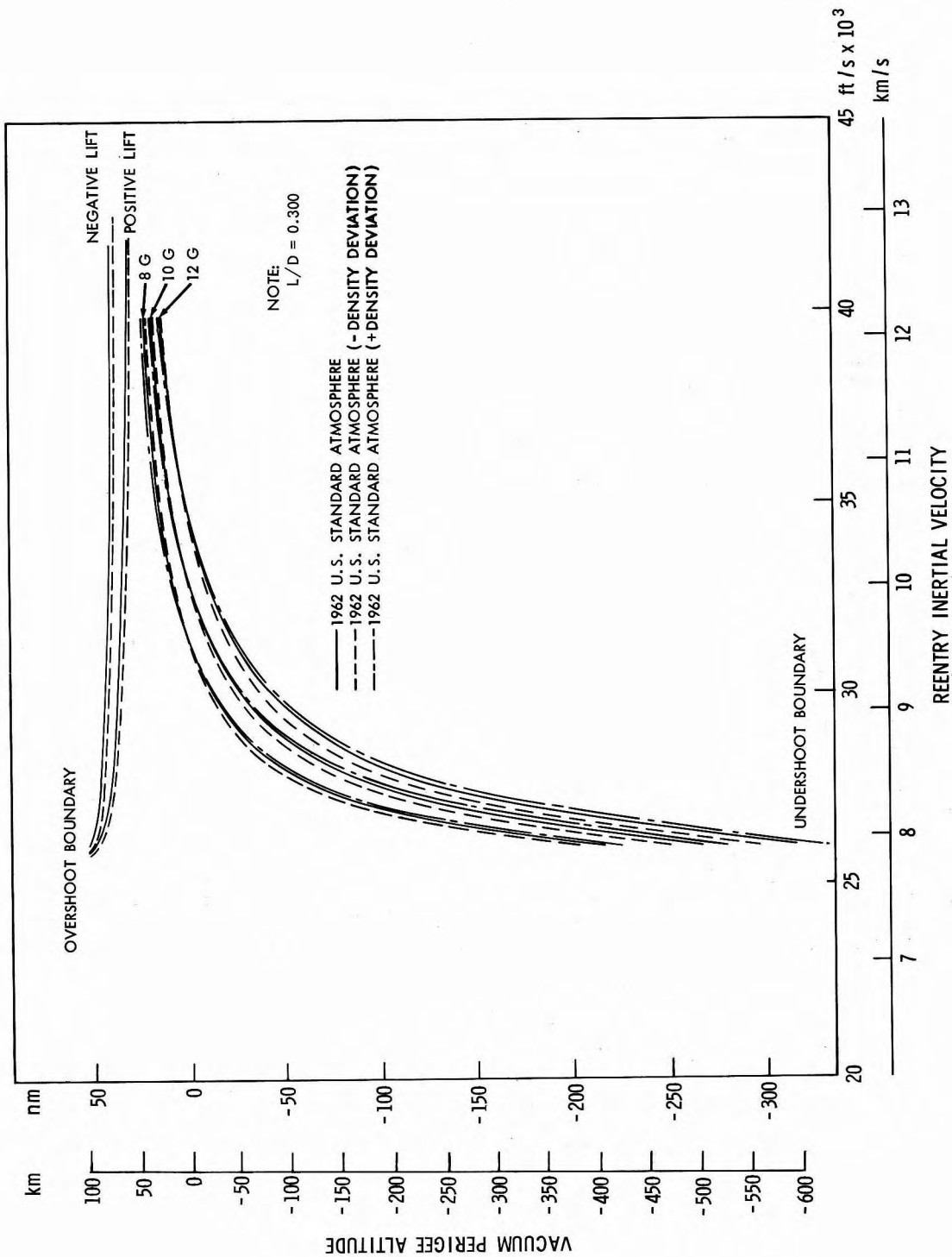


Figure 9.3f—Reentry corridor as a function of vacuum perigee altitude,  $L/D = 0.300$ .

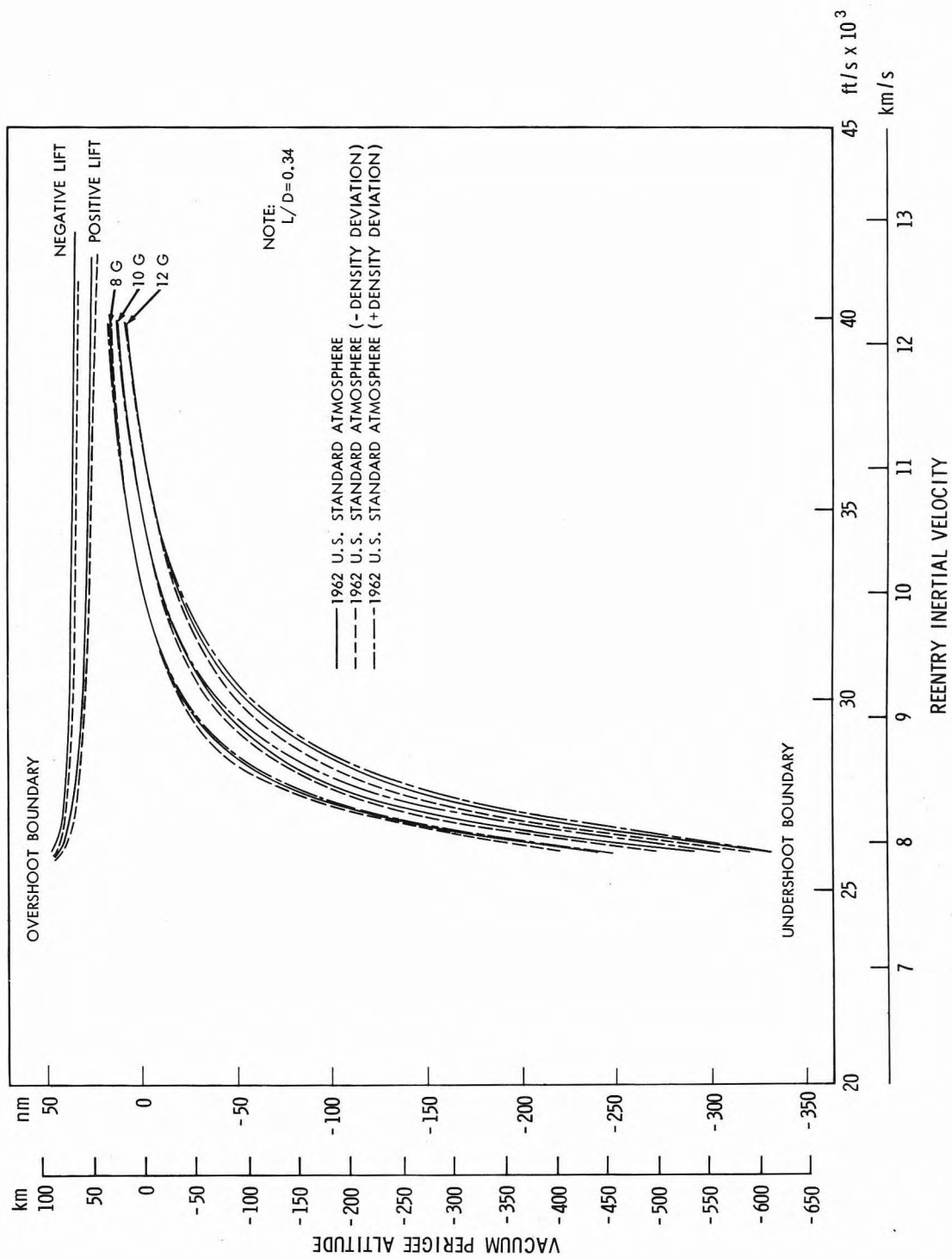


Figure 9.3g—Reentry corridor as a function of vacuum perigee altitude,  $L/D = 0.340$ .



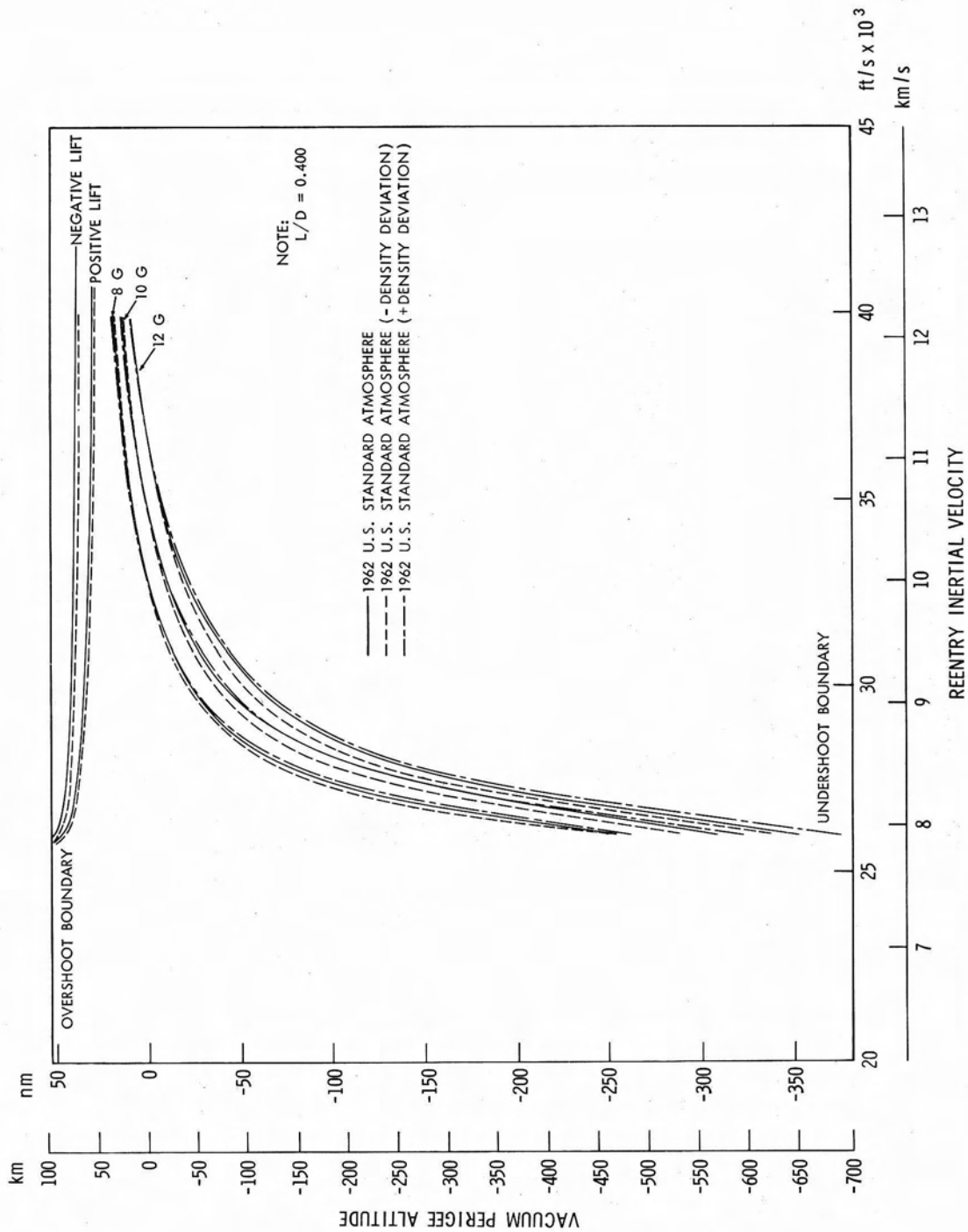


Figure 9.3h—Reentry corridor as a function of vacuum perigee altitude,  $L/D = 0.400$ .

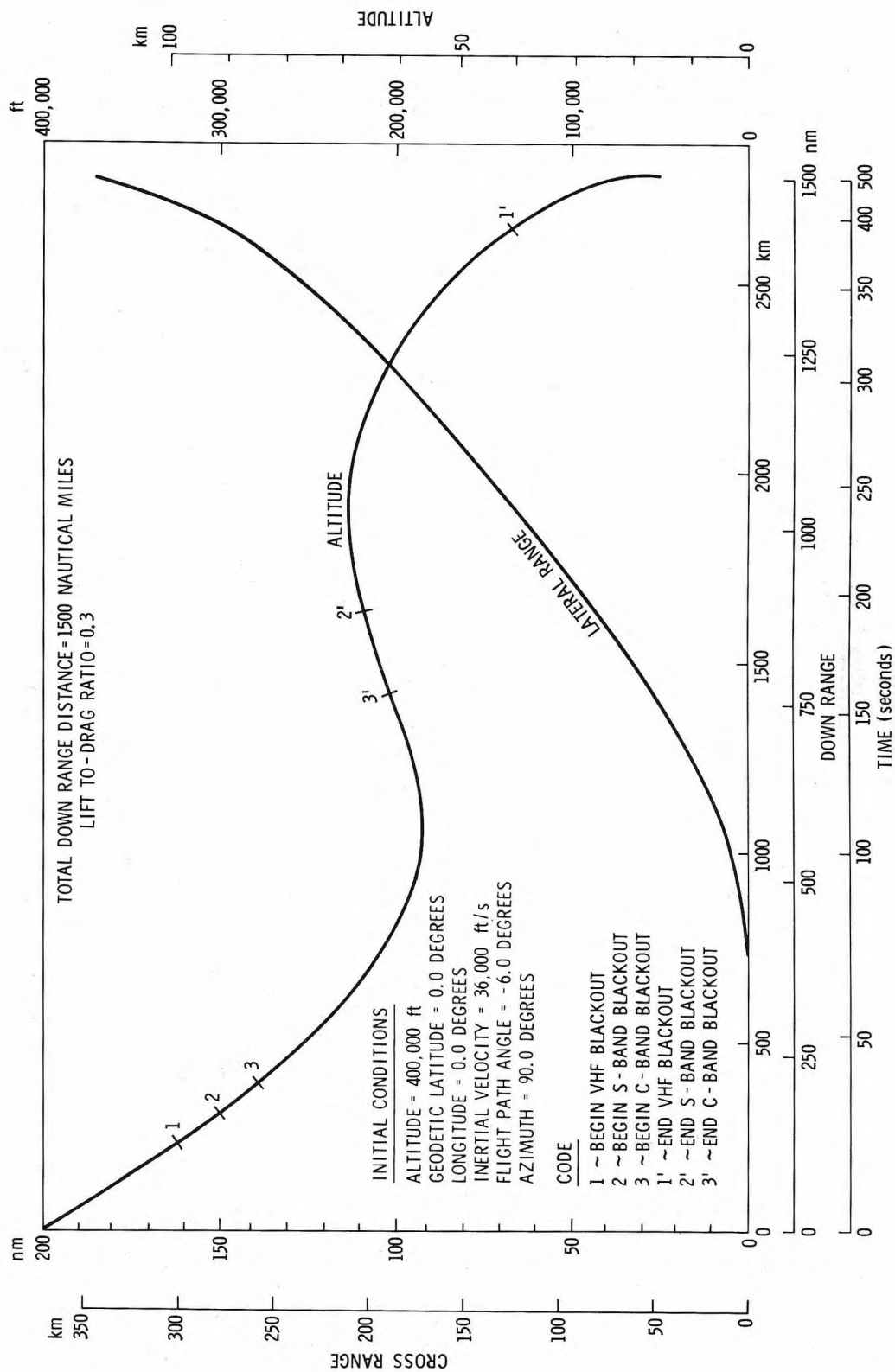


Figure 9.4a—Total down range distance = 1500 nautical miles. Lift-to-drag ratio = 0.3.

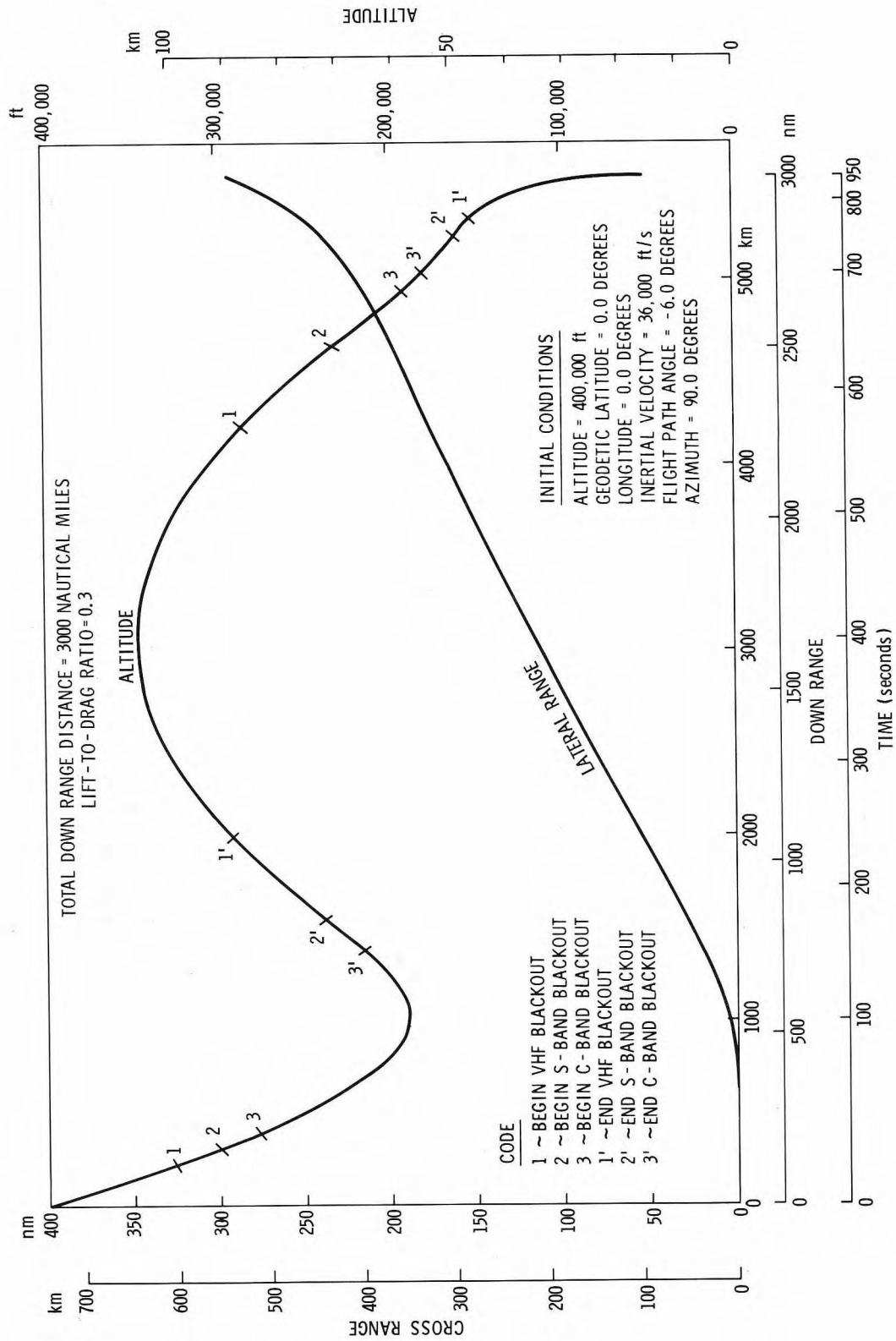


Figure 9.4b—Total down range distance = 3000 nautical miles. Lift-to-drag ratio = 0.3.

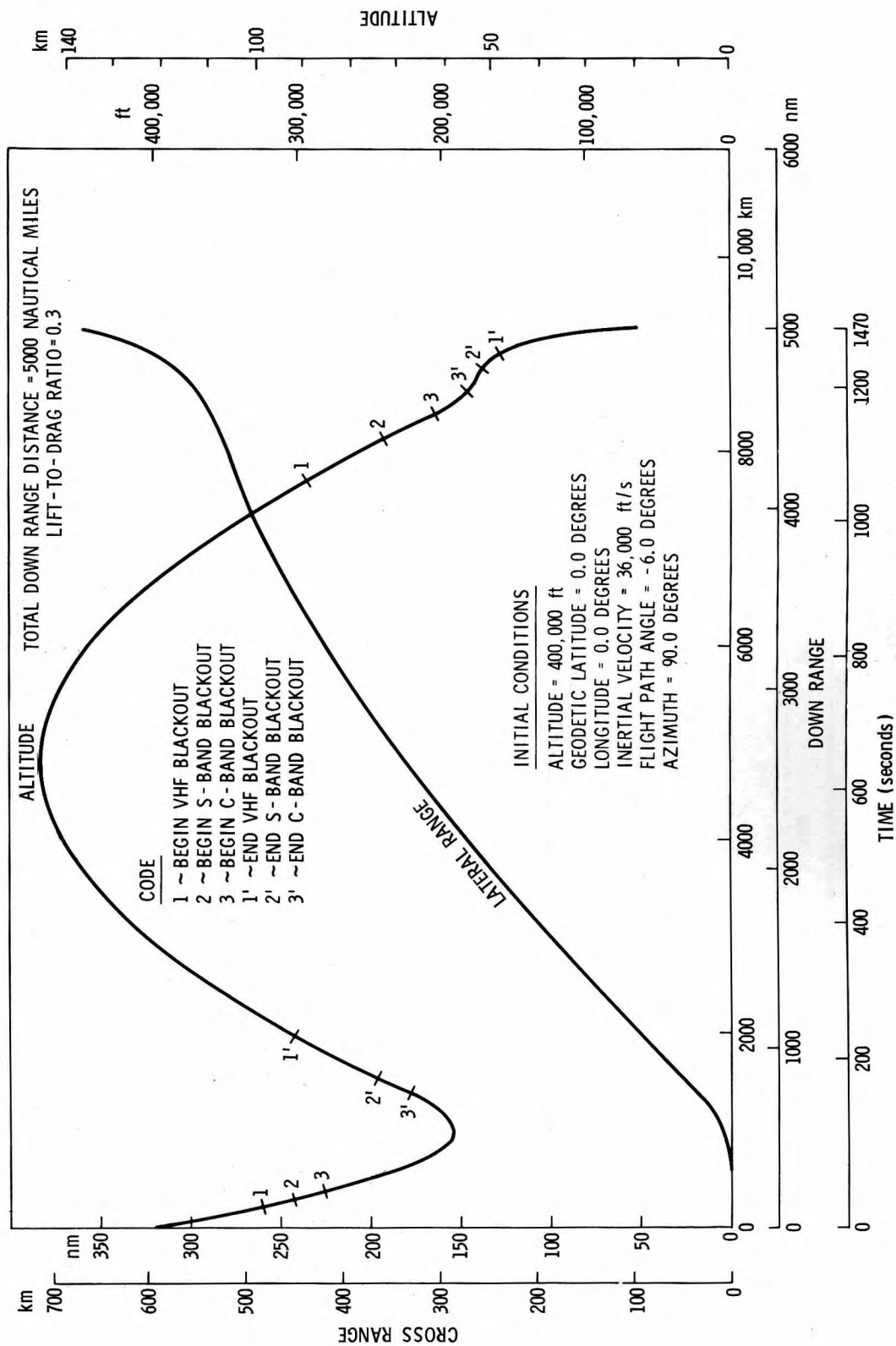


Figure 9.4c—Total down range distance = 5000 nautical miles. Lift-to-drag ratio = 0.3

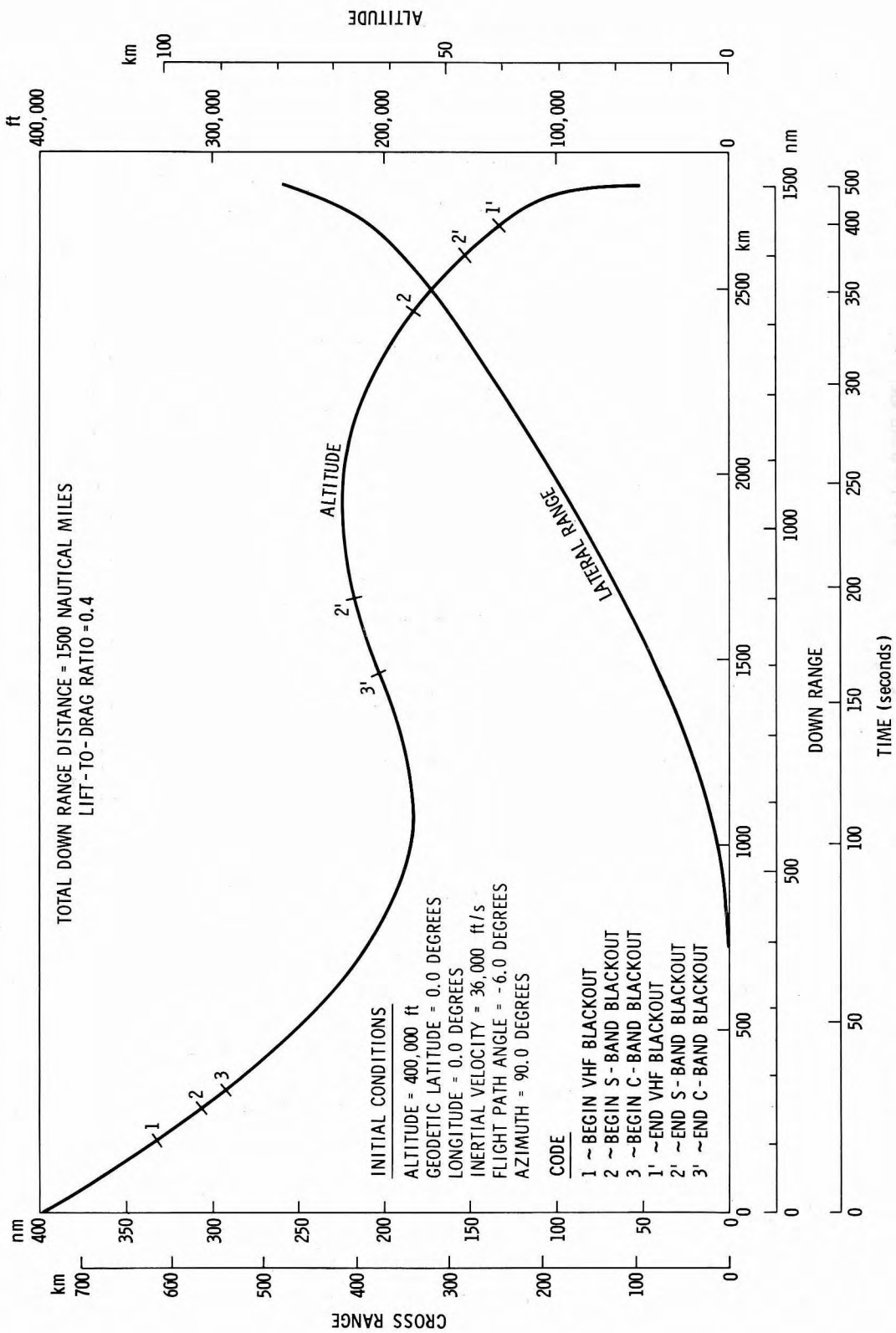


Figure 9.4d—Total down range distance = 1500 nautical miles. Lift-to-drag ratio = 0.4.

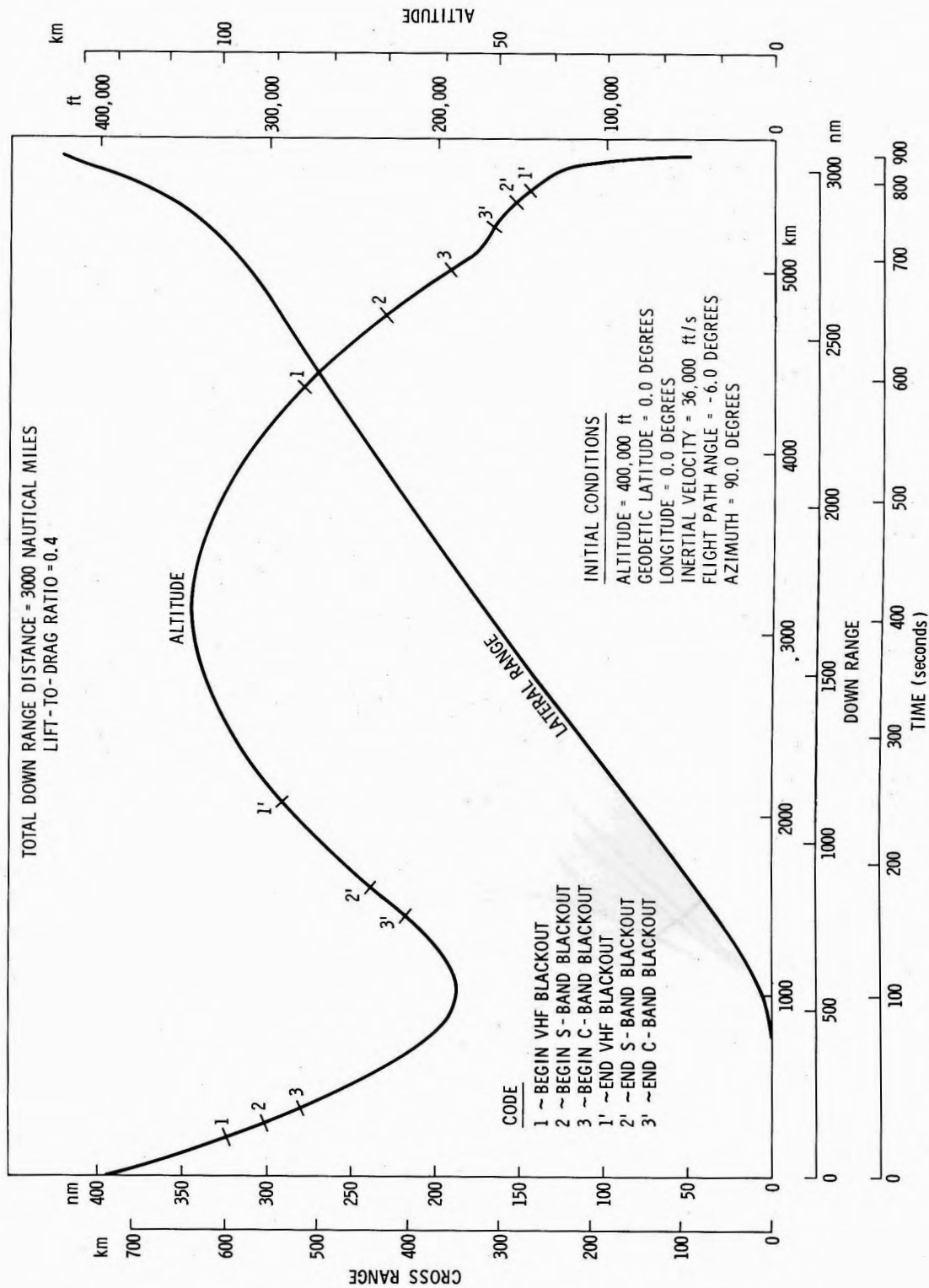


Figure 9.4e—Total down range distance = 3000 nautical miles. Lift-to-drag ratio = 0.4.

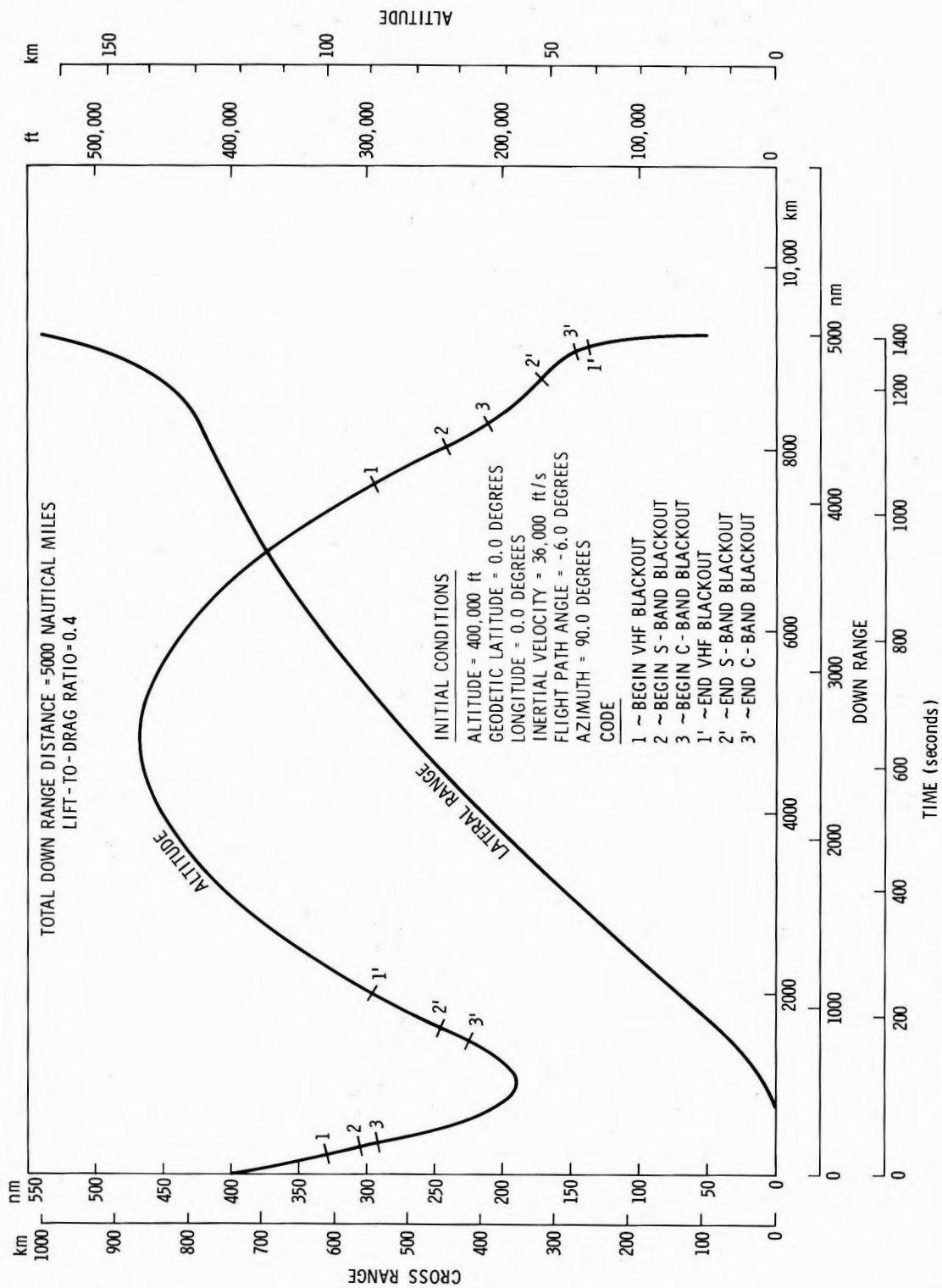


Figure 9.4f—Total down range distance = 5000 nautical miles. Lift-to-drag ratio = 0.4.

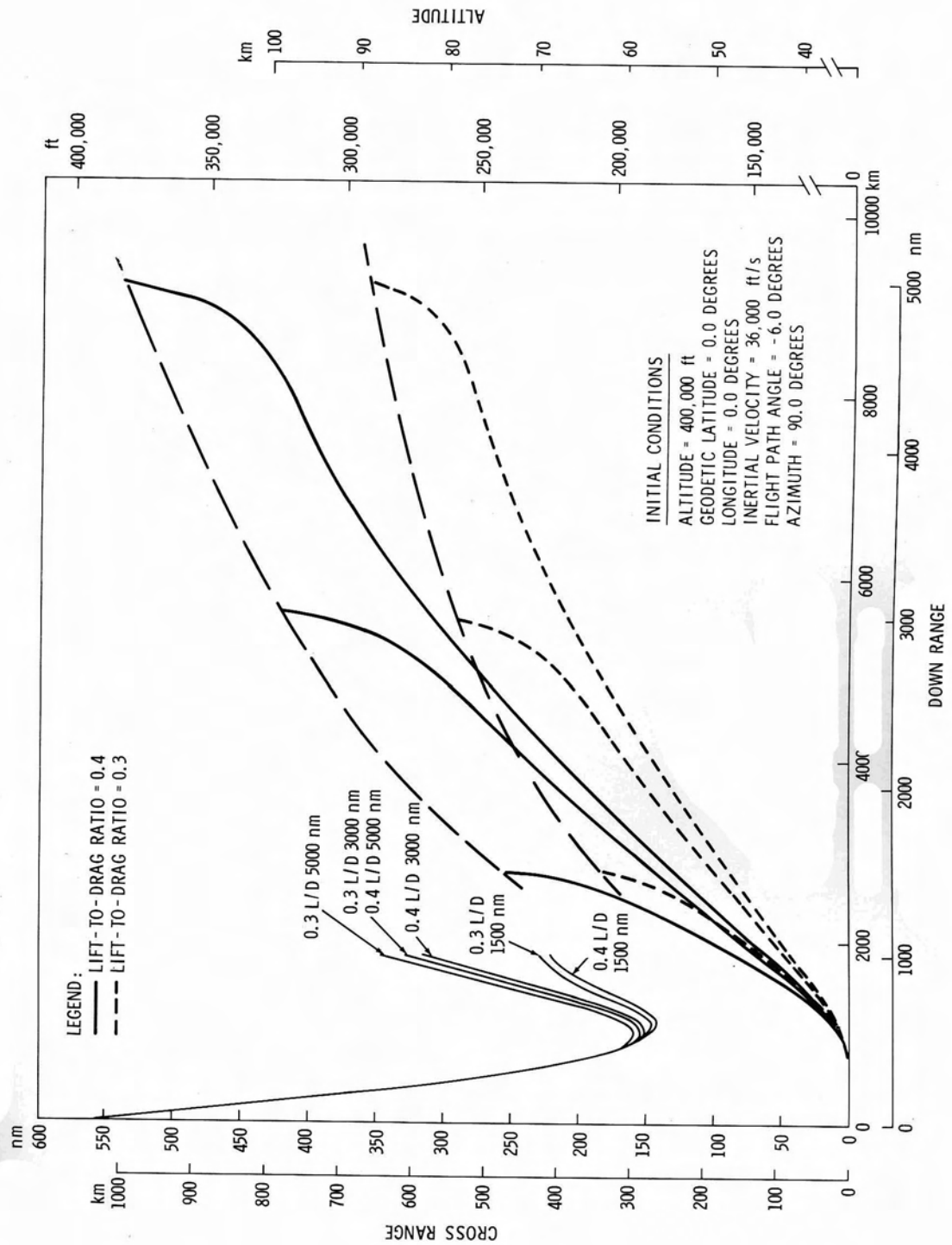


Figure 9.4g